



UNIVERSITY OF
LIVERPOOL

Development of Phosphazene-Polyoxometalate
Catalyst Systems for Multiphase Oxidations with
Hydrogen Peroxide

Thesis submitted in accordance with the requirements of the
University of Liverpool for the degree of Doctor in
Philosophy by Michael James Craven

September 2017

Abstract

Development of Phosphazene-Polyoxometalate Catalyst Systems for Multiphase Oxidations with Hydrogen Peroxide

Michael James Craven

Olefin epoxidation and oxidative desulfurization are two important reactions in both industry and academia. Olefin epoxidation produces epoxides which are important precursors and intermediates in materials and organic syntheses, respectively. Oxidative desulfurization is an emerging technology for the removal of heavy aromatic organosulfur compounds from vehicular diesel fuels which produce harmful SO_x gases from their combustion and are difficult to remove using the conventional hydrodesulfurization technology. Hydrogen peroxide is an attractive oxidising agent for these reactions as it has a high oxygen atom efficiency in oxidation reactions and its only by-product is typically water. Reactions with H_2O_2 are commonly conducted in liquid-liquid biphasic systems due to immiscibility of the aqueous H_2O_2 and the fuel/olefin-containing organic solvent. Keggin-type polyoxometalates (POM, $[\text{XM}_{12}\text{O}_{40}]^{8-n}$, where $\text{M} = \text{Mo}^{\text{VI}}, \text{W}^{\text{VI}}$ and $\text{X} = \text{P}^{\text{V}} (n = 5), \text{Si}^{\text{IV}} (n = 4)$) are often used as catalyst precursors which transform in the presence of H_2O_2 to form active peroxo polyoxometalate (peroxo-POM) species. A suitable phase transfer catalyst (PTC) is required to transfer the peroxo POM to the organic layer where oxidation of the target substrate takes place. Many PTCs have been reported for these reactions over the years - typically quaternary ammonium cations - which are often cumbersome to prepare. In this work, organoaminocyclotriphosphazenes ($\text{P}_3\text{N}_3(\text{NHR})_6$, RPN, R = Bz, benzyl; iBu, *iso*-butyl; iPr, *iso*-propyl; n-Bu, n-butyl; Hex, hexyl; and Cy, cyclohexyl) are presented as alternative PTCs for these reactions, which are easily prepared in one-step reaction of commercially-available $\text{P}_3\text{N}_3\text{Cl}_6$ with a range of primary amines. RPN-POM catalysts were formed by simply combining RPN and POM species together in suitable solvents or *in situ*. Three systems have been developed for olefin epoxidation and oxidative desulfurization with H_2O_2 using RPN-POM catalysts: homogeneous RPN-POM salt catalysts in aqueous biphasic solvent systems

(System One); heterogeneous POM/RPN-SiO₂ solid catalysts for aqueous biphasic solvent systems (System Two); and eutectic RPN-POM “ionic liquid” multifunctional solvent-catalyst systems for reactions in the absence of organic solvents (System Three).

Reactions were conducted under mild conditions (atmospheric pressure and reaction temperature ≤ 60 °C). With BzPN-PMo based catalysts, up to 100% dibenzothiophene (DBT) conversion could be achieved in 0.5 and 3h using Systems one and Two, respectively. Cyclooctene oxide yields of up to 99% were obtained in 0.5h using System One and in 4h using System Two with BzPN-PMo and HexCyPN-PMo as catalysts, respectively. These results compare well with some of the best results reported in the literature, which used similar catalyst-types and reaction conditions. A 76% cyclooctene oxide yield was obtained after 5h with PMo/BzPN-SiO₂ in system two, which was a modest performance compared with other results reported for heterogenous catalysts under similar conditions. In all three systems, the final yield of cyclooctene oxide or conversion of DBT typically increased with decreasing aqueous stability and increasing oxidative potential of POM in the order: PMo > PW > SiW. With respect to benzothiophene in oxidative desulfurization, activity decreased in the order: DBT > (4,6-dimethyldibenzothiophene) DMDBT > (benzothiophene) BT due to the electron-donating and steric effects of the aromatic rings and methyl groups of benzothiophenes. Activity with respect to RPN was relative to the catalyst type, reactant and the solvent system that was used.

The results show that RPN-POMs are promising catalysts for biphasic oxidations with H₂O₂ that can be modified to give homogeneous, heterogeneous and solventless catalyst systems. Mechanisms have been proposed for all three systems.

Acknowledgements

Firstly, I would like to offer my sincerest thanks to my supervisors, Professor Ivan Kozhevnikov and Dr Alexander Steiner, for not only providing me with the opportunity to study for a Ph.D, but also for their continuous support, guidance and (limitless) patience throughout. I could not have asked for better mentors and I will never forget the knowledge and advice they have imparted on me over the last 5 years. I would also like to thank Dr Elena Kozhevnikova for all her tireless help and support in the lab. Without her, I am certain I would still be stuck trying to conduct my first experiment!

I would like to thank Dr Konstantin Luzyanin and Dr Craig Robertson for their contributions to this work and for their friendship.

My deepest gratitude is extended to Dr Frederic Blanc, Dong Xiao, Dr David Bergbreiter and Peerada Samunual for the expertise and for their contributions to our collaborative works.

It has been a privilege to work alongside Rana Yahya, Rebekah Upton, Sophie Hodgkiss, Coral Rogers, Hossein Bayahia, Abdullah Alotaibi, Walaa Alharbi, Khadijah Alharbi, Matthew Wallace, Safer Almutairi, Abdulrahman Alazman, Olivia Poole, Jessica Smith and Vinicius Costa, and I wish them all the best in their future endeavours.

I have enjoyed demonstrating for undergraduate laboratory and workshop courses during my studies, and thank Dr Gita Sedghi and Dr James Gaynor for the opportunity.

I greatly appreciate all the help I have received from university staff members in the Department of Chemistry.

During my studies, my taekwondo training provided me with an outlet for any stress that I experienced – work-related or otherwise. I would like to thank my teacher, Dr Konstantinos Mavorokoridis, and all the members of the UOL TKD club for their friendship and for helping me to unwind when I needed it the most.

Without the support and inspiration from my incredible friends throughout this journey, I may have lost my sanity years ago. Thank you all for being such amazing people! I'd like to extend special thanks to Mike Davidson, Faye Hern, Ste Danks, Casper Kunstmann, Bob Smith, Chris

Thomas, Alex Hill, Dan Bradley, Iain Aldous, Iain Burgess, Hollyann Prince, Adam Byrne, TJ, Ric Lyons, Matt Singh, John Anders, Eleanor Veil, Jenna Redman, Andrew Flanagan and Sarah Horspole for all the great memories and for listening to my awesome (read: terrible) jokes. Cheers!

I would like to thank my wife's family for all their love and moral support, and for always treating me as one of their own. My heart-felt thanks go to my mother-in-law, Jeanette, and to my father-in-law, Ste, for always helping when work began to get on top of us both.

I would like to thank all my family for their unwavering love and support which has helped me to realise many of my aspirations in life thus far. In particular, I would like to thank my parents, my sister and my brother-in-law; undoubtedly, without their sacrifices and constant encouragement, I would not have been able to do this and for that I will never be able to thank them enough.

Finally, I would like to thank my amazing wife and better half, Sarah-Jayne Craven, for her infallible love and unflagging support. The amount of patience and understanding she has shown me over the last few years has been inspirational. A few lines of text cannot convey how thankful I am of her sacrifices. I am truly grateful that she has chosen to stand by me, everlong.

Publications and Presentations

Published Literature

1. **M. Craven**, R. Yahya, E. F. Kozhevnikova, C. M. Robertson, A. Steiner, I. V. Kozhevnikov, *Alkylaminophosphazenes as efficient and tuneable phase transfer agents for polyoxometalate catalyzed biphasic oxidation with hydrogen peroxide*, ChemCatChem 8 (2016) 200-208.
2. R. Yahya, **M. Craven**, E. F. Kozhevnikova, A. Steiner, P. Samunual, I. V. Kozhevnikov, D. E. Bergbreiter, *Polyisobutylene oligomer-bound polyoxometalates as efficient and recyclable catalysts for biphasic oxidations with hydrogen peroxide*, Catal. Sci. Technol. 5 (2015) 818-821.
3. **M. Craven**, R. Yahya, E. Kozhevnikova, R. Boomishankar, C. Robertson, A. Steiner and I. Kozhevnikov, *Novel polyoxometalate–phosphazene aggregates and their use as catalysts for biphasic oxidations with hydrogen peroxide*, Chem. Commun. 49 (2013) 349-351.

Oral and Poster Presentations

1. *Alkylaminocyclophosphazene-functionalized silica as solid support for polyoxometalate-catalyzed biphasic oxidation with hydrogen peroxide*, Poster presented at Designing New Heterogeneous Catalysts Faraday Discussion, (2016).
2. *Novel Polyoxometalate–Phosphazene Aggregates and Their use as Catalysts for Biphasic Oxidations with Hydrogen Peroxide*, Poster presented at EPSRC Fundamentals and Practice Summer School, Liverpool, United Kingdom, (2015).
3. *Phosphazene-Bound Polyoxometalates as Efficient Catalysts for Biphasic Oxidations with Hydrogen Peroxide*, Oral presentation at the 8th European School on Molecular Nanoscience, Paris, France, (2015).
4. *Novel Polyoxometalate–Phosphazene Aggregates and Their use as Catalysts for Biphasic Oxidations with Hydrogen Peroxide*, Poster presented at Northern Sustainable Chemistry (NORSC) symposium, Huddersfield, United Kingdom, (2014).

Abbreviations

AC	Activated Carbon
AU	Arbitrary Units
BT	Benzothiophene
BET	Brunauer-Emmett-Teller
BHJ	Barrett-Joyner-Halenda
Bu	n-Butyl
Bz	Benzyl
BzPN	Benzylaminocyclotriphosphazene
Cy	Cyclohexyl
DBT	Dibenzothiophene
DES	Deep Eutectic Solvents
DMDBT	4,6-Dimethyldibenzothiophene
DRIFTS	Diffuse Reflectance Infrared Fourier Transform Spectroscopy
DCE	1,2- Dichloroethane
DSC	Differential Scanning Calorimetry
DTA	Differential Thermal Analysis
DTG	Derivative Thermogravimetric Analysis
EDS	Extractive Desulfurization
EPA	Environmental Protection Agency
FID	Flame Ionisation Detector
GLC	Gas Liquid Chromatography
GC-FID	Gas Chromatography- Flame Ionisation Detector

HDS	Hydrodesulfuration
Hex	Hexyl
HexPN	Hexylaminocyclotriphosphazene
HPA	Heteropoly Acid
iBu	<i>iso</i> -Butyl
iBuPN	<i>iso</i> -Butylaminocyclotriphosphazene
ICP-OES	Inductively Coupled Plasma Optical Emission Spectroscopy
IL	Ionic Liquid
iPr	<i>iso</i> -Propyl
iPrPN	<i>iso</i> -Propylaminocyclotriphosphazene
IR	Infrared
MAS	Magic Angle Spinning
MOF	Metal Organic Framework
NMR	Nuclear Magnetic Resonance
ODS	Oxidative Desulfurization
PMo	Phosphomolybdic Acid
PN	Phosphazene
POM	Polyoxometalate
PTC	Phase-Transfer Catalyst
PW	Phosphotungstic Acid
RPN	Aminocyclotriphosphazene
RTIL	Room Temperature Ionic Liquid
SiO ₂	Silica
SiW	Silicotungstic Acid
SO _x	Sulfur Oxides

TGA	Thermal Gravimetric Analysis
ULSD	Ultra-Low Sulfur Diesel
UV/Vis	Ultraviolet–Visible Spectroscopy
XRD	X-Ray Diffractometry

Contents

Abstract	i
Acknowledgements	iii
Publications and Presentations	v
Published Literature	v
Oral and Poster Presentations.....	vi
Abbreviations	vii
Contents	x
List of Figures	xvii
List of Tables	xxvi
Project Aims and Thesis Outline	xxviii
1. Introduction	1
1.1 Catalysis	1
1.1.1 Homogeneous Catalysis	3
1.1.2 Heterogeneous Catalysis	4
1.1.3 Heterogeneous vs. Homogeneous Catalysis.....	6
1.1.4 Aqueous Biphasic Catalysis	8
1.1.4.1 Phase-Transfer Catalysis.....	10
1.1.5 Catalysis-Performing Solvents	15
1.1.5.1 Ionic Liquids	15
1.1.5.2 Deep Eutectic Solvents	17
1.2 Polyoxometalates	18
1.2.1 Scope	18
1.2.2 Introduction	19
1.2.3 Nomenclature	20
1.2.4 Heteropolyoxometalates	21
1.2.5 Structure	21
1.2.5.1 Structural Hierarchy of Polyoxometalates	21
1.2.5.2 The Keggin Structure	23
1.2.5.3 Lacunary Keggin Anions	25

1.2.6 Thermal Stability of Solid Compounds.....	26
1.2.7 Properties of POMs in Solution.....	27
1.2.7.1 Solubility.....	27
1.2.7.2 Acidity in Solution.....	28
1.2.7.3 Stability in Solution	29
1.2.8 Use in Catalysis	32
1.2.8.1 Polyoxometalates as Catalysts for Selective Oxidation in Liquid-Phase Reactions	34
1.3 Selective Oxidation Reactions with Hydrogen Peroxide	36
1.3.1 The Venturello-Ishii System for the Phase-Transfer Oxidation of Substrates Catalysed by Peroxo Polyoxometalates	39
1.3.2 Epoxidation of Alkenes Using H ₂ O ₂ as an Oxidant	42
1.3.3 Desulfurization of Diesel Fuels	44
1.3.3.1 Why is Desulfurization of Diesel Fuels Necessary?.....	44
1.3.3.2 Oxidative Desulfurization.....	47
1.4 Phosphazenes	49
1.4.1 Scope	49
1.4.2 Introduction	49
1.4.3 General Properties of Phosphazenes	50
1.4.4 Cyclotriphosphazenes.....	52
1.4.4.1 Structure.....	52
1.4.4.2 Synthesis of Cyclotriphosphazenes.....	53
1.4.4.3 Substitution of Pendant Groups (Reactions of Halophosphazenes)	54
1.4.4.4 Basicity	55
1.4.4.5 Cyclophosphazene Salts.....	58
1.4.4.6 Organoaminocyclotriphosphazenes	59
1.4.4.6.1 Synthesis.....	59
1.4.4.6.2 Aminocyclophosphazene Supramolecular Structures.....	60
1.4.5 Previous Examples of Phosphazene-Polyoxometalate Salt Aggregates	65
1.4.6 Suitability as Phase-Transfer Moieties for POM-Catalysed Oxidations with Hydrogen Peroxide.....	67
References	69

2. Experimental	94
2.1 Sample Preparation	94
2.1.1 Organoaminocyclotriphosphazene Preparation.....	94
2.1.1.1 Hexa(isobutylamino)cyclotriphosphazene	94
2.1.1.2 Hexa(isopropylamino)cyclotriphosphazene	95
2.1.1.3 Hexa(benzylamino)cyclotriphosphazene	95
2.1.1.4 Hexa(hexylamino)cyclotriphosphazene	96
2.1.2 RPN-POM Preparation.....	97
2.1.2.1 BzPN-PW.....	97
2.1.2.2 iBuPN-PW	97
2.1.2.3 iPrPN-PW	98
2.1.3 Preparation of Intermediate $[W(O_2)_4](iBuPNH)_2$	98
2.1.4 Preparation of POM/RPN-SiO ₂	98
2.1.4.1 Preparation of RPN-SiO ₂	98
2.1.4.1.1 iBuPN-Modified Hypersil APS-2 (iBuPN-SiO ₂)	99
2.1.4.1.2 BzPN-Modified Hypersil APS-2 (BzPN-SiO ₂)	100
2.1.4.1.3 iPrPN-Modified Hypersil APS-2 (iPrPN-SiO ₂)	100
2.1.4.2 Preparation of PMo/RPN-SiO ₂	100
2.1.5 Preparation of Eutectic RPN-POMs	101
2.1.5.1 Preparation of Eutectic RPNs	101
2.1.5.1.1 HexBzPN.....	102
2.1.5.1.2 HexCyPN.....	103
2.1.5.1.3 CyBzPN.....	103
2.1.5.1.4 HexBzCyPN	104
2.1.5.1.5 HexiBuPN.....	104
2.1.5.1.6 HexBuPN.....	105
2.1.5.1.7 iBuBuPN.....	105
2.1.5.1.8 HexiBuBuPN	106
2.1.5.2 Preparation of Eutectic RPN-Cl and Eutectic RPN-NO ₃ IL	106
2.1.5.2.1 Eutectic RPN-Cl	106
2.1.5.2.1.1 HexBzPN-Cl.....	106
2.1.5.2.1.2 HexCyPN-Cl.....	107
2.1.5.2.1.3 CyBzPN-Cl	107

2.1.5.2.1.4 HexBzCyPN-Cl.....	108
2.1.5.2.1.5 HexiBuPN-Cl.....	108
2.1.5.2.1.6 HexBuPN-Cl.....	108
2.1.5.2.1.7 iBuBuPN-Cl.....	109
2.1.5.2.1.8 HexiBuBuPN-Cl.....	109
2.1.5.2.1.9 HexPN-Cl.....	109
2.1.5.2.1.10 BzPN-Cl.....	110
2.1.5.2.2 Eutectic RPN-NO ₃	110
2.1.5.2.2.1 HexBzPN-NO ₃	110
2.1.5.2.2.2 HexCyPN-NO ₃	110
2.1.5.2.2.3 CyBzPN-NO ₃	111
2.1.5.2.2.4 HexBzCyPN-NO ₃	111
2.1.5.2.2.5 HexiBuPN-NO ₃	111
2.1.5.2.2.6 HexBuPN-NO ₃	112
2.1.5.2.2.7 iBuBuPN-NO ₃	112
2.1.5.2.2.8 HexiBuBuPN-NO ₃	112
2.1.5.2.2.9 HexPN-NO ₃	113
2.1.5.2.2.10 BzPN-NO ₃	113
2.1.5.3 Preparation of Eutectic RPN-POM IL Catalysts.....	113
2.1.5.3.1 HexBzPN-PMo.....	114
2.1.5.3.2 HexCyPN-PMo.....	114
2.1.5.3.3 BzCyPN-PMo.....	114
2.1.5.3.4 HexBzCyPN-PMo.....	115
2.1.5.3.5 HexiBuPN-PMo.....	115
2.1.5.3.6 HexBuPN-PMo.....	115
2.1.5.3.7 iBuBuPN-PMo.....	116
2.1.5.3.8 HexiBuBuPN-PMo.....	116
2.1.5.3.9 HexPN-PMo.....	117
2.1.5.3.10 BzPN-PMo.....	117
2.1.5.3.11 HexCyPN-SiW.....	117
2.1.5.3.12 HexCyPN-PW.....	118
2.1 Catalyst Characterization Techniques.....	118
2.2.1 Elemental Analysis.....	118

2.2.1.1 Inductively Coupled Plasma Optical Emission Spectroscopy (ICP-OES)	118
2.2.1.2 CHN Analysis	120
2.2.2 Microscopy	120
2.2.2.1 Scanning Electron Microscopy (SEM)	120
2.2.3 Thermal Analysis.....	121
2.2.3.1 Thermogravimetric Analysis (TGA).....	121
2.2.3.2 Differential Scanning Calorimetry (DSC)	122
2.2.4 Spectroscopy.....	123
2.2.4.1 UV-Visible Spectroscopy	124
2.2.4.2 Fourier Transform Infra-Red Spectroscopy (FTIR)	126
2.2.4.3 Nuclear Magnetic Resonance Spectroscopy (NMR)	128
2.2.4.3.1 Solution-State Nuclear Magnetic Resonance Spectroscopy.....	131
2.2.4.3.2 Solid-State Magic Angle Spinning Nuclear Magnetic Resonance Spectroscopy (MAS NMR)	134
2.2.5 X-Ray Diffractometry	136
2.2.5.1 Single Crystal X-Ray Diffractometry	137
2.2.5.2 X-Ray Powder Diffractometry (XRD).....	138
2.2.6 Surface Area and Porosimetry Studies	138
2.3 Catalyst Reaction Studies	144
2.3.1 Product Analysis.....	144
2.3.1.1 Gas-Liquid Chromatography	144
2.3.1.1.1 Injection Port – Split/Splitless Inlet.....	145
2.3.1.1.2 Column	147
2.3.1.1.3 Stationary Phase	148
2.3.1.1.4 Column Oven and Temperature	148
2.3.1.1.5 Detector	149
2.3.1.1.6 Chromatogram	151
2.3.1.2 Calibration of Compounds.....	151
2.3.1.3 Chromatograph Specifications	156
2.3.2 Titrations.....	157
2.3.3 Reaction Studies	158
2.3.3.1 RPN-POM Catalysed Biphasic Oxidation Reactions with H ₂ O ₂	160
2.3.3.1.2 Epoxidation of Olefins	160
2.3.3.1.2 Oxidative Desulfurization	161

2.3.3.2 POM/RPN-SiO ₂ Catalysed Biphasic Oxidation Reactions with H ₂ O ₂	162
2.3.3.2.1 Oxidative Desulfurization	162
2.3.3.2.2 Epoxidation of Olefins	163
2.3.3.3 Epoxidation of Olefins Catalysed by Eutectic RPN-POMs.....	164
References	165
3. System One: Homogeneous Catalysis – Biphasic Oxidation Reactions with Hydrogen Peroxide Catalysed by RPN-POM Salt Aggregates	168
3.1 Introduction	168
3.1.1 RPN-POM Aggregate Salts.....	171
3.2 Phase-Transfer of POM Facilitated by RPN	177
3.3 Epoxidation of Alkenes	181
3.4 Search for Intermediates.....	190
3.5 Oxidation of Benzothiophenes	195
3.6 Conclusions	200
References	201
4. System Two: Heterogeneous catalysis – Oxidation Reactions with H₂O₂ in Multiphase Systems Catalysed by POM Immobilized on RPN-Functionalized Silica Support	206
4.1 Introduction	206
4.2 Phosphazene-Modified Silica Support	212
4.3 POM Immobilized on Phosphazene-Functionalized Silica.....	225
4.4 Oxidation of Benzothiophenes by H ₂ O ₂ Catalysed by POM/RPN-SiO ₂	229
4.5 Epoxidation of Olefins	238
4.6 Conclusions	247
References	250
5. System Three: Epoxidation of Olefin with H₂O₂ Catalysed by Eutectic RPN-POMs	256
5.1 Introduction	256
5.1.1 Combinatorial Approach to Forming Eutectic RPNs.....	258
5.2 Preparation of Eutectic RPNs.....	264
5.3 Preparation of Eutectic RPN Salts	273
5.4 Epoxidation of Olefins Catalysed by Eutectic RPN-POM.....	281
5.5 Conclusions	290
References	291
6. General Conclusions	295

References..... 308

List of Figures

Fig. 1.1	Energy vs. reaction coordinate diagram to show the effect of a catalyst on the activation energy (E_a) of a reaction.	2
Fig. 1.2	Steps of heterogeneous catalysis cycle.	5
Fig. 1.3	Primary, secondary, and tertiary structures of heteropoly compounds.	23
Fig. 1.4	Keggin structure.	24
Fig. 1.5	Geometrical isomers of Keggin-type polyoxometalates.	25
Fig. 1.6	Monovacant and trivacant lacunary POM species.	26
Fig. 1.7	Hammett acidity function (H_o) of $H_nXW_{12}O_{40}$ as a function of the charge of the polyanion.	29
Fig. 1.8	pH range of existence of heteropoly acids.	30
Fig. 1.9	Structure of the Venturello complex, $\{PO_4[WO(O_2)_2]_4\}^{3-}$.	40
Fig. 1.10	The qualitative relationship between the type and size of sulfur molecules in various distillate fuel fractions and their relative reactivities in HDS processes.	47
Fig. 1.11	Structure of a cyclotriphosphazene.	52
Fig. 1.12	Schematic representations of the bonding in cyclotriphosphazenes.	53
Fig. 1.13	Structure of $[(P_3N_3R_6)H]^+ X^-$ salts.	58
Fig. 1.14	Arrangement of hydrogen-bonded organoaminophosphazenes, $P_3N_3(NHR)_6$, in lipid bilayers.	61
Fig. 1.15	Schematic representation of H-bridging motifs observed in solid-state structures of $P_3N_3(NHR)_6$ including single, double, triple, quadruple and septuple H-bridges.	62

Fig. 1.16	Crystallographic structures of RPNs.	64
Fig. 1.17	Schematic hydrogen bonding modes of phosphazanium ions towards anions.	65
Fig. 1.18	The average bond lengths in the rings of the phosphazene cations in $[\text{HP}_3\text{N}_3(\text{NMe}_2)_6]^+[\text{Mo}_6\text{O}_{19}^{2-}]$.	66
Fig. 1.19	Arrangement of the ions in $[\text{HP}_3\text{N}_3(\text{NMe}_2)_6]^+[\text{Mo}_6\text{O}_{19}^{2-}]$.	67
Fig. 2.1	The electromagnetic spectrum.	124
Fig. 2.2	Set-up of FTIR spectrometer operating in DRIFTS mode.	127
Fig. 2.3	Energy levels for a spin $I = \frac{1}{2}$ nucleus in an externally applied field.	129
Fig. 2.4	Precession of a nucleus around an applied external field.	130
Fig. 2.5	Generation of net magnetization vector of nuclear spins in a sample with application of an external magnetic field.	132
Fig. 2.6	Stages of a typical NMR experiment.	133
Fig. 2.7	Bragg diffraction by a set of parallel lattice planes.	136
Fig. 2.8	Types of pores.	139
Fig. 2.9	The four types of adsorption isotherms usually observed by nitrogen adsorption on solid catalysts.	140
Fig. 2.10	The four hysteresis types of adsorption isotherm usually found by N_2 adsorption.	141
Fig. 2.11	General set-up of gas chromatographic instrumentation.	145
Fig. 2.12	Split/splitless injection port.	146
Fig. 2.13	Organisation of layers in an open tubular capillary column.	147
Fig. 2.14	Diagram of a flame ionisation detector (FID).	150
Fig. 2.15	Cyclooctene calibration.	153
Fig. 2.16	Epoxycyclooctane calibration.	153

Fig. 2.17	1-Hexene calibration.	153
Fig. 2.18	1,2-Epoxyhexane calibration.	153
Fig. 2.19	Cyclohexene calibration.	154
Fig. 2.20	Epoxycyclohexane calibration.	154
Fig. 2.21	Epoxyoctane calibration.	154
Fig. 2.22	Benzothiophene calibration.	154
Fig. 2.23	Dibenzothiophene calibration.	154
Fig. 2.24	4,6-Dimethyldibenzothiophene calibration.	154
Fig. 2.25	Temperature programme for the GC column for analysis of olefin epoxidation reaction.	156
Fig. 2.26	Temperature programme for the GC column for analysis of benzothiophene oxidation reaction samples.	156
Fig. 2.27	Set-up of equipment for reactions.	158
Fig. 2.28	Plot of conversion of DBT versus time for desulfurization of heptane model diesel fuel with H ₂ O ₂ and PMo/BzPN-SiO ₂ catalyst.	159
Fig. 3.1	Crystal structure of [iBuPNH] ₄ [SiW]·2CH ₃ OH.	172
Fig. 3.2	Crystal structure of [iPrPNH][iPrPNH ₂][PW]·6CH ₃ OH highlighting the disorder of the extra RPN cation proton between the two rings through a chain of hydrogen-bonded MeOH molecules.	173
Fig. 3.3	Octahedral assembly of [iBuPN] ₃ [iBuPNH] ₃ [PW] modelled from the positions of W and P atoms.	174
Fig. 3.4	FTIR spectra of PW and BzPN-PW.	175
Fig. 3.5	TGA for iBuPN and iBuPN-PW under N ₂ .	176
Fig. 3.6	TGA for iPrPN and iPrPN-PW under N ₂ .	176
Fig. 3.7	TGA for BzPN and BzPN-PW under N ₂ .	177

- Fig. 3.8 ^{31}P NMR of organic phase separated from toluene (5 mL) – water (1 mL) biphasic system containing PW (0.15 mmol) and iBuPN (0.31 mmol) after stirring for 20 min at room temperature. 178
- Fig. 3.9 UV-Vis spectrum of DCE phase after shaking the PW-BzPN (1:6)/DCE-H₂O system {PW ($6.48 \cdot 10^{-3}$ mmol), BzPN ($38.9 \cdot 10^{-3}$ mmol), DCE (10 mL), H₂O (0.5 mL)}. DCE phase was diluted 1:10 with fresh DCE. 178
- Fig. 3.10 UV-Vis absorbance of PW in the DCE phase in DCE/H₂O system at different RPN/PW molar ratios. 180
- Fig. 3.11 ^{31}P NMR of organic phase separated from toluene (3 mL) – water (1 mL) biphasic system containing PW ($6.48 \cdot 10^{-2}$ mmol), H₂O₂ (10 mmol) and iBuPN (0.39 mmol) after stirring for 20 minutes at room temperature. 180
- Fig. 3.12 UV-Vis spectrum of DCE phase after shaking the PW-BzPN (1:6)/DCE-H₂O₂-H₂O system {PW ($6.48 \cdot 10^{-3}$ mmol), BzPN ($38.9 \cdot 10^{-3}$ mmol), H₂O₂ (1.01 mmol), DCE (10 mL), H₂O (0.3 mL)}. 181
- Fig. 3.13 Effect of POM for cyclooctene epoxidation catalysed by POM-BzPN in toluene-H₂O system. 183
- Fig. 3.14 Arrhenius plot for epoxidation of cyclooctene catalysed by BzPN-PMo in toluene-H₂O system. 183
- Fig. 3.15 First-order plot for cyclooctene epoxidation catalysed by BzPN-PW in PhMe-H₂O system. 184
- Fig. 3.16 Initial rate of cyclooctene epoxidation catalysed by BzPN-PW in DCE-H₂O two-phase system versus UV-Vis absorbance of PW in the

	DCE phase at different BzPN/PW molar ratios in the presence and absence of hydrogen peroxide.	186
Fig. 3.17	Epoxide yield versus reaction time for cyclooctene epoxidation catalysed by BzPN-PW in DCE-H ₂ O system at various PW/BzPN molar ratios.	187
Fig. 3.18	Initial rate of cyclooctene epoxidation catalysed by iBuPN-PW in DCE-H ₂ O two-phase system versus UV-Vis absorbance of PW in the DCE phase at different iBuPN/PW molar ratios in the presence and absence of hydrogen peroxide.	187
Fig. 3.19	Epoxide yield versus reaction time for cyclooctene epoxidation catalysed by iBuPN-PW in DCE-H ₂ O system at various PW/iBuPN molar ratios.	188
Fig. 3.20	Catalyst reuse for cyclooctene epoxidation catalysed by BzPN-PMo in toluene-H ₂ O system.	189
Fig. 3.21	Effect of stirring speed for cyclooctene epoxidation catalysed by BzPN-PMo in PhMe-H ₂ O system.	190
Fig. 3.22	³¹ P NMR of yellow powder in MeOH (CDCl ₃ lock) isolated from a PhMe/H ₂ O ₂ system in the absence of olefin and standard with 1:6 [PW]:[iBuPN] at 60°C for 30 minutes.	192
Fig. 3.23	Selected bond lengths (Å) and angles (°) of the crystal structure of (iBuPNH) ₂ [W(O ₂) ₄]·2CH ₃ OH.	193
Fig. 3.24	Crystal structure of (iBuPNH) ₂ [W(O ₂) ₄]·2CH ₃ OH highlighting the ribbon-like assembly of anions and cations.	193
Fig. 3.25	Supramolecular structure of (iBuPNH) ₂ [W(O ₂) ₄]·2CH ₃ OH including methanol molecules.	194

Fig. 3.26	Yield of cyclooctene oxide produced over a 2 hour period in the presence of H ₂ O ₂ using pre-formed (iBuPNH) ₂ [W(O ₂) ₄] as a catalyst.	195
Fig. 4.1	Reaction processes for an organic molecule at the surface of a supported metal catalyst in a liquid-solid system.	207
Fig. 4.2	¹³ C CP MAS (14 kHz) NMR and ³¹ P DE MAS (12 kHz) NMR spectra and quantification of different phosphorus sites of (P ₃ N ₃ Cl _{6-n})-SiO ₂ and BzPN-SiO ₂ .	213
Fig. 4.3	²⁹ Si CP MAS NMR spectra of Hypersil APS-2, BzPN-SiO ₂ , iBuPN-SiO ₂ , iPrPN-SiO ₂ .	214
Fig. 4.4	¹³ C CP MAS NMR spectra of Hypersil APS-2, iBuPN-SiO ₂ , iPrPN-SiO ₂ .	215
Fig. 4.5	³¹ P DE MAS NMR spectra and the deconvolution and quantification of different phosphorus sites of iBuPN-SiO ₂ and iPrPN-SiO ₂ .	217
Fig. 4.6	SEM images of Hypersil APS-2 and BzPN-SiO ₂ .	222
Fig. 4.7	Nitrogen adsorption isotherms for Hypersil APS-2, BzPN-SiO ₂ , iBuPN-SiO ₂ , iPrPN-SiO ₂ and PMo/BzPN-SiO ₂ .	223
Fig. 4.8	SEM images of fresh PMo/BzPN-SiO ₂ catalyst and spent catalysts recovered after desulfurization reaction.	226
Fig. 4.9	¹³ C CP MAS (14 kHz), ²⁹ Si CP MAS (10 kHz) and ³¹ P DE MAS (12 kHz) NMR spectra for PMo/BzPN-SiO ₂ .	227
Fig. 4.10	FTIR spectra of PMo/BzPN-SiO ₂ and H ₃ PMo ₁₂ O ₄₀ (KBr powder).	228
Fig. 4.11	Comparison of activity of POM/BzPN-SiO ₂ catalysts in DBT oxidation by H ₂ O ₂ in heptane-H ₂ O system.	231
Fig. 4.12	Comparison of activity of PMo catalyst with different RPN-SiO ₂ supports for the conversion of DBT to the corresponding sulfone.	232

Fig. 4.13	Comparison of activity of PMo/BzPN-SiO ₂ at different temperatures in DBT oxidation by H ₂ O ₂ in heptane-H ₂ O system.	233
Fig. 4.14	Arrhenius plot of initial rates for DBT oxidation by H ₂ O ₂ catalysed by PMo/BzPN-SiO ₂ in heptane-H ₂ O ₂ system.	233
Fig. 4.15	Comparison of heterogeneous PMo/BzPN-SiO ₂ (PMo/BzPN = 1:1) and homogeneous PMo-BzPN (PMo/BzPN = 1:1 or 1:6) catalysts for oxidation of DBT with H ₂ O ₂ in heptane-H ₂ O system.	234
Fig. 4.16	Reuse of PMo/BzPN-SiO ₂ catalyst for DBT conversion to DBT sulfone by H ₂ O ₂ in heptane/H ₂ O system.	236
Fig. 4.17	Comparison of catalytic activity of Hypersil APS-2-PMo and PMo/iBuPN-SiO ₂ in biphasic epoxidation of cyclooctene by H ₂ O ₂ .	239
Fig. 4.18	Effect of POM on biphasic epoxidation of cyclooctene with H ₂ O ₂ catalysed by POM/iBuPN-SiO ₂ .	241
Fig. 4.19	Reuse of PMo/BzPN-SiO ₂ catalyst for biphasic epoxidation of cyclooctene by H ₂ O ₂ .	243
Fig. 4.20	UV-Vis spectrum of DCE layer after stirring BzPN-SiO ₂ , PMo and H ₂ O ₂ in DCE-H ₂ O system to check for catalyst leeching.	244
Fig. 4.21	UV-Vis spectrum of DCE layer after shaking PMo-BzPN (1:6)/DCE-H ₂ O ₂ -H ₂ O system {PMo (0.0065 mmol), BzPN (0.0039 mmol), H ₂ O ₂ (1.01 mmol), DCE (10 mL), H ₂ O (0.3 mL)}.	245
Fig. 4.22	Comparison of biphasic epoxidation of cyclooctene by H ₂ O ₂ using PMo/BzPN-SiO ₂ or BzPN-PMo as a catalyst.	246
Fig. 5.1	FTIR spectra of P ₃ N ₃ Cl ₆ and HexCyPN.	265

Fig. 5.2	^{31}P NMR spectra of mixed RPNs synthesized from mono (HexPN), binary (HexiBuPN) and ternary (HexiBuBuPN) mixtures of primary amines.	266
Fig. 5.3	Comparison of the ^{31}P NMR spectra of CyPN, HexPN and HexCyPN showing the preferred substitution of HexNH ₂ over CyNH ₂ in the synthesis of HexCyPN.	267
Fig. 5.4	Mass spectrum of BzCyPN	269
Fig. 5.5	$^1\text{H}^{13}\text{C}$ HMQC for HexCyPN.	270
Fig. 5.6	^1H COSY for HexCyPN.	270
Fig. 5.7	DSC curve for BzCyPN.	272
Fig. 5.8	DSC curve for HexiBuPN.	272
Fig. 5.9	DSC curve for HexBuPN.	272
Fig. 5.10	DSC curve for HexiBuBuPN.	272
Fig. 5.11	DSC curve for HexBzPN	272
Fig. 5.12	DSC curve for HexBzCyPN	272
Fig. 5.13	DSC curve for HexCyPN	273
Fig. 5.14	DSC curve for iBuBuPN	273
Fig. 5.15	FTIR spectra of HexBzCyPN-PMo and H ₃ PMo ₁₂ O ₄₀ .	274
Fig. 5.16	XRD of HexCyPN-Cl.	276
Fig. 5.17	XRD of HexBuPN-NO ₃ .	276
Fig. 5.18	Schematic representation of the proposed ordering of RPNH ⁺ and Cl ⁻ or NO ₃ ⁻ in bilayers in microcrystalline RPN-Cl and RPN-NO ₃ waxes.	277
Fig. 5.19	Single-crystal X-ray structure of BzPN-Cl.	278
Fig. 5.20	XRD of HexiBuPN-PMo.	279

Fig. 5.21	Schematic representation of the proposed packing of RPNH^+ and POM ions in eutectic RPN-POM composites.	280
Fig. 5.22	XRD of BzCyPN-PMo.	280
Fig. 5.23	Effect of stirring speed on cyclooctene epoxidation by H_2O_2 with HexCyPN-PMo catalyst at 60 °C.	287
Fig. 5.24	Comparison of epoxide yields achieved after 60 min at 60 °C and different stirring speeds for cyclooctene epoxidation by H_2O_2 with HexCyPN-PMo catalyst.	287
Fig. 5.25	Structure of POM-RTILs, comprised of alkylimidazolium cations and Venturello ions, which were used as catalysts for the epoxidation of olefins with H_2O_2 in the absence of solvent.	288

List of Tables

Table 1.1	Comparison of the Properties of Homogeneous and Heterogeneous Catalysis.	7
Table 1.2	Main species identified at various pH values in decomposition studies of $H_3PW_{12}O_{40}$ in aqueous solution.	31
Table 1.3	Industrial processes catalysed by heteropoly acids.	33
Table 1.4	pK_a values for assorted cyclophosphazenes in nitrobenzene.	57
Table 2.1	Boiling points, retention times and relative response factors (R_f) of compounds in olefin epoxidation and dibenzothiophene oxidation	155
Table 3.1	Epoxidation of olefins catalysed by BzPN-POM in toluene- H_2O biphasic system.	182
Table 3.2	Effect of RPN on cyclooctene epoxidation catalysed by PW in toluene- H_2O two-phase system.	185
Table 3.3	Oxidation of benzothiophenes by H_2O_2 in toluene- H_2O two-phase system in the presence of BzPN-POM catalyst at 60 °C.	196
Table 3.4	Effect of RPN and [RPN]/[POM] ratio on oxidation of DBT by H_2O_2 in toluene- H_2O two-phase system.	198
Table 4.1	Immobilized POM catalysts and their corresponding reaction studies.	209
Table 4.2	Composition of RPN- SiO_2 samples.	220
Table 4.3	Surface and porosity data for Hypersil APS-2 and RPN- SiO_2 functionalized supports.	222
Table 4.4	Oxidation of benzothiophenes by H_2O_2 in heptane- H_2O system using POM/RPN- SiO_2 as catalysts.	230

Table 4.5	Comparison of RPNs and effect of solvent on biphasic epoxidation of cyclooctene by H ₂ O ₂ .	242
Table 5.1	Possible permutations for RPN synthesized using binary mixture of amines.	261
Table 5.2	The maximum number of unique compounds that can be achieved from amine mixtures.	262
Table 5.3	Melting points of RPN-X DESs.	275
Table 5.4	Optimization of reaction conditions for HexCyPN-PMo catalysed epoxidation of cyclooctene with H ₂ O ₂ .	282
Table 5.5	Comparison of RPNs with PMo as catalysts for epoxidation of cyclooctene with H ₂ O ₂ .	283
Table 5.6	Comparison of POM's as catalysts with HexCyPN for epoxidation of cyclooctene with H ₂ O ₂ .	284
Table 5.7	Catalyst reuse experiments for epoxidation of cyclooctene with H ₂ O ₂ catalysed by HexCyPN-PMo.	285
Table 5.8	Epoxidation of 1-hexene with H ₂ O ₂ catalysed by HexCyPN-PMo.	286

Project Aims and Thesis Outline

Prior to this study, we published preliminary results demonstrating that polyoxometalate-phosphazene (POM-RPN) salts show promise as catalysts for biphasic oxidations with hydrogen peroxide.¹ The salts could be formed from the POM and RPN components in MeOH, or *in situ* in two-phase PhMe/H₂O systems, and were isolated by evaporation of the solvent and analysed using a range of analytical techniques. The aim of this study is to build on this preliminary work and to investigate the catalytic properties and operational mechanisms of RPN-POMs, and the development of different systems for their use in oxidations with H₂O₂. The oxidations that will be used to test the catalyst systems will be the epoxidation of olefins, and the oxidation of aromatic organosulfur compounds of the benzothiophene family for oxidative desulfurization of diesel fuels.

Three different RPN-POM catalyst systems will be developed in this study. System One will be oxidation of a target substrate (an olefin or benzothiophene) with H₂O₂ catalysed by RPN-POM in an aqueous biphasic system. This system will provide a more comprehensive investigation of the biphasic systems used in our previous work and will focus on developing a better understanding of the effect of RPN phase-transfer catalyst moiety on the catalytic activity with respect to the organic solvent used.

System Two will use a heterogeneous RPN-POM catalyst, POM immobilised on RPN-functionalised silica (POM/RPN-SiO₂), for oxidation reactions with H₂O₂ in a triphasic system. This system will be employed with the aim of achieving good conversions or yields of benzothiophenes or epoxides, respectively, whilst improving the ease of catalyst-product separation (compared to System One) by utilizing the three immiscible phases.

In System Three, eutectic ionic liquids, comprised of RPNs with mixed organoamino substituent groups (eutectic RPNs) and POMs, will be presented as multifunctional solvent-catalysts for epoxidation of olefins with H₂O₂. This is as a greener reaction system than the other systems as reactions are conducted in the absence of volatile organic solvents.

The following are brief overviews of each of the chapters contained within this work:

Chapter 1 provides a broad introduction to catalysts and the different catalyst systems that are relevant in this study; the properties of POMs and their use in catalysis; selective oxidations with hydrogen peroxide and the Venturello-Ishii system for biphasic oxidations with H₂O₂ catalysed by POM; a background on oxidative desulfurization and epoxidation of olefins, the target reactions used in this study; and the properties of RPNs and their suitability as phase-transfer catalysts (PTC) or surfactants in oxidation reactions catalysed by POM.

Chapter 2, the experimental chapter, describes the methods used for the synthesis of the catalysts and their components, the procedure for catalytic testing in each of the three different catalyst systems, and the techniques that were employed for their characterization. The basic theory of the techniques is outlined along with the context in which they were used in this study.

Chapter 3 reports the study of biphasic oxidation reactions with H₂O₂ catalysed by RPN-POMs (System One). Context for this work will be provided in a brief introduction, followed by analysis of the phase-transfer capabilities of the RPN moieties, results of the oxidative desulfurization and olefin epoxidation catalyst tests, and concluding remarks on the catalyst performance in these systems. Catalyst activity is tested for different POMs and RPNs with a range of different benzothiophenes and olefins in two-phase systems with either n-heptane, PhMe or 1,2-dichloroethane (DCE) as organic solvent.

Chapter 4 outlines the results of catalysis with POM immobilized on RPN functionalized silica, POM/RPN-SiO₂, for both oxidation reactions (System Two). Characterization of the RPN-SiO₂ support and POM/RPN-SiO₂ catalyst describes their morphologies and the species immobilized on the surface of the silica support. Oxidative desulfurization of three benzothiophenes is tested in n-heptane/H₂O₂ system to model a system with diesel fuel, whereas olefin epoxidation is tested in a range of organic solvent/H₂O systems. The reactions are tested using different RPNs and POMs to find the best surfactant/POM catalyst combination for each system.

Chapter 5 details the results of epoxidation of olefins with H₂O₂ using eutectic RPN-POMs as multifunctional solvent/catalysts (System Three). The effect of temperature, different POMs and different eutectic RPNs on the rate of catalysis are investigated. The properties of different eutectic RPNs with different mixed primary amine substituents and the properties of eutectic RPN-POMs are discussed. The effect of counter ion on materials properties and phases of eutectic RPN-X (where X = POM, Cl⁻ or NO₃⁻) are also examined using X-ray diffraction and thermal studies.

Finally, **Chapter 6** concludes this study, providing a summary of the results from previous chapters and remarking on the significance of the findings in this work in the field of catalysis.

References

- 1 M. Craven, R. Yahya, E. F. Kozhevnikova, R. Boomishankar, C. M. Robertson, A. Steiner and I. V. Kozhevnikov, *Chem. Commun.*, 2013, **49**, 349–351.

1. Introduction

1.1 Catalysis

A catalyst was defined by Berzelius as a substance that is added to a chemical reaction to increase the rate, but is not itself consumed by the reaction;¹ hence, a catalyst remains chemically unchanged at the end of a reaction and can be recovered and reused. Catalysis is, therefore, the acceleration of a reaction caused by the addition of a catalyst. Catalysis is vitally important for the modern industrial economy, with approximately 90% of processes using catalysts in one or more stages in the production of chemicals and materials.²

A catalyst operates in a reaction by lowering the activation energy (E_a) - the energy that must be added to a system for the reaction to proceed - but does not alter the thermodynamics of the system (i.e. it does not alter the energies of the reactants or products themselves), nor does it change the equilibrium composition of the reaction (Fig. 1.1). It can do this by stabilising reactive transition states of one or more of the reactants, by bringing reactants together (proximity and orientation effects), and/or can enable otherwise inaccessible reaction pathways.

In a reaction mechanism, a catalyst typically reacts with one or more of the reactants to form a temporary intermediate, or transition, species which reacts further along the catalytic cycle as the product is generated and the catalyst is regenerated. As a catalyst undergoes no permanent change at the end of a reaction, it can be reused numerous times for the same reaction and can be used in very small quantities. However, catalytic activity or small amounts of a catalyst can be slowly lost over time through transfer processes between vessels or effects such as poisoning.³

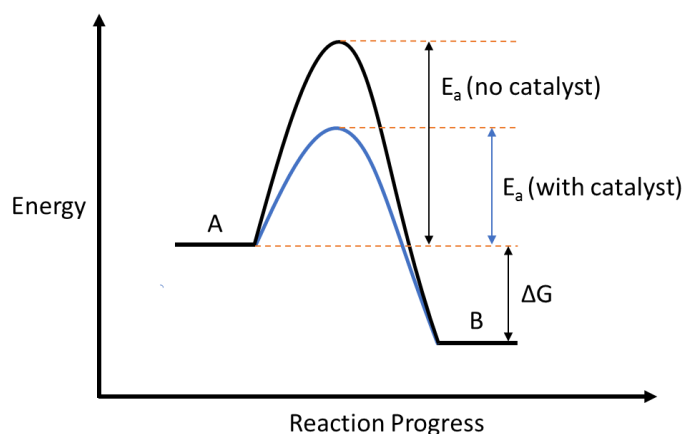


Fig. 1.1. Energy vs. reaction coordinate diagram to show the effect of a catalyst on the activation energy (E_a) of a reaction. In this reaction, reactant A is converted to product B.

The benefits of using catalysts can be numerous. One of the main reasons for using catalysts in industry is that they can improve the economy of a reaction.² Lowering E_a for a reaction lowers the energy requirements of the system and thus lowers the cost of the energy that needs to be put into the system to force the reaction to go. This can also force reactions to occur on an appreciable timescale that otherwise occur over a long period of time, or would not occur at all (e.g. the production of ammonia from N_2 and H_2 gas in the Haber process). Catalyst use can also provide environmental benefits by avoiding use of harmful reagents by making other safer and more sustainable reagents accessible, reducing reaction waste, reducing the volume of a reaction, and removing the requirement of toxic or volatile solvents, to name a few.

Currently, the world is experiencing a “climate crisis” which has forced governments from many of the largest nations to push initiatives to reduce the production of environmental pollutants.^{4,5} There is a requirement for industries to reduce the possible environmental impact of chemical processes by reducing their waste and emissions. The production of more efficient catalysts and processes are, therefore, high priority to conform with regulations. New catalysts

must minimise the level of harmful by-products whilst not contributing impurities into the process themselves (e.g. through poor separation from the products, gradual decomposition etc.).

There are two types of catalysis: homogeneous and heterogeneous; both types will be discussed briefly along with their merits and demerits with respect to each other.

1.1.1 Homogeneous Catalysis

A homogeneous catalyst is one which operates in the same phase as the reactants in a reaction. Homogeneous catalysis is most commonly carried out in a single solution phase in which both the catalyst and the reactants are dissolved and can react together.

Many commonly used homogeneous catalysts are metal complexes. These are comprised of an active metal centre coordinated to a number of suitable ligands. The coordinated ligands often provide multiple operations such as solubilising the active metal centre in the solvent reaction medium, promoting the catalytic activity of the metal centre, and improving selectivity of reactants and products (e.g. coordinate regioselectivity, chemoselectivity and enantioselectivity). Substrates can be introduced onto the metal centre by: simple coordination at a vacant site on the metal centre; substitution of coordinated ligands through dissociative (S_N1) or associative (S_N2) mechanisms; oxidative addition, whereby the metal centre donates electrons to the incoming substrate; or sigma bond metathesis, which occurs when the metal is already in its highest oxidation state (d^0). Coordinated substrates can then react through migratory insertion, nucleophilic attack of a second reactant with the coordinated substrate, or β -hydride elimination. The dissociation of the substrate(s) from the metal centre most frequently occurs by the reverse operation of its initial introduction. These processes are discoordination, substitution, reductive elimination or sigma-bond metathesis.⁶

Homogeneous systems have many advantages; the reactions are usually fast as all metal centres are available for reaction in solution, the selectivity can be tuned by altering ligands around the metal centre, it is very easy to study in situ reactions using spectroscopic techniques, and some reactions can only be performed homogeneously such as the hydroformylation of alkenes.

The inherent problems with homogeneous catalysis are in separation of the catalyst from reactants and products. This is often done by distillation which requires extra energy expenditure and can cause the catalyst to deactivate or the product to degrade. Catalyst recycling often requires extraction of the catalyst between runs which can lead to long “turn around” times between runs and some catalyst may be lost through transfer. Besides, the use of volatile organic solvents, which are commonly used as a reaction medium, is extremely hazardous to health and the environment.

The problem of product separation can be solved by using aqueous biphasic catalysis (*vide infra*). The requirement of volatile organic solvents can be either reduced or removed entirely by using ionic liquids as a reaction medium, or by solventless reactions which can also involve liquid catalysts (*vide supra*).

1.1.2 Heterogeneous Catalysis

A heterogeneous catalyst is one which operates in a different phase to the reactants in a reaction. For instance, a catalyst may be a solid and the reactants may be gases. Many industrial catalysts are heterogeneous and important examples include bulk metal surfaces and zeolites for the reactions of gasses and liquids. Well-known examples include catalytic converters in vehicles which use mixtures of Pd, Pt and Rh to catalyse the oxidation of CO and the reduction of NO_x,⁷⁻⁹ the Haber process which produces ammonia from N₂ and H₂ over an α -Fe catalyst,¹⁰ and zeolite catalysts which are used for the cracking of heavy petroleum distillates.¹¹

Reactions occur at the active sites on the surface of a catalyst. Various types of active site have been reported in the literature through the years, ranging from a specific arrangement of atoms on the surface of a metal to transition metal complexes tethered to a solid support such as silica or alumina. All heterogeneously catalysed reactions occur in cycles following the same generic steps:

1. Transport of substrates to the catalyst
2. Interaction with the catalyst (adsorption)
3. Reaction to form product
4. Desorption of product
5. Transport of product away from the catalyst

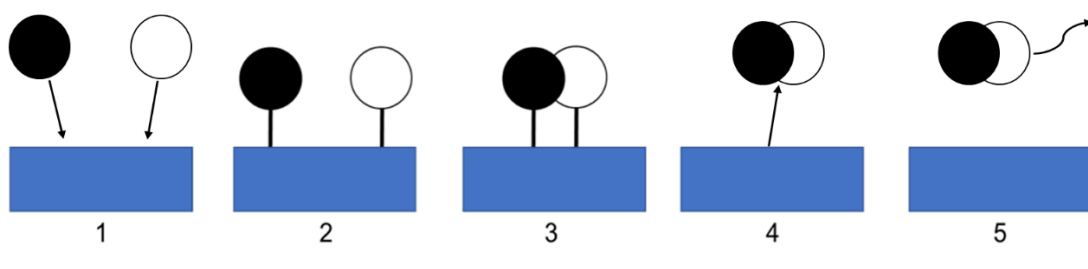


Fig. 1.2. Steps of heterogeneous catalysis cycle.

Often the rate of the reaction is determined by the mass transport of the reactants and products to and from the surface of the catalyst, respectively, and the total number of available active sites on the catalyst surface.

The main advantage of heterogeneous catalysis is that it is easy to separate the catalyst from the product. Other advantages are that some processes can only be conducted with heterogeneous catalysts, such as exhaust gas catalysis, and heterogeneous catalysts usually have high thermal stabilities.

The inherent problems with heterogeneous catalysis are that only the surface atoms are available to perform catalysis which means reactions are slower. They often provide poor selectivity, and catalyst poisoning, caused by chemical bonding of the reactants and products to the active sites, can cause partial or total deactivation of the catalyst. Sintering by cohesion of active sites on the surface (i.e. the growth of metal crystallites by migration of metal active sites) is also a common problem with these types of catalyst.

Nonetheless, porous catalysts or porous supports can be used to increase the surface area and the number of available active sites to improve catalytic activity, and templating with other molecules when forming the catalyst can be employed to influence the shape and size of pores to improve catalyst selectivity. Another method to improve catalyst selectivity is controlled poisoning (e.g. Lindlar's catalyst¹²).³

1.1.3 Heterogeneous vs. Homogeneous Catalysis

Table 1.1 compares some of the most important properties of heterogeneous and homogeneous catalysis. It is important to note that some processes can only be carried out exclusively by heterogeneous or homogeneous catalysis (e.g. exhaust catalysis and hydroformylation of alkenes, respectively). Notable advantages of homogeneous catalysis over heterogeneous catalysis include: up to 100% availability of all active sites, whereas only surface active sites are available in heterogeneous catalysts, which can improve the rates of reaction and reduce the weight and amount of catalyst used in the reaction mixture; tuneable selectivity at the catalysts active sites; and the ability to track the processes in a reaction using *in situ* spectroscopic techniques, which can help to discern the mechanism of the reaction. However, product separation is much more difficult, often requiring the application of techniques such as distillation to separate the catalyst from the product which requires the use of additional energy,

whereas in heterogeneous catalysis the catalyst is inherently separated from the product and can often be separated by simple decantation.

Table 1.1. Comparison of the Properties of Homogeneous and Heterogeneous Catalysis.¹³

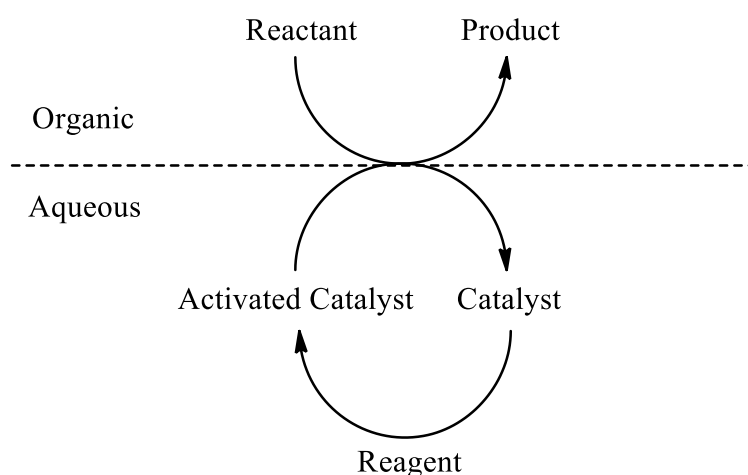
Property	Heterogeneous	Homogeneous
Typical Composition(s)	Solid metal Metal oxide Supported metal	Metal complex
Solvent	Not required	Usually required
Thermal Stability	Robust	Sensitive
Availability of Active Sites	Surface only	All metal centres available
Selectivity	Can be poor	Can be tuned
<i>In Situ</i> Analysis	Difficult	Can use spectroscopic techniques
Product Separation	Easy	Difficult

Homogeneous catalysis generally requires the use of a volatile organic solvent as a reaction medium to solubilise the catalyst and the reactants which are often toxic, harmful to the environment, and increase the waste from the process if they cannot be recycled. In comparison, in heterogeneous catalysis the reactant only has to pass over the surface of the catalyst to interact with the active sites for a reaction to take place, so the use of additional solvents is often not required.

Aqueous biphasic catalysis and ionic liquids can be applied to homogeneous catalytic systems to improve catalyst-product separation and reduce waste.

1.1.4 Aqueous Biphasic Catalysis

The application of aqueous biphasic systems in catalytic reactions was first theorised by Manassen in 1973.¹⁴ It has since become a developed area of catalysis which aims to combine the high conversions and selectivities of homogeneously catalysed reactions, whilst providing the easy separation of catalyst, reactants and products afforded by heterogeneously catalysed reactions. The systems for these reactions are composed of two immiscible solvents, an organic solvent and water, in which the catalyst operates in one phase and the products form in the other. Scheme 1.1 details a typical mechanism for catalysis in an aqueous biphasic system.



Scheme 1.1. Typical mechanism for a reaction catalysed in an aqueous biphasic system.

Initially, the catalyst reacts with a reagent in one phase, here the aqueous phase, to form a catalytically active species. The reaction occurs through interaction between the catalyst and the reactant at the phase boundary (or interface) between the two layers, which is largely aided by emulsification of the two-phase solvents through stirring.¹⁵ The product then remains in the organic phase and the catalytically active species is regenerated in the aqueous phase by reacting with more reagent. Once the reaction has run to completion, the product can be extracted by simple phase separation techniques (e.g. decantation) whilst the catalyst remains in the aqueous phase ready for reuse. Immobilisation of the catalyst in the solvent renders the

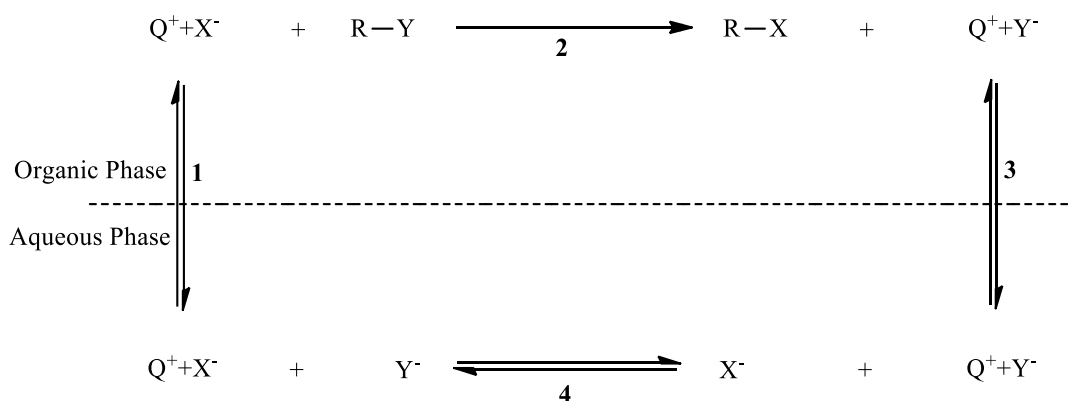
reaction “green” as the catalyst does not enter the environment after the reaction has been completed, allowing for safer, more environmentally friendly methods of reuse and disposal.^{16,17} Owing to their versatility and “green” properties, biphasic homogeneous systems have been used in a wide variety of catalytic processes such as the Shell Higher Olefin Process (SHOP) in the production of detergent-ranged alcohols,¹⁸ the Ruhrchemie/Rhone-Poulenc process for the hydroformylation of propene,^{19,20} and the polymerisation of THF.²¹

The main problem often encountered in aqueous biphasic reactions is long reaction times due to limited interaction of the catalyst and reactant(s) at the interface resulting from phase immiscibility. As previously intimated, emulsification of the phases to increase the area of the interface through stirring can improve reaction times, but often the improvement is only small. The problem of immiscibility has often been solved using co-solvents which have both organic and polar features (e.g. ethanol, methanol etc.) that provide miscibility in both phases, reducing/eliminating the phase boundary effect and improving accessibility between the two reactants. However, rate acceleration of the reaction also tends to be minimal due to excessive solvation of the catalyst and the use of expensive aprotic co-solvents such as dimethyl formamide (DMF), dimethyl sulfoxide (DMSO), N-methyl-2-pyrrolidone (NMP) etc. drives up reaction costs and makes post-reaction separation of the solvents more difficult.^{22,23} The addition of emulsifiers to increase the interfacial surface area has also been used to promote reaction at the interface, but this usually results in difficulty in separating the product from the reaction matrix due to high stability of the emulsion.

A more elegant solution to overcoming the phase barrier problem is through the addition of a phase-transfer catalyst to the reaction mixture.

1.1.4.1 Phase-Transfer Catalysis

The term “phase-transfer catalysis” (PTC) was originally coined by Starks²⁴ to describe the acceleration of a reaction that is directly caused by use of a phase-transfer catalyst. A phase-transfer catalyst is a compound which facilitates the migration of a reactant in a two-phase system from one phase into the other where the reaction occurs.²⁵ They are most commonly lipophilic cations that are added to aqueous biphasic systems to facilitate the migration of hydrophilic anionic reactants between phases through the formation of amphiphilic ion pairs. They are often added to the reaction mixture in the form of a salt. The mechanism for a primitive phase-transfer catalysed reaction - a simple nucleophilic substitution in an aqueous biphasic system - is illustrated in Scheme 1.2. In this system, the PTC is a cationic species (Q^+) and the reactant, solubilised in the aqueous phase, is an anionic species (X^-). The Q^+ complexes with X^- in the aqueous phase to form an intermediate complex (Q^+X^-) which can transfer reversibly between the two phases facilitated by Q^+ (step 1). Once in the organic phase, the complexed X^- , can react with the second lipophilic reactant ($R-Y$) in step 2 to give the product ($R-X$). Q^+ complexes with by-product anion (Y^-) and the resulting intermediate (Q^+Y^-) can then reversibly transfer between the two phases (step 3). Once in the aqueous phase, Q^+ can regenerate Q^+X^- with X^- (step 4) and the cycle repeats until one or both of the reactants are used up.

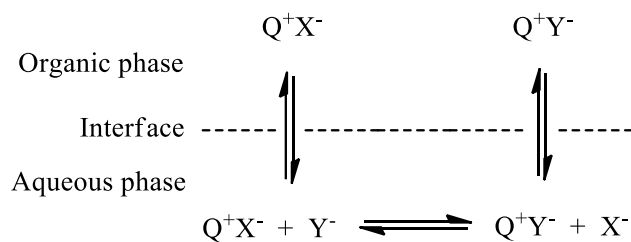


Scheme 1.2. Mechanism for liquid-liquid biphasic phase-transfer catalysis.²⁶

PTC reactions often occur in two important steps which determine the mechanism of the overall reaction: i) the intrinsic reaction step and ii) the phase-transfer step. The intrinsic reaction step is the target reaction step, which in Scheme 1.2 is the displacement reaction of Y^- with X^- in the organic phase. The phase-transfer step is the transfer of a reactant between the two phases. If the intrinsic reaction step is the rate-limiting step, then the phase-transfer operates by an *extraction* mechanism; if the phase-transfer step is the rate-limiting step, then the reaction operates *via* an *interfacial* mechanism. The extraction mechanism was described by Starks and the intrinsic mechanism for phase-transfer in a biphasic system was described by Brandstrom and Montanari, and Makosza, and can be seen in Scheme 1.3.²⁵

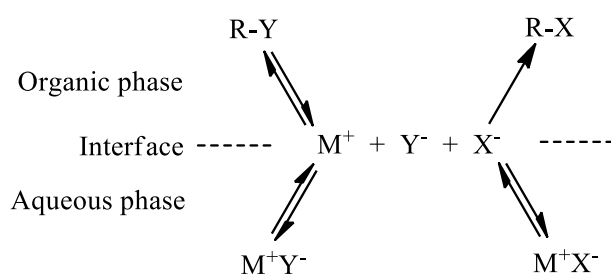
The extraction mechanism was first presented by Starks for the reaction of 1-chlorooctane and aqueous sodium cyanide.²⁷ In this mechanism, the PTC is amphiphilic and can operate in both phases. In the interfacial mechanism, the PTC operates only at the interface. The interfacial mechanism can be sub-divided into two further mechanisms: the Makosza modification and the Brandstrom-Montanari modification.²⁵ In the Makosza mechanism, an anionic reactant from the aqueous phase is first transferred into the interfacial region by the PTC to form the intermediate catalytic reagent. The intermediate is usually too hydrophilic to enter the organic phase and so reaction with the second reactant occurs at the interface to yield the desired product.²⁸ In the Brandstrom-Montanari mechanism, the PTC is too lipophilic to enter the aqueous phase and instead complexes with the aqueous reagent at the interface to form the intermediate salt. The intermediate can then react with the second reactant in the organic phase to yield the final product.²⁹

Extraction Mechanism - complex extracted from the aqueous phase into the organic phase

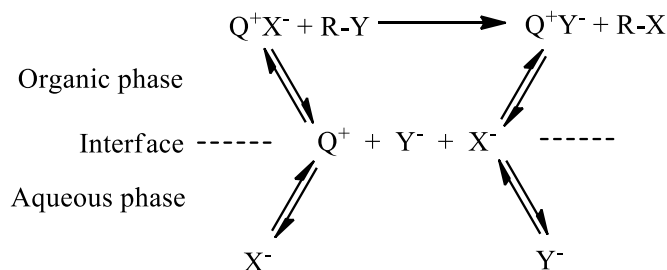


Interfacial Mechanism - complex remains outside of the organic phase

Makosza Modification



Brandstrom-Montanari Modification



Scheme 1.3. Extraction and interfacial mechanisms for phase-transfer.

The rate of all phase-transfer catalysed reactions depends on the efficiency of the phase-transfer step. Increasing the interfacial area between the two phases improves phase-transfer efficiency and makes the reactants available for reaction faster. The interfacial area can be increased: by decreasing the interfacial tension through the use of smaller amounts of non-polar solvents in the organic phase; by agitating the mixture through the use of faster stirring or ultrasound to

create disperse droplets; by introducing surfactants to the mixture to aid the formation of disperse, tiny droplets; or by the formation of a *third-phase* composed of the PTC.³⁰ The bulkiness of the PTC will also affect the rate of phase-transfer. Quaternary ammonium cations are often used for a variety of reactions such as nucleophilic substitutions, eliminations, reduction and oxidation reactions, to name a few. The lipophilicity of these catalysts is provided by their alkyl chains and so most reactions they catalyse operate by an interfacial mechanism as a result. As these chains increase in size, the cation becomes much more lipophilic and bulky, which gives the cation a greater affinity for the organic phase but reduces availability of the cation centre for binding through steric hindrance and reduces the catalyst concentration at the interface. These factors will reduce the rate of transfer. The use of asymmetrical quaternary cations (i.e. with two shorter alkyl chains and two longer alkyl chains) can improve availability of the cationic centre to the interface for anion binding, yet still provide the necessary lipophilicity to solubilise the resulting complex in the organic phase.

The choice of PTC not only influences the rate of the phase-transfer step, but can also have a marked influence on the rate of the intrinsic step also. For a reaction to occur in the organic layer the transferred anion must be in a highly reactive form and, whilst many organic-phase reactions are so fast that they do not require activation of the anion beyond delivery into the organic phase, some anions need to be activated to achieve more practical reaction rates. The first method of activation occurs through greater separation of the cation and anion in the intermediate complex salts which results in looser anion binding and makes the anionic reactant more available for reaction. The second method is through reduced water of hydration around the anion or the entire salt which, when present, can provide steric hindrance and dampen the effective charge of the anion, thus reducing its reactivity. The third, and probably most obvious method, is by dispersion of the anion throughout the organic layer to provide better availability to the second reactant.

Aside from choice of PTC, the rate of the intrinsic step can also be improved by other factors such as agitation, heating, and the use of a cocatalyst. Cocatalysts are widely used in both laboratory practices and industrial applications. In these processes both catalysts operate independently, but when applied together improve the efficiency of the system. The nature in which cocatalysts operate within PTC systems can be subdivided into three categories. The first category of cocatalyst embraces reactions of hydrophilic anions of low lipophilicity that cannot be transferred efficiently between phases in simple phase-transfer catalysed systems. For example, the addition of alcohols to a system can significantly improve hydroxide transfer,³¹ or the addition of triphenyl fluoride to aid transfer of anhydrous KF in biphasic fluorination processes with quaternary ammonium salts.^{32,33}

The second category involves the use of transition metal catalysts with a PTC in biphasic systems. These reactions can often proceed independently of the PTC in either homogeneous or heterogeneous systems, but addition of the PTC often provides significant advantages such as easy catalyst or product separation once the reaction is complete. Examples of such reactions include the catalytic phase-transfer carbonylation of benzyl halides with iron pentacarbonyl or cobalt tetracarbonyl.^{34,35}

In the third category of cocatalytic process, the catalyst activates the reagent in the aqueous phase *via* association. The resulting active complex is then transferred into the organic layer facilitated by the PTC. Once the organic phase reaction has taken place, the catalyst migrates to the interface or into the aqueous phase to activate another molecule of reagent. Molybdate and tungstate have proved to be highly effective cocatalysts with quaternary onium salts in biphasic epoxidation of olefins with hydrogen peroxide.³⁶⁻³⁸

1.1.5 Catalysis-Performing Solvents

In this work, eutectic RPN-POMs were used as multifunctional solvent-catalysts for the epoxidation of cyclooctene with H₂O₂ with the aim of designing a system which avoided using volatile organic solvents in the reaction mixture. The eutectic RPN-POMs are eutectic ionic liquids and so this section introduces ionic liquids and deep eutectic solvents and their uses in catalysis.

1.1.5.1 Ionic Liquids

Ionic liquids (ILs) are molten salts that exist in the liquid state at temperatures below 100 °C,³⁹ though many ionic liquid compounds are liquids under ambient conditions (room temperature ionic liquids- RTILs).⁴⁰⁻⁴² Composed of organic cations and inorganic or organic anions, they exist in a liquid state due to poorly coordinated ions in low symmetry arrangements that exhibit ionic-covalent crystalline structures but do not form well-ordered crystal lattice structures.^{43,44} Many reported examples of ILs in the literature are often halide salts of alkyl ammonium, imidazolium and phosphonium cations.^{40,45-48} The synthesis of a variety of other ILs typically involves reaction of halide salts with an appropriate Lewis acid.⁴⁹⁻⁵¹

The formation of IL solids requires low temperatures, though, glass transitions are often observed instead of melting points due to the difficulty in forming well-ordered arrangements, especially when long aliphatic side chains are involved.^{52,53} Interactions between the ions affect mechanical, chemical and electrical properties of ILs. Species with complex arrays of strong ionic, hydrogen-bonding and van-der-Waals interactions between ions regularly show negligible vapour pressure in the absence of decomposition, giving rise to non-flammable substances with high thermal and electronic stabilities.⁵⁴ Properties such as viscosity, melting point, solubility and hydrophobicity can be manipulated by careful choice of cations and anions to fulfil a specific role; these are often called “designer solvents” or “task specific ionic liquids”.⁵⁵⁻⁵⁷ Appropriate functionalization has seen them used in a variety of applications

including solvents,^{58,59} electrolytes,^{60,61} separation,^{62,63} heat storage,⁶⁴ pre-treatment of biomass,⁶⁵ corrosion resistant coatings for reactive metals⁶⁶ and lubricants⁶⁷ amongst other uses.

Use of ILs as solvents is one their most well researched applications. Often regarded as “green solvents” in the literature, their high thermal stability, non-flammability and recyclability has seen them used as suitable replacements for volatile organic solvents in reactions; indeed, there is a wealth of literature that is available which document the use of ILs as solvents for numerous organic and inorganic reactions.⁶⁸⁻⁷⁴

The melting point of an ionic liquid is an important factor with these compounds, particularly when viewed with regards to use as a reaction solvent. In this case, it is imperative that the IL chosen as a reaction solvent has a melting point below the temperature of the desired reaction in order for the reaction to take place; hence, IL melting points is a topic that has been extensively investigated over the last 30 years, and much of this work has been reviewed.^{75,76}

Use of the “green” moniker, however, can be a point of contention as volatile organics are sometimes used as a synthetic medium to prepare ionic liquids, and data on biodegradation and the toxicology of ILs is often unknown.⁷⁷

Much interest in using ILs as solvents has focussed on their use in catalytic reactions; a topic that has been the subject of many reviews.⁷⁸⁻⁸⁰ More recent work has seen the development of multifunctionality to the ILs in these systems by appropriation of one of the ions (often organometallic cations) to also perform catalytic reactions.^{39,81-84}

The first report of an IL used as a catalyst was in Freidel-Crafts acylation in 1986.⁸⁵ Since then, many different ILs have been developed for use as catalysts in a diverse range of reactions such as halogenation,⁸⁶ carbonylation,⁸⁷ hydrogenation⁸⁸ and oxidation.⁸⁹ Some reported benefits of

using ILs as solvent-catalysts include minimising the volume of reaction mixture, improving stabilisation of catalytically active species through ionic interactions with counter ions, and use of counter-ions as catalyst promoters. Some IL catalysts can even operate as reaction controlled catalysts, whereby they solubilise under a specific set of reaction conditions and alteration of the conditions at the end of the reaction causes the catalyst to self-separate, thus improving catalyst-product separation.⁸⁹⁻⁹²

1.1.5.2 Deep Eutectic Solvents

The approach of using mixtures of different ion constituents or different molten salt components to influence the properties of ionic liquids has been investigated previously in the literature and, indeed, there are a few recently published reviews on the subject.^{41,93,94} Using this approach, low-temperature ionic liquids have been produced by combining different nitrate salts for use as heat-transfer fluids,^{95,96} or by using compositions of a range of different ions.^{93,97} The combination of one or more compounds in a mixture creates a *eutectic* with a melting point lower than the individual components. These mixtures are otherwise known as *eutectic mixtures*, *deep eutectic solvents* or *deep eutectic ionic liquids*.⁹⁷⁻⁹⁹ In addition, hydrogen-bond donating species may also be added to these mixtures to further influence the properties.⁹⁷

Like their conventional ionic liquid analogues, Deep eutectic solvents (DESs) have found applications in catalysis,¹⁰⁰ organic synthesis,¹⁰¹ dissolution and extraction processes,¹⁰²⁻¹⁰⁴ electrochemistry,¹⁰⁵ gas adsorption,¹⁰⁶ separation,¹⁰⁷ and materials chemistry,^{108,109} due to the tuneability of their physiochemical properties such as melting point, solubility, viscosity, and density, among others.⁹⁸ They are most commonly used as reaction media in place of volatile organic solvents for catalysis and organic synthesis as they often have low-cost components, low volatility with high thermal stability, are non-flammable, bio renewable, biodegradable,

non-toxic, and can even be water compatible.^{98,100,101,107} Furthermore, some eutectic ionic liquids have been functionalized to also perform catalysis in addition to operating as a solvent for a variety of reactions.

The use of DESs in catalysis is a rapidly developing area of research. They have been reported for their use as green and sustainable media as well as catalysts in many chemical processes. Some of the recent advances in these areas have been reviewed.^{100,110} Phosphonium-based deep eutectic (P-DES) solvents and an alkali were reported as catalysts for the production of low grade crude palm oil (LGCPO)-based biodiesel using a two-stage process.¹¹¹ The P-DES showed high catalytic activity in the pre-treatment of LGCPO. Choline chloride/zinc chloride eutectic solvents have also been reported as catalysts for a three-component Mannich type reaction of aldehydes, amines and ketones (acetone and acetophenones) at room temperature to give amino carbonyls in 60 to 98 % yields.¹¹² The catalyst could be recycled at least four times without a remarkable decrease in its catalytic activity. Halogen- free Brønsted acidic DESs of quaternary ammonium methanesulfonate salts (e.g. TCyAMsO, TBnAMsO, TOAMsO or TCyATos) with p-toluenesulfonic acid have been used as dual solvent-catalysts for esterification of several carboxylic acids with different alcohols.¹¹³ Yields of up to 97% were reported for the best performing reaction of lauric acid with methanol in 2 h at 60 °C using TCyAMsO-p-TSA DES as a catalyst.

1.2 Polyoxometalates

1.2.1 Scope

In this work polyoxometalates (POMs) were used as precursors for catalytically active peroxo polyoxometalate species in aqueous biphasic oxidations with H₂O₂. POMs were introduced to the reaction systems in their conjugate heteropoly acid (HPA) forms as these are commercially

available and provide acidic protons for the protonation of RPN phase-transfer moieties to their corresponding cationic species, which are required to form ionic and hydrogen bonding interactions with the anionic POMs (and peroxy POMs) to make the POM-RPN aggregate catalysts. The relative activity of POMs in these systems depends on their HPA acid strength, oxidation potential, and hydrolytic stability. The POMs used in this work are $\text{PW}_{12}\text{O}_{40}^{3-}$ (PW), $\text{PMo}_{12}\text{O}_{40}^{3-}$ (PMo) and $\text{SiW}_{12}\text{O}_{40}^{4-}$ (SiW), and their properties are listed below:¹¹⁴

Acid strength (HPA): $\text{PW} > \text{SiW} \geq \text{PMo}$

Oxidation potential: $\text{PMo} \gg \text{PW} > \text{SiW}$

Hydrolytic stability: $\text{SiW} > \text{PW} > \text{PMo}$

This section will introduce the nomenclature for POMs and their derivative species that have been used in this work, and will also provide the background on the relevant properties and chemistry of POMs required to explain the experimental observations and conclusions made in this study.

1.2.2 Introduction

Polyoxometalates are a very diverse class of nano-sized metal-oxide clusters that are unique in their structural variety and functional versatility, with applications in various disciplines of current technological, environmental and economic interest (e.g. catalysis, materials science, medicine and energy).¹¹⁵⁻¹¹⁷ The arrangement of the clusters forms an extensive array of anionic structures constituting early transition-metal elements in their highest oxidation states. These structures are categorised as either *isopoly* or *heteropoly* anions with the general formulas $[\text{M}_m\text{O}_y]^{p-}$ and $[\text{X}_x\text{M}_m\text{O}_y]^{q-}$ ($x \leq m$), respectively, where M represents the *addendum atom* (typically Mo^{VI} , W^{VI} , V^{V} etc.) and X is the *heteroatom* (usually P^{5+} , Si^{4+} , As^{5+} , B^{3+} , etc.). These compounds, both comprising oxygen-sharing MO_y polyhedra, readily form in acidic

aqueous solutions *via* a self-assembly process involving the condensation of one or more oxoanions and can be isolated as solids with an appropriate counter-cation such as H⁺, alkali metal cations (K⁺, Na⁺, Cs⁺ etc.) and NH₄⁺. Examples for the formation of an *isopolyanion* ([Mo₇O₂₄]⁶⁻) and a *heteropolyanion* ([PW₁₂O₄₀]³⁻) are outlined in equations 1.1 and 1.2, respectively.¹¹⁶



1.2.3 Nomenclature

A simplified nomenclature is used for POMs in which they are considered *pseudo* coordination complexes. If a heteroatom is present then this is regarded as the central atom of the complex and the addenda atoms as the ligands and, as such, a complex consisting of a phosphorus heteroatom and twelve tungsten addenda atoms would be written [PW₁₂O₄₀]³⁻. In acid form – referred to as *polyacids* or *polyoxoacids* – the proton counterions are placed outside of the brackets or, often, the brackets are completely dropped to give H₃[PW₁₂O₄₀] or H₃PW₁₂O₄₀. The same nomenclature is also used for other counter cations, for instance Na⁺ in Na₃[PW₁₂O₄₀]. For simplicity, it is common practice to omit the charge, counter ion and even the oxygen atoms; for example, H₃PW₁₂O₄₀ may be abbreviated to PW₁₂, PW or HPW.

In this work, we will mostly deal with heteropoly anions and will use the term ‘heteropoly compounds’ as a general term referring to all heteropoly anions and their derivatives, including the anions themselves, their conjugate heteropoly acids (HPAs) and their heteropoly salts. We will particularly focus on the use of Keggin-type heteropoly compounds with the general structural formula [XM₁₂O₄₀]ⁿ⁻, as these will be used as precursors to the active catalysts used in our reactions. The polyoxometalate or heteropoly anion form will be abbreviated to ‘XM’,

the heteropoly acid will be abbreviated to ‘HXM’ and the heteropoly salts will be abbreviated to ‘Y-XM’ for brevity, where X = heteroatom, M = addendum atom and Y = the salt counter cation.

1.2.4 Heteropolyoxometalates

Heteropoly compounds are most notably distinguished from their isopoly counterparts by the presence of a heteroatom situated in well-defined sites at the centre of the polyanions.¹¹⁵ These compounds are of particular interest in catalysis: an area in which heteropoly acids (HPAs) in particular have attracted much attention over the last three decades due to their strong Brønstead acidity, ability to undergo fast redox transformations under mild conditions, wide range of adjustable acid-base redox properties, good thermal and oxidative stabilities compared with common organometallic complexes, good solubility in polar solvents, and *pseudo*-liquid phase behaviour.¹¹⁶ Indeed, these attributes have seen applications of heteropoly compounds in various areas of catalysis from acid to oxidation catalysis in a plethora of different homogeneous and heterogeneous systems.¹¹⁸ The properties of a given heteropoly compound originate from both the molecular and electronic structures provided by the bonding between its constituent hetero atom, addendum and counter cation.

1.2.5 Structure

1.2.5.1 Structural Hierarchy of Polyoxometalates

Apart from being relatively complex structures themselves, POM particles (individual POM molecules) are also part of a structural hierarchy in which they can be considered a single repeating unit within much larger structural frameworks. This hierarchy (Fig 1.3) was proposed

by Misono et al. to highlight the structural diversity of solid heteropoly compounds,¹¹⁸ and consists of a 3-tiered system of primary (individual particles), secondary (crystal structure and packing) and tertiary (textural properties) structures to describe the solid and its properties.

In the hierarchy, the POM particles are considered the primary structures. In solution, individual POMs can be more easily observed coordinated to solvent molecules or in their acid form. These “primary structures” can adopt many different configurations which can be identified starting from 3 highly symmetrical “parent structures” with tetrahedral and octahedral central polyhedra – the Keggin¹¹⁹ and Wells-Dawson,¹²⁰ and Anderson-Evans¹²¹ structures, respectively – and any other POM structures are considered as their derivatives.¹²² The stability of these structures in aqueous solution relies heavily on the pH; acidic solutions (pH > 2) are required to prevent them from degrading *via* hydrolysis. Though the chemistry of the Wells-Dawson and Anderson-Evans structures is fascinating and has been well researched,^{120,121,123,124} these POMs were not used in this work and, as such, will not be discussed in depth.

In the solid state, heteropoly acids form ionic crystalline structures using linkers such as hydrated protons (H_5O_2^+). The complex formed between the linkers and the POMs comprise the “secondary structure” of the hierarchy. The 3-dimensional structures created by the POMs and the linkers, as they are assembled, are the “tertiary structures”; the size of the primary ions and secondary complexes, the structure of the pores and the distribution of protons and cations are all elements of the tertiary structure.

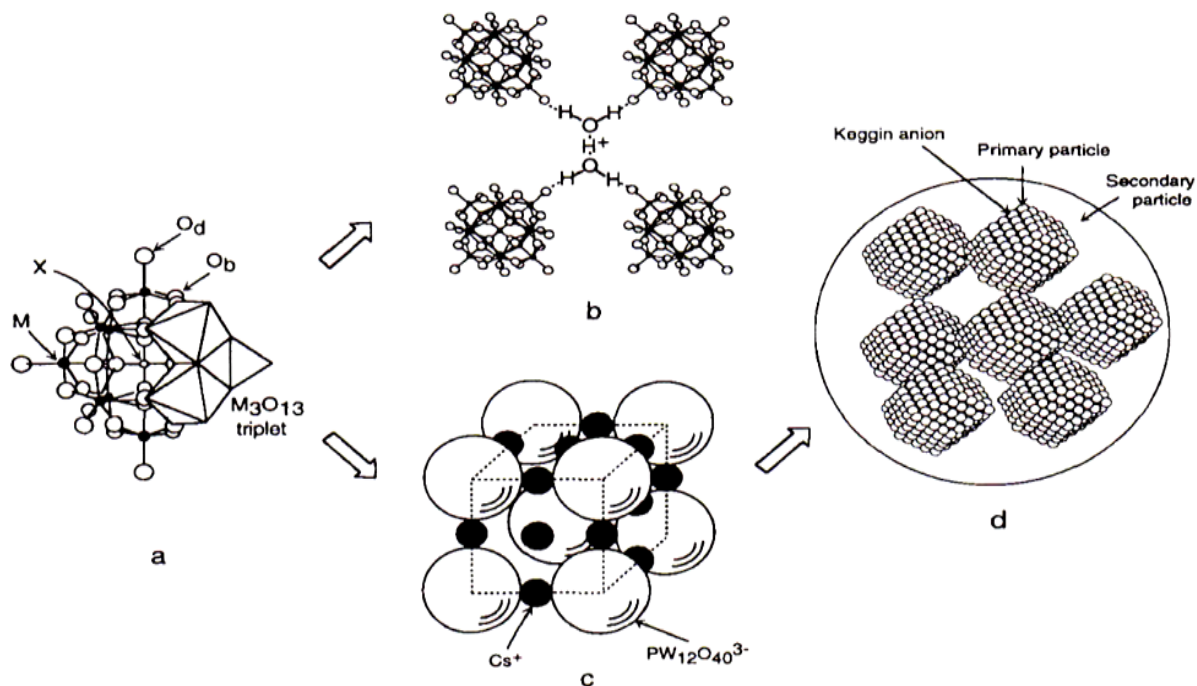


Fig. 1.3. Primary, secondary, and tertiary structures of heteropoly compounds: (a) primary structure (Keggin structure, $\text{XM}_{12}\text{O}_{40}$); (b) secondary structure ($\text{H}_3\text{PW}_{12}\text{O}_{40}\cdot 6\text{H}_2\text{O}$); (c) secondary structure ($\text{Cs}_3\text{PW}_{12}\text{O}_{40}$ unit cell); (d) tertiary structure of bulk $\text{Cs}_{2.5}\text{H}_{0.5}\text{PW}_{12}\text{O}_{40}$.¹¹⁸

1.2.5.2 The Keggin Structure

The most comprehensively researched of the polyoxometalate structures, by far, is the 12:1 Keggin structure (Fig 1.4).^{119,125-127} Among a wide variety of heteropoly compounds, Keggin POMs are the most stable, the easiest to synthesize and the most commercially available. These compounds, together with their derivatives, are the most important for catalysis.

Keggin heteropoly acids have a diameter of ca. 1.2 nm and consist of 12 edge and corner O-sharing MO_6 octahedra (most commonly $\text{M} = \text{Mo}^{\text{VI}}$, W^{VI} or V^{V}) which are arranged into a spherical structured framework encapsulating a central, charged tetrahedron ($[\text{XO}_4]^{n-}$, typically $\text{X} = \text{P}^{\text{V}}$, Si^{VI} , Al^{III} etc.). The structure contains a total of 40 oxygen atoms: four M_3O_{13} groups made up of twelve internally bridging M-O-M bonds, twelve edge-bridging angular M-O-M

bonds between the octahedra, and twelve terminal M=O bonds and four X-O-M bonds which comprise the tetrahedral centre. The most frequently used addenda atoms are Mo^{VI} and W^{VI} due to their favourable ionic radius and charge combinations which improves accessibility of the empty metal d-orbitals to the filled oxygen 2p orbitals for oxygen-metal π -bonding.

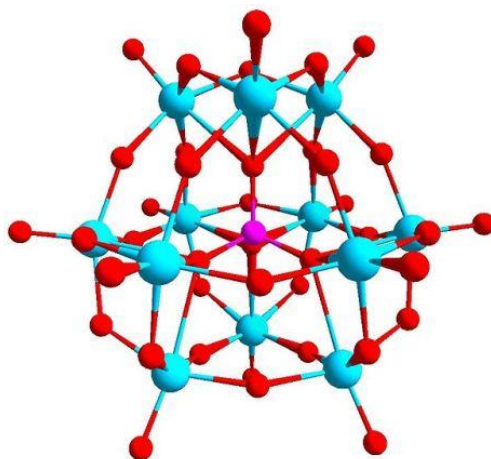


Fig. 1.4. Keggin structure: The heteroatom (purple) can be seen in the centre of the tetrahedron, formed between itself and 4 surrounding oxygen atoms (red). The addenda atoms are depicted in blue.¹²⁸

Each of the M₃O₁₃ groups can be rotated about its 3-fold axis which leads to geometrical isomers, of which there are a total of 5: α , β , γ , δ and ϵ . The most common isomer is α and rotation of one of its M₃O₁₃ groups by 60° produces the β isomer, rotation of two gives the γ isomer and rotation of 3 and 4 groups gives the δ and ϵ isomers, respectively (Fig. 1.5).

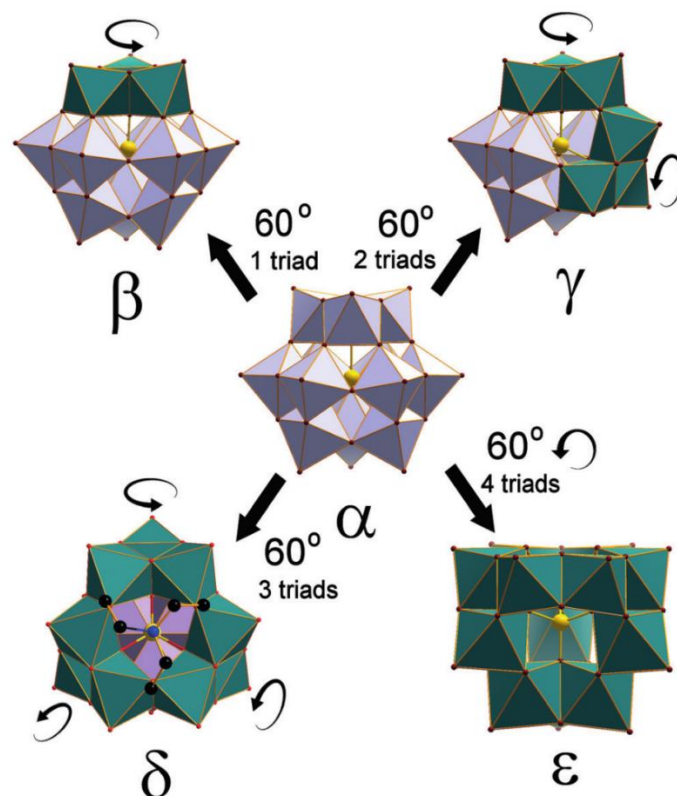


Fig. 1.5. Geometrical isomers of Keggin-type polyoxometalates. The α isomer is shown in the centre. Rotation of one or more of the M_3O_{13} groups in the α isomer by 60° produces the β , γ , δ and ϵ isomers.¹²⁹

1.2.5.3 Lacunary Keggin Anions

Lacunary or defective derivatives of the Keggin POM are produced by the removal of one or more addendum atoms.¹¹⁵ This produces vacancies in the Keggin structure which have been used as binding sites and/or active sites in many reactions, including oxidation reactions.^{130,131}

Fig. 1.6 illustrates examples of a monovacant $[XM_{11}O_{39}]^{n-}$ and a trivacant $[XM_9O_{34}]^{n-}$ species in which a Keggin compound has lost one and three MO_6 octahedra, respectively. The formation of lacunary species often depends on pH in solution and, as such, this subject will be discussed further in section 1.2.7.3.

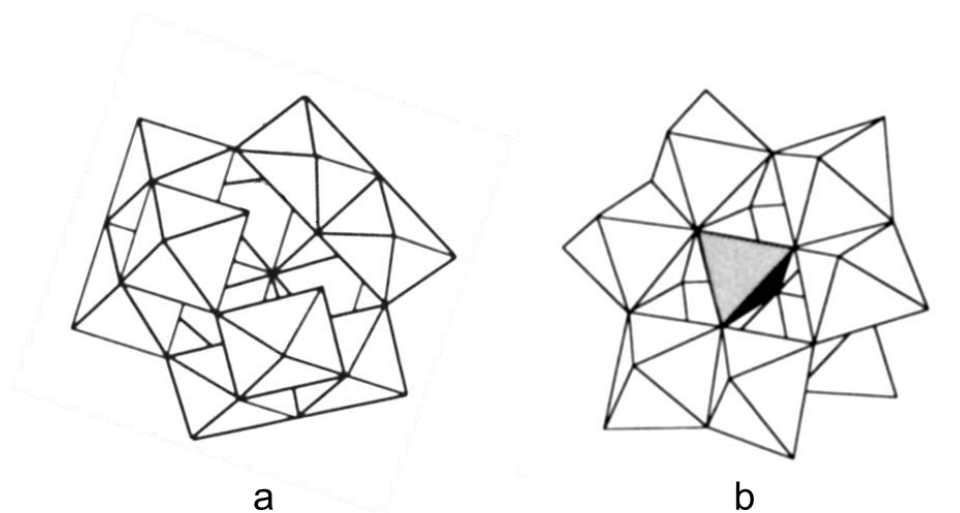


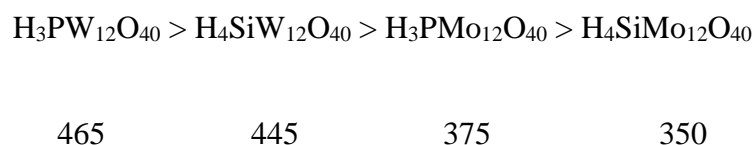
Fig. 1.6. Monovacant (a) and trivacant (b) lacunary POM species.^{115,118} The central XO_4 tetrahedron is not shown in the monovacant structure.

1.2.6 Thermal Stability of Solid Compounds

Heteropoly compounds are thermally robust and are solids at room temperature. The thermal stability of these compounds is measured by methods such as thermal gravimetric analysis (TGA), differential thermal analysis (TG-DTA), differential scanning calorimetry (DSC) and X-ray diffraction (XRD). Simple solubility tests have also been successfully used to test the thermal stability of heteropoly compounds in which the compound is first heated to a desired temperature and then water is added; if the sample solubilises then the structure is deemed to have remained intact, otherwise decomposition has taken place.¹³² In general, the Keggin-type heteropoly compounds are the most stable of the various types of polyoxometalates. Moderately high temperatures are often required for the onset of thermal decomposition.¹¹⁶

The thermal decomposition of POMs often occurs through a complex multi-stage process. For heteropoly acid hydrate $\text{H}_3\text{PW}_{12}\text{O}_{40} \cdot x\text{H}_2\text{O}$, physisorbed water is lost at temperatures just below 100 °C, water hydrogen bonded to hydrated acidic protons is lost

between 100-280 °C, and the loss of the acidic protons and the onset of thermal decomposition of the Keggin structure occurs in the range of 370-600 °C.¹¹⁶⁻¹¹⁸ The same observations were made for the thermal degradation of H₃PMo₁₂O₄₀ at similar temperatures, indicating that the loss of the acidic protons is required before the Keggin structure is sufficiently destabilised to thermally decompose.¹³³ The decomposition temperature (°C) for the most typical Keggin heteropoly acids, as estimated from TGA, decreases in the following series:¹³⁴



1.2.7 Properties of POMs in Solution

1.2.7.1 Solubility

The lattice energies of heteropoly compounds and solvation energies of heteropoly anions are low. Heteropoly acids are highly soluble in water and small chain oxygen-containing organic solvents, such as lower alcohols and ethers, but are highly insoluble in nonpolar solvents such as alkanes. Salts with small cations such as Na⁺ and Li⁺ are also readily soluble in aqueous media in contrast to salts with larger cations, such as K⁺ and NH₄⁺, which are not soluble in water. Salts of large organic cations such as quaternary ammonium salts are soluble in nonpolar organic solvents but insoluble in water which is useful in applications such as biphasic catalysis and the extraction and/or isolation of POMs.^{118,135}

1.2.7.2 Acidity in Solution

Heteropoly acids of the Keggin type are usually strong Brønsted acids which, when dissolved in an aqueous solution, completely dissociate into their constituent protons and heteropoly anions. Heteropoly acids are much stronger than mineral acids such as H_2SO_4 , HNO_3 , HCl etc. This can be rationalized by the large size of the heteropoly anions and delocalization of the electronegative charge through its greater structure, which leads to weaker electrostatic interactions with its acidic protons making them easier to lose. By comparison, the much smaller anions created by the dissociation of mineral acids have much smaller structures with much more localized and less disperse anionic charges, which creates stronger electrostatic interactions with protons and thus more effectively binds them. A comparison of the acid strengths of heteropoly acids gives the order:¹³⁶



The acid strength is diminished when W^{VI} is replaced with Mo^{VI} and V^{V} or when the heteroatom P^{V} is replaced with Si^{IV} . Misono et al. demonstrated the effect of heteroatom on the acidity by measuring the Hammett acidity as a function of the heteropolyanion charge for different heteropoly acids in acetonitrile (Fig 1.7).¹³⁷ Typically, as the charge on the heteropoly anion decreases and the valence of the heteroatom increases, electrostatic interactions with acidic protons decrease and so the acidity of the heteropoly acid increases in response.

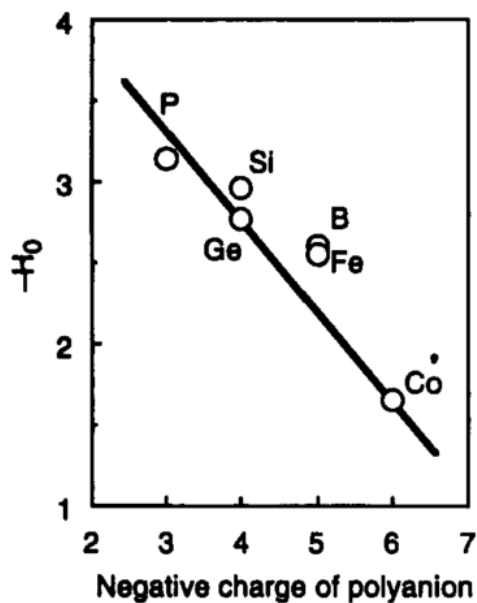


Fig. 1.7. Hammett acidity function (H_0) of $H_nXW_{12}O_{40}$ as a function of the charge of the polyanion.¹³⁷

1.2.7.3 Stability in Solution

Keggin heteropoly acids - and some Keggin salts - are highly soluble in polar solvents and usually fully dissociate in aqueous solution, making them strongly acidic. The near-spherical POMs that are formed are weakly solvated due to the low charge density on the external bridging and terminal oxygen atoms, which form only weak hydrogen bonding interactions with the solvating water molecules. This is evidenced by hydrodynamic radii measurements, which often correspond with the crystallographic radii for a given heteropoly acid.¹³⁸

The structure and stability of solvated POMs is dependent on the pH of the solution. Fig. 1.8 shows the effect of pH on the stability of some common Keggin type POMs. In acidic media ($pH \leq 1.5$) all POMs are present in their Keggin heteropoly anion form $[XM_{12}O_{40}]^{n-}$. As the pH is increased the POMs start to degrade and addenda atoms are lost to form lacunary species.

The initial degradation is, therefore, dependent on addendum atom type and stability decreases in the order of:

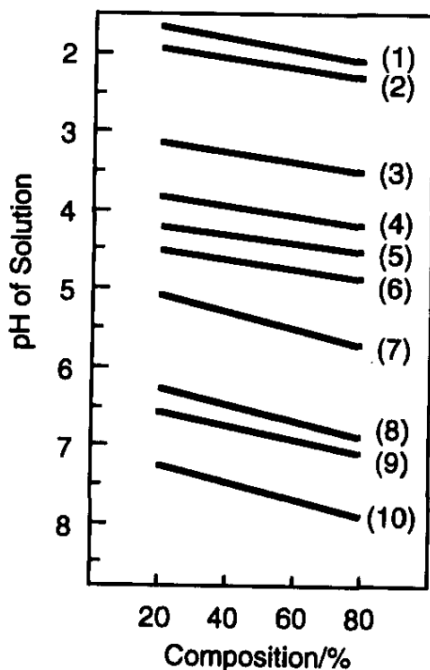
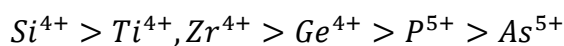


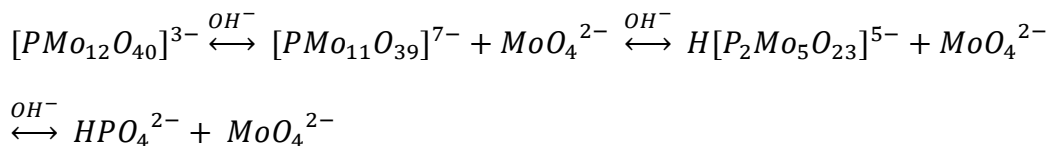
Fig. 1.8. pH range of existence of heteropoly acids:¹³⁹ (1) $PMo_{12}O_{40}^{3-}$, (2) $PW_{12}O_{40}^{3-}$, (3) $GeMo_{12}O_{40}^{4-}$, (4) $GeW_{12}O_{40}^{4-}$, (5) $P_2W_{18}O_{62}^{6-}$, (6) $SiW_{12}O_{40}^{4-}$, (7) $PMo_{11}O_{39}^{7-}$, (8) $P_2Mo_5O_{23}^{6-}$, (9) $H_2W_{12}O_{40}^{6-}$, (10) $PW_{11}O_{39}^{7-}$.¹¹⁸

The heteroatom is also influential on the stability of the POM; for instance, the stability of Mo^{VI} heteropoly anions decreases with respect to the heteroatom of the order:



The choice of addenda and heteroatoms consequently affects the state of the POM at a given pH. Petterson et al. demonstrated that a variety of POM species can be formed by a solution of 1:12 HPO_4^{2-} and MoO_4^{2-} at different pH values.¹⁴⁰ The Keggin $[PMo_{12}O_{40}]^{3-}$ exists in solution at $pH \leq 1.5$, but as the pH increases it experiences alkaline hydrolysis. At higher concentrations

($\sim 10^{-1}$ M) hydrolysis occurs *via* the formation of a dimeric $[P_2Mo_{18}O_{62}]^{6-}$ intermediate. In more dilute ($< 10^{-3}$ M) solutions the process occurs through a $[PMo_{11}O_{39}]^{7-}$ intermediate as outlined in the following scheme:¹³⁵



Zhu et al. studied the decomposition behaviour of $[PW_{12}O_{40}]^{3-}$ in aqueous solution with respect to pH and identified the main species present at various pH values.¹⁴¹ The results are outlined in Table 1.2. Decomposition of $[PW_{12}O_{40}]^{3-}$ was reduced in the presence of acetone or ethanol at pH less than 8.

Table 1.2. Main species identified at various pH values in decomposition studies of $[PW_{12}O_{40}]^{3-}$ in aqueous solution.¹⁴¹

pH	Main components
1.0	$[PW_{12}O_{40}]^{3-}$
2.2	$[PW_{12}O_{40}]^{3-}$, $[P_2W_{21}O_{71}]^{6-}$, $[PW_{11}O_{39}]^{7-}$
3.5	$[PW_{12}O_{40}]^{3-}$, $[P_2W_{21}O_{71}]^{6-}$, $[PW_{11}O_{39}]^{7-}$, $[P_2W_{18}O_{62}]^{6-}$, $[P_2W_{19}O_{67}]^{10-}$
5.4	$[P_2W_{21}O_{71}]^{6-}$, $[PW_{11}O_{39}]^{7-}$, $[P_2W_{18}O_{62}]^{6-}$
7.3	$[PW_9O_{34}]^{9-}$
8.3	PO_4^{3-} , WO_4^{2-}

The degradation of most POM species occurs within a small pH range, from the formation of the first lacunary species through to complete decomposition to their constituent addenda and hetero atoms. Within this range, many complex equilibria involving the formation and degradation of numerous degraded POM species are established. It is well known that

equilibria are slow in tungstate systems and rapid in molybdate systems.^{115,142} In liquid phase catalysis by polyoxometalates (particularly oxidation reactions), unless the system requires a very particular structure of POM, and thereby precise buffering of the pH, it is often the case that there are numerous degraded POM species present and many of these may be involved in the catalysis.¹¹⁶

1.2.8 Use in Catalysis

The first attempts at using POMs for catalysis date back to the early twentieth century. Since then, catalysis by heteropoly compounds has been at the forefront of fundamental and applied catalysis. The success of heteropoly compounds in the field of catalysis is due to their unique physiochemical properties, most importantly their multifunctionality and their structural mobility.¹³⁵ They are strong Brønsted acids and can undergo reversible redox transformations under mild conditions. These properties can be tuned by careful selection of the structural components (i.e. addenda, heteroatom, counter cations etc.) which comprise their discrete ionic structures. The structures are frequently maintained upon cation substitution or reduction/oxidation which leads to high proton mobility and a ‘pseudo-liquid’ phase – in which the diffusion of the reactant through the solid lattice is faster than the reaction, allowing reactant molecules in the gas or liquid phase to penetrate in between the polyanions (primary structure) and react inside the bulk solid. Consequently, POMs/HPAs are often used in acid catalysis and selective oxidation reactions.^{118,143-145} These reactions can be performed homogeneously in liquid systems or heterogeneously in solid-liquid, solid-gas or even liquid-liquid systems due to the high solubility of most POMs in polar solvents and their high thermal stability in the solid state. Systematic mechanistic studies of heteropoly compounds on the molecular level have resulted in the application of these catalysts in many large-scale industrial processes for the synthesis of organic compounds. Examples of these reactions are listed in Table 1.3.

Table 1.3. Industrial processes catalysed by heteropoly acids.¹⁴⁶

Reaction	Catalyst	Type ^a	Year Production Started
$\text{CH}_2=\text{C}(\text{CH}_3)\text{CHO} + \text{O}_2 \rightarrow \text{CH}_2=\text{C}(\text{CH}_3)\text{COOH}$	Mo-V-P-HPA	Het	1982
$\text{CH}_2=\text{CH}_2 + \text{O}_2 \rightarrow \text{CH}_3\text{COOH}$	Pd-H ₄ SiW ₁₂ O ₄₀ /SiO ₂	Het	1997
$\text{CH}_2=\text{CHCH}_3 + \text{H}_2\text{O} \rightarrow \text{CH}_3\text{CH}(\text{OH})\text{CH}_3$	H ₄ SiW ₁₂ O ₄₀	Hom	1972
$\text{CH}_2=\text{C}(\text{CH}_3)_2 + \text{H}_2\text{O} \rightarrow (\text{CH}_3)_3\text{COH}$	H ₃ PMo ₁₂ O ₄₀	Hom	1984
$\text{CH}_3\text{CH}=\text{CHCH}_3 + \text{H}_2\text{O} \rightarrow$ $\text{CH}_3\text{CH}(\text{OH})\text{CH}_2\text{CH}_3$	H ₃ PMo ₁₂ O ₄₀	Hom	1989
$n\text{THF} + \text{H}_2\text{O} \rightarrow \text{HO}-[-(\text{CH}_2)_4\text{-O-}]_n\text{-H}$	H ₃ PW ₁₂ O ₄₀	Bip	1985
$\text{CH}_2=\text{CH}_2 + \text{CH}_3\text{COOH} \rightarrow \text{CH}_3\text{CH}_2\text{OOCCH}_3$	H ₄ SiW ₁₂ O ₄₀ /SiO ₂	Het	2001

a) Hom = homogeneous, Het = heterogeneous, and Bip = biphasic.

In this work, aqueous biphasic systems were used to carry out oxidation of organic compounds in the presence of both homogeneous and heterogeneous POM derivative catalysts. For this reason, only POM catalysed oxidation reactions will be discussed further in this section and in later chapters. Many reviews on catalysis by polyoxometalates have been published, however, which summarise the findings of all areas of POM catalysis since its inception. These include: acid and oxidation catalysis by POMs in liquid phase reactions;^{114,136, 147-149} POMs as catalysts for fine chemical synthesis;^{116,150} heterogeneous acid and oxidation catalysis by POMs;^{118,149,151-155} industrial applications of POMs;²¹ light alkane functionalization by POM catalysis;¹⁵⁶ photocatalysis by POMs;^{149,157} transition metal-substituted POMs for liquid-phase oxidation;¹⁴⁹ the use of POMs for studies of catalyst active sites;¹⁵⁸ HPAs as ‘green’ catalysts;¹⁵⁹ POM-based phase-transfer catalysis for organic reactions;¹⁶⁰ POM-based heterogeneous catalysts for liquid-phase organic transformations;¹⁵⁰ and general overviews of POM catalysis.^{118,161}

1.2.8.1 Polyoxometalates as Catalysts for Selective Oxidation in Liquid-Phase Reactions

Selective oxidation of organic compounds catalysed in homogeneous and heterogeneous systems by heteropoly compounds has garnered much interest over the last 50 years.^{143,145,162-165} Reactions are most frequently carried out in homogeneous liquid-phase or liquid-liquid biphasic systems - although heterogeneous liquid-solid systems are known¹⁶⁵ - and can occur *via* two processes: the removal of hydrogen from the target substrate (oxidative dehydrogenation) or by catalytic oxo-transfer oxidation (oxygenation). These processes can be summarised by Eq. 1.1 and Eq. 1.2 respectively:¹⁶⁶





Where: Sub = substrate; OX = oxidant; RED = reduced form of oxidant; and OD = oxygen donor.

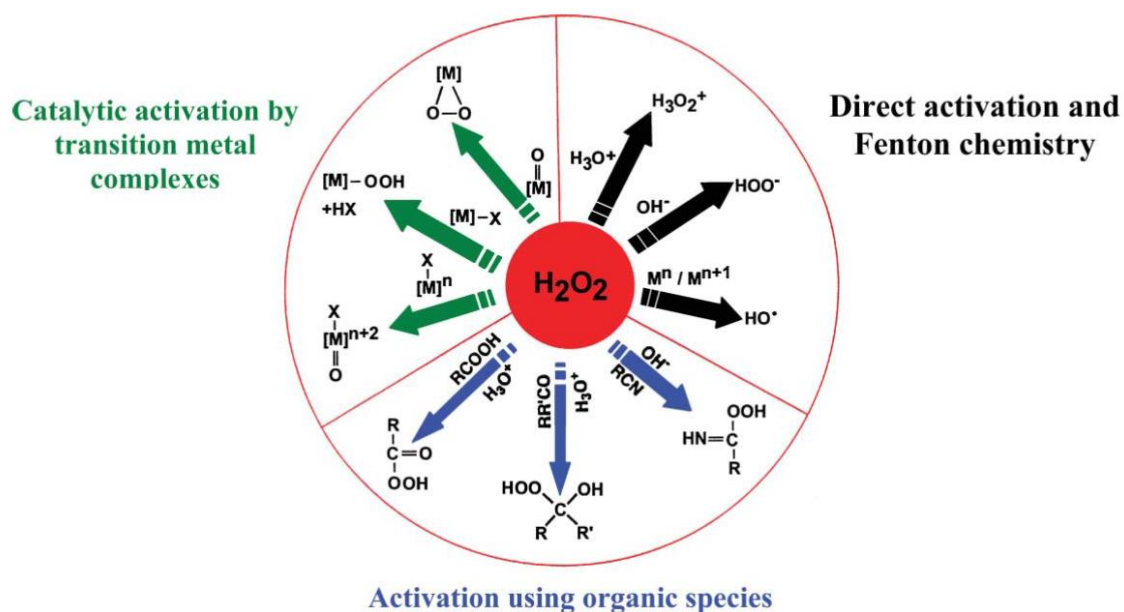
A variety of different oxidants have been investigated for use in metal-catalysed processes, many of which operate as oxygen donors. The most attractive oxidants generally have a high percentage of active oxygen, a high selectivity towards the formation of active species or products, are cheap to purchase and have few associated environmental issues. Amongst the most desirable oxidants which best suit these criteria are O₂ and H₂O₂; however, the oxidation chemistry of these compounds is often complex and difficult to control with regards to metal-catalysed oxidation processes (see Hill¹⁶⁶ for a complete description). Indeed, many of these reactions can suffer loss in catalytic activity due to either reversible and/or irreversible μ-oxo dimer formation, or the oxidative degradation of organic ligands (commonly porphyrins or other macrocycles) which are often required to drive stereochemistry and/or solubilise and stabilize the metal catalyst in the reaction medium. Polyoxometalates are viewed as a viable substitute for metallo-macrocyclic catalysts in these reactions due to their superior thermal stability and resistance to oxidative degradation.¹¹⁶ However, the solvolytic stability of polyoxometalates in liquid-phase reactions can be a problem for some reactions and beneficial for others. As discussed in Section 1.2.7.3, polyoxometalates in solution can decompose to form a variety of lacunary polyanions and mononuclear metallospecies that exist in a series of pH-dependent equilibria. In reactions that use H₂O₂ as an oxidant, these lacunary species can interact with the H₂O₂ to form peroxo polyoxometalate (or peroxo POM for convenience) species which are catalytically active in selective oxidation reactions.^{162,167}

1.3 Selective Oxidation Reactions with Hydrogen Peroxide

Oxidation is an important technology for converting organic and inorganic materials into useful chemicals with a higher oxidation state. A compound reaches a higher oxidation state through the loss of electrons and/or through the addition of oxygen atoms. Examples of oxidation can be found in everyday processes around us such as respiration (oxidation of haemoglobin), the rusting of metal (production of iron oxide from the reaction of iron with oxygen from the air) and the browning of fruit (production of melanins from the oxidation of natural phenols catalysed by enzymes).

In industry, oxidation reactions are used for a variety of applications including the manufacture of chemicals, materials, fuels, and the production of key intermediates in the synthesis of drugs. The oxidation reactions carried out in these processes are selective oxidations as they target specific reactant(s) to produce specific product(s).¹⁶⁸⁻¹⁷⁰

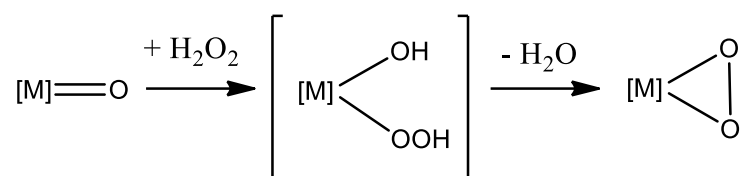
Selective oxidation of compounds requires the use of an oxidizing reagent. Hydrogen peroxide is an attractive agent for liquid-phase oxidations.^{171,172} It is relatively cheap to purchase, it has an atom efficiency of 47% in oxidation reactions, and its only by-product is water.¹⁷³ It has been demonstrated as an effective oxidising reagent in a number of reactions including:¹⁷⁴ oxidation of alcohols;¹⁷⁵ oxidation of aldehydes to carboxylic acids;¹⁷⁶ epoxidation of olefins;¹⁶⁴ and oxidation of sulfides and sulfoxides (used in oxidative desulfurization processes).¹⁷⁷ However, the peroxygen atom of H₂O₂ cannot be transferred to a target reactant unless it is activated in a peracid, a dioxirane or a transition metal complex (Scheme. 1.4).^{38,178}



Scheme 1.4. Routes for activation of hydrogen peroxide.³⁸

Organic and inorganic peroxides and peroxyacids are amongst some of the most commonly used oxidizing reagents for oxidative transformations.^{179–182} The peroxides/peracids are prepared from the reaction of the corresponding organic acids or acid anhydrides,¹⁸³ or inorganic persalts of alkali metals (M_2O_2) with hydrogen peroxide.¹⁸⁴ However, these can be hazardous to handle and produce stoichiometric amounts of acid waste which are both economically and environmentally unfriendly.^{184–188}

An alternative method of activation is to use transition metals as catalysts/activators. Activation of the hydrogen peroxide by Fenton chemistry (Fe^{II} catalyst) produces oxygen radical species which can carry out a range of homogeneous and biphasic oxidation reactions.^{189,190} Other transition metal species react with H_2O_2 to form active peroxometalate complexes. Scheme 1.5 gives the synthesis route for the formation of peroxo complexes from the reaction of d^0 transition metal oxo complexes with hydrogen peroxide.

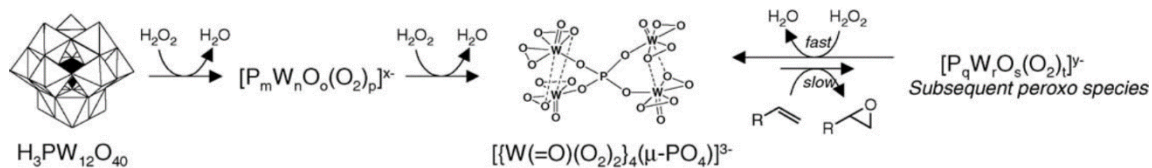


Scheme 1.5. Synthesis of peroxo complexes from the reaction of d^0 transition metal oxo complexes with hydrogen peroxide.³⁸

Vanadium, tungsten, molybdenum and rhenium oxo species react well with hydrogen peroxide and their resulting peroxo species are particularly active oxidising agents for a number of organic transformations. Their easy and stable interconversion (redox) between oxo and peroxo species enables them to establish catalytic systems.³⁸

The addition of different XO^n ligands ($X = Se^{VI}, S^{VI}, As^V, P^V, Si^{IV}$ etc.) can influence oxygen transfer activity of the peroxometalate species in epoxidation and sulfoxidation reactions by mediation of the Lewis acidity of these groups through choice of the heteroatom.^{191,192} Through use of these ligands, Venturello complexes (e.g. $[\{W(=O)(O_2)_2\}_4(\mu-PO_4)]^{3-}$) can be formed which are particularly effective catalysts in these reactions.^{167,193–196} Indeed, it is generally accepted that Venturello complexes are the main active catalyst species in biphasic oxidation reactions with hydrogen peroxide in which heteropolyoxometalates are used as an active catalyst precursor.^{143,164} The operation of these species is outlined in Scheme 1.6.

Reactions in these systems are typically biphasic, with the target olefin in the organic phase and the catalyst and H_2O_2 reagent in the aqueous phase. Most often, the phase boundary effect is overcome through the use of a phase-transfer catalyst,³⁷ which is typically a quaternary ammonium cation.^{164,193,196–202} The mechanism for the operation of polyoxometalate-catalysed phase-transfer oxidation with H_2O_2 is called the Venturello-Ishii system.



Scheme 1.6. Schematic representation for the formation of peroxometalate species (Venturello complex, $[\{W(=O)(O_2)_2\}_4(\mu-PO_4)]^{3-}$) from POM precursor ($H_3PW_{12}O_{40}$) and their subsequent catalytic activity in oxidation reactions with H_2O_2 .¹⁶⁴

1.3.1 The Venturello-Ishii System for the Phase-Transfer Oxidation of Substrates Catalysed by Peroxo Polyoxometalates

Much work has been done in the area of H_2O_2 oxidation catalysed by heteropoly compounds.^{143,160,161,164,165} Keggin-type tungsten and molybdenum polyoxometalates in particular have proven to be effective in catalysis for the oxidation of various organic compounds by H_2O_2 such as olefin epoxidation, oxidation of thiophenes, alcohols, phenols, glycols etc. which are often carried out in homogeneous or liquid-liquid biphasic systems.¹⁴³ In these reactions, the polyoxometalates are not actually the catalyst themselves, but are instead precursors to monomeric, dimeric and tetrameric catalytically active peroxo-POM intermediate species which form as the POMs degrade in the presence of excess H_2O_2 . These peroxo-POM species are believed to be the effective catalysts that are formed in two highly efficient systems for hydroperoxide oxidation that were developed simultaneously but independently by Venturello and Ishii. Venturello *et al.*^{167,194,203} investigated the epoxidation of alkenes in a DCE- H_2O biphasic system with H^+ , WO_4^{2-} and PO_4^{3-} catalyst precursors, 15 % H_2O_2 oxidant at 60 °C in the presence of a quaternary ammonium cation phase-transfer catalyst (PTC). From this system, a peroxo-POM, $\{PO_4[WO(O_2)_2]_4\}^{3-}$ (the ‘‘Venturello complex’’, Fig 1.9), was isolated and characterised.¹⁶⁷ This species showed significant catalytic activity when tested in

the biphasic oxidation of alkenes (epoxidation of 1-octene with 15 % H₂O₂ gave remarkable stereoselective yield of 89 % *cis*-epoxycyclooctane) and was presumed to be the active oxygen mediator in their initial systems.

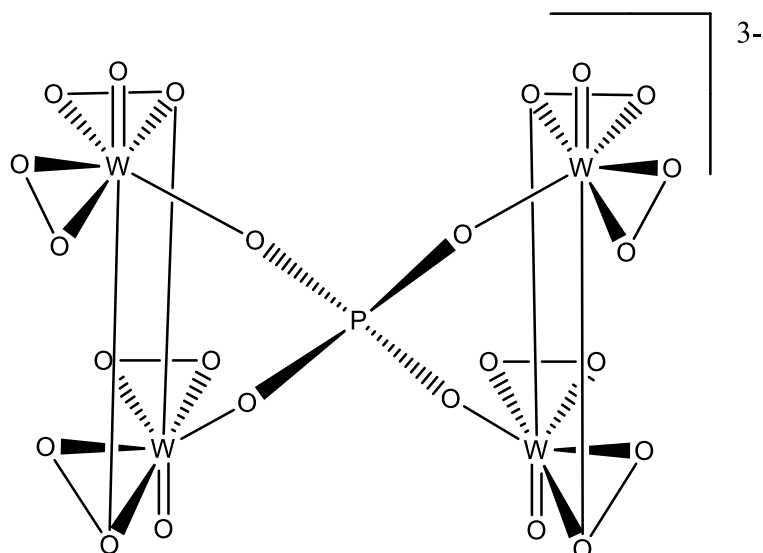
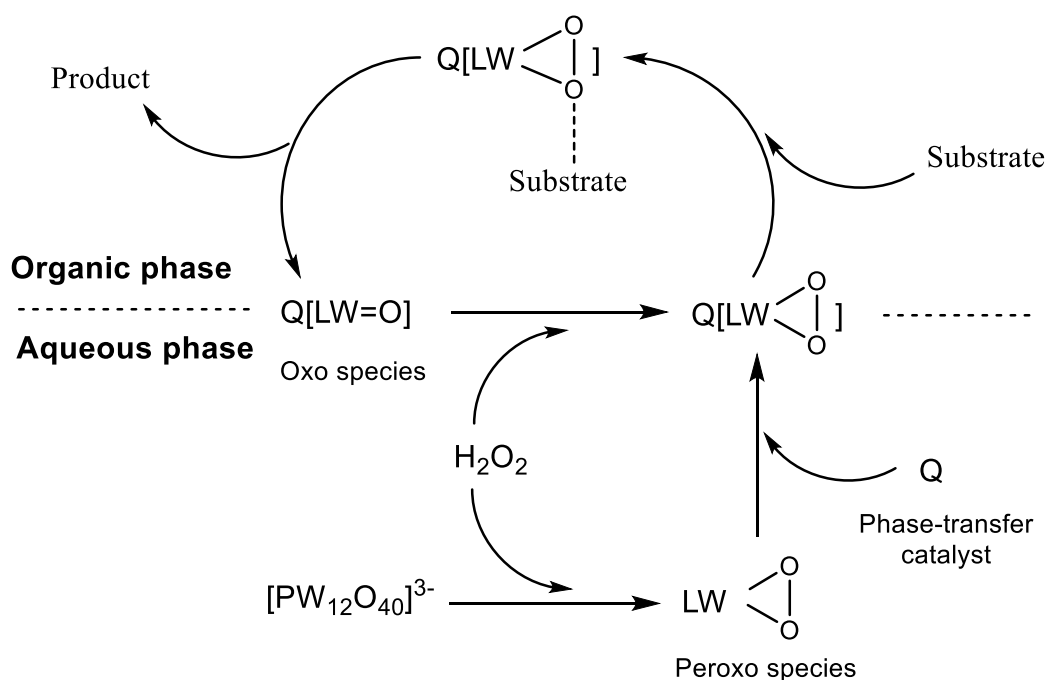


Fig. 1.9. Structure of the Venturello complex, $\{\text{PO}_4[\text{WO}(\text{O}_2)_2]_4\}^{3-}$.¹⁶⁷

Ishii *et al.*^{195,196,204–207} focused on the oxidation of various organic substrates with 35 % H₂O₂ and H₃PW₁₂O₄₀ or H₃PMo₁₂O₄₀ catalyst in CHCl₃-H₂O biphasic systems using cetylpyridinium chloride as a phase-transfer agent. The system was shown to effectively catalyse the epoxidation of relatively electron-poor terminal alkenes¹⁹⁶ and allylic alcohols²⁰⁵ amongst other reactions. Later studies by Brégeault,²⁰⁸ using Venturello's conditions, and Hill,²⁰⁹ using Ishii's conditions, discovered that both systems were in fact effectively identical, with both forming catalytically active $\{\text{PO}_4[\text{WO}(\text{O}_2)_2]_4\}^{3-}$, both required a PTC to operate, and the only difference between the two systems was the choice of catalyst precursors. The Venturello-Ishii system, as it later became known, was developed from the research of both groups and is used to describe the oxidation of organic substrates by H₂O₂ in the presence of a POM catalyst precursor and a PTC, which is typically a quaternary ammonium cation.^{164,193,196–198,199–202} The

schematic mechanism for the system is outlined in Scheme 1.7 and has been adapted from the mechanism first proposed by Ishii *et al.*¹⁹⁶ for more general applications.



Scheme 1.7. Mechanism of alkene epoxidation with H_2O_2 catalysed by POM in a two-phase system.¹⁹⁶

The system is composed of two phases: an organic phase containing the target substrate, and an aqueous phase containing the POM catalyst precursor and H_2O_2 oxidant. In step **1** of the reaction, the polyoxometalate decomposes in the presence of excess H_2O_2 to form a peroxy-POM species which can facilitate transfer of the active oxygen. The PTC then complexes with the active peroxy-POM at the interface and transfers the peroxy-POM into the organic phase (**2**). The active oxygen on the peroxy-POM interacts with the target substrate (**3**) before reacting to give the oxidized product (**4**) and the reduced oxo peroxy-POM species. The oxo peroxy-POM is then regenerated by H_2O_2 at the interface (**5**) ready to react with more substrate. The

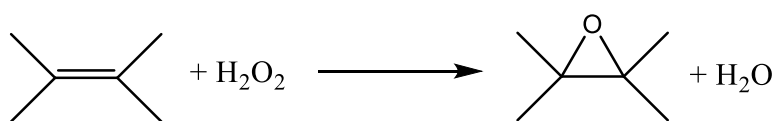
cycle repeats through steps 3-5 until all of the substrate has reacted or until the H₂O₂ has been used up.

The system was used to describe the epoxidation of olefins by H₂O₂ catalysed by peroxo-POMs under phase-transfer conditions.

1.3.2 Epoxidation of Alkenes Using H₂O₂ as an Oxidant

The epoxidation of olefins is an important reaction for both academic and industrial applications. The epoxide products are used as raw materials for epoxy resins, surfactants and paints, and are key intermediates in organic syntheses (i.e. functionalising hydrocarbons and quickly building functionality into molecules, often with good control over selectivity).^{164,210–}

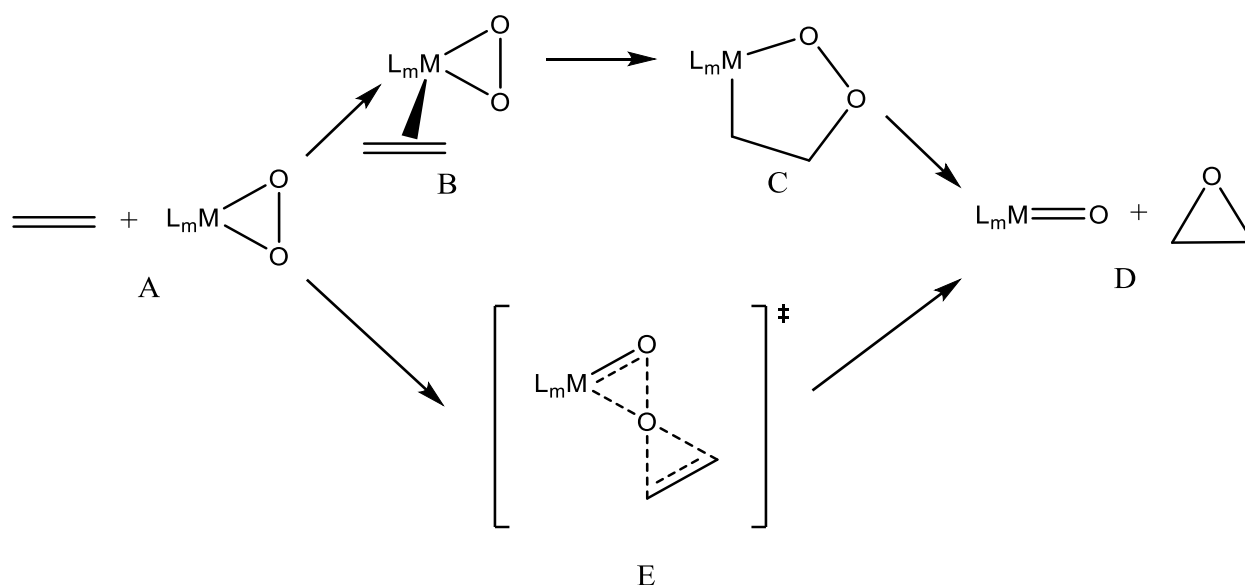
²¹³ Although an extensive number of epoxidation processes are known and have been used for these applications, such as the chlorohydrin process and those using organic peroxides and peracids,^{179,180} they often suffer both economic and environmental disadvantages such as high cost or produce toxic waste by-products. Instead, catalytic epoxidation with H₂O₂ is often researched as a “greener” alternative (Scheme 1.8).^{174,214,215}



Scheme 1.8. Oxidation of an olefin by H₂O₂.

Many different transition-metal compounds have been used as catalysts in both homogeneous and heterogeneous epoxidations with hydrogen peroxide such as metalloporphyrins,^{216, 217} titanosilicates,²¹⁸ methyltrioxorheneum,²¹⁹ tungsten compounds^{194,196} and manganese complexes.²²⁰ Transition metal catalysts typically operate *via* the formation of oxo/peroxo

species in these reactions (Scheme 1.5) and their mechanisms have been well investigated, with particular focus on peroxomolybdate species.^{192,221–227} Two mechanisms have been proposed to explain the reaction between the olefin and metalperoxo species; both are shown in Scheme 1.9. The first mechanism, proposed by Mimoun, is a multistep process which proceeds through species A-D.^{225,226} The first step involves coordination of the olefin to the metal centre to yield intermediate B. In the second step, the olefin is cyclo-inserted into one of the molybdenum-peroxo bonds to give molybdo-2,3-dioxolane, C, and in the final step is the cycloextrusion of the epoxide product which gives the transition metal oxide which then reacts with more H₂O₂ to regenerate the peroxo complex to complete the catalytic cycle.



Scheme 1.9. Schematic representations of the reaction mechanisms suggested by Mimoun^{225,226} (top) and Sharpless²²⁸ (bottom).

The alternative mechanism, proposed by Sharpless,²²⁸ suggests that a transition state, E, is formed through the attack of a peroxo group oxygen atom by the olefin.

Although there have been decades of controversy over which mechanism is correct, computational studies conducted by numerous groups using quantum-chemical calculations have concluded that the Sharpless mechanism is most likely the correct mechanism as this system requires less activation energy than one which follows the Mimoun mechanism.^{192,221,227} Activation and cleavage of the O–O bond in the transition state of the reaction (E) occurs through direct nucleophilic attack of the $\pi(\text{C}=\text{C})$ HOMO of the olefin towards the $\sigma^*(\text{O}=\text{O})$ LUMO of the peroxy group.^{221,227} In addition, it was also suggested that decomposition of the five-membered metallocyclic intermediate (C) in the Mimoun mechanism would not produce an epoxide but instead would lead to the formation of aldehydes or ketones.²²¹

As discussed above, epoxidation with H_2O_2 can be conducted with polyoxometalates using Venturello-Ishii conditions, and these reactions have been reviewed extensively.^{114,161,163,164,229} Reactivity with respect to polyoxometalates generally increases with decreasing stability in aqueous solution and increasing oxidation potential,¹¹⁴ in line with their ease in forming peroxy-POM species in the presence of aqueous H_2O_2 . The PTCs used in these systems are typically quaternary ammonium cations.^{164,193,196-202}

1.3.3 Desulfurization of Diesel Fuels

1.3.3.1 Why is Desulfurization of Diesel Fuels Necessary?

In the modern world, we rely heavily on vehicles driven by combustion of fossil and bio fuels to transport our goods and ourselves. Indeed, many of us travel to our places of work using vehicles such as cars or busses, which, in many cases, require the combustion of diesel oil fuels to operate. These fuels, in their purest forms, are composed of aliphatic and aromatic hydrocarbons which are burned in the presence of oxygen to release energy, CO_2 and H_2O . In

their crude forms, they also contain organosulfur compounds such as thiols, thiophenes and sulfides. If these compounds are not removed from the fuels they can corrode pipelines and engines, deactivate catalysts in vehicles and oil refining processes, and, when combusted, will produce SO_x gases (e.g. SO_2 , sulfates and sulfur trioxide) which are harmful to human health and the environment. For instance, SO_x can dissolve in atmospheric water vapour to produce acid rain (H_2SO_4) which can damage buildings and crops.²³⁰

Strict environmental regulations have been put in place by the world's governing bodies which have seen the sulfur content of diesel fuels used in transportation vehicles decrease dramatically from 2000 to 10 ppm over the last 20 years.²³¹⁻²³³ As stricter environmental legislation develops, the requirement of cleaner diesel fuels will impose heavier restrictions on their sulfur content; not only will the fuels need to become cleaner, but so too must the technology used to produce them.

The most widely used method for removing sulfur from diesel fuels in petroleum refineries is hydrodesulfurization (HDS) which uses hydrogenolysis to cleave C-S bonds to form C-H and S-H bonds. Industrial applications of this process commonly use a fixed-bed reactor operated at high temperatures (300-400 °C) and pressures (30-130 atm) in the presence of a catalyst, typically Co-Mo or Ni-Mo sulfided oxides on an alumina support.²³⁴⁻²³⁸ Sulfur is removed from the fuel as H_2S and converted to elemental sulfur using the Claus process or to sulfuric acid using the contact process.^{234,239,240}

Fig. 1.10 shows the qualitative relationship between the type and size of sulfur molecules in various distillate fuel fractions and their relative reactivities in HDS processes. For disulfides, sulfides, thiols, and tetrahydrothiophene - sulfur compounds without conjugation between the lone pairs on S atom and the π -electrons in an aromatic ring - HDS occurs directly through the hydrogenolysis pathway. These sulfur compounds display much higher HDS reactivity than

that of thiophene because they have higher electron density on the S atom and a weaker C–S bond. The reactivities of the 1- to 3-ring sulfur compounds decrease in the order of thiophenes >benzothiophenes >dibenzothiophenes.^{241–244} Removal of these heavier, aromatic compounds, therefore, requires much more severe reaction conditions,^{245–247} which can reduce catalyst lifetimes, compromise fuel quality by saturation of olefins and loss of octane number, and drive up operating and capital costs.^{248,249} As stricter legislation continues to demand lower sulfur content, the removal of heavier aromatic compounds will become imperative and alternative techniques to HDS will be required for their removal that are more efficient and cost effective. Thus, alternative desulfurization methods have been subject to widespread investigation in recent years with the view to operate these in tandem with HDS, or even replace the process altogether. These include oxidative desulfurization (ODS),^{249–253} extraction,^{254–256} adsorption^{257–259} and bio-desulfurization.^{260–263} Of these processes, ODS appears most promising for deep desulfurization of diesel fuel.

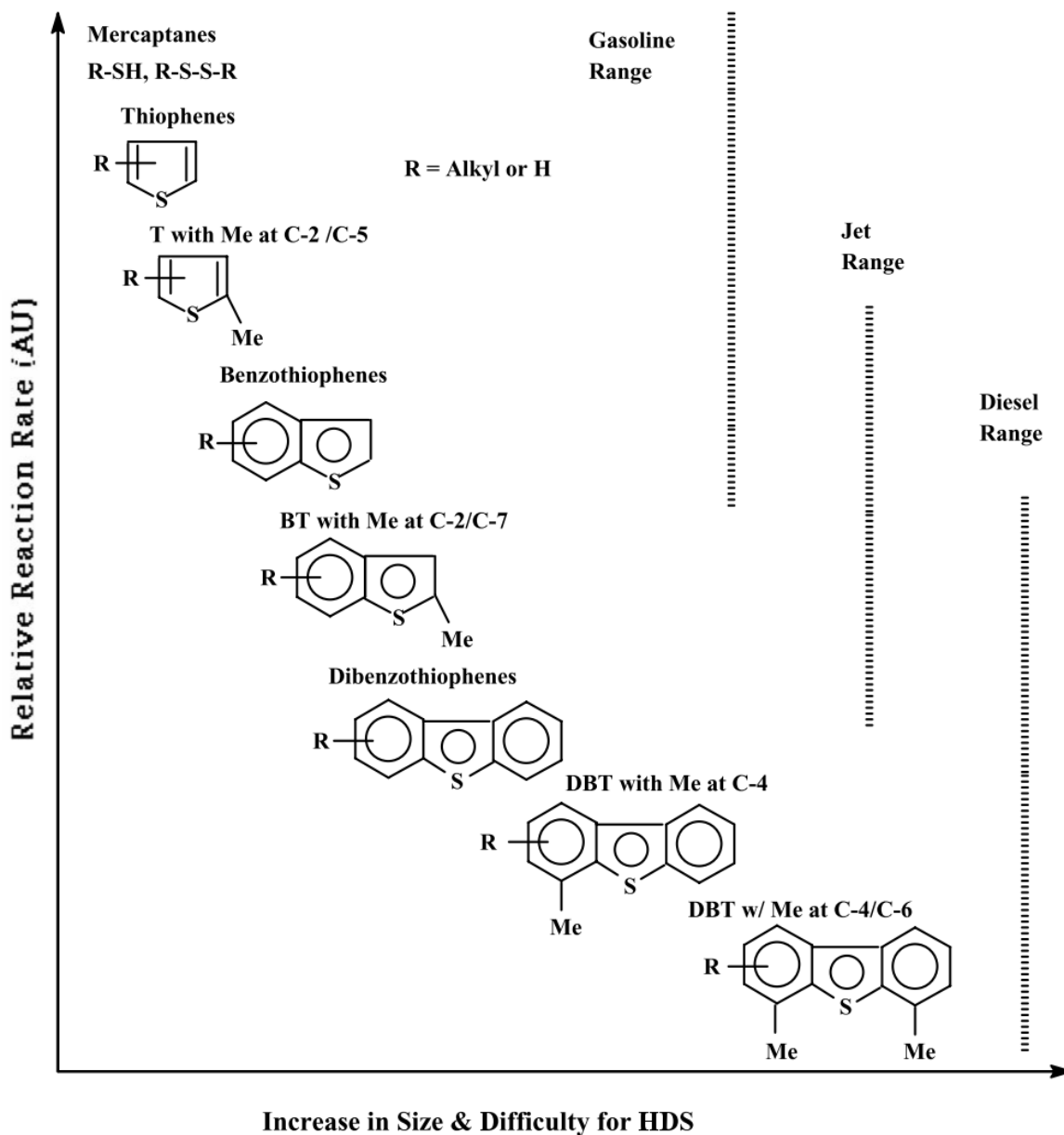
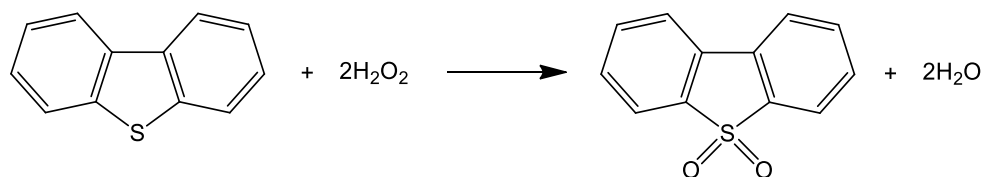


Fig. 1.10. The qualitative relationship between the type and size of sulfur molecules in various distillate fuel fractions and their relative reactivities in HDS processes.²⁴⁴

1.3.3.2 Oxidative Desulfurization

In this technology, oxidising reagents are used at low temperatures (< 80 °C) and atmospheric pressure to add one or two oxygen atoms to the sulfur atoms of heavy sulfur compounds to yield sulfones and sulfoxides, respectively (Scheme 1.10). The oxidized products are more

polar and heavier than their parent compounds and so separation from the fuel can be facilitated through extraction,²⁶⁴ distillation,¹⁸² or adsorption.²⁶⁵ Thus, ODS processes are comprised of two stages: i) oxidation, followed by; ii) separation operations. This method is highly efficient for removing aromatic organosulfur compounds such as thiols and benzothiophenes, which, as previously discussed, are difficult to remove by HDS.^{250,266}



Scheme 1.10. Oxidation of dibenzothiophene to the corresponding sulfone with H_2O_2 .

Many oxidants for ODS have been investigated that include molecular oxygen,²⁶⁷ organic and inorganic peroxy acids,^{181,182} NO_2 ,²⁶⁸ ozone²⁶⁹ etc.²⁷⁰ However, H_2O_2 is the most commonly used oxidant as it is cheap, its only by-product is water and it has a high amount of active oxygen per mass unit.²¹⁵ Various catalytic systems such as HCOOH , CCl_3COOH , polyoxometalates, CF_3COOH , methyl-trioxorhenium(VII), and titanate silicates have been investigated in the oxidation of sulfur compounds with H_2O_2 .^{270–277} Some of the most efficient systems are based on transition metal salts in a high oxidation state with Lewis acidity.^{266,278–282} Under these conditions, reaction times can be cut to under 2 h, though, these times are still considered too long to be integrated into refinery processes.²⁵⁰ Another problem with these systems is that they are biphasic, with the sulfur-containing fuel phase separated from the H_2O_2 -containing aqueous phase. This can help with catalyst-product separation, but without overcoming the phase-barrier problem, the reactions are slow. This problem has often been overcome through the application of phase-transfer catalysts (PTCs) to the system.^{145,199,201,202,283–285} The operational mechanism of these systems is analogous to that of

the Venturello-Ishii system for olefin epoxidation (see Section 1.3.1): The transition metal catalyst precursors react with hydrogen peroxide in the aqueous layer to form the catalytically active peroxo species which then complexes with the PTC. The PTC then facilitates phase migration of the active peroxo species for the reaction to take place. Polyoxometalates are often used in these systems as a precursor for active transition metal catalyst species,^{167,285} and quaternary ammonium cations are most commonly used as PTC.^{199–202} However, these systems can sometimes suffer from poor catalyst separation from the fuel layer once the reaction has reached completion. Many research groups have resolved this problem by heterogenizing the catalyst on solid supports such as silica and alumina, though, this can result in lower yields or slower reaction times.^{145,285–289}

1.4 Phosphazenes

1.4.1 Scope

In this work, organoaminocyclotriphosphazenes have been applied as phase-transfer moieties for a variety of active POM-based catalysts for use in biphasic oxidations with hydrogen peroxide. This section will introduce phosphazenes primarily focussing on the synthesis, structures, properties and applications of cyclotriphosphazenes to justify their suitability as PTC moieties, in particular, those with organoamino substituent groups. Discussion of other classifications of phosphazenes will be added to provide a broader scope where needed.

1.4.2 Introduction

Phosphazenes (phosponitriles) are a class of formally unsaturated inorganic-organic materials with distinctive $-P=N$ structural units (PN units). The phosphorus atoms in these units are

pentavalent and the nitrogen atoms are trivalent which enables bonding between these units or other molecules to create phosphazene compounds. These compounds can be classified into categories such as monomeric ($R_3P=NR'$), dimeric, polymeric $(NPR_2)_n$, and cyclic $(NPR_2)_n$ phosphazenes. The simplest phosphazenes, monophosphazenes (phosphoranimines) and diphosphazenes, consist of only one or two PN units, respectively. Polyphosphazenes and cyclophosphazenes, however, are more complex. Their structures are characterised by repeating units, $-[R_2P=N]_n-$, which are linked together through covalent bonds, creating a backbone of alternating nitrogen and phosphorus atoms in the structure. Linear polyphosphazene derivatives containing up to 15000 repeating units have been reported, whereas cyclophosphazenes with ring sizes of between three to forty repeating units are known. As the phosphorus atoms are pentavalent and tetracoordinate, two attachment points exist per PN unit which enables the addition of pendant groups onto the phosphazene, including halogeno, aryl, alkyl, alkoxy, hydroxyl and alkylamino units. The choice of pendant group(s) functionalises the phosphazene compounds which, depending on their composition, can exhibit properties typically attributed to organic, inorganic and highly polymeric molecular compounds as a result (e.g. good resistance to high and low temperatures, biocompatibility, radiation resistance, hydrophobicity, hydrophilicity and bioerodibility). Investigation of links between properties and structure has led to the design of phosphazenes for specific applications such as high performance elastomers, flame retardants,²⁹⁰ polymeric electrolytes,²⁹¹ biomedicines,²⁹² catalysts²⁹³ and batteries.²⁹⁴

1.4.3 General Properties of Phosphazenes

Though there are many varieties of phosphazene compounds, the feature that defines them collectively is the presence of P-N bonding. The atypical bonding exhibited by these P-N bonds provides phosphazenes with many unique and characteristic structural properties. The

following is a summary of some of the most commonly observed properties of phosphazenes that has been adapted from Allcock's "*Phosphorus-Nitrogen Compounds*":²⁹⁵

- i) Phosphazene ring and chain structures are thermally and hydrolytically stable
- ii) The P-N bond lengths in phosphazenes are shorter than is expected for purely covalent σ -bonds, and the distances in these bonds are often shortened further by the presence of more electronegative pendant groups on the phosphorus atoms.
- iii) The bond lengths in the skeletal structure of cyclophosphazenes are usually equivalent around the ring unless the pendant groups are unsymmetrical, or one or two ring nitrogen atoms are involved in Lewis acid-base pairing.
- iv) Cyclophosphazene rings can be planar or puckered, but either conformation appears to have little to no effect on molecular stability.
- v) The ring nitrogen atoms in cyclophosphazenes can function as basic coordination sites, and this property is enhanced by the presence of more electron-donating pendant groups attached to phosphorus.
- vi) Many reactions with phosphazenes involve nucleophilic attack on the phosphorus atoms, removing one of the pendant substituent groups.
- vii) Unlike aromatic systems, the phosphazene skeleton is difficult to reduce electrolytically.
- viii) Spectral effects associated with delocalization in organic π -electron systems are not observed for cyclo- or polyphosphazenes.

1.4.4 Cyclotriphosphazenes

Although cyclophosphazenes with between three and forty phosphazene ring units are known, cyclotriphosphazenes with their rigid and thermally stable three-membered phosphazene rings have found the most success as building blocks for supramolecular assemblies or functionalized complexes.^{296–298} Indeed, they have been found to be excellent ligands/surfactants for transition metal ions due to their robust structure and wide range of substituents that can be tuned for use as active sites or linkers (*vide infra*).^{298,299}

1.4.4.1 Structure

Cyclotriphosphazenes are inorganic heterocyclic compounds with a six-membered ring composed of three repeat PN units; each unit consists of a nitrogen atom with an electron lone pair and a tetrahedral phosphorus centre with two pendant substituent groups (Fig. 1.11).³⁰⁰ The majority of cyclotriphosphazenes are planar or close to planar and, unlike organic aromatic ring species, moderate puckering has little to no effect on the molecular stability.³⁰¹

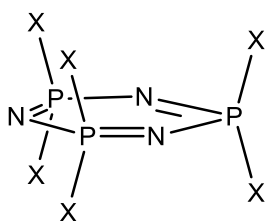


Fig. 1.11. Structure of a cyclotriphosphazene.^{302–304}

The rings are not aromatic; instead they have a zwitterionic structure in which the nitrogen and phosphorus atoms are linked through σ -bonding frameworks with ionic bonding contributions.³⁰⁵ The zwitterionic structure is formed by transfer of an electron from

phosphorus to nitrogen through subsidiary negative hyperconjugation contributions.³⁰⁶ The negative hyperconjugation contributions require interaction of the (σ^* P-N) and (σ^* P-X) orbitals with the in-phase and out-of-phase lone pair orbitals, which can be enhanced by increasing the electronegativity of the phosphorus pendant groups (X). In phosphazenes with equivalent pendant groups (i.e. with formula (NPX₂)₃) equivalent bond lengths between all of the ring P-N bonds have been observed, though, these lengths have been reported to change depending on the electron withdrawing or donating behaviour of the substituent groups.^{301,307}

Double bonds are almost always used in schematic diagrams of cyclotriphosphazenes as a relic of past (incorrect) bonding theories to keep track of electrons in the structure (Fig 1.12, (1)).³⁰¹ A more accurate schematic representation of the structure based on current models is shown in Fig. 1.12 (2). However, the double bond scheme will be used in this work to maintain consistency with the literature.

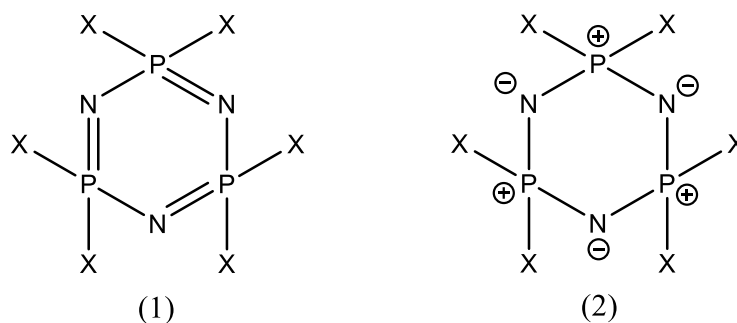
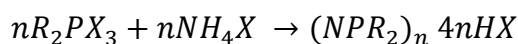


Fig. 1.12. Schematic representations of the bonding in cyclotriphosphazenes: (1) valence bonding model and (2) zwitterionic model.

1.4.4.2 Synthesis of Cyclophosphazenes

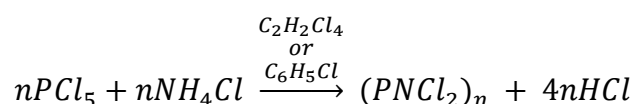
Many cyclophosphazenes have been reported in the literature. Some are prepared by direct synthesis whilst others are prepared by performing substitution reactions on appropriate

precursors. Halogenated cyclophosphazene compounds can be prepared by reacting halophosphoranes with ammonium halides, which can be represented by the equation²⁹⁵



where R can be a halo or organo group and X is a halogen atom (typically Cl or Br). Trimers and tetramers usually form in the highest yields in these reactions, though small quantities of larger cyclo species and linear species may also be produced.

By far the most important and heavily investigated halocyclophosphazene is the trimer, (NPCl₂)₃.³⁰⁸ This is synthesized by reacting ammonium chloride with phosphorus pentachloride.^{309–311} The general scheme for this reaction is³¹²

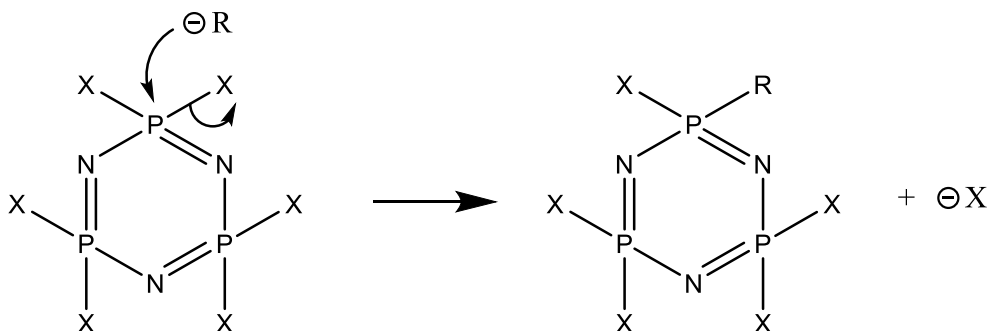


This compound is important as it often serves as a precursor in the production of many different hexa-substituted cyclotriphosphazene species by simple nucleophilic substitution of the chlorine groups.

1.4.4.3 Substitution of Pendant Groups (Reactions of Halophosphazenes)

Halocyclotriphosphazenes are important starting materials for the abundant and diverse chemistry of cyclophosphazenes. They are commonly used as precursors for the synthesis of more desirable and often more complex compounds, as their stable rings allow the introduction of a wide variety of nucleophilic substituents into exocyclic positions at the phosphorus centres (Scheme. 1.11).³⁰¹ In these reactions, incoming nucleophiles supplant the original halo substituents (i.e. Cl, F or Br) sequentially through a series of nucleophilic substitutions to produce either *homo-* or *hetero-* substituted derivatives, which include *organo* derivatives with

P-N, P-O, P-S or P-C bonds.^{301,313,314} These reactions occur smoothly and the spatial arrangement of the groups is determined by the size of the substituent group and the size of neighbouring substituent groups (with regards to heterosubstituted derivatives).³¹⁴



Scheme. 1.11. Nucleophilic substitution of halocyclotriphosphazene halide group.

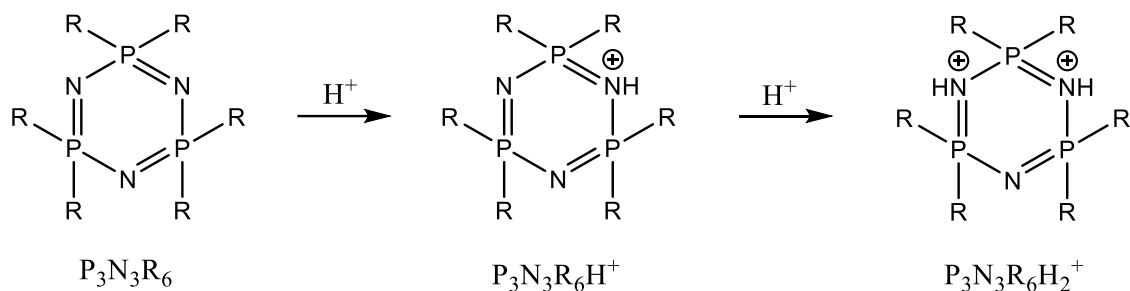
The most widely used halocyclotriphosphazene precursor is $P_3N_3Cl_6$ due to the amenability of its P-Cl bonds to facile synthetic manipulations. Its rigid and highly stable six-membered ring provides a D_{3h} symmetrical support for the six exocyclic, P-bonded pendant groups which in *homo*-substituted compounds orient with 3 groups above and three groups below the ring. Numerous nucleophilic substitutions of these compounds have been reported over the years which include, hydrolysis;^{309,310,315} aminolysis,³¹⁶ and reactions with alkoxides, aryloxides and thiolates^{295,317} to list a few.

Substitution of the halide groups with the appropriate group can also tune the basic properties of the cyclotriphosphazene ring.

1.4.4.4 Basicity

The skeletal nitrogen atoms in cyclophosphazene rings are basic and can be protonated in the presence of strong Brønsted acids through donation of their lone electron pairs. Their basicity

can be enhanced using electron donating substituent groups on the neighbouring phosphorous atoms and, through functionalization with strong nucleophilic substituents (e.g. amines), cyclophosphazenes can be strong bases with one or two ring nitrogens able to be protonated to yield mono- and dicationic species (Scheme 1.12).



Scheme 1.12. Protonation of the basic ring N sites to yield mono- and dicationic species (R = nucleophilic substituent).

The pK_a values for many cyclophosphazenes bearing different substituent groups have been measured previously and representative values are given in Table 1.4.^{318–323}

Chlorocyclophosphazenes have very low basic strengths due to the electron withdrawing nature of the chloro groups which reduces the availability of the ring nitrogen lone electron pairs. The base strength of aryl-, alkoxy- and alkylphosphazenes increases of the order R = CF₃ < Ph < Et in line with the electron donating characteristics of the groups. Aminophosphazenes have the highest recorded base strengths which tend to have pK_{a1} values that are similar to or higher than the parent amines.³¹⁸ Nevertheless, unlike the other types of substituent groups, the base strengths of aminophosphazenes cannot be rationalised explicitly by the electron donating or withdrawing abilities of the R groups. Instead, a “saturation effect” has been suggested to explain the insensitivity of the pK_{a1} values with respect to subtle electronic differences between this type of substituent group, yet the electron releasing powers become more distinguished in the spread of pK_{a2} values.³¹⁸

Table 1.4. pK_a values for assorted cyclophosphazenes in nitrobenzene. ³¹⁸⁻³²³

Compound	pK_{a1}	pK_{a2}
$P_3N_3Cl_6$	<-6.0	-
$P_3N_3(CF_3)_6$	<-6.0	-
$P_3N_3Ph_6$	1.50	-
$P_3N_3Et_6$	6.40	-
$P_3N_3(OMe)_6$	-1.9	-
$P_3N_3(OPr^i)_6$	1.4	-
$P_3N_3(OBu^t)_6$	0.1	-
$P_3N_3(OCH_2Ph)_6$	-2.1	-
$P_3N_3(OPh)_6$	-5.8	-
$P_3N_3(SPh)_6$	-4.8	-
$P_3N_3(NHMe)_6$	8.8 ± 0.6	-2.0 ± 0.4
$P_3N_3(NHEt)_6$	8.2	3.4
$P_3N_3(NHBu^t)_6$	7.9	-1.8
$P_3N_3(NMe_2)_6$	7.6	-3.3
$P_3N_3(NEt_2)_6$	8.5	-3.9
$P_3N_3(NH(C_6H_{11}))_6$	7.9	-1.4
$P_3N_3Cl_3(NC_5H_{10})_6$	8.4	-3.2 ± 0.4
$P_3N_3(NMePh)_6$	3.5	-
$P_3N_3Cl_3(NC_5H_{10})_3$ (<i>gem</i>)	-3.9	-
$P_3N_3Cl_3(NC_5H_{10})_3$ (<i>trans</i>)	-5.3	-
$P_3N_3Ph_3(NMe)_3$ (<i>gem</i>)	5.7	-5.2
$P_3N_3Ph_3(NMe)_3$ (<i>trans</i>)	5.8	-5.2

1.4.4.5 Cyclophosphazene Salts

Due to the relative basic strengths of cyclotriphosphazenes, many of these compounds have been able to form salt-like adducts when reacted with acids. Examples include: hydrohalide salts, such as $[\text{P}_3\text{N}_3(\text{NHBu}^n)_6]\cdot\text{HCl}$,³²⁴ $[\text{P}_3\text{N}_3(\text{NHPr}^n)_6]\cdot\text{HCl}$,³²⁴ $[\text{P}_3\text{N}_3(\text{NHPr}^n)_6]\cdot\text{HBr}$,³²⁴ $[\text{P}_3\text{N}_3\text{F}_6]\cdot 2\text{HF}\cdot 2\text{H}_2\text{O}$,³²⁵ $[\text{P}_3\text{N}_3(\text{NHPh})_6]\cdot\text{HCl}$,³²⁶ and $[\text{P}_3\text{N}_3\text{Cl}_4(\text{NHCH}_2\text{H}_4\text{NH}_2)_2]\cdot 2\text{HCl}$;³²⁶ acetate salts, $[\text{P}_3\text{N}_3(\text{NH}_2)_6]\cdot\text{HOOCCH}_3$;³²⁷ perchlorate salts, $[\text{P}_3\text{N}_3\text{Cl}_6]\cdot\text{HClO}_4$, $[\text{P}_3\text{N}_3\text{Cl}_6]\cdot 2\text{HClO}_4$, $[\text{P}_3\text{N}_3(\text{NHPh})_6]\cdot\text{HClO}_4$, and $[\text{P}_3\text{N}_3\text{Cl}_4(\text{NHMe})_2]\cdot\text{HClO}_4$;³²⁶ and, more recently, superacid adducts with the general formula $[\text{P}_3\text{N}_3\text{Cl}_6]\cdot\text{HMX}_4$ ($\text{M} = \text{Al}$ and Ga , and $\text{X} = \text{Cl}$ or Br).³²⁸ Hydrohalide, perchlorate and acetate salts can be synthesized by simply mixing the components in non-aqueous media,^{324–327} whereas synthesis of the superacid salts requires inert conditions and minimal exposure to light.³²⁸ In all cases, the final products are formed through protonation of the cyclophosphazene to give a “phosphazanium” cation and a counterion with the general formula $[(\text{P}_3\text{N}_3\text{R}_6)\text{H}]^+ \text{X}^-$ (Fig. 1.13).^{47,107,331} Protonation of N sites in the constituent phosphazanium rings can be detected in the crystallographic data of the salts through elongation of the flanking P-N bonds.^{328–330,332}

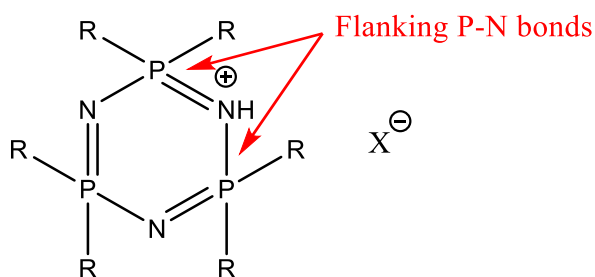


Fig. 1.13. Structure of $[(\text{P}_3\text{N}_3\text{R}_6)\text{H}]^+ \text{X}^-$ salts.³⁰¹

Indeed, a cyclophosphazene-isopolyoxometalate compound, $[\text{P}_3\text{N}_3(\text{NMe})_6\text{H}]_2^+[\text{Mo}_6\text{O}_{19}^{2-}]$, has been reported previously and X-ray diffraction studies confirmed protonation of the

phosphazene ring within the structure.^{332,333} This compound will be discussed in more detail below.

The cyclophosphazene ring nitrogen atoms can also operate as Lewis bases towards appropriate Lewis acids through use of their lone electron pairs to form salts.^{295,334,335} Lewis acid adducts $P_3N_3Cl_6 \cdot AlCl_3$ and $P_3N_3Cl_6 \cdot GaCl_3$ show dative N-Al and N-Ga bonding between the cyclic N sites and the metals in the corresponding crystallographic X-ray data, as well as considerable lengthening of the flanking P-N bonds as has been seen in the protonated species mentioned above.³³⁵

Acylation and alkylation of organoaminocyclotriphosphazenes, $(RNH)_6P_3N_3$ (R = *n*-propyl, isobutyl, isopropyl, cyclohexyl, *tert*-butyl, benzyl), through reaction of the phosphazene with alkyl- or acylhalides results from the formation of N-alkyl and N-acyl bonds at the ring nitrogen sites.³³⁶ X-ray crystal structures showed that the alkylation and acylation of ring N sites leads to substantial elongation of the associated P-N bonds, with bond lengthening more pronounced in N-acylated species than in N-alkylated species.

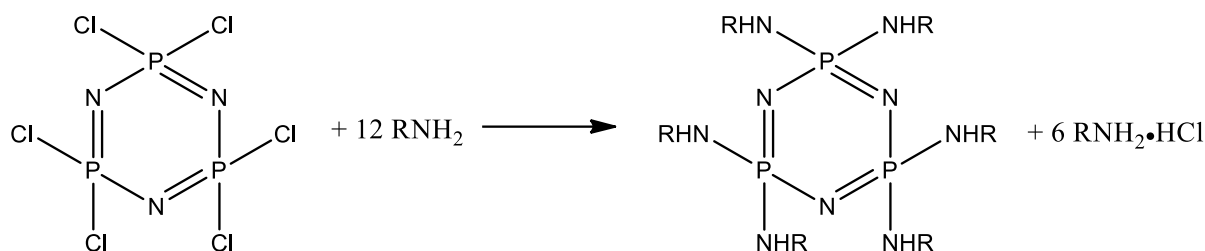
1.4.4.6 Organoaminocyclotriphosphazenes

These compounds have the general formula $P_3N_3(NHR)_6$ which will, henceforth, be abbreviated to RPN, where R is the corresponding alkyl group of the organoamine substituents.

1.4.4.6.1 Synthesis

Halocyclotriphosphazenes, such as $P_3N_3Cl_6$, react with primary or secondary amines (aminolysis) to produce amino-substituted phosphazenes (Scheme 1.13). Excess amine is often added to the reaction as a hydrohalide acceptor to form ammonium hydrogen halide as a side

product. The choice of a suitable solvent can ensure that ammonium hydrogen halide is removed from the reaction medium through insolubility. This prevents the halide from reacting further in the mixture. The synthesis of amino-substituted cyclophosphazenes through the aminolysis of halophosphazenes has been reviewed.³¹⁶



Scheme 1.13. Synthesis of amino-substituted cyclophosphazenes through the aminolysis of halophosphazenes.

1.4.4.6.2 Aminocyclophosphazene Supramolecular Structures

Hexa-substituted organoaminocyclotriphosphazenes are attractive prospects as building blocks for supramolecular assemblies³³⁷ and multi-site coordination ligands for metallic complexes.³³⁸

These compounds are amphiphilic and their basic ring nitrogen centres can function as proton acceptors or hydrogen-bond acceptor sites, whilst the exocyclic amino NH groups (RNH) operate as hydrogen-bond donor sites. These interactions allow formation of intermolecular NH \cdots N bonds between the neighbouring P₃N₃(NHR)₆ groups, as illustrated in Fig. 1.14.³³⁷

This results in the formation of amphiphilic bilayers, with the hydrophilic rings and amino groups sandwiched between two hemispheres of lipophilic R groups. Subtle variations in the shape and size of these R groups alters the topography of the supramolecular networks, as evidenced by X-ray determination of their crystallographic structures. Free rotation about the P-N exocyclic bonds enables variable directionalities of the NH bonds which results in ten

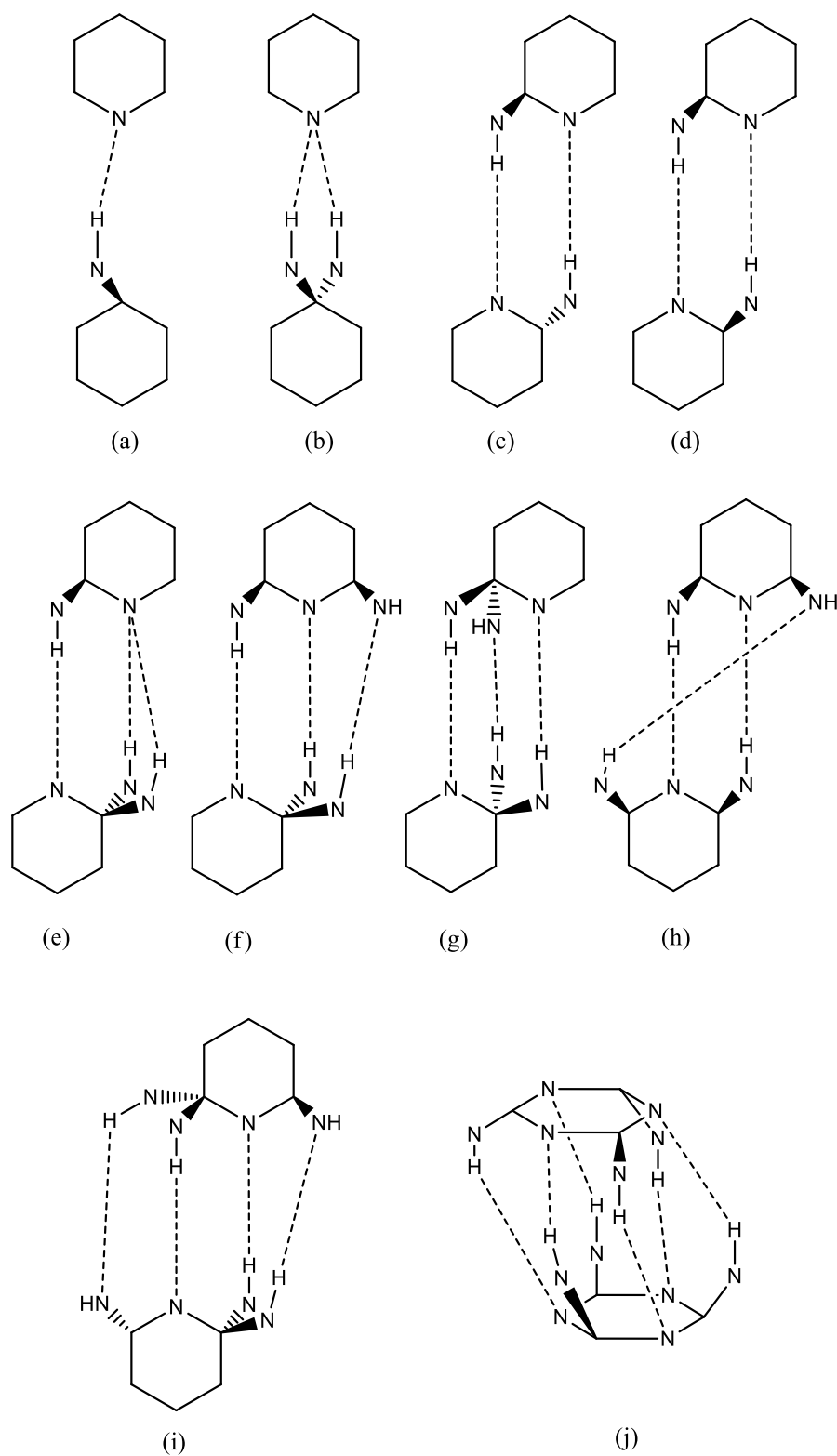


Fig. 1.15. Schematic representation of H-bridging motifs observed in solid-state structures of $P_3N_3(NHR)_6$ including single **(a)**, double **(b, c, d)**, triple **(e, f, g, h)**, quadruple **(i)** and septuple **(j)** H-bridges.

The crystal structures for a selection of RPNs are presented in Fig. 1.16. Intermolecular NH \cdots N interactions are not present in the crystal structure of tBuPN as the steric bulk of the tBu substituents hinders the formation of these bonds. In contrast, CyPN forms dimers with **c**-bridges between the two units as the less bulky Cy groups can be arranged to reduce steric hindrance; the dimers can be packed in different arrangements which results in triclinic or monoclinic modifications in the crystal structure. The structure of iPrPN displays hexameric ring structures with S_6 symmetry held together by six **e**-bridges. The smaller size of the iPr substituents makes the NH and N sites more available for intermolecular bonding. The crystal structure of BzPN is composed of monoclinic and triclinic zig-zag chain polymorphs. The BzPN units in these chains are linked via **c**-bridges. iBuPN also forms a chain structure, however, each repeat unit consists of five crystallographically unique molecules connected by an alternating **g-j-f-h-g** bridge pattern.

In addition to intermolecular NH \cdots N interactions, aryl derivatives such as PhPN displayed NH \cdots π interactions in the solid state. The PhPN units arrange in a linear chain with **b**-bridging units and neighbouring chains can interact through NH \cdots π interactions to form layered sheets. Presumably, these interactions were not evident in the BzPN structure due to steric hindrance of the benzyl group.³³⁷

Organoaminocyclotriphosphazene supramolecular structures, however, are not limited to forming intermolecular interactions only with other cyclophosphazene derivatives. As discussed above, due to their strong basicity facilitated by electron donation from the exocyclic organoamino substituents, one or two ring nitrogen sites can be protonated in the presence of strong Brønsted acids, such as HCl, to give phosphazanium mono- and dication (Scheme 1.12). The cationic species can form salts through coordination with the conjugate base of the acid (Fig. 1.13), which readily crystallize upon evaporation of the solvent. The structures of these crystals often display ion pairing facilitated by hydrogen bonding from exocyclic and

ring NH functions. The bonding in RPN salts has been discussed previously,²⁹⁶ and the hydrogen bonding modes of the phosphazenum ions towards the conjugate anions in these adducts were highlighted and are shown in Fig. 1.17.

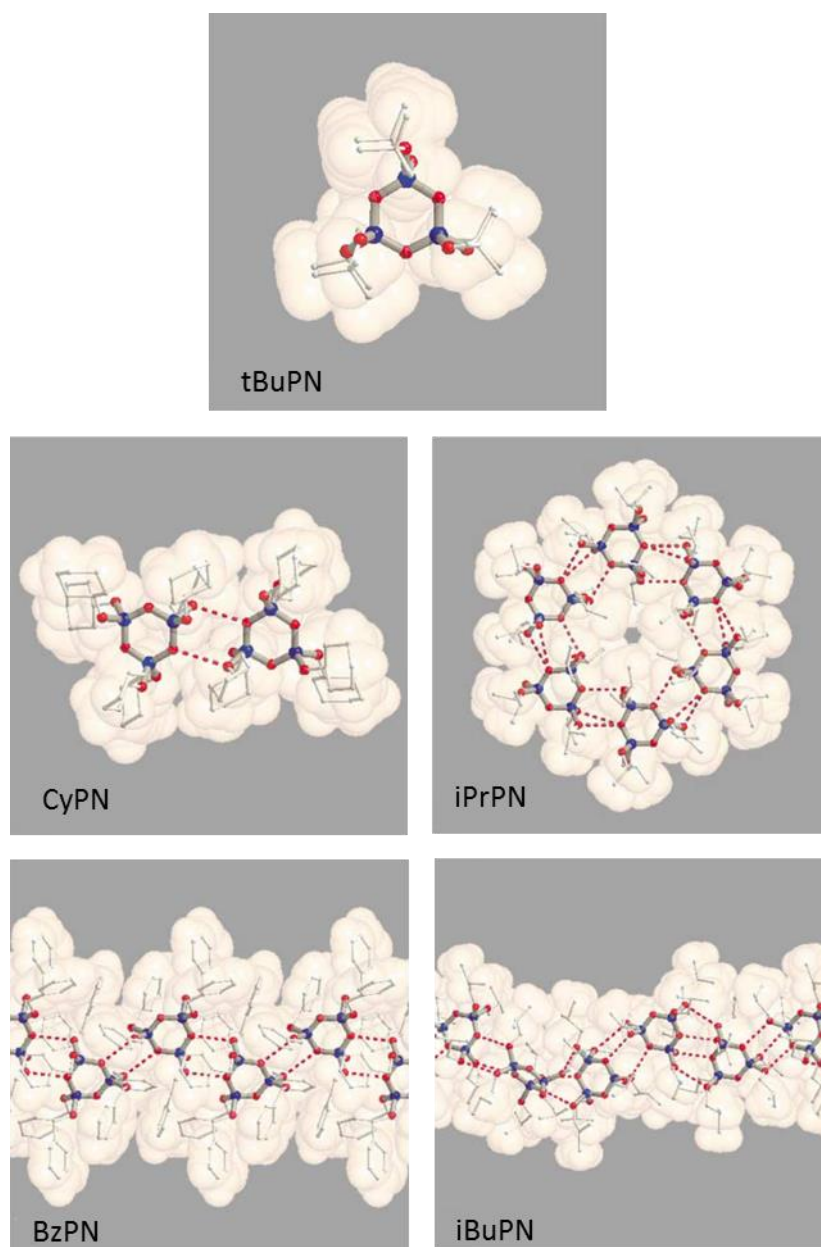


Fig. 1.16. Crystallographic structures of RPNs. H-bonds are represented by dashed lines.³³⁷

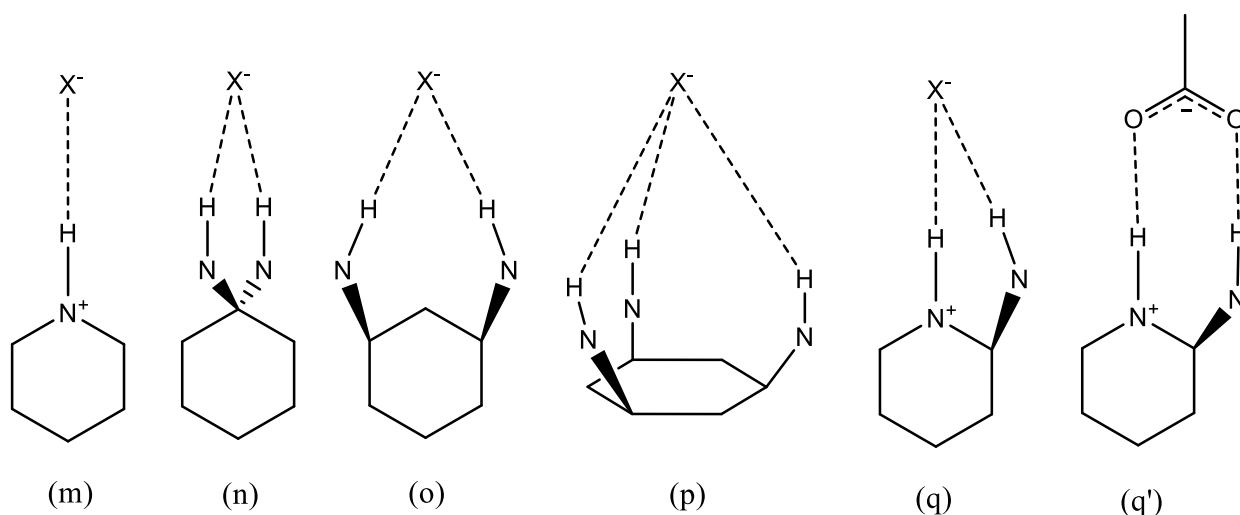


Fig. 1.17. Schematic hydrogen bonding modes of phosphazanium ions towards anions.²⁹⁶

Monoprotonated RPN, $[\text{RPNH}]^+$, has a ring NH site that can bind anions directly with monodentate (**m**) interactions, or through bidentate (**q**) interactions with support from an exocyclic NH group. **q**-Bonding interactions are particularly favourable with carboxylate anions (**q'**) and these anions can also bridge two neighbouring phosphazanium ions through $\text{NH}\cdots\text{O}$ bonds. Other bidentate interactions (**n** and **o**) involve bonding from only the exocyclic NH groups. Both mono- and bidentate interactions were seen frequently in structures with halides. The tridentate interactions, **p**, were observed in halides of *N,N'*-dialkyl phosphazanium ions.

1.4.5 Previous Examples of Phosphazene-Polyoxometalate Salt Aggregates

To our knowledge (that is, both of my supervisors and I) the only RPN-POM salt aggregate in the literature reported by another research group was $[\text{HP}_3\text{N}_3(\text{NMe}_2)_6]^+[\text{Mo}_6\text{O}_{19}^{2-}]$ in 1972.^{332,333} The salt was formed by the reaction of $\text{P}_3\text{N}_3(\text{NMe}_2)_6$ with molybdenum trioxide in boiling water and was isolated as large yellow-green crystals and had a melting point of 215-

216 °C (also temperature of onset decomposition). It was insoluble in water, 2-butanol, ethyl acetate, tetrahydrofuran, carbon tetrachloride, benzene, and hexane. It was slightly soluble in boiling ethanol and soluble in dichloromethane, acetone, acetonitrile and nitromethane.

Bands in the FTIR analysis at 2595 and 2340 cm^{-1} were assigned to ν_{NH^+} modes.

A broad singlet peak at δ -19.5 ppm (56 Hz wide) in the ^{31}P NMR (referenced to H_3PO_4) could be assigned to the $\text{P}_3\text{N}_3\text{P}$ sites, with the suggestion of fast NH proton exchange between the ring N sites in solution.

X-ray structure determination indicated that the unit cell consisted of a polymolybdate dianion flanked by two phosphazene cations in an extended arrangement. The proton in each cation was situated at a phosphazene ring nitrogen and the resulting N-H bonds were pointed directly towards the bridging oxygen atoms in the anions. The position of the cation proton on the ring could be determined from a difference Fourier map and elongation of the flanking P-N bonds. The average bond lengths in the rings of the phosphazene cations are given in Fig. 1.18.

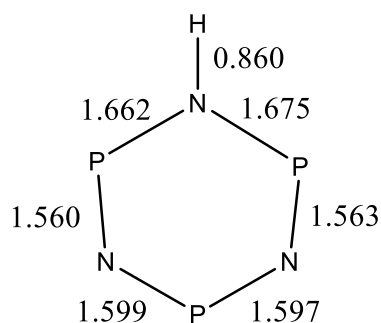


Fig. 1.18. The average bond lengths in the rings of the phosphazene cations in $[\text{HP}_3\text{N}_3(\text{NMe}_2)_6]^+[\text{Mo}_6\text{O}_{19}^{2-}]$

The arrangement of the ions in the $[\text{HP}_3\text{N}_3(\text{NMe}_2)_6]^+[\text{Mo}_6\text{O}_{19}^{2-}]$ unit cell is illustrated in Fig. 1.19.

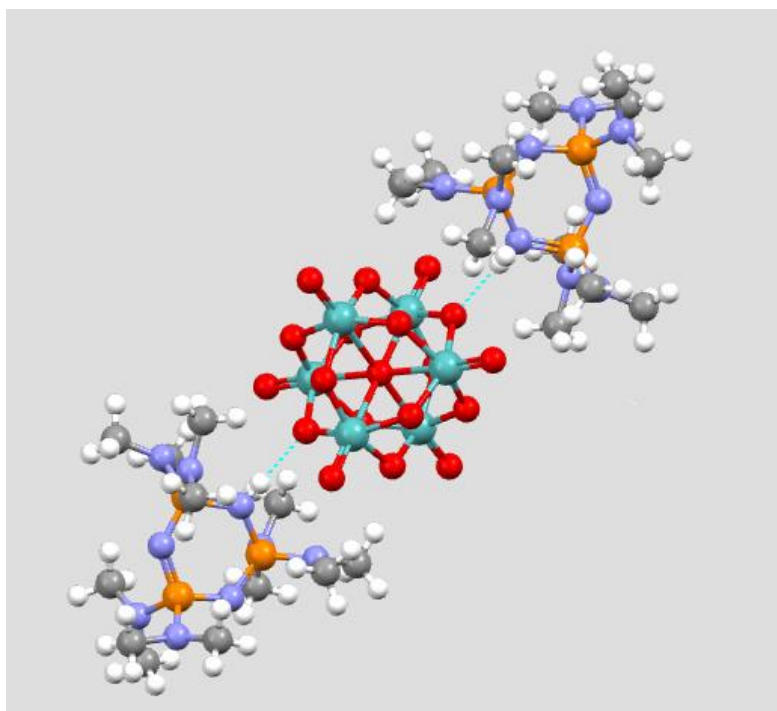


Fig. 1.19. Arrangement of the ions in $[\text{HP}_3\text{N}_3(\text{NMe}_2)_6]^+]_2[\text{Mo}_6\text{O}_{19}^{2-}]$.³³³

1.4.6 Suitability as Phase-Transfer Moieties for POM-Catalysed Oxidations with Hydrogen Peroxide

The following points provide a summary of some of the key reasons why RPNs are suitable phase-transfer catalyst moieties for POM-catalysed oxidations with H_2O_2 :

- Organoaminocyclotriphosphazenes are robust and remain stable when exposed to extreme conditions such as strongly acidic or basic media and hydrothermal treatment.^{339,340}
- They are soluble in organic solvents. Their solubility can be tuned by selection of different lipophilic R groups on the exocyclic amino substituents.³¹⁶
- The strong basicity of their ring nitrogen sites allows them to operate as Brønsted or Lewis bases, enabling the introduction of groups to provide additional functionalities.³³⁸
- Addition of a strong Brønsted acid often results in the formation of salt adducts.²⁹⁶
- Acid precursors of polyoxometalates, heteropoly acids, are strong Brønsted acids.

- A RPN-POM salt aggregate, $[\text{HP}_3\text{N}_3(\text{NMe}_2)_6]^+[\text{Mo}_6\text{O}_{19}^{2-}]$, has already been synthesized previously.^{332,333} The compound had a high thermal stability (215 °C mp and onset temperature for decomposition) and could be solubilized in a range of organic solvents. As POM is otherwise insoluble in most organic solvents, this indicates that the coordinated RPN cations operated as a ligand/surfactant which solubilised the POM species in the organic media, with both component ions remaining intact.
- Cyclotriphosphazenes have been used as supports for Schiff base moieties for the hydroxylation of benzene with hydrogen peroxide at reaction temperatures of up to 80 °C. Catalyst reuse in these reactions suggests that both the ring structure and aminopropyl substituents used to tether the cyclophosphazene supports to the surface of the solid silica support remain intact during the reaction. This suggests cyclotriphosphazenes with organoamino substituents are stable under reaction conditions similar to those proposed in this work.³⁴¹
- PTCs for biphasic oxidations with POMs are often quaternary ammonium salts with long chain alkyl groups with one or two shorter chains to make the cation centre more accessible. These can be difficult to synthesize.
- RPNs can be synthesized with long chains positioned above and below the plane of the ring which maintains accessibility of cationic ring centre and can potentially improve solubility of complexes in solution. In addition, RPNs can provide hydrogen bonding interactions for improved stability of catalytically active intermediate species.

References

- 1 J. J. Berzelius, *Årsberättelsen om framsteg i fysik och kemi*, Stockholm, Sweden, 1835.
- 2 J. G. de Vries and S. D. Jackson, *Catal. Sci. Technol.*, 2012, **2**, 2009.
- 3 M. Bowker, *The Basis and Applications of Heterogeneous Catalysis*, Oxford University Press, Oxford, 1998.
- 4 United States Environmental Protection Agency (EPA), *The Plain English Guide to the Clean Air Act: Clean Air Act Overview*, Washington DC, 2007.
- 5 Legislation.gov.uk, Clean Air Act 1993, <http://www.legislation.gov.uk/ukpga/1993/11/introduction>, (accessed 1 September 2017).
- 6 R. A. Henderson, *The Mechanisms of Reactions at Transition Metal Sites*, Oxford University Press, Oxford, 1995.
- 7 K. C. Taylor, *Catal. Rev.*, 1993, **35**, 457–481.
- 8 J. Wang, H. Chen, Z. Hu, M. Yao and Y. Li, *Catal. Rev.*, 2015, **57**, 79–144.
- 9 M. Shelef and G. W. Graham, *Catal. Rev.*, 1994, **36**, 433–457.
- 10 in *Ullmann's Encyclopedia of Industrial Chemistry*, Wiley-VCH Verlag GmbH & Co. KGaA, 2000.
- 11 H. Shimada, K. Sato, K. Honna, T. Enomoto and N. Ohshio, *Catal. Today*, 2009, **141**, 43–51.
- 12 H. Lindlar and R. Dubuis, *Org. Synth.*, 1966, **46**, 89.
- 13 D. Cole-Hamilton, in *Catalysis Fundamentals and Practice*, University of Liverpool,

- Liverpool, 2015.
- 14 J. Manassen, D. D. Whitehurst, J. C. Bailar, S. Carra, M. Graziani, K. Mosbach, R. C. Pitkethly, E. K. Pye and J. J. Rooney, eds. F. Basolo and R. L. Burwell, Springer US, Boston, MA, 1973, pp. 177–185.
 - 15 W. Keim, *Green Chem.*, 2003, **5**, 105–111.
 - 16 W. M. Nelson, *Green Solvents for Chemistry: Perspectives and Practice*, Oxford University Press, New York, 2003.
 - 17 R. A. Sheldon, *Green Chem.*, 2005, **7**, 267–268.
 - 18 E. F. Lutz, *J. Chem. Educ.*, 1986, **63**, 202–203.
 - 19 W. A. Herrmann and C. W. Kohlpaintner, *Angew. Chemie*, 1993, **32**, 1524–1544.
 - 20 C. W. Kohlpaintner, R. W. Fischer and B. Cornils, *Appl. Catal. A Gen.*, 2001, **221**, 219–225.
 - 21 M. Misono and N. Nojiri, *Appl. Catal.*, 1990, **64**, 1–30.
 - 22 S. D. Naik and L. K. Doraiswamy, *AIChE J.*, 1998, **44**, 612–646.
 - 23 T. Hashimoto and K. Maruoka, in *Asymmetric Phase Transfer Catalysis*, ed. K. Maruoka, Wiley, Weinheim, 2008, pp. 1–8.
 - 24 C. M. Starks, *J. Am. Chem. Soc.*, 1971, **93**, 195–199.
 - 25 C. M. Starks and M. Halper, *Phase-Transfer Catalysis: Fundamentals, Applications, and Industrial Perspectives*, Springer Netherlands, 1994.
 - 26 C. L. Liotta, J. Berkner, J. Wright and B. Fair, in *Phase-Transfer Catalysis*, ed. M. E. Halpern, American Chemical Society, 1997, pp. 29–40.

- 27 C. M. Starks and R. M. Owens, *J. Am. Chem. Soc.*, 1973, **95**, 3613–3617.
- 28 M. Małkosza and M. Fedoryński, *Catal. Rev.*, 2003, **45**, 321–367.
- 29 F. Montanari, S. Quici and P. Tundof, 1983, 199–202.
- 30 D.-H. Wang and H.-S. Weng, *Chem. Eng. Sci.*, 1988, **43**, 2019–2024.
- 31 E. V Dehmlow, R. Thieser, Y. Sasson and E. Pross, *Tetrahedron*, 1985, **41**, 2927–2932.
- 32 S. Dermeik and Y. Sasson, *J. Org. Chem.*, 1985, **50**, 879–882.
- 33 S. Dermeik and Y. Sasson, *J. Org. Chem.*, 1989, **54**, 4827–4829.
- 34 H. Abbayes, A. Buloup and G. Tanguy, *Organometallics*, 1983, **2**, 1730–1736.
- 35 G. Tanguy, B. Weinberger and H. des Abbayes, *Tetrahedron Lett.*, 1983, **24**, 4005–4008.
- 36 O. Bortolini, V. Conte, F. Di Furia and G. Modena, *J. Org. Chem.*, 1986, **51**, 2661–2663.
- 37 O. Bortolini, F. Di Furia, G. Modena and R. Seraglia, *Aldrichimica Acta*, 1985, **50**, 2688–2690.
- 38 J.-M. Brégeault, *Dalt. Trans.*, 2003, (6), 3289–3302.
- 39 P. Wasserscheid and W. Keim, *Angew. Chemie Int. Ed.*, 2000, **39**, 3772–3789.
- 40 J. S. Wilkes, J. A. Levisky, R. A. Wilson and C. L. Hussey, *Inorg. Chem.*, 1982, **21**, 1263–1264.
- 41 K. N. Marsh, J. A. Boxall and R. Lichtenthaler, *Fluid Phase Equilib.*, 2004, **219**, 93–98.
- 42 S. K. Poole, P. H. Shetty and C. F. Poole, *Anal. Chim. Acta*, 1989, **218**, 241–264.

- 43 P. Wasserscheid and T. Welton, Eds., *Ionic Liquids in Synthesis*, Wiley-VCHVerlag, Stuttgart, Germany, Second., 2008.
- 44 R. D. Rogers and K. R. Seddon, Eds., *Ionic Liquids IIIA: Fundamentals, Progress, Challenges, and Opportunities*, American Chemical Society, Washington, USA, first., 2005.
- 45 J. G. Huddleston, A. E. Visser, W. M. Reichert, H. D. Willauer, G. A. Broker and R. D. Rogers, *Green Chem.*, 2001, **3**, 156–164.
- 46 C. J. Bradaric, A. Downard, C. Kennedy, A. J. Robertson and Y. Zhou, *Green Chem.*, 2003, **5**, 143–152.
- 47 Y. Zhang, S. Zhang, X. Lu, Q. Zhou, W. Fan and X. Zhang, *Chem. - A Eur. J.*, 2009, **15**, 3003–3011.
- 48 D. J. Kim, K. H. Oh and J. K. Park, *Green Chem.*, 2014, **16**, 4098–4101.
- 49 B. Clare, A. Sirwardana and D. R. MacFarlane, ed. B. Kirchner, Springer Berlin Heidelberg, Berlin, Heidelberg, 2010, pp. 1–40.
- 50 J. S. Wilkes and M. J. Zarawotko, *J. Chem. Soc. Chem. Commun.*, 1992, 965–967.
- 51 L. Cammarata, S. G. Kazarian, P. A. Salter and T. Welton, *Phys. Chem. Chem. Phys.*, 2001, **3**, 5192–5200.
- 52 S. A. Mirkhani, F. Gharagheizi, P. Ilani-Kashkouli and N. Farahani, *Thermochim. Acta*, 2012, **543**, 88–95.
- 53 W. Xu, E. I. Cooper and C. A. A. Angell, *J. Phys. Chem. B*, 2003, **107**, 6170–6178.
- 54 C. Maton, N. De Vos and C. V Stevens, *Chem. Soc. Rev.*, 2013, **42**, 5963–77.

- 55 M. T. Zafarani-Moattar and R. Majdan-Cegincara, *J. Chem. Eng. Data*, 2007, **52**, 2359–2364.
- 56 J. H. Davis, Jr., *Chem. Lett.*, 2004, **33**, 1072–1077.
- 57 H. L. Ngo, K. LeCompte, L. Hargens and A. B. McEwen, *Thermochim. Acta*, 2000, **357–358**, 97–102.
- 58 J. P. Hallett and T. Welton, *Chem. Rev.*, 2011, **111**, 3508–3576.
- 59 T. Welton, *Chem. Rev.*, 1999, **99**, 2071–2083.
- 60 M. Armand, F. Endres, D. R. MacFarlane, H. Ohno and B. Scrosati, *Nat. Mater.*, 2009, **8**, 621–9.
- 61 M. Galiński, A. Lewandowski and I. Stepniak, *Electrochim. Acta*, 2006, **51**, 5567–5580.
- 62 A. Berthod, M. J. Ruiz-Ángel and S. Carda-Broch, *J. Chromatogr. A*, 2008, **1184**, 6–18.
- 63 S. P. M. Ventura, F. A. E. Silva, M. V. Quental, D. Mondal, M. G. Freire and J. A. P. Coutinho, *Chem. Rev.*, 2017.
- 64 Z. Zhang, A. Salih, M. Li and Y. Bolun, *Energy & Fuels*, 2014, **28**, 2802–2810.
- 65 Q. Zhang, J. Hu and D.-J. Lee, *Renew. Energy*, 2017, **111**, 77–84.
- 66 W. C. Neil, M. Forsyth, P. C. Howlett, D. R. MacFarlane, C. R. Hutchinson and B. R. W. Hinton, in *47th Annual Conference of the Australasian Corrosion Association 2007: Corrosion Control 2007*, 2007, pp. 675–682.
- 67 J. Qu, J. J. Truhan, S. Dai, H. Luo and P. J. Blau, *Tribol. Lett.*, 2006, **22**, 207–214.
- 68 M. Lombardo, M. Chiarucci and C. Trombini, *Green Chem.*, 2009, **11**, 574–579.

- 69 P. Mastrorilli, C. F. Nobile, R. Paolillo and G. P. Suranna, *J. Mol. Catal. A Chem.*, 2004, **214**, 103–106.
- 70 S. Anjaiah, S. Chandrasekhar and R. Grée, *J. Mol. Catal. A Chem.*, 2004, **214**, 133–136.
- 71 S. T. Handy, *J. Org. Chem.*, 2006, **71**, 4659–4662.
- 72 E. Janus, I. Goc-Maciejewska, M. Lozynski and J. Pernak, *Tetrahedron Lett.*, 2006, **47**, 4079–4083.
- 73 Y. Xiao and S. V. Malhotra, *Tetrahedron Lett.*, 2004, **45**, 8339–8342.
- 74 C. E. Song, *Chem. Comm.*, 2004, **82**, 1033–1043.
- 75 S. Aparicio, M. Atilhan and F. Karadas, *Ind. Eng. Chem. Res.*, 2010, **49**, 9580–9595.
- 76 D. Rooney, J. Jacquemin and R. Gardas, *Top. Curr. Chem.*, 2009, 290, 185–212.
- 77 P. J. Scammells, J. L. Scott and R. D. Singer, *Aust. J. Chem.*, 2005, **58**, 155–169.
- 78 J. S. Wilkes, *J. Mol. Catal. A Chem.*, 2004, **214**, 11–17.
- 79 H. Olivier-Bourbigou and L. Magna, *J. Mol. Catal. A Chem.*, 2002, **182–183**, 419–437.
- 80 R. A. Sheldon, *Chem. Commun.*, 2001, 2399–2407.
- 81 T. Welton, *Coord. Chem. Rev.*, 2004, **248**, 2459–2477.
- 82 S. V Malhotra, V. Kumar and V. S. Parmar, *Curr. Org. Synth.*, 2007, **4**, 370–380.
- 83 H. Olivier-Bourbigou, L. Magna and D. Morvan, *Appl. Catal. A Gen.*, 2010, **373**, 1–56.
- 84 A. C. Cole, J. L. Jensen, I. Ntai, K. L. T. Tran, K. J. Weaver, D. C. Forbes and J. H. Davis, *J. Am. Chem. Soc.*, 2002, **124**, 5962–5963.

- 85 J. A. Boon, J. A. Levisky, J. L. Pflug and J. S. Wilkes, *J. Org. Chem.*, 1986, **51**, 480–483.
- 86 R. Cristiano, K. Ma, G. Pottanat and R. G. Weiss, *J. Org. Chem.*, 2009, **74**, 9027–9033.
- 87 B. Yu, H. Zhang, Y. Zhao, S. Chen, J. Xu, L. Hao and Z. Liu, *ACS Catal.*, 2013, **3**, 2076–2082.
- 88 X. Liu, C. Chen, Y. Xiu, A. Chen, L. Guo, R. Zhang, J. Chen and Z. Hou, *Catal. Commun.*, 2015, **67**, 90–94.
- 89 J. Chen, L. Hua, W. Zhu, R. Zhang, L. Guo, C. Chen, H. Gan, B. Song and Z. Hou, *Catal. Commun.*, 2014, **47**, 18–21.
- 90 Y. Leng, J. Wang, D. Zhu, X. Ren, H. Ge and L. Shen, *Angew. Chemie - Int. Ed.*, 2009, **48**, 168–171.
- 91 X. Ding, W. Chai and D. Kang, *Spec. Petrochemicals*, 2011, **28**, 49–53.
- 92 X. Meng, H.-Y. He, Y. Nie, X. Zhang, S.-J. Zhang and J. Wang, *ACS Sustain. Chem. Eng.*, 2017, **5**, 3081–3086.
- 93 H. Niedermeyer, J. P. Hallett, I. J. Villar-Garcia, P. A. Hunt and T. Welton, *Chem. Soc. Rev.*, 2012, **41**, 7780–7802.
- 94 G. Chatel, J. F. B. Pereira, V. Debbeti, H. Wang and R. D. Rogers, *Green Chem.*, 2014, **16**, 2051–2083.
- 95 *Us 7,588,694 B1*, 2009, 1–9.
- 96 J. W. Raade and D. Padowitz, 2011, **133**, 1–6.
- 97 E. L. Smith, A. P. Abbott and K. S. Ryder, *Chem. Rev.*, 2014, **114**, 11060–11082.

- 98 Q. Zhang, K. De Oliveira Vigier, S. Royer and F. Jérôme, *Chem. Soc. Rev.*, 2012, **41**, 7108–7146.
- 99 M. Skopek, M. A. Mohamoud, K. S. Ryder and A. R. Hillman, *Chem. Commun.*, 2009, **44**, 935–937.
- 100 P. Liu, J.-W. Hao, L.-P. Mo and Z.-H. Zhang, *RSC Adv.*, 2015, **5**, 48675–48704.
- 101 S. Khandelwal, Y. K. Tailor and M. Kumar, *J. Mol. Liq.*, 2016, **215**, 345–386.
- 102 Z. Helalat-Nezhad, K. Ghanemi and M. Fallah-Mehrjardi, *J. Chromatogr. A*, 2015, **1394**, 46–53.
- 103 M. Sharma, C. Muskesh, D. Mondal and K. Prasad, *RCS Adv.*, 2013, **3**, 18149–18155.
- 104 B. Tang, H. Zhang and K. H. Row, *J. Sep. Sci.*, 2015, **38**, 1053–1064.
- 105 C. A. Nkuku and R. J. LeSuer, *J. Phys. Chem. B*, 2007, **111**, 13271–7.
- 106 S. Sun, Y. Niu, Q. Xu, Z. Sun and X. Wei, *Ind. Eng. Chem. Res.*, 2015, **54**, 8019–8024.
- 107 G. Garcia, S. Aparicio, R. Ullah and M. Atilhan, *Energy & Fuels*, 2015, **29**, 2616–2644.
- 108 D. Freudenmann, S. Wolf, M. Wolff and C. Feldmann, *Angew. Chemie - Int. Ed.*, 2011, **50**, 11050–11060.
- 109 R. E. Morris, *Chem. Commun.*, 2009, 2990–2998.
- 110 J. García-Álvarez, in *Green Technologies for the Environment*, American Chemical Society, 2014, vol. 1186, pp. 3–37.
- 111 A. Hayyan, M. Ali Hashim, F. S. Mjalli, M. Hayyan and I. M. AlNashef, *Chem. Eng. Sci.*, 2013, **92**, 81–88.

- 112 F. Keshavarzipour and H. Tavakol, *Catal. Letters*, 2015, **145**, 1062–1066.
- 113 V. De Santi, F. Cardellini, L. Brinchi and R. Germani, *Tetrahedron Lett.*, 2012, **53**, 5151–5155.
- 114 I. V. Kozhevnikov, *Chem. Rev.*, 1998, **98**, 171–198.
- 115 M. T. Pope, *Heteropoly and Isopoly Oxometalates*, Springer-Verlag Berlin, Heidelberg, 1983.
- 116 I. V. Kozhevnikov, *Catalysts for Fine Chemical Synthesis: Catalysis by Polyoxometalates*, Wiley, West Sussex, 2002.
- 117 M. T. Pope and A. Muller, Eds., *Polyoxometalates: From Platonic Solids to Anti-Retroviral Activity*, Kluwer Academic Publishers, Dordrecht, 1994.
- 118 T. Okuhara, N. Mizuno and M. Misono, *Adv. Catal.*, 1996, **41**, 113–252.
- 119 J. A. Dias, S. C. L. Dias, E. Caliman, J. Bartis and L. Francesconi, in *Inorganic Syntheses: Volume 36*, John Wiley & Sons, Inc., 2014, pp. 210–217.
- 120 L. E. Briand, G. T. Baronetti and H. J. Thomas, *Appl. Catal. A Gen.*, 2003, **256**, 37–50.
- 121 A. Blazevic and A. Rompel, *Coord. Chem. Rev.*, 2016, **307**, 42–64.
- 122 M. T. Pope and A. Muller, *Angew. Chemie Int. Ed. English*, 1991, **30**, 34–48.
- 123 J. M. Clemente, E. Coronado and B. S. Tsukerblat, 1995, **195**, 17–28.
- 124 P. A. Lorenzo-Luis and P. Gili, *ChemInform*, 2002, **33**, 221.
- 125 A. Chaumont and G. Wipff, *J. Phys. Chem. C*, 2009, **113**, 18233–18243.
- 126 S. Ganapathy, M. Fournier, J. F. Paul, L. Delevoye and M. Guelton, 2002, **114**, 7821–

- 7828.
- 127 J. M. Maestre, X. Lopez, C. Bo, J.-M. Poblet and N. Casañ-Pastor, *J. Am. Chem. Soc.*, 2001, **123**, 3749–3758.
- 128 H. Li, J. Gupta, S. Wang, N. Zhang and C. Bubeck, *J. Colloid Interface Sci.*, 2014, **427**, 25–28.
- 129 H. Sartzi, H. N. Miras, L. Vilà-Nadal, D. L. Long and L. Cronin, *Angew. Chemie - Int. Ed.*, 2015, **54**, 15488–15492.
- 130 K. Kamata, K. Yonehara, Y. Sumida, K. Yamaguchi, S. Hikichi and N. Mizuno, *Science*, 2003, **300**, 964–6.
- 131 X. López, J. J. Carbó, C. Bo and J. M. Poblet, *Chem. Soc. Rev.*, 2012, **41**, 7537–71.
- 132 G. A. Tsigdinos, Springer Berlin Heidelberg, Berlin, Heidelberg, 1978, pp. 1–64.
- 133 T. V Andrushkevich, V. M. Bondareva, R. I. Maksimovskaya, G. Y. Popova, L. M. Plyasova, G. S. Litvak and A. V Ziborov, *Stud. Surf. Sci. Catal.*, 1994, 82, 837–844.
- 134 J. B. Moffat, in *Acidity and Basicity of Solids: Theory, Assessment and Utility*, eds. J. Fraissard and I. Petrokis, Kluwer, Dordrecht, 1993.
- 135 Ref [116], pp. 9–45.
- 136 I. V. Kozhevnikov, *Russ. Chem. Rev.*, 1987, **56**, 811–825.
- 137 C. Hu, M. Hashimoto, T. Okuhara and M. Misono, *J. Catal.*, 1993, **143**, 437–448.
- 138 L. C. W. Baker and D. C. Glick, *Chem. Rev.*, 1998, **98**, 3–50.
- 139 P. Souchay, *Ions minéraux condensés*, Masson, Paris, 1969.

- 140 L. Pettersson, I. Andersson and L. Ohman, *Inorg. Chem.*, 1986, **25**, 4726–4733.
- 141 Z. Zhu, R. Tain and C. Rhodes, *Can. J. Chem.*, 2003, **81**, 1044–1050.
- 142 L. Pettersson, in *Polyoxometalates, From Platonic Solids to Anti-Retroviral Activity*, eds. M. T. Pope and A. Muller, Kluwer Academic Publishers, Dordrecht, 1994, p. 27.
- 143 Ref [116], pp. 117–166.
- 144 P. Zhao, M. Zhang, Y. Wu and J. Wang, *Ind. Eng. Chem. Res.*, 2012, **51**, 6641–6647.
- 145 C. Komintarachat and W. Trakarnpruk, *Ind. Eng. Chem. Res.*, 2006, **45**, 1853–1856.
- 146 Ref [116], pp. 175–182.
- 147 I. V. Kozhevnikov and K. I. Matveev, *Appl. Catal.*, 1983, **5**, 135–150.
- 148 R. J. J. Jansen, H. M. van Veldhuizen, M. A. Schwegler and H. van Bekkum, *Recl. des Trav. Chim. des Pays-Bas*, 1994, **113**, 115–135.
- 149 E. Papaconstantinou, *Chem. Soc. Rev.*, 1989, **18**, 1–31.
- 150 I. V. Kozhevnikov, *Catal. Rev.*, 1995, **37**, 311–352.
- 151 M. Misono, *Catal. Rev.*, 1987, **29**, 269–321.
- 152 J. B. Moffat, *Rev. Chem. Intermed.*, 1987, **8**, 1–20.
- 153 J. B. Moffat, *Chem. Eng. Commun.*, 1989, **83**, 9–29.
- 154 A. Corma, *Chem. Rev.*, 1995, **95**, 559–614.
- 155 T. Okuhara, N. Mizuno and M. Misono, *Appl. Catal. A Gen.*, 2001, **222**, 63–77.
- 156 M. Misono and N. Mizuno, *Catalytic activation and functionalization of light alkanes:*

- advances and challenges*, Kluwer, Dordrecht, 1997.
- 157 T. Yamase, *Chem. Rev.*, 1998, **98**, 307–326.
- 158 L. I. Kuznetsova, G. M. Maksimov and V. A. Likholobov, *Kinet. Catal.*, 1999, **40**, 622–637.
- 159 M. Misono, I. Ono, G. Koyano and A. Aoshima, *Pure Appl. Chem.*, 2000, **72**, 1305–1311.
- 160 Y. Zhou, Z. Guo, W. Hou, Q. Wang and J. Wang, *Catal. Sci. Technol.*, 2015, **5**, 4324–4335.
- 161 S.-S. Wang and G.-Y. Yang, *Chem. Rev.*, 2015.
- 162 J.-M. Brégeault, M. Vennat, J.-Y. Piquemal, Y. Mahha, E. Briot, P. C. Bakala, A. Atlamsani and R. Thouvenot, *J. Mol. Catal. A Chem.*, 2006, **250**, 177–189.
- 163 N. Mizuno and K. Yamaguchi, *Chem. Rec.*, 2006, **6**, 12–22.
- 164 N. Mizuno, K. Yamaguchi and K. Kamata, *Coord. Chem. Rev.*, 2005, **249**, 1944–1956.
- 165 Y. Zhou, G. Chen, Z. Long and J. Wang, *RSC Adv.*, 2014, **4**, 42092–42113.
- 166 C. L. Hill and C. M. Prosser-McCartha, *Coord. Chem. Rev.*, 1995, **143**, 407–455.
- 167 C. Venturello, J. C. J. Bart and M. Ricci, *J. Mol. Catal.*, 1985, **32**, 107–110.
- 168 G. Centi and S. Perathoner, in *Encyclopedia of Catalysis*, John Wiley & Sons, Inc., 2002.
- 169 A. Weiss, in *Modern Biooxidation*, Wiley-VCH Verlag GmbH & Co. KGaA, 2007, pp. 193–209.
- 170 A. Scarso and G. Strukul, in *Stereoselective Synthesis of Drugs and Natural Products*,

- John Wiley & Sons, Inc., 2013.
- 171 C. W. Jones, J. H. Clark and M. J. Braithwaite, *Applications of Hydrogen Peroxide and Derivatives*, The Royal Society of Chemistry, Cambridge, 1999.
- 172 G. Strukul, Ed., *Catalytic Oxidations with Hydrogen Peroxide as Oxidant*, Springer Netherlands, 1992.
- 173 R. Noyori, M. Aoki and K. Sato, *Chem. Commun.*, 2003, 1977–1986.
- 174 R. Noyori, M. Aoki, K. Sato and R. Noyori, *Chem. Commun.*, 2003, 1977–1986.
- 175 J. J. Dong, D. Unjaroen, F. Mecozzi, E. C. Harvey, P. Saisaha, D. Pijper, J. W. de Boer, P. Alsters, B. L. Feringa and W. R. Browne, *ChemSusChem*, 2013, **6**, 1774–1778.
- 176 K. Sato, M. Hyodo, J. Takagi, M. Aoki and R. Noyori, *Tetrahedron Lett.*, 2000, **41**, 1439–1442.
- 177 A. K. Sharipov, Z. A. Suleimanova, I. S. Faizrakhmanov and R. M. Masagutov, *Pet. Chem.*, 1991, **31**, 90–96.
- 178 W. R. Sanderson, *Pure Appl. Chem.*, 2000, **72**, 1289–1304.
- 179 K. A. Jorgensen, *Chem. Rev.*, 1989, **89**, 431–458.
- 180 D. Swern, *Organic Peroxides*, Wiley Interscience, New York, vol. 2., 1971.
- 181 X. Zhou, C. Zhao, J. Yang and S. Zhang, *Energy and Fuels*, 2007, **21**, 7–10.
- 182 G. E. Dolbear and E. R. Skov, *Am. Chem. Soc. Div. Pet. Chem. Prepr.*, 2000, **45**, 375–378.
- 183 US5977403 A, 1999, 6.

- 184 D. E. Clark, *Chem. Heal.*, 2001, **9098**, 12-22.
- 185 E. S. Shanley, in “*Organic Peroxides*”, ed. D. Swern, Wiley Interscience, New York, 1972.
- 186 R. Curci and J. O. Edwards, in *Organic Peroxides*, ed. D. Swern, Wiley Interscience, New York, 1970.
- 187 M. Schultz and K. Kirschke, in *Organic Peroxides*, ed. D. Swern, Wiley Interscience, 1972.
- 188 O. L. Mageli and C. S. Sheppard, in *Organic Peroxides*, ed. D. Swern, Wiley Interscience, New York, 1970.
- 189 J. W. Kück, M. R. Anneser, B. Hofmann, A. Pöthig, M. Cokoja and F. E. Kühn, *ChemSusChem*, 2015, **8**, 4056–4063.
- 190 A. A. S. Oliveira, I. F. Teixeira, T. Christofani, J. C. Tristão, I. R. Guimarães and F. C. C. Moura, *Appl. Catal. B Environ.*, 2014, **144**, 144–151.
- 191 K. Kamata, T. Hirano, S. Kuzuya and N. Mizuno, *J. Am. Chem. Soc.*, 2009, **131**, 6997–7004.
- 192 B. Zhu, Z. L. Lang, L. K. Yan, M. R. S. A. Janjua and Z. M. Su, *Int. J. Quantum Chem.*, 2014, **114**, 458–462.
- 193 C. Venturello and R. D’Aloisio, *J. Org. Chem.*, 1988, **53**, 1553–1557.
- 194 C. Venturello, E. Alneri and M. Ricci, *J. Org. Chem.*, 1983, **48**, 3831–3833.
- 195 S. Sakaue, T. Tsubakino, Y. Nishiyama and Y. Ishii, *J. Org. Chem.*, 1993, **58**, 3633–3638.

- 196 Y. Ishii, K. Yamawaki, T. Ura, H. Yamada, T. Yoshida and M. Ogawa, *J. Org. Chem.*, 1988, **53**, 3587–3593.
- 197 C. Aubry, G. Chottard, N. Platzler, J.-M. Brégeault, R. Thowenot, F. Chauveau, C. Huet, H. Ledonl, E. Ali and C. C. R. A. Sci, *Inorg. Chem.*, 1991, **30**, 4409–4415.
- 198 Y. Ding, W. Zhao, H. Hua and B. Ma, *Green Chem.*, 2008, **10**, 910–913.
- 199 F. M. Collins, A. R. Lucy and C. Sharp, *J. Mol. Catal. A Chem.*, 1997, **117**, 397–403.
- 200 D. Huang, Y. J. Wang, L. M. Yang and G. S. Luo, *Ind. Eng. Chem. Res.*, 2006, **45**, 1880–1885.
- 201 X. Jiang, H. Li, W. Zhu, L. He, H. Shu and J. Lu, *Fuel*, 2009, **88**, 431–436.
- 202 D. Huang, Z. Zhai, Y. C. Lu, L. M. Yang and G. S. Luo, *Ind. Eng. Chem. Res.*, 2007, **46**, 1447–1451.
- 203 C. Venturello and M. Gambaro, *Synthesis (Stuttg.)*, 1989, **4**, 295–297.
- 204 G. D. Yadav and A. A. Pujari, *Org. Process Res. Dev.*, 2000, **4**, 88–93.
- 205 Y. Matoba, H. Inoue, J.-I. Akagi, T. Okabayashi, Y. Ishii and M. Ogawa, *Synth. Commun.*, 1984, **14**, 865–873.
- 206 S. Sakaguchi, S. Watase, Y. Katayama, Y. Sakata, Y. Nishiyama and Y. Ishii, *J. Org. Chem.*, 1994, **58**, 5681–5686.
- 207 H. Yamamoto, M. Tsuda, S. Sakaguchi and Y. Ishii, *J. Org. Chem.*, 1997, **62**, 7174–7177.
- 208 L. Salles, C. Aubry, R. Thouvenot, F. Robert, C. Doremieux-Morin, G. Chottard, H. Ledon, Y. Jeannin and J.-M. Brégeault, *Inorg. Chem.*, 1994, **33**, 871–878.

- 209 D. C. Duncan, R. C. Chambers, E. Hecht and C. L. Hill, *J. Am. Chem. Soc.*, 1995, **117**, 681–691.
- 210 R. A. Sheldon and J. K. Kochi, *Metal-catalyzed oxidations of organic compounds: mechanistic principles and synthetic methodology including biochemical processes*, Academic Press, Michigan, 1981.
- 211 C. L. Hill, in *Advances in Oxygenated Processes vol. 1*, ed. A. L. Baumstark, Jai Press Inc., London, 1988, p. 210.
- 212 M. Hudlicky, *Oxidations in Organic Chemistry*, Wiley VCH, 1990.
- 213 A. H. Tullo, *Chem. Eng. News Arch.*, 2004, **82**, 25–31.
- 214 B. S. Lane and K. Burgess, *Chem. Rev.*, 2003, **103**, 2457–2473.
- 215 J. M. Campos-Martin, G. Blanco-Brieva and J. L. G. Fierro, *Angew. Chemie - Int. Ed.*, 2006, **45**, 6962–6984.
- 216 I. D. Cunningham, T. N. Danks, J. N. Hay, I. Hamerton, S. Gunathilagan and C. Janczak, *J. Mol. Catal. A Chem.*, 2002, **185**, 25–31.
- 217 B. Meunier, *Chem. Rev.*, 1992, **92**, 1411–1456.
- 218 B. Notari, *Adv. Catal.*, 1996, **41**, 253–334.
- 219 C. C. Romão, F. E. Kühn and W. a. Herrmann, *Chem. Rev.*, 1997, **97**, 3197–3246.
- 220 D. E. De Vos, J. L. Meinershagen and T. Bein, *Angew. Chemie Int. Ed*, 1996, **35**, 2211–2213.
- 221 I. V Yudanov, *J. Struct. Chem.*, 2007, **48**, 1227–1244.
- 222 D. I. Metelitsa, *Russ. Chem. Rev.*, 1972, **41**, 807–821.

- 223 I. V Yudanov, C. Di Valentin, P. Gisdakis and N. Rosch, *J. Mol. Catal.*, 2000, **158**, 189–197.
- 224 F. Jin, H. Ding, Y. Luan and G. Wang, *Prog. Chem.*, 2008, **20**, 1886–1895.
- 225 H. Mimoun, I. Seree de Roch and L. Sajus, *Tetrahedron*, 1970, **26**, 37–50.
- 226 H. Mimoun, *Angew. Chemie Int. Ed.*, 1982, **21**, 734–750.
- 227 D. V. Deubel, J. Sundermeyer and G. Frenking, *J. Am. Chem. Soc.*, 2000, **122**, 10101–10108.
- 228 D. R. Sharpless, K.B., Townsend, J.M., Williams, 1972, **94**, 295–296.
- 229 G. Grigoropoulou, J. H. Clark and J. a Elings, *Green Chem.*, 2003, **5**, 1–7.
- 230 B. Freedman, in *Environmental Ecology: The Ecological Effects of Pollution, Disturbance, and Other Stresses*, Academic Press, Inc., London, 2nd edn., 1995, pp. 12–17.
- 231 N. Palaić, K. Sertić-Bionda, D. Margeta and Š. Podolski, *Chem. Eng. J. Biochem. Eng. J.*, 2015, **29**, 323–327.
- 232 European Union, *Off. J. Eur. Union*, 2009, L140/88-L140/113.
- 233 *Tier 3 Gasoline Sulfur Standard's Impact on Gasoline Refining*, 2014.
- 234 J. Gary, G. Handwerk and M. J. Kaiser, *Petroleum Refining.*, CRC Press, London, 5th edn., 2007.
- 235 F. van Looij, P. van der Laan, W. H. . Stork, D. . DiCamillo and J. Swain, *Appl. Catal. A Gen.*, 1998, **170**, 1–12.
- 236 T. C. Ho, *Catal. Today*, 2004, **98**, 3–18.

- 237 I. Mochida, K. Sakanishi, X. Ma, S. Nagao and T. Isoda, *Catal. Today*, 1996, **29**, 185–189.
- 238 T. Takatsuka, S.-I. Inoue and Y. Wada, *Catal. Today*, 1997, **39**, 69–75.
- 239 P. Grancher, *Hydrocarb. Process.*, 1978, **57**, 155–160.
- 240 P. Grancher, *Hydrocarb. Process.*, 1978, **57**, 257–262.
- 241 C. G. Frye and J. F. Mosby, *Chem. Eng. Prog.*, 1967, **63**, 66.
- 242 D. R. Kilanowski, H. Teeuwen, V. H. J. de Beer, B. C. Gates, G. C. A. Schuit and H. Kwart, *J. Catal.*, 1978, **55**, 129–137.
- 243 P. T. Vasudevan and J. L. G. Fierro, *Catal. Rev. - Sci. Eng.*, 1996, **38**, 161–188.
- 244 C. Song, *Catal. Today*, 2003, **86**, 211–263.
- 245 B. C. Gates and H. Topsoe, *Polyhedron*, 1997, **16**, 3213–3217.
- 246 T. Kabe, A. Ishihara and H. Tajima, *Ind. Eng. Chem. Res.*, 1992, **31**, 1577–1580.
- 247 X. Ma, K. Sakanishi and I. Mochida, *Ind. Eng. Chem. Res.*, 1994, **33**, 218–222.
- 248 H. Y. Zhang, G. B. Shan, H. Z. Liu and J. M. Xing, *Chem. Eng. Commun.*, 2007, **194**, 938–945.
- 249 A. W. Bhutto, R. Abro, S. Gao, T. Abbas, X. Chen and G. Yu, *J. Taiwan Inst. Chem. Eng.*, 2016, **62**, 84–97.
- 250 J. M. Campos-Martin, M. C. Capel-Sanchez, P. Perez-Presas and J. L. G. Fierro, *J. Chem. Technol. Biotechnol.*, 2010, **85**, 879–890.
- 251 R. Gatan, P. Barger, V. Gembicki, A. Cavanna and D. Molinari, *ACS Div. Fuel Chem.*

- Prepr.*, 2004, **49**, 577–579.
- 252 A. Seeberger and A. Jess, *Green Chem.*, 2010, **12**, 602–608.
- 253 D. Wang, N. Liu, J. Zhang, X. Zhao, W. Zhang and M. Zhang, *J. Mol. Catal. A Chem.*, 2014, **393**, 47–55.
- 254 U. Domańska, K. Walczak and M. Królikowski, *J. Chem. Thermodyn.*, 2014, **77**, 40–45.
- 255 C. Li, J. Zhang, Z. Li, J. Yin, Y. Cui, Y. Liu and G. Yang, *Green Chem.*, 2016, 3789–3795.
- 256 C. Li, D. Li, S. Zou, Z. Li, J. Yin, A. Wang, Y. Cui, Z. Yao and Q. Zhao, *Green Chem.*, 2013, **15**, 2793–2799.
- 257 M. Muzic, K. Sertic-Bionda, Z. Gomzi, S. Podolski and S. Telen, *Chem. Eng. Res. Des.*, 2010, **88**, 487–495.
- 258 C. Marín-Rosas, L. F. Ramírez-Verduzco, F. R. Murrieta-Guevara, G. Hernández-Tapia and L. M. Rodríguez-Otal, *Ind. Eng. Chem. Res.*, 2010, **49**, 4372–4376.
- 259 J. Bu, G. Loh, C. G. Gwie, S. Dewiyanti, M. Tasrif and A. Borgna, *Chem. Eng. J.*, 2011, **166**, 207–217.
- 260 D. Boniek, D. Figueiredo, A. F. B. Dos Santos and M. A. De Resende Stoianoff, *Clean Technol. Environ. Policy*, 2014, **17**, 29–37.
- 261 K. A. Gray, G. T. Mrachkott and C. H. Squires, *Curr. Opin. Microbiol.*, 2003, **6**, 229–235.
- 262 S. F. Sousa, J. F. M. Sousa, A. C. C. Barbosa, C. E. Ferreira, R. P. P. Neves, A. J. M.

- Ribeiro, P. A. Fernandes and M. J. Ramos, *J. Phys. Chem. A*, 2016, **120**, 5300-5306.
- 263 M. Soleimani, A. Bassi and A. Margaritis, *Biotechnol. Adv.*, 2007, **25**, 570–596.
- 264 P. S. Tam, J. R. Kittrell and J. W. Eldridge, *Ind. Eng. Chem. Res.*, 1990, **29**, 321–324.
- 265 M. A. Safa, R. Al-Majren, T. Al-Shamary, J. Il Park and X. Ma, *Fuel*, 2017, **194**, 123–128.
- 266 A. K. Sharipov and V. R. Nigmatullin, *Chem. Technol. Fuels Oils*, 2005, **41**, 309–312.
- 267 S. Murata, K. Murata, K. Kiden and M. Nomura, *Div. Fuel Chem.*, 2003, **48**, 531.
- 268 A. Attar and W. H. Corcoran, *Ind. Eng. Chem. Prod. Res. Dev.*, 1978, **17**, 102–109.
- 269 S. Otsuki, T. Nonaka, W. Qian, A. Ishihara and T. Kabe, *Sekiyu Gakkaishi (Journal Japan Pet. Institute)*, 1999, **42**, 315–320.
- 270 V. Chandra Srivastava, *RSC Adv.*, 2012, **2**, 759–783.
- 271 Y. Shiraishi, K. Tachibana, T. Hirai and I. Komasaawa, *Ind. Eng. Chem. Res.*, 2002, **41**, 4362–4375.
- 272 Y. Shiraishi, Y. Taki, T. Hirai and I. Komasaawa, *Ind. Eng. Chem. Res.*, 2001, **40**, 1213–1224.
- 273 C. Lanju, G. Shaohui, Z. Dishun, W. Jialin and M. Tong, *Energy Sources, Part A Recover. Util. Environ. Eff.*, 2008, **30**, 370–376.
- 274 F. Al-Shahrani, T. Xiao, S. A. Llewellyn, S. Barri, Z. Jiang, H. Shi, G. Martinie and M. L. H. Green, *Appl. Catal. B Environ.*, 2007, **73**, 311–316.
- 275 K. Yazu, Y. Yamamoto, T. Furuya, K. Miki and K. Ukegawa, *Energy and Fuels*, 2001, **15**, 1535–1536.

- 276 S. Herbstman and J. Patel, *Preprints*, 1982, **27**, 826–836.
- 277 N. D’Alessandro, L. Tonucci, M. Bonetti, M. Di Deo, M. Bressan and A. Morvillo, *New J. Chem.*, 2003, **27**, 989–993.
- 278 D. Borah, M. K. Baruah and I. Haque, *Fuel*, 2001, **80**, 1475–1488.
- 279 M. Te, C. Fairbridge and Z. Ring, *Appl. Catal. A Gen.*, 2001, **219**, 267–280.
- 280 E. V Fedorova, N. P. Zhirkov, A. V Tarakanova, A. A. Ivanov, V. M. Senyavin, A. V Anisimov, E. V Tulyakova and S. A. Surin, *Pet. Chem.*, 2002, **42**, 253–256.
- 281 A. K. Sharipov and V. R. Nigmatullin, *Pet. Chem.*, 2005, **45**, 371–377.
- 282 K. Yazu, Y. Yamamoto, T. Furuya, K. Miki and K. Ukegawa, *Energy and Fuels*, 2001, **15**, 1535–1536.
- 283 M. C. Capel-Sanchez, P. Perez-Presas, J. M. Campos-Martin and J. L. G. Fierro, *Catal. Today*, 2010, **157**, 390–396.
- 284 O. Etemadi and T. F. Yen, *Energy and Fuels*, 2007, **21**, 2250–2257.
- 285 A. de Angelis, P. Pollesel, D. Molinari, J. Parker Wallace O’Neal, A. Frattini, F. Cavani, S. Martins and C. Perego, *Pure Appl. Chem.*, 2007, **79**, IUPAC.
- 286 Z. Karimi and A. R. Mahjoub, *J. Surfaces Interfaces Mater.*, 2013, **1**, 155–162.
- 287 B. Maleki, S. Hemmati, A. Sedrpoushan, S. S. Ashrafi and H. Veisi, *RSC Adv.*, 2014, **4**, 40505–40510.
- 288 B. Karimi, M. Ghoreishi-Nezhad and J. H. Clark, *Org. Lett.*, 2005, **7**, 625–628.
- 289 S. Xun, D. Zheng, S. Yin, Y. Qin, M. Zhang, W. Jiang, W. Zhu and H. Li, *RSC Adv.*, 2016, **6**, 42402–42412.

- 290 M. S. Yang, J. W. Liu and L. K. Li, *Adv. Mater. Res.*, 2011, **216**, 474–478.
- 291 S. Jankowsky, M. M. Hiller, O. Fromm, M. Winter and H. D. Wiemhöfer, *Electrochim. Acta*, 2015, **155**, 364–371.
- 292 M. Carezza, S. Lora and L. Fambri, in *Biomaterials: From Molecules to Engineered Tissue*, eds. N. Hasirci and V. Hasirci, Springer US, Boston, MA, 2004, pp. 113–122.
- 293 A. Kondoh, K. Ando and M. Terada, *Chem. Commun.*, 2013, **49**, 10254–10256.
- 294 E. J. Dufek, M. L. Stone, D. K. Jamison, F. F. Stewart, K. L. Gering, L. M. Petkovic, A. D. Wilson, M. K. Harrup and H. W. Rollins, *J. Power Sources*, 2014, **267**, 347–355.
- 295 H. R. Allcock, *Phosphorus-Nitrogen Compounds*, Academic Press, Inc., London, 1972.
- 296 A. Steiner, in *Polyphosphazenes for Biomedical Applications*, ed. A. K. Andrianov, John Wiley & Sons, Inc., 2009, pp. 411–453.
- 297 V. Chandrasekhar and K. R. J. Thomas, *Appl. Organomet. Chem.*, 1993, **7**, 1–31.
- 298 V. Chandrasekhar and S. Nagendran, *Chem. Soc. Rev.*, 2001, **30**, 193–203.
- 299 M. Gall and M. Breza, *Polyhedron*, 2009, **28**, 521–524.
- 300 K. H. Meyer, W. Lotmar and G. W. Pankow, *Helv. Chem. Acta*, 1936, **19**, 930–948.
- 301 H. R. Allcock, *Chem. Rev.*, 1972, **72**, 315–356.
- 302 M. W. Dougill, *J. Chem. Soc.*, 1963, 3211–3217.
- 303 A. Wilson and D. F. Carroll, *J. Chem. Soc.*, 1960, 2548–2552.
- 304 G. J. Bullen, *J. Chem. Soc. A.*, 1971, 1450–1453.
- 305 V. Luan, a M. Penda, A. Costales, G. A. Carriedo and F. J. Garcı, 2001, 5280–5291.

- 306 A. B. Chaplin, J. A. Harrison and P. J. Dyson, *Inorg. Chem.*, 2005, **44**, 8407–17.
- 307 K. A. R. Mitchell, *Chem. Rev.*, 1969, **69**, 419–419.
- 308 J. Liebig, *Justus Liebigs Ann. Chem.*, 1834, **11**, 139.
- 309 H. N. Stokes, *Am. Chem. J.*, 1895, **17**, 275.
- 310 H. N. Stokes, *Chem. Ber.*, 1895, **28**, 437.
- 311 H. N. Stokes, *Am. Chem. J.*, 1897, **19**, 782.
- 312 M. L. Nielsen, G. Cranford and O. T. Quimby, in *Inorganic Syntheses*, John Wiley & Sons, Inc., 2007, pp. 94–97.
- 313 V. Chandrasekhar, *Adv. Inorg. Chem.*, 2002, **53**, 159–211.
- 314 C. W. Allen, *Chem. Rev.*, 1991, **91**, 119–135.
- 315 M. Yokoyama, H. Cho and M. Sakuma, *kogyo kagaku zasshi*, 1963, **66**, 422–427.
- 316 H. R. Allcock, in *Phosphorus-Nitrogen Compounds*, Academic Press, Inc., London, 1972, pp. 175–204.
- 317 H. R. Allcock, in *Phosphorus-Nitrogen Compounds*, Academic Press, London, 1972, pp. 150–174.
- 318 D. Feakins, *J. Chem. Soc.*, 1964, 4464–4471.
- 319 D. Feakins, W. A. Last, N. Neemuchwala and R. A. Shaw, *J. Chem. Soc.*, 1965, 2804–2811.
- 320 D. Feakins, W. A. Last, N. Nabi and R. A. Shaw, *J. Chem. Soc. A.*, 1966, 1831–1834.
- 321 D. Feakins, S. N. Nabi, R. A. Shaw and P. Watson, *J. Chem. Soc. A.*, 1968, 10–15.

- 322 D. Feakins, W. A. Last, S. N. Nabi, R. A. Shaw and P. Watson, *J. Chem. Soc. A.*, 1969, 196–202.
- 323 D. Feakins, R. A. Shaw and P. Watson, *J. Chem. Soc. A.*, 1969, 2468–2475.
- 324 T. Moeller and S. G. Kokalis, *J. Inorg. Nucl. Chem.*, 1963, **25**, 875–881.
- 325 O. Schmitz-Dumont and H. Kùlkens, *Z. Anorg. Allg. Chem.*, 1938, **238**, 189–200.
- 326 H. Bode, K. Bütow and G. Lienau, *Chem. Ber.*, 1948, **81**, 547–552.
- 327 D. B. Sowerby and L. F. Audrieth, *Chem. Ber.*, 1961, **94**, 2670–2675.
- 328 Z. Tun, A. J. Heston, M. J. Panzner, V. Scionti, D. A. Medvetz, B. D. Wright, N. A. Johnson, L. Li, C. Wesdemiotis, P. L. Rinaldi, W. J. Youngs and C. A. Tessier, *Inorg. Chem.*, 2016, **55**, 3283–3293.
- 329 N. V Mani and A. J. Wagner, *Chem. Commun.*, 1968, 658–660.
- 330 N. V Mani and A. J. Wagner, *Acta Crystallogr. Sect. B Struct. Crystallogr. Cryst. Chem.*, 1971, **27**, 51–58.
- 331 I. I. Vorontsov, D. R. Tur, V. S. Papkov and M. Y. Antipin, *J. Mol. Struct.*, 2009, **928**, 1–11.
- 332 H. R. Allcock, E. C. Bissell and E. T. Shawl, *J. Am. Chem. Soc.*, 1972, **94**, 8603–8604.
- 333 H. R. Allcock, E. C. Bissell and E. T. Shawl, *Inorg. Chem.*, 1973, **12**, 2963–2968.
- 334 Z. Tun, A. J. Heston, M. J. Panzner, D. A. Medvetz, B. D. Wright, D. Savant, V. R. Dudipala, D. Banerjee, P. L. Rinaldi, W. J. Youngs and C. A. Tessier, *Inorg. Chem.*, 2011, **50**, 8937–8945.
- 335 A. J. Heston, M. J. Panzner, W. J. Youngs and C. A. Tessier, *Inorg. Chem.*, 2005, **44**,

- 6518–6520.
- 336 M. A. Benson, S. Zacchini, R. Boomishankar, Y. Chan and A. Steiner, *Inorg. Chem.*, 2007, **46**, 7097–7108.
- 337 J. F. Bickley, R. Bonar-Law, G. T. Lawson, P. I. Richards, F. Rivals, A. Steiner and S. Zacchini, *Dalt. Trans.*, 2003, 1235–1244.
- 338 V. Chandrasekhar, P. Thilagar and B. Murugesu Pandian, *Coord. Chem. Rev.*, 2007, **251**, 1045–1074.
- 339 H. R. Allcock, T. J. Fuller and K. Matsumura, *Inorg. Chem.*, 1982, **21**, 515–521.
- 340 H. R. Allcock, in *Phosphorus-Nitrogen Compounds*, Academic Press, Inc., London, 1972, pp. 134–149.
- 341 P. K. Khatri, B. Singh, S. L. Jain, B. Sain and A. K. Sinha, *Chem. Commun.*, 2011, **47**, 1610–1612.

2. Experimental

This chapter will outline the experimental processes that were used in this study on the development of RPN-POM catalyst systems for multiphase oxidation reactions with hydrogen peroxide. It will begin by discussing the preparation of samples, which includes synthesis of: organoaminocyclotriphosphazene (RPN) catalyst phase-transfer moieties; RPN-POM catalysts; an RPN-POM reaction intermediate; RPN-POM heterogenization on solid silica supports; eutectic RPN mixtures and their salts; and eutectic RPN-POM catalysts. It will then move on to describe the techniques that were used to characterise the structure, stability and properties of these compounds. Finally, it will conclude by outlining the processes for the reaction studies in which the catalysts are used for the epoxidation of olefins and/or oxidative desulfurization of a model diesel fuel with H₂O₂. All materials used were purchased from Sigma-Aldrich, Lancaster or Thermo Fischer Scientific. N₂ and H₂ gasses were supplied by BOC.

2.1 Sample Preparation

2.1.1 Organoaminocyclotriphosphazene Preparation

Alkylaminocyclophosphazenes were prepared with slight modifications to previously reported methods.¹

2.1.1.1 *Hexa(isobutylamino)cyclotriphosphazene*

Isobutylamine (575 mmol) was added to a stirred solution of hexachlorocyclotriphosphazene (28.8 mmol) in toluene (200 mL, dried over KOH pellets) in a 500 mL flask. The mixture, which formed a white precipitate, was heated at reflux for 24 h until the reaction had gone to

completion (monitored with ^{31}P NMR). Aqueous KOH (30%) was added and stirred for 30 min before the mixture was transferred into a separating funnel. The organic layer was separated and most of the solvent was distilled off. The remaining solvent was removed under vacuum to produce a white solid, which was re-crystallised from *n*-pentane to afford the product in 97 % yield (15.8 g). m.p.: 60.5 °C; elemental analysis calcd (%) for $(i\text{BuPN})_6\text{P}_3\text{N}_3$: C 50.77, H 10.65, N 22.20; found: C 50.21, H 10.53, N 21.95; FTIR (KBr powder, cm^{-1}): 3217 (N-H); 2954, 2868 (C-H_{alkyl}), 1466, 1400 (C-C_{alkyl}), 1197, 1089 (P-N); δ ^{31}P NMR (toluene, CDCl_3): 19.6 ppm (s).

2.1.1.2 Hexa(isopropylamino)cyclotriphosphazene

Hexa(isopropylamino)cyclotriphosphazene was synthesised from isopropylamine and hexachlorocyclotriphosphazene similarly to *i*BuPN in 87 % yield. m.p.: 76 °C; elemental analysis calcd (%) for $(i\text{PrNH})_6\text{P}_3\text{N}_3$: C 44.17, H 10.01, N 25.80; found: C 43.15, H 9.82, N 25.51; FTIR (KBr powder, cm^{-1}): 3212 (N-H), 2962 (C-H_{alkyl}), 1400 (C-C_{alkyl}), 1076 (P-N); δ ^{31}P NMR (toluene, CDCl_3): 15.1 ppm (s).

2.1.1.3 Hexa(benzylamino)cyclotriphosphazene

Toluene (200 mL, dried over KOH pellets) was added to hexachlorocyclotriphosphazene (28.8 mmol) in a 1 L flask followed by triethylamine (358 mmol) and benzylamine (578 mmol). The mixture, which formed a white precipitate, was heated at reflux for 24 h until the reaction had gone to completion (monitored with ^{31}P NMR). The mixture was cooled to room temperature to produce a white precipitate (triethylamine hydrochloride), which was filtered off by suction using a Büchner funnel. Filtration was repeated two more times to ensure the precipitate was removed from the solution. The solvent was removed on a rotary evaporator to give a

yellow/brown oil. Hexane (200 mL) was added to the oil and stirred for 15 min, resulting in the formation of a white precipitate. The hexane was then decanted off and petroleum ether (200 mL, b.p. 40-60 °C) was added to the precipitate and heated at reflux for 15 min. The white powder was isolated by filtration using a Büchner funnel in 85 % yield (18.94 g). m.p.: 83 °C; elemental analysis calcd (%) for (PhCH₂NH)₆P₃N₃: C 65.37, H 6.23, N 16.34; found: C 65.17, H 6.24, N 16.09; FTIR (KBr powder, cm⁻¹): 3380, 3176 (N-H), 3032 (C-H_{arom}), 2888 (C-H_{alkyl}), 1602, 1493, 1451 (C-C), 1200 (P-N); δ ³¹P NMR (toluene, CDCl₃): 17.4 ppm (s).

2.1.1.4 Hexa(hexylamino)cyclotriphosphazene

Toluene (40 mL, dried over KOH pellets) was added to hexachlorocyclotriphosphazene (5.76 mmol) in a 250 mL flask followed by hexylamine (115 mmol). The mixture, which fumed and formed clear crystals, was heated at reflux for 24 h until the reaction had gone to completion (monitored with ³¹P NMR). The mixture was cooled to room temperature and washed twice with HCl (2.81 M, 65 mL). The orange/brown solution was stirred for 5 min with 30 wt. % KOH (10 mL). Toluene (30 mL) and H₂O (30 mL) were stirred with the solution for 2 min then separated off. The bulk of the toluene was removed by using a rotary evaporator, leaving an orange/brown oil. The oil was heated under vacuum to 70 °C to remove solvent traces. The oil was slowly cooled to room temperature to produce an orange wax in 86 % yield (3.64 g). m.p.: 40 °C; elemental analysis calcd (%) for (C₆H₁₃NH)₆P₃N₃: C 58.70, H 11.41, N 17.12; found: C 57.9, H 11.40, N 16.70; FTIR (KBr powder, cm⁻¹): 3359 (N-H), 2955, 2927, 2857 (C-H_{alkyl}), 1465, 1405 (C-C_{alkyl}), 1254, 1093 (P-N); δ ³¹P NMR (CDCl₃): 18.4 ppm (s).

2.1.2 RPN-POM Preparation

RPN-POM aggregates were obtained by dissolving heteropoly acid hydrates (0.1 mmol) and phosphazenes (0.3 – 0.6 mmol) in methanol at 40 °C. The salt aggregates crystallised upon slow evaporation of the solvent at room temperature and were isolated by filtration using a Büchner funnel.

Samples detailed in this section were synthesized and isolated prior to this study. Analysis of 6:1 [RPN]/[POM] samples will be included as they are believed to closely resemble assemblies formed *in situ* in biphasic systems in the absence of H₂O₂.

2.1.2.1 BzPN-PW

Elemental analysis calcd (%) for (BzPN)₆-PW: C 40.23, H 3.91, N 10.06, W 29.37, P 7.42; found: C 37.12, H 3.55, N 9.25, W 27.65, P 8.40; FTIR, cm⁻¹: 3570 (N-H), 2978 (C-H_{alkyl}), 1547 (C-C_{arom}), 1392, 1258 (C-C_{alkyl}), 1188 (P-N), 1072 (P-O), 944 (W=O), 795, 636 (W-O-W_{bridge}); δ ³¹P NMR (CDCl₃): 14.3 ppm (s, br, [BzPNH]⁺). -10.5 (s, br, PW); UV/vis, λ_{max} (nm): 260 (W-O); TGA: -33.6 % wt. (100-550 °C).

2.1.2.2 iBuPN-PW

Elemental analysis calcd (%) for (iBuPN)₆-PW: C 27.46, H 5.82, N 12.02, W 35.37, P 8.87; found: C 22.39, H 4.98, N 6.28, W 17.56, P 4.44; FTIR, cm⁻¹: 3300 (N-H), 2970 (C-H_{alkyl}), 1385 (C-C_{alkyl}), 1138 (P-N), 1045 (P-O), 945 (W=O), 894, 783 (W-O-W_{bridge}); δ ³¹P NMR (CDCl₃): 10.3 ppm (m, br, [iBuPNH]⁺). -10.5 (s, br); UV/vis, λ_{max} (nm): 263.9 (W-O); TGA: -26.5 % wt. (150-575 °C).

2.1.2.3 *iPrPN-PW*

Elemental analysis calcd (%) for (iBuPN)₆-PW: C 22.40, H 5.08, N 13.07, W 38.16, P 9.64; found: C 20.72, H 4.61, N 12.23, W 29.01, P 8.04; FTIR, cm⁻¹: 3210 (N-H), 2970 (C-H_{alkyl}), 1384, 1254 (C-C_{alkyl}), 1138 (P-N), 1045 (P-O), 941 (W=O), 894, 810 (W-O-W_{bridge}); δ ³¹P NMR (CDCl₃): 9.7 ppm (m, br, [iPrPNH]⁺), -11 (s, br); UV/vis, λ_{max} (nm): 263.9 (W-O); TGA: -26.4 % wt. (150-575 °C).

2.1.3 Preparation of Intermediate [W(O₂)₄](iBuPNH)₂

H₂WO₄ (1.00 mmol) was dissolved in 30 % w/v H₂O₂ (0.167 mol) and stirred for 20 min at 60 °C. The solution was then allowed to cool to room temperature and *i*BuPN (3.00 mmol) in toluene (5 mL) was added and stirred at room temperature for a further 10 min. A white/yellow powder precipitated out of the mixture, which was filtered under low pressure and washed with toluene to obtain the product in 92 % yield (1.99 g). M.p.: 82 °C; FTIR (KBr powder, cm⁻¹): 3275 (N-H), 2955 (CH₃), 2872 (CH₂), 1470 (C-C), 1082 (P-N), 821 (ν_{sym} (O-O)), (ν_{sym} W-(O₂)); δ ³¹P NMR (CDCl₃ solvent and lock): 15.3 ppm (s, P-*i*BuPN).

2.1.4 Preparation of POM/RPN-SiO₂

2.1.4.1 Preparation of RPN-SiO₂

Hypersil APS-2 (2 g, 0.8 mmol aminopropyl groups), dry toluene (40 mL), hexachlorocyclotriphosphazene (P₃N₃Cl₆) (0.8 mmol) and triethylamine (20 mmol) were added to a 250 mL two-neck round bottomed flask equipped with a magnetic stirring bar, a reflux condenser and a bubbler. The flask was flushed through with nitrogen at ambient temperature for 5 min. The mixture was then heated to reflux (120 °C) under nitrogen with stirring and left

for 24 h. Then the mixture was left to cool to room temperature. Nitrogen flow was stopped, the bubbler was removed and primary amine RNH₂ (R= benzyl (Bz), *iso*-butyl (iBu) or *iso*-propyl (iPr), 8 mmol) in dry toluene (10 mL) was added to the mixture. This was then heated to reflux (120 °C) with stirring and left for 24 h. The mixture (faint yellow/brown coloured) was then cooled to room temperature forming clear crystals and a yellow/brown powder. The mixture was then filtered and washed with toluene under low pressure to produce a mix of white powder/white crystals. These were transferred to a beaker with methanol (20 mL); the resulting creamy/white precipitate was stirred for 10 min and then filtered and washed with methanol under low pressure to give a white powder. The powder was stirred with aqueous KOH (30 mL, 10% w/v) for 5 min, filtered under low pressure, washed with distilled H₂O and dried under vacuum in a desiccator.

2.1.4.2 *iBuPN-Modified Hypersil APS-2 (iBuPN-SiO₂)*

Elemental analysis calcd (%) for 0.12 mmol g⁻¹ loading of iBuPN: C 3.13, N 1.55, P 1.16; found: C 3.69, N 1.87, P 1.15; FTIR (KBr powder, Hypersil APS-2 background, cm⁻¹): 3335 (N-H), 2963, 2876 (C-H_{alkyl}), 1466, 1406 (C-C_{alkyl}), 1114 (P-N); δ ³¹P DE (Direct-Excitation with ¹H high power decoupling) NMR (161.9 MHz, 12 kHz MAS (Magic Angle Spinning)): (R'/R'' = Pr or iBu), 18 and 14 ppm {P(NHR')NHR''}, 9 and 4 ppm {P(=O)NHR'}, -3 ppm (PO₂); δ ²⁹Si CP (Cross-Polarization) NMR (79.4 MHz, 10 kHz MAS): -59 ppm (T²), -67 ppm (T³), -102 ppm (Q³), -111 ppm (Q⁴); δ ¹³C CP NMR (100.5 MHz, 10 kHz MAS): 49, 30 and 19 ppm (iBuNH), 43, 25 and 10 ppm (PrNH); iBuPN loading was found to be 0.12 mmol g⁻¹ determined by P content from ICP analysis.

2.1.4.3 BzPN-Modified Hypersil APS-2 (BzPN-SiO₂)

Elemental analysis calcd (%) for 0.14 mmol g⁻¹ loading of BzPN: C 5.71, N 1.76, P 1.30; found: C 5.58, N 1.88, P 1.32. FTIR (KBr powder, Hypersil APS-2 background, cm⁻¹): 3403 (N-H), 3248 (N-H broad), 3028 (C-H_{arom}), 2849 (C-H_{alkyl}), 1664, 1496 (C-C), 1448 (C-C_{alkyl}), 1274, 1107 (P-N), 878 (P-O), 731, 699 (C-H_{arom}); δ ³¹P DE NMR (161.9 MHz, 12 kHz MAS): (R'/R'' = Pr or Bz), 19 and 14 ppm {P(NHR')NHR''}, 5 ppm {P(=O)NHR'}, -3 ppm (PO₂); δ ²⁹Si CP NMR (79.4 MHz, 10 kHz MAS): -59 ppm (T²), -67 ppm (T³), -102 ppm (Q³), -111 ppm (Q⁴); δ ¹³C CP NMR (100.5 MHz, 14 kHz MAS): 142, 128 and 45 ppm (BzNH), 43, 25 and 10 ppm (PrNH); BzPN loading was found to be 0.14 mmol g⁻¹ determined by P content from ICP analysis.

2.1.4.4 iPrPN-Modified Hypersil APS-2 (iPrPN-SiO₂)

Elemental analysis calcd (%) for 0.14 mmol g⁻¹ loading of iPrPN: C 3.02, N 1.76, P 1.30; found: C 3.17, N 1.73, P 1.29. FTIR (KBr powder, Hypersil APS-2 background, cm⁻¹): 3333 (N-H), 3225 (N-H broad), 2971, 2880 (C-H_{alkyl}), 1466, 1409 (C-C_{alkyl}), 1310 (P-N), 896 (P-O), 718, 650, 626; δ ³¹P DE NMR (161.9 MHz, 12 kHz MAS): (R'/R'' = Pr or iPr), 18 and 12 ppm {P(NHR')NHR''}, 5 ppm {P(=O)R'}, -2 ppm (PO₂); δ ²⁹Si CP NMR (79.4 MHz, 10 kHz MAS): -59 ppm (T²), -67 ppm (T³), -102 ppm (Q³), -111 ppm (Q⁴); δ ¹³C CP NMR (100.5 MHz, 10 kHz MAS): 43 and 24 ppm (iPrNH), 43, 25 and 10 ppm (PrNH); iPrPN loading was found to be 0.14 mmol g⁻¹ determined by P content from ICP analysis.

2.1.4.5 Preparation of PMo/BzPN-SiO₂

H₃PMo₁₂O₄₀ (0.0332 g, 0.014 mmol), BzPN-SiO₂ (0.1 g, 0.014 mmol surface BzPN groups), H₂O (0.3 mL) and heptane (10 mL) was stirred in a 50 ml beaker at ambient temperature and

pressure for 30 min. The product, a yellow powder, was then filtered under low pressure and washed with heptane. The powder was dried under vacuum overnight; it gradually turned yellow-green. Elemental analysis calcd (%) for [PMo]/[BzPN] = 1:1 mol/mol loading: C 4.55 and N 1.41; found: C 4.37, N 1.55. FTIR (KBr powder, Hypersil APS-2 background, cm^{-1}): 3577 (N-H), 3346 (N-H), 1408 (C-C), 1328 (P-N), 1099 (P-O), 965 (Mo=O), 874, 818 (Mo-O-Mo_{bridge}); δ ^{31}P DE NMR (161.9 MHz, 12 kHz MAS): (R'/R'' = Pr or Bz), 11 ppm {P(NHR')NHR''}, -3.7 and -4.4 ppm (PMo); δ ^{29}Si CP NMR (79.4 MHz, 10 kHz MAS): -59 ppm (T²), -67 ppm (T³), -102 ppm (Q³), -111 ppm (Q⁴); δ ^{13}C CP NMR (100.5 MHz, 14 kHz MAS): 140, 128 and 45 ppm (BzNH), 43, 25 and 10 ppm (PrNH).

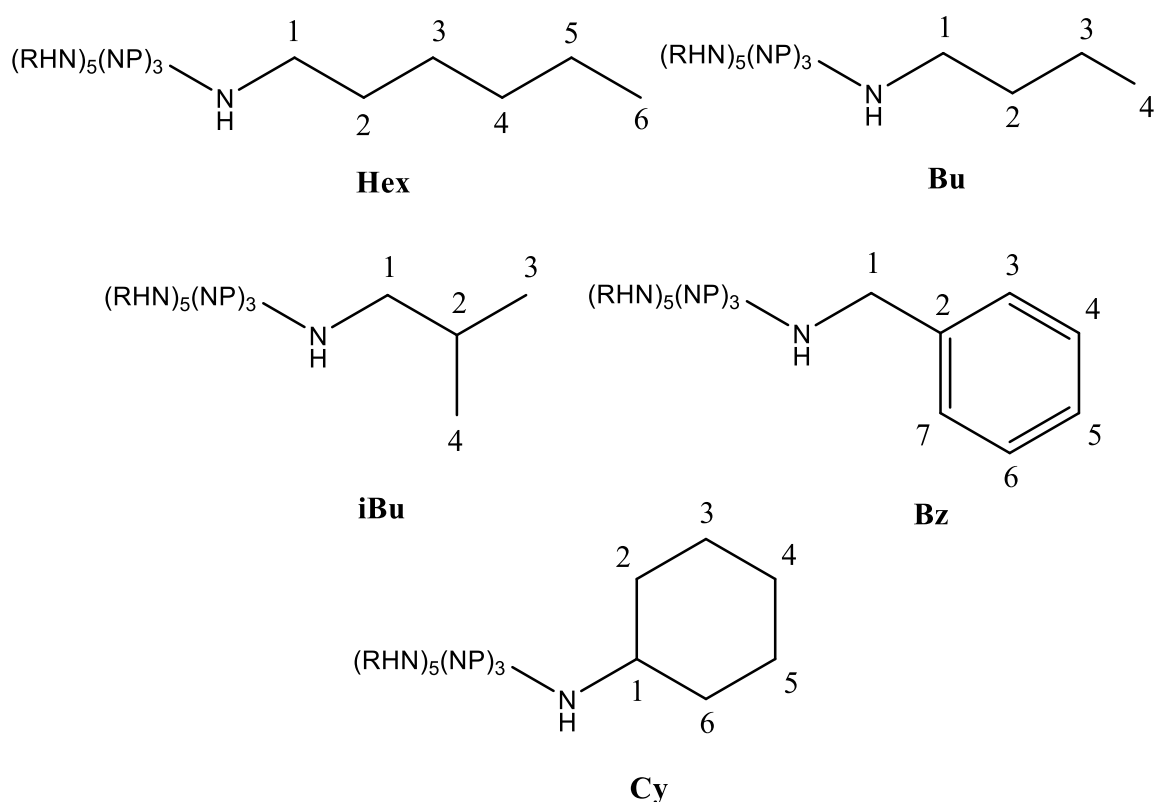
2.1.5 Preparation of Eutectic RPN-POMs

Synthesis of, and data collection for, samples in this section was done by Rebekah Upton (masters student) under the supervision of Dr A. Steiner and I. Analysis and discussion of the data in this manuscript is my own work.

2.1.5.1 Preparation of Eutectic RPNs

Hexachlorocyclotriphosphazene (5.75 mmol) was added to a 250 mL two-necked round bottomed flask equipped with a Schlenk line, a septum cap on one neck, a reflux condenser, oil bath, and a hot plate with a thermoregulator and magnetic stirrer. The flask was flushed with nitrogen to create an inert atmosphere. Dry toluene (100 mL) was injected into the flask and stirred to dissolve hexachlorocyclotriphosphazene. Amines (2 or 3 different amines) - dried over molecular sieves and pre-mixed in a vial prior to addition - were injected into the flask. The reaction mixture was stirred and heated to reflux under a N₂ atmosphere for 24 hours. After 24 hours, the mixture was filtered under vacuum. The filtrate was worked-up in a separation flask with three HCl_{aq} (80 mL, 1 M) washes, one Milli-Q water wash, one KOH_{aq} (6 g, 50 mL)

wash, and one distilled water wash. The organic layer was then stirred for 30 minutes at ambient conditions over ground KOH pellets, separated by decantation and the solvent was removed using a rotary evaporator to yield the final product. Carbons and hydrogens have been assigned for each R group as illustrated below:



Scheme 2.1. Carbon and hydrogen assignments for RPN R groups.

2.1.5.1.1 HexBzPN

Pale yellow liquid/wax; 3.45 g, 84.35%; elemental analysis calcd (%): C 60.74, H 8.50, N 17.71; found: C 61.09, H 8.74, N 16.34; FTIR (cm^{-1}): 3400 (N-H), 3208 (N-H broad), 3063, 3029 (C-H_{arom}), 2955, 2926 2856 ($\text{C-H}_{\text{alkyl}}$), 1597, 1552, 1495 (C=C_{arom}), 1453, 1400 ($\text{C-C}_{\text{alkyl}}$) 1170, 1089, 1067 (P-N), 900, 776, 727, 695; $\delta^{31}\text{P}$ NMR (162 MHz, CDCl_3): 18.22 (m); $\delta^1\text{H}$

NMR (400 MHz, CDCl₃): 7.27 (m, BzNH), 4.14 (s, CH₂ BzNH), 4.11 (s, NH HexNH/BzNH), 2.89 (s, CH₂; C1 HexNH), 1.44 (s, CH₂; C2 HexNH), 1.25 (t, CH₂; C3, C4, C5 HexNH), 0.85 (m, CH₃, HexNH); m/z (A= HexNH, B= BzNH): 736.6 (1.2%, M+H⁺, A₆), 742.6 (16, M+H⁺, A₅B), 748.5 (75, M+H⁺, A₄B₂), 754.5 (100, M+H⁺, A₃B₃), 760.4 (41, M+H⁺, A₂B₄), 766.4 (5, M+H⁺, AB₅), 772.3 (0.5, M+H⁺, B₆).

2.1.5.1.2 HexCyPN

Pale yellow liquid; 4.11 g, 97.86%; elemental analysis calcd (%): C 59.23, H 10.77, N 17.27; found: C 59.17, H 11.42, N 16.99; FTIR (cm⁻¹): 3500 (N-H), 3177 (N-H broad), 2956, 2923, 2854 (C-H_{alkyl}), 1466, 1400, (C-C_{alkyl}), 1165, 1088, 1050 (P-N), 998, 888, 856, 772, 723; δ ³¹P NMR (162 MHz, CDCl₃): 18.11 (m), 16.70 (m); δ ¹H NMR (400 MHz, CDCl₃): 3.06 (s, NH HexNH/CyNH), 2.86 (m, CH CyNH/ CH₂; C1 HexNH), 2.03 (m, CH₂; C2 HexNH), 1.68/1.46 (m, CH₂; C2, C4, C6 CyNH), 1.27 (m, CH₂; C3, C4, C5 HexNH/ C3, C5 CyNH), 0.87 (t, CH₃ HexNH); m/z (A= CyNH, B= HexNH): 728.5 (1%, M+H⁺, A₄B₂), 730.6 (7, M+H⁺, A₃B₃), 732.6 (53.5, M+H⁺, A₂B₄), 734.6 (100, M+H⁺, AB₅), 736.6 (29, M+H⁺, B₆).

2.1.5.1.3 CyBzPN

Pale yellow liquid; 3.84 g, 94.58%; elemental analysis calcd (%): C 61.26, H 7.71, N 17.86; found: C 64.18, H 7.08, N 16.53; FTIR (cm⁻¹): 3384 (N-H), 3180 (N-H broad), 3062, 3027 (C-H_{arom}), 2925, 2950, 2850 (C-H_{alkyl}), 1604, 1494 (C-C_{arom}), 1451, 1402, (C-C_{alkyl}), 1179, 1090, 1065, 1027 (P-N), 903, 776, 723, 693; δ ³¹P NMR (162 MHz, CDCl₃): 17.90 (m), 16.48 (m); δ ¹H NMR (400 MHz, CDCl₃): 7.21 (m, BzNH), 4.06 (m, CH₂ BzNH), 3.87 (s, NH; BzNH), 3.08 (m, NH; CyNH), 2.40 (m, CH CyNH), 1.87 (s, CH₂; C2, C6; CyNH), 1.55 (m, CH₂; C2, C4, C6 CyNH), 1.00 (m, CH₂; C3, C5 CyNH); m/z (A= CyNH, B= BzNH): 732.5 (0.1%, M+H⁺,

A₅B), 740.5 (2, M+H⁺, A₄B₂), 748.4 (13, M+H⁺, A₃B₃), 756.4 (72, M+H⁺, A₂B₄), 764.3 (100, M+H⁺, AB₅), 772.3 (24, M+H⁺, B₆).

2.1.5.1.4 HexBzCyPN

Yellow liquid; 3.27 g, 79.37%; elemental analysis calcd (%): C 60.40, H 9.01, N 17.61; found: C 62.21, H 9.36, N 16.62; FTIR (cm⁻¹): 3384 (N-H), 3209 (N-H broad), 3063, 3028 (C-H_{arom}), 2955, 2924, 2853 (C-H_{alkyl}), 1494, (C-C_{arom}), 1452, 1397 (C-C_{alkyl}) 1179, 1089, 1028 (P-N), 902, 843, 779, 728, 696; δ ³¹P NMR (162 MHz, CDCl₃): 18.18 (m), 16.60 (m); δ ¹H NMR (400 MHz, CDCl₃): 7.29 (m, BzNH), 4.15 (m, CH₂, BzNH), 3.08br (s, NH), 2.88br (s, CH₂; C1 HexNH), 2.46 (m, CH, CyNH), 2.05 (m, CH₂; C2, C6 CyNH), 1.66 (m, CH₂; C2 HexNH), 1.44 (m, CH₂; C2, C4, C6 CyNH), 1.27 (t, CH₂; C3, C4, C5 HexNH/ CH₂; C3, C5 CyNH), 1.10 (m, CH₂; C3, C5 CyNH), 0.87 (t, CH₃ HexNH); m/z (A= CyNH, B= HexNH, C= BzNH): 724.5 (0.1%, M+H⁺ - A₆), 726.9 (1, M+H⁺, A₅B), 729.5 (1, M+H⁺, A₄B₂), 730.6 (2, M+H⁺, A₃B₃), 732.6 (7, M+H⁺, A₂B₄/ A₅C), 734.6 (14, M+H⁺, A₄BC/ AB₅), 736.6 (12, M+H⁺, A₃B₂C/B₆), 738.5 (15, M+H⁺, A₂B₃C), 740.5 (74, M+H⁺, A₄C₂/AB₄C), 742.5 (52, M+H⁺, A₃BC₂/B₅C), 744.5 (22.5, M+H⁺, A₂B₂C₂), 746.5 (97, M+H⁺, AB₃C₂), 748.5 (100, M+H⁺, A₃C₃/ B₄C₂), 749.5 (24, M+H⁺, A₂BC₃), 752.4 (42.5, M+H⁺, AB₂C₃), 754.4 (78, M+H⁺, B₃C₃), 766.4 (5, M+H⁺, BC₅), 772.4 (0.1, M+H⁺, C₆).

2.1.5.1.5 HexiBuPN

Pale yellow liquid; 3.35 g, 89.33%; elemental analysis calcd (%): C 55.27, H 11.13, N 19.34; found: C 56.57, H 11.22, N 18.43; FTIR (cm⁻¹): 3400 (N-H), 3209 (N-H broad), 2955, 2925, 2856 (C-H_{alkyl}), 1466, 1397 (C-C_{alkyl}), 1182, 1100, 1050 (P-N); δ ³¹P NMR (162 MHz, CDCl₃): 18.52 (m); δ ¹H NMR (400 MHz, CDCl₃): 2.88 (s, CH₂; C1 HexNH), 2.70 (s, CH₂, iBuNH),

2.07br (d, NH), 1.68 (m, CH, iBuNH), 1.46 (m, CH₂; C2 HexNH), 1.27br (m, CH₂; C3, 4, 5 HexNH), 0.88 (m, CH₃, HexNH/iBuNH); m/z (A= iBuNH, B= HexNH): 568.4 (2.2%, M+H⁺, A₆), 596.4 (25, M+H⁺, A₅B), 624.5 (73, M+H⁺, A₄B₂), 652.5 (100, M+H⁺, A₃B₃), 680.5 (67, M+H⁺, A₂B₄), 708.6 (21, M+H⁺, AB₅), 736.6 (3, M+H⁺, B₆).

2.1.5.1.6 HexBuPN

Pale yellow liquid; 3.69 g, 98.40%; elemental analysis calcd (%): C 55.27, H 11.13, N 19.34; found: C 55.35, H 11.15, N 18.69; FTIR (cm⁻¹): 3200 (N-H broad), 2950, 2900, 2800 (C-H_{alkyl}), 1465, 1399 (C-C_{alkyl}), 1200, 1125, 1085 (P-N), 951, 775, 727; δ ³¹P NMR (162 MHz, CDCl₃): 18.37br (s); δ ¹H NMR (400 MHz, CDCl₃): 2.87 (m, CH₂; C1 HexNH/BuNH), 2.02 (s, NH), 1.44 (m, CH₂; C2 HexNH/BuNH), 1.28 (m, CH₂; C3,4,5 HexNH), 0.86 (m, CH₃ HexNH/BuNH); m/z (A= iBuNH, B= HexNH): 569.4 (5%, M⁺, A₆), 596.5 (26, M⁺, A₅B), 624.5 (74, M⁺, A₄B₂), 652.5 (100, M⁺, A₃B₃), 680.6 (65, M⁺, A₂B₄), 708.6 (20, M⁺, AB₅), 736.6 (4, M⁺, B₆).

2.1.5.1.7 iBuBuPN

Colourless liquid; 2.49 g, 76.15%; elemental analysis calcd (%): C 50.77, H 10.65, N 22.20; found: C 51.53, H 10.66, N 21.50; FTIR (cm⁻¹): 3400 (N-H), 3210 (N-H broad), 2955, 2929, 2868 (C-H_{alkyl}), 1465, 1398, (C-C_{alkyl}), 1182, 1118, 1083 (P-N), 951, 770, 729; δ ³¹P NMR (162 MHz, CDCl₃): 18.57 (m); δ ¹H NMR (400 MHz, CDCl₃): 2.82/2.63 (s, NH iBuNH/BuNH), 2.05/1.96 (s, CH₂; C1 iBuNH/ CH₂; C1 BuNH), 1.62 (hept, CH iBuNH), 1.39 (m, CH₂; C2 BuNH), 1.27 (m, CH₂; C3 BuNH), 0.83 (m, CH₃ iBuNH/BuNH); m/z (A= iBuNH/BuNH): 568.4 (100%, M+H⁺, A₆), 569.4 (M+2H⁺, A₆).

2.1.5.1.8 HexiBuBuPN

Pale yellow liquid; 3.18 g, 88.58%; elemental analysis calcd (%): C 53.91, H 10.99, N 20.21; found: C 53.14, H 10.76, N 20.49; FTIR (cm^{-1}): 3400 (N-H), 3208 (N-H broad), 2955, 2926, 2858 (C-H_{alkyl}), 1465, 1398 (C-C_{alkyl}), 1182, 1120, 1087 (P-N), 951, 905, 772, 728; δ ^{31}P NMR (162 MHz, CDCl_3): 18.42 (m); δ ^1H NMR (400 MHz, CDCl_3): 2.88 (m, CH_2 ; C1 HexNH/ CH_2 ; C1 BuNH), 2.70 (m, CH_2 iBuNH), 2.12 (s, NH HexNH), 2.03 (3, NH iBuNH/BuNH), 1.69 (hept, CH iBuNH), 1.46 (m, CH_2 ; C2 HexNH/BuNH), 1.27 (m, CH_2 ; C3, C4, C5 HexNH, C3 BuNH), 0.90 (m, CH_3 HexNH/iBuNH/BuNH); m/z (A= iBuNH/BuNH, B= HexNH): 568.4 (6%, $\text{M}+\text{H}^+$, A_6), 596.4 (75, $\text{M}+\text{H}^+$, A_5B), 624.5 (100, $\text{M}+\text{H}^+$, A_4B_2), 652.5 (57, $\text{M}+\text{H}^+$, A_3B_3), 680.5 (15, $\text{M}+\text{H}^+$, A_2B_4), 708.6 (2, $\text{M}+\text{H}^+$, AB_5).

2.1.5.2 Preparation of Eutectic RPN-Cl and Eutectic RPN- NO_3 IL

Eutectic RPN-X IL prepared in 1:1 stoichiometric ratio $[\text{X}]/[\text{RPN}]$ (where $\text{X} = \text{Cl}^-$ or NO_3^-) based on ionic charges assuming monocationic RPN species were formed *in situ*. A solution of RPN (0.685 mmol) in dichloromethane (10 mL) was first prepared which was then combined with $\text{HCl}_{(\text{aq})}$ or $\text{HNO}_{3(\text{aq})}$ (0.685 mmol) in a flask. The resulting mixture was stirred for 2 hours (20.5 °C). Distilled water (10 mL) was then added and the layers were separated using a separating funnel. The organic layer was then rotary evaporated off to give the final product.

2.1.5.2.1 Eutectic RPN-HCl

2.1.5.2.1.1 HexBzPN-Cl

White wax; 0.47 g, 90 %; m.p. 60-64 °C; elemental analysis calcd (%): C 57.78, H 8.22, N 16.85; found: C 59.34, H 8.49, N 15.89; FTIR (cm^{-1}): 3205 (N-H broad), 3062, 3031 (C-H_{arom}),

2956, 2928, 2857 (C-H_{alkyl}), 2649 (N-H⁺), 1605, 1496 (C-C_{arom}), 1453, 1428 (C-C_{alkyl}), 1236, 1191 1093, 1070 (P-N), 1028, 906,780, 726, 696 (Cl); δ ³¹P NMR (162 MHz, CDCl₃): 13.65 (m); δ ¹H NMR (400 MHz, CDCl₃): 7.27 (m, BzNH), 4.08 (m, CH₂ BzNH), 3.54br (s, NH HexNH/BzNH), 2.84 (m, CH₂; C1 HexNH), 1.43 (m, CH₂; C2 HexNH), 1.24 (t, CH₂; C3, C4, C5 HexNH), 0.85 (m, CH₃, HexNH).

2.1.5.2.1.2 *HexCyPN-Cl*

White wax; 0.49 g, 94 %; m.p. 64-68 °C; elemental analysis calcd (%): C 56.41, H 10.39, N 16.45; found: C 55.33, H 10.77, N 15.98; FTIR (cm⁻¹): 3203 (N-H broad), 2957, 2925, 2854 (C-H_{alkyl}), 2661 (N-H⁺), 1448, 1378 (C-C_{alkyl}), 1239, 1394, 1094 (P-N), 905, 775, 723, 700s (Cl); δ ³¹P NMR (162 MHz, CDCl₃): 12.59 (m); δ ¹H NMR (400 MHz, CDCl₃): 3.04 (s, NH HexNH/CyNH), 2.90 (s, CH CyNH/ CH₂; C1 HexNH), 1.95/1.70/1.51 (m, CH₂; C2 HexNH/ CH₂; C2, C4, C6 CyNH), 1.30 (s, CH₂; C3, C4, C5 HexNH/ C3, C5 CyNH), 0.88 (t, CH₃ HexNH).

2.1.5.2.1.3 *CyBzPN-Cl*

Cream wax; 0.25 g, 78 %; m.p. 48-52 °C; elemental analysis calcd (%): C 58.25, H 7.47, N 16.98; found: C 59.59, H 6.68, N 15.51; FTIR (cm⁻¹): 3369 (N-H), 3186 (N-H broad), 3061, 3029 (C-H_{arom}), 2927, 2852 (C-H_{alkyl}), 2636 (N-H⁺), 1605, 1496 (C-C_{arom}), 1452, 1410, (C-C_{alkyl}), 1236, 1198, 1092, 1069 (P-N), 1027, 912, 779, 727, 694; δ ³¹P NMR (162 MHz, CDCl₃): 12.47 (m); δ ¹H NMR (400 MHz, CDCl₃): 7.26 (m, BzNH), 4.00 (s, CH₂ BzNH), 3.73 (s, NH; BzNH), 2.99 (s, NH; CyNH), 2.36 (s, CH CyNH) 1.85 (s, CH₂; C2, C6; CyNH), 1.50 (d, CH₂; C2,C4, C6 CyNH), 1.13 (t, CH₂; C3, C5 CyNH).

2.1.5.2.1.4 *HexCyBzPN-Cl*

White wax; 0.45 g, 87 %; m.p. 55-60 °C; elemental analysis calcd (%): C 57.47, H 8.71, N 16.76; found: C 58.11, H 8.91, N 15.79; FTIR (cm⁻¹): 3205 (N-H), 3062, 3031 (C-H_{arom}), 2955, 2927, 2856 (C-H_{alkyl}), 2650 (N-H⁺), 1606, 1496 (C-C_{arom}), 1455, 1428, (C-C_{alkyl}), 1236, 1198, 1093, 1070 (P-N), 1028, 907, 780, 726, 695; δ ³¹P NMR (162 MHz, CDCl₃): 12.47 (m); δ ¹H NMR (400 MHz, CDCl₃): 7.27 (m, BzNH), 4.45br (s, NH BzNH) 4.08 (d, CH₂ BzNH), 3.71br (s, NH HexNH/CyNH), 2.85 (m, CH CyNH/ CH₂; C1 HexNH), 1.90 (s, CH₂; C2, C6; CyNH), 1.67 (s, CH₂; C2 HexNH), 1.49 (m, CH₂; C2, C4, C6 CyNH), 1.27 (m, CH₂; C3, C4, C5 HexNH/ CH₂; C3, C5 CyNH), 0.85 (m, CH₃ HexNH).

2.1.5.2.1.5 *HexiBuPN-Cl*

Colourless wax; 0.48 g, 92 %; m.p. 54-58 °C; elemental analysis calcd (%): C 52.35, H 10.69, N 18.31; found: C 52.31, H 10.63, N 17.55; FTIR (cm⁻¹): 3204 (N-H broad), 2956, 2927, 2859 (C-H_{alkyl}), 2718 (N-H⁺), 1466, 1422, (C-C_{alkyl}), 1244, 1200, 1090 (P-N), 915, 773; δ ³¹P NMR (162 MHz, CDCl₃): 12.58 (m); δ ¹H NMR (400 MHz, CDCl₃): 3.70br (s, NH HexNH/iBuNH), 2.90 (s, CH₂; C1 HexNH), 2.73 (s, CH₂ iBuNH), 1.71 (m, CH iBuNH), 1.51 (m, CH₂; C2 HexNH), 1.28 (m, CH₂; C3, C4, C5 HexNH), 0.91 (m, CH₃ HexNH/iBuNH).

2.1.5.2.1.6 *HexBuPN-Cl*

White solid; 0.43 g, 83%; m.p. 73-76 °C; elemental analysis calcd (%): C 52.35, H 10.69, N 18.31; found: C 51.78, H 10.53, N 17.27; FTIR (cm⁻¹): 3212 (N-H broad), 2957, 2927, 2858 (C-H_{alkyl}), 2650 (N-H⁺), 1430 (C-C_{alkyl}), 1236, 1195, 1118 1097 (P-N), 913, 816, 775, 725; δ ³¹P NMR (162 MHz, CDCl₃): 13.20 (d); δ ¹H NMR (400 MHz, CDCl₃): 3.71br (s, NH HexNH/BuNH), 2.91 (s, CH₂; C1 HexNH/ CH₂; C1 BuNH), 1.51 (s, CH₂; C2 HexNH/ CH₂; C2 BuNH), 1.28 (m, CH₂; C3, C4, C5 HexNH/ CH₂; C3 BuNH), 0.91 (m, CH₃ HexNH/BuNH).

2.1.5.2.1.7 *iBuBuPN-Cl*

White solid; 0.50 g, 94 %; m.p. 142-144 °C; elemental analysis calcd (%): C 47.71, H 10.18, N 20.86; found: C 42.00, H 8.93, N 18.28; FTIR (cm⁻¹): 3204 (N-H broad), 2956, 2931, 2869 (C-H_{alkyl}), 2717 (N-H⁺) 1464, 1420 (C-C_{alkyl}), 1243, 1199, 1087 (P-N), 915, 770; δ ³¹P NMR (162 MHz, CDCl₃): 13.42 (d); δ ¹H NMR (400 MHz, CDCl₃): 3.71br (s, NH *i*BuNH/*Bu*NH), 2.92/2.73 (s, CH₂; C1 *i*BuNH/ CH₂; C1 *Bu*NH), 1.73 (m, CH *i*BuNH), 1.50 (m, CH₂; C2 *Bu*NH), 1.33 (m, CH₂; C3 *Bu*NH), 0.93 (m, CH₃ *i*BuNH/*Bu*NH).

2.1.5.2.1.8 *HexiBuBuPN-Cl*

Colourless wax; 0.48 g, 91 %; m.p. 58-64 °C; elemental analysis calcd (%): C 50.93, H 10.53, N 19.09; found: C 50.42, H 10.48, N 18.81; FTIR (cm⁻¹): 3198 (N-H broad), 2956, 2929, 2861 (C-H_{alkyl}), 2718 (N-H⁺), 1417 (C-C_{alkyl}), 1244, 1198, 1090 (P-N), 913, 772, 725; δ ³¹P NMR (162 MHz, CDCl₃): 13.08 (m); δ ¹H NMR (400 MHz, CDCl₃): 2.91 (s, CH₂; C1 HexNH/ CH₂; C1 *i*BuNH/ CH₂; C1 *Bu*NH), 2.73 (s, NH HexNH, *i*BuNH, *Bu*NH), 1.73 (m, CH *i*BuNH), 1.51 (m, CH₂; C2 HexNH/ CH₂; C2 *Bu*NH), 1.28 (m, CH₂; C3, C4, C5 HexNH/ CH₂; C3 *Bu*NH), 0.93 (m, CH₃ HexNH/*i*BuNH/*Bu*NH).

2.1.5.2.1.9 *HexPN-Cl*

White solid; 0.48 g, 92 %; m.p. 106-109 °C; FTIR (cm⁻¹): 3366 (N-H), 3168 (N-H broad), 2958, 2926, 2857 (C-H_{alkyl}), 2708 (N-H⁺), 1466, 1434, 1378 (C-C_{alkyl}), 1243, 1122, 1095 (P-N), 937, 778, 724; δ ³¹P NMR (162 MHz, CDCl₃): 13.89 (m); δ ¹H NMR (400 MHz, CDCl₃): 3.49 (s, NH), 2.90br (s, CH₂; C1), 1.50 (s, CH₂; C2), 1.28 (m, CH₂; C3,4,5), 0.88 (m, CH₃);

2.1.5.2.1.10 *BzPN-Cl*

Cream solid; 0.99 g, 94 %; m.p. 128-130 °C; elemental analysis calcd (%): C 62.41, H 6.07, N 15.60; found: C 62.38, H 6.12, N 15.67; FTIR (cm^{-1}): 3400 (N-H), 3200 (N-H broad), 3100, 3050, 3000 (C-H_{arom}), 2900, 2850, 2800 ($\text{C-H}_{\text{alkyl}}$), 1600, 1500 (C-C_{arom}), 1200, 1100, 1050 (P-N), 700; δ_{P} (162 MHz, CDCl_3) 13.63 (s); δ_{H} (400 MHz, CDCl_3): 7.22 (m, Ar H), 4.03 (s, CH_2), 3.33br (s, NH);

2.1.5.2.2 *Eutectic RPN-NO₃*

2.1.5.2.2.1 *HexBzPN-NO₃*

White wax; 0.53 g, 98 %; m.p. 72-78°C; elemental analysis calcd (%): C 55.80, H 7.94, N 18.08; found: C 57.75, H 8.30, N 16.97; FTIR (cm^{-1}): 3259 (N-H broad), 3062, 3031 (C-H_{arom}), 2956, 2927, 2857 ($\text{C-H}_{\text{alkyl}}$), 2662 (N-H^+), 1605, 1496 (C-C_{arom}), 1363 (NO_3^-), 1452 ($\text{C-C}_{\text{alkyl}}$), 1239, 1197, 1094, 1070 (P-N), 1027, 906, 781, 725, 695; $\delta^{31\text{P}}$ NMR (162 MHz, CDCl_3): 13.43 (m); $\delta^1\text{H}$ NMR (400 MHz, CDCl_3): 7.27 (m, BzNH), 4.07 (m, CH_2 BzNH), 3.30br (s, NH HexNH/BzNH), 2.84 (s, CH_2 ; C1 HexNH), 1.42 (m, CH_2 ; C2 HexNH), 1.24 (t, CH_2 ; C3, C4, C5 HexNH), 0.85 (m, CH_3 , HexNH).

2.1.5.2.2.2 *HexCyPN-NO₃*

White solid; 0.44 g, 81 %; m.p. 60-63 °C; elemental analysis calcd (%): C 54.53, H 10.04, N 17.66; found: C 54.39, H 10.43, N 17.36; FTIR (cm^{-1}): 3272 (N-H broad), 2956, 2925, 2854 ($\text{C-H}_{\text{alkyl}}$), 1345 (NO_3^-), 2662 (N-H^+), 1447 ($\text{C-C}_{\text{alkyl}}$), 1238, 1199, 1100 (P-N), 926, 824, 778, 723; $\delta^{31\text{P}}$ NMR (162 MHz, CDCl_3): 12.26 (m); $\delta^1\text{H}$ NMR (400 MHz, CDCl_3): 3.29 (s, NH HexNH/CyNH), 2.89 (s, CH CyNH/ CH_2 ; C1 HexNH), 1.92/1.68/1.49 (m, CH_2 ; C2 HexNH/

CH₂; C2, C4, C6 CyNH), 1.28 (s, CH₂; C3, C4, C5 HexNH/ C3, C5 CyNH), 0.88 (t, CH₃ HexNH).

2.1.5.2.2.3 *CyBzPN-NO₃*

Cream solid; 0.31 g, 94 %; m.p. 96-102 °C; elemental analysis calcd (%): C 56.24, H 7.21, N 18.22; found: C 56.75, H 6.52, N 16.10; FTIR (cm⁻¹): 3356 (N-H), 3247 (N-H broad), 3062, 3030 (C-H_{arom}), 2928, 2853 (C-H_{alkyl}), 2661 (N-H⁺), 1605, 1496 (C-C_{arom}), 1349 (NO₃⁻), 1452 (C-C_{alkyl}), 1236, 1199, 1100, 1094, 1070 (P-N), 1028, 911, 784, 726, 634; δ ³¹P NMR (162 MHz, CDCl₃): 12.07 (m); δ ¹H NMR (400 MHz, CDCl₃): 7.23 (m, BzNH), 4.01 (s, CH₂ BzNH), 3.71 (s, NH BzNH), 2.99br (s, NH CyNH), 2.45br (s, CH CyNH), 1.85 (m, CH₂; C2, C6; CyNH), 1.62br (s, CH₂; C2, C4, C6 CyNH), 1.13 (m, CH₂; C3, C5 CyNH).

2.1.5.2.2.4 *HexCyBzPN-NO₃*

White solid; 0.50 g, 93 %; m.p. 82-85 °C; elemental analysis calcd (%): C 55.51, H 8.41, N 17.98; found: C 56.65, H 8.62, N 17.19; FTIR (cm⁻¹): 3261 (N-H broad), 3063, 3031 (C-H_{arom}), 2956, 2927, 2856, 2825 (C-H_{alkyl}), 2650 (N-H⁺), 1606, 1496 (C-C_{arom}), 1348 (NO₃⁻), 1451 (C-C_{alkyl}), 1237, 1198, 1099, 1071 (P-N), 1028, 907, 782, 726, 695; δ ³¹P NMR (162 MHz, CDCl₃): 12.44 (m); δ ¹H NMR (400 MHz, CDCl₃): 7.26 (m, BzNH), 4.11 (s, CH₂ BzNH), 3.26br (s, NH BzNH), 3.05br (s, NH HexNH/CyNH), 2.87 (m, CH CyNH/ CH₂; C1 HexNH), 1.88 (s, CH₂; C2, C6; CyNH), 1.66 (s, CH₂; C2 HexNH), 1.43 (m, CH₂; C2, C4, C6 CyNH), 1.24 (m, CH₂; C3, C4, C5 HexNH/ CH₂; C3, C5 CyNH), 0.85 (m, CH₃ HexNH).

2.1.5.2.2.5 *HexiBuPN-NO₃*

White wax; 0.46 g, 84 %; m.p. 52-58 °C; elemental analysis calcd (%): C 50.40, H 10.29, N 19.59; found: C 50.90, H 10.28, N 19.04; FTIR (cm⁻¹): 3270 (N-H broad), 2730 (N-H⁺), 2956,

2927, 2859 (C-H_{alkyl}), 1347 (NO₃⁻), 1437 (C-C_{alkyl}), 1237, 1199, 1097 (P-N), 927, 827, 778, 724; δ ³¹P NMR (162 MHz, CDCl₃): 13.41 (m); δ ¹H NMR (400 MHz, CDCl₃): 3.36br (d, NH HexNH/iBuNH), 2.89 (s, CH₂; C1 HexNH), 2.73 (s, CH₂ iBuNH), 1.71 (m, CH iBuNH), 1.49 (m, CH₂; C2 HexNH), 1.28 (m, CH₂; C3, C4, C5 HexNH), 0.90 (m, CH₃ HexNH/iBuNH).

2.1.5.2.2.6 *HexBuPN-NO₃*

White solid; 0.50 g, 91 %; m.p. 44-51 °C; elemental analysis calcd (%): C 50.40, H 10.29, N 19.59; found: C 51.23, H 10.38, N 19.24; FTIR (cm⁻¹): 3263 (N-H broad), 2675 (N-H⁺), 2957, 2927, 2859 (C-H_{alkyl}), 1343 (NO₃⁻), 1440, 1375 (C-C_{alkyl}), 1238, 1196, 1118, 1094, 1041 (P-N), 918, 827, 777, 726; δ ³¹P NMR (162 MHz, CDCl₃): 13.32(m); δ ¹H NMR (400 MHz, CDCl₃): 2.90 (s, CH₂; C1 HexNH/ CH₂; C1 BuNH), 1.48 (m, CH₂; C2 HexNH/ CH₂; C2 BuNH), 1.28 (m, CH₂; C3, C4, C5 HexNH/ CH₂; C3 BuNH), 0.91 (m, CH₃ HexNH/BuNH).

2.1.5.2.2.7 *iBuBuPN-NO₃*

White solid; 0.51 g, 91 %; m.p. 130-132 °C; elemental analysis calcd (%): C 45.70, H 9.75, N 22.21; found: C 45.36, H 9.66, N 22.19; FTIR (cm⁻¹): 3275 (N-H broad), 2957, 2932, 2869 (C-H_{alkyl}), 2720 (N-H⁺), 1348 (NO₃), 1436 (C-C_{alkyl}), 1237, 1200, 1093, 1042 (P-N), 918, 827, 774, 732, 673; δ ³¹P NMR (162 MHz, CDCl₃): 13.39 (s); δ ¹H NMR (400 MHz, CDCl₃): 3.34br (d, NH iBuNH/BuNH), 2.91/2.73 (s, CH₂; C1 iBuNH/ CH₂; C1 BuNH), 1.71 (m, CH iBuNH), 1.49 (m, CH₂; C2 BuNH), 1.34 (m, CH₂; C3 BuNH), 0.90 (m, CH₃ iBuNH/BuNH).

2.1.5.2.2.8 *HexiBuBuPN-NO₃*

Colourless wax; 0.49 g, 89 %; m.p. 34-39 °C; elemental analysis calcd (%): C 48.96, H 10.13, N 20.39; found: C 49.78, H 10.27, N 20.14; FTIR (cm⁻¹): 3272 (N-H broad), 2956, 2928, 2860 (C-H_{alkyl}), 2671 (N-H⁺), 1367 (NO₃⁻), 1428 (C-C_{alkyl}), 1240, 1194, 1092, 1042 (P-N), 925, 827,

775, 726; δ ^{31}P NMR (162 MHz, CDCl_3): 14.07 (s); δ ^1H NMR (400 MHz, CDCl_3): 2.90 (s, CH_2 ; C1 HexNH/ CH_2 ; C1 iBuNH/ CH_2 ; C1 BuNH), 2.72 (s, NH HexNH, iBuNH, BuNH), 1.71 (m, CH iBuNH), 1.48 (m, CH_2 ; C2 HexNH/ CH_2 ; C2 BuNH), 1.28 (m, CH_2 ; C3, C4, C5 HexNH/ CH_2 ; C3 BuNH), 0.90 (m, CH_3 HexNH/iBuNH/BuNH).

2.1.5.2.2.9 HexPN- NO_3

White solid; 0.50 g, 93 %; m.p. 90-93 °C; FTIR (cm^{-1}): 3272 (N-H broad), 2956, 2928, 2860 ($\text{C-H}_{\text{alkyl}}$), 2662 (N-H^+), 1367 (NO_3^-), 1428 ($\text{C-C}_{\text{alkyl}}$), 1240, 1194, 1092, 1042 (P-N), 925, 827, 775, 726; δ ^{31}P NMR (162 MHz, CDCl_3): 14.32br (s); δ ^1H NMR (400 MHz, CDCl_3): 2.89 (s, CH_2 ; C1), 2.67br (s, NH), 1.48, (m, CH_2 ; C2), 1.28 (m, CH_2 ; C3,4,5), 0.88 (m, CH_3).

2.1.5.2.2.10 BzPN- NO_3

Cream solid; 0.91 g, 83 %; m.p. 129-133 °C; FTIR (cm^{-1}): 3400 (N-H), 3200 (N-H broad), 3050, 3000, 2950 (C-H_{arom}), 2900, 2800 ($\text{C-H}_{\text{alkyl}}$), 1600 (C-C_{arom}), 1380 (NO_3^-), 1250, 1100, 1075 (P-N); elemental analysis calcd (%): C 60.43, H 5.88, N 16.79; found: C 58.98, H 5.95, N 16.19; δ ^{31}P NMR (162 MHz, CDCl_3): 12.91 (m); δ ^1H NMR (400 MHz, CDCl_3): 7.22 (m, Ar H), 4.00 (s, CH_2), 3.25br (s, NH).

2.1.5.3 Preparation of Eutectic RPN-POM IL Catalysts

RPN-POM IL catalysts were prepared in stoichiometric ratios $[\text{POM}]/[\text{RPN}]$ based on anionic charge of POM and assuming formation of monocationic RPN species *in situ*. A solution of RPN (0.345 mmol) in ethanol (3 mL) and a solution of POM (0.114 mmol) in ethanol (3 mL) were combined in a flask and stirred at room temperature for 2 hours. The solvent was then removed by rotary evaporation.

2.1.5.3.1 *HexBzPN-PMo*

Green glass; 0.43 g, 93.48%; m.p. 50-57 °C; elemental analysis calcd (%): C 32.77, H 4.58, N 9.55; found: C 31.71, H 4.65, N 8.61; FTIR (cm⁻¹): 3500 (N-H), 3351 (N-H broad), 3063, 3031 (C-H_{arom}), 2956, 2927, 2857 (C-H_{alkyl}), 1496 (C-C_{arom}), 1454, 1406 (C-C_{alkyl}), 1254, 1092 (P-N), 1059 (P-O), 951 (Mo=O), 877, 798 (Mo-O-Mo); δ ³¹P NMR (162 MHz, CDCl₃): 11.97 (m, RPN), -3.69 (s, PMo); δ ¹H NMR (400 MHz, CDCl₃): 7.26 (m, BzNH), 4.16br (s, CH₂ BzNH), 3.28br (s, NH HexNH/BzNH), 2.92 (s, CH₂; C1 HexNH), 1.47br (s, CH₂; C2 HexNH), 1.22 (m, CH₂; C3, C4, C5 HexNH), 0.84 (m, CH₃, HexNH).

2.1.5.3.2 *HexCyPN-PMo*

Green viscous liquid; 0.41 g, 87.23%; elemental analysis calcd (%): C 32.33, H 5.88, N 9.43; found: C 31.34, H 6.12, N 9.22; FTIR (cm⁻¹): 3545 (N-H), 3360 (N-H broad), 2954, 2927, 2855 (C-H_{alkyl}), 1495, 1451, 1407 (C-C_{alkyl}), 1252, 1093 (P-N), 1059 (P-O), 952 (Mo=O), 875, 791 (Mo-O-Mo); δ ³¹P NMR (162 MHz, CDCl₃): 11.30 (m, RPN), -3.76 (s, PMo); δ ¹H NMR (400 MHz, CDCl₃): 3.72br (s, NH HexNH/CyNH), 2.90 (s, CH CyNH/ CH₂; C1 HexNH), 1.93/1.69/1.51 (m, CH₂; C2 HexNH/ CH₂; C2, C4, C6 CyNH), 1.28 (s, CH₂; C3, C4, C5 HexNH/ C3, C5 CyNH), 0.88 (t, CH₃ HexNH).

2.1.5.3.3 *BzCyPN-PMo*

Green solid; 0.43 g, 89.58%; m.p. 96-104 °C; elemental analysis calcd (%): C 32.92, H 4.14, N 9.60; found: C 30.95, H 3.54, N 8.12; FTIR (cm⁻¹): 3400 (N-H broad), 3050, 3000 (C-H_{arom}), 2900, 2850 (C-H_{alkyl}), 1600, 1500 (C-C_{arom}), 1453, 1405 (C-C_{alkyl}), 1250, 1100 (P-N), 1050 (P-O), 950 (Mo=O), 900 and 775 (Mo-O-Mo); δ ³¹P NMR (162 MHz, CDCl₃): 12.70 (m, RPN), 10.83 (m, RPN), -3.64 (s, PMo); δ ¹H NMR (400 MHz, CDCl₃): 7.26 (m, BzNH), 4.13 (s, CH₂;

BzNH), 3.91 (s, NH; BzNH), 3.79 (s, NH; CyNH), 2.17 (m, CH CyNH), 1.91 (s, CH₂; C2, C6; CyNH), 1.58 (s, CH₂; C2,C4, C6 CyNH), 1.25/0.87 (s, CH₂; C3, C5 CyNH);

2.1.5.3.4 *HexBzCyPN-PMo*

Green glass; 0.37 g, 80.43%; m.p. 56-63 °C; elemental analysis calcd (%): C 32.67, H 4.87, N 9.53; found: C 11.58, H 1.82, N 2.99; FTIR (cm⁻¹): 3357 (N-H broad), 3062, 3023 (C-H_{arom}), 2928, 2853 (C-H_{alkyl}), 1496 (C-C_{arom}), 1453, 1405 (C-C_{alkyl}), 1257, 1090 (P-N), 1059 (P-O), 950 (Mo=O), 873, 781 (Mo-O-Mo), 694; δ ³¹P NMR (162 MHz, CDCl₃): 10.83 (m, RPN), -3.70 (s, PMo); δ ¹H NMR (400 MHz, CDCl₃): 7.26 (m, BzNH), 4.19 (s, CH₂ BzNH), 3.87br (s, NH BzNH), 3.30br (s, NH HexNH/CyNH), 2.94 (s, CH CyNH/ CH₂; C1 HexNH), 1.93 (s, CH₂; C2, C6; CyNH), 1.54br (m, CH₂; C2 HexNH/ CH₂; C2, C4, C6 CyNH), 1.27 (s, CH₂; C3, C4, C5 HexNH/ CH₂; C3, C5 CyNH), 0.87(m, CH₃ HexNH).

2.1.5.3.5 *HexiBuPN-PMo*

Green glass; 0.42 g, 85.71%; m.p. 56-62 °C; elemental analysis calcd (%): C 28.59, H 5.84, N 10.00; found: C 26.35, H 5.38, N 8.85; FTIR (cm⁻¹): 3362 (N-H broad), 2955, 2927, 2858 (C-H_{alkyl}), 1466, 1406 (C-C_{alkyl}), 1256, 1091 (P-N), 1059 (P-O), 952 (Mo=O), 874, 780 (Mo-O-Mo); δ ³¹P NMR (162 MHz, CDCl₃): 11.09 (m, RPN), -3.75 (s, PMo); δ ¹H NMR (400 MHz, CDCl₃): 3.32br (s, NH HexNH/iBuNH), 2.98 (s, CH₂; C1 HexNH), 2.80 (s, CH₂ iBuNH), 1.76br (s, CH iBuNH), 1.56br (s, CH₂; C2 HexNH), 1.29 (m, CH₂; C3, C4, C5 HexNH), 0.93 (m, CH₃ HexNH/iBuNH).

2.1.5.3.6 *HexBuPN-PMo*

Green viscous liquid; 0.41 g, 83.67%; elemental analysis calcd (%): C 28.38, H 5.81, N 10.04; found: C 28.03, H 5.98, N 9.45; FTIR (cm⁻¹): 3363 (N-H) , 2956, 2927 and 2858 (C-H_{alkyl}),

1465, 1405 (C-C_{alkyl}), 1253, 1092 (P-N), 1059 (P-O), 952 (Mo=O), 875, 791 (Mo-O-Mo); δ ³¹P NMR (162 MHz, CDCl₃): 13.47 (t, RPN), 11.24 (d, RPN), -3.75 (s, PMo); δ ¹H NMR (400 MHz, CDCl₃): 3.21 (s, NH HexNH/BuNH), 2.93 (d, CH₂; C1 HexNH/ CH₂; C1 BuNH), 1.47 (m, CH₂; C2 HexNH/ CH₂; C2 BuNH), 1.22 (m, CH₂; C3, C4, C5 HexNH/ CH₂; C3 BuNH), 0.85 (m, CH₃ HexNH/BuNH).

2.1.5.3.7 *iBuBuPN-PMo*

Green viscous liquid; 0.45 g, 86.54%; elemental analysis calcd (%): C 24.51, H 5.23, N 10.72; found: C 22.73, H 4.91, N 9.91; FTIR (cm⁻¹): 33363 (N-H broad), 2957, 2930, 2870 (C-H_{alkyl}), 1465, 1405 (C-C_{alkyl}), 1257, 1089 (P-N), 1058 (P-O), 951 (Mo=O), 873, 781 (Mo-O-Mo); δ ³¹P NMR (162 MHz, CDCl₃): 11.38 (m, RPN), -3.75 (s, PMo); δ ¹H NMR (400 MHz, CDCl₃): 3.33 (s, NH *i*BuNH/BuNH), 3.00/2.81 (s, CH₂; C1 *i*BuNH/ CH₂; C1 BuNH), 1.76 (s, CH *i*BuNH), 1.54 (s, CH₂; C2 BuNH), 1.36 (m, CH₂; C3 BuNH), 0.93 (m, CH₃ *i*BuNH/BuNH).

2.1.5.3.8 *HexiBuBuPN-PMo*

Green viscous liquid; 0.42 g, 85.71%; elemental analysis calcd (%): C 27.29, H 5.64, N 10.23; found: C 26.33, H 5.50, N 9.79; FTIR (cm⁻¹): 3365 (N-H broad), 2957, 2929, 2871 (C-H_{alkyl}), 1465, 1406 (C-C_{alkyl}), 1252, 1091 (P-N), 1059 (P-O), 953 (Mo=O), 876, 796 (Mo-O-Mo); δ ³¹P NMR (162 MHz, CDCl₃): 11.24 (m, RPN), -3.75 (s, PMo); δ ¹H NMR (400 MHz, CDCl₃): 3.33 (s, NH HexNH, *i*BuNH, BuNH), 2.97 (s, CH₂; C1 *i*BuNH/ CH₂; C1 BuNH), 2.79 (s, CH₂; C1 HexNH), 1.75 (s, CH *i*BuNH), 1.53 (s, CH₂; C2 HexNH/ CH₂; C2 BuNH), 1.29 (m, CH₂; C3, C4, C5 HexNH/ CH₂; C3 BuNH), 0.92 (m, CH₃ HexNH/*i*BuNH/BuNH).

2.1.5.3.9 *HexPN-PMo*

Green viscous liquid; 0.84 g, 92.31%; analysis calcd (%): C 32.16, H 6.37, N 9.38; found: C 31.12, H 6.34, N 8.83; FTIR (cm^{-1}): 3359 (N-H broad), 2955, 2927, 2857 (C-H_{alkyl}), 1465, 1405 (C-C_{alkyl}), 1254, 1093 (P-N), 1060 (P-O), 953 (Mo=O), 876, 799 (Mo-O-Mo); δ ^{31}P NMR (162 MHz, CDCl_3): 11.21 (m, RPN), -3.77 (s, PMo); δ ^1H NMR (400 MHz, CDCl_3): 3.32br (s, NH HexNH), 2.97 (s, CH_2 ; C1 HexNH), 1.54 (s, CH_2 ; C2 HexNH), 1.29 (m, CH_2 ; C3, C4, C5 HexNH), 0.89 (m, CH_3 HexNH).

2.1.5.3.10 *BzPN-PMo*

Green solid; 0.71 g, 79 %; m.p. 74-80 °C; elemental analysis calcd (%): C 33.36, H 2.88, N 9.73; found: C 36.20, H 3.70, N 8.87; FTIR (cm^{-1}): 3357 (N-H broad), 3062, 3029 (C-H_{arom}), 1604, 1495 (C-C_{arom}), 1454, 1403 (C-C_{alkyl}), 1257, 1090 (P-N), 1060 (P-O), 952 (Mo=O), 873, 784 (Mo-O-Mo), 726, 693 ; δ ^{31}P NMR (162 MHz, CDCl_3): 12.82 (t, RPN), 10.87 (d, RPN), -3.72 (s, PMo); δ ^1H NMR (400 MHz, CDCl_3): 7.18 (m, ArH), 4.13 (s, CH_2), 3.89 (s, NH).

2.1.5.3.11 *HexCyPN-SiW*

Green viscous liquid; 0.46 g, 92.00%; elemental analysis calcd (%): C 29.83, H 5.49, N 8.70; found: C 30.94, H 6.00, N 8.99; FTIR (cm^{-1}): 3317 (N-H broad), 2925, 2854 (C-H_{alkyl}), 1451, 1410 (C-C_{alkyl}), 1250 , 1094 (P-N), 968 (W=O), 916, 884 (W-O-W), 783 (Si-O); δ ^{31}P NMR (162 MHz, CDCl_3): 13.53 (m, RPN), 11.67 (m, RPN), 9.87 (m, RPN); δ ^1H NMR (400 MHz, CDCl_3): 3.67 (s, NH HexNH/CyNH), 2.18 (m, CH CyNH/ CH_2 ; C1 HexNH), 1.96/1.70/1.54 (m, CH_2 ; C2 HexNH/ CH_2 ; C2, C4, C6 CyNH), 1.28 (s, CH_2 ; C3, C4, C5 HexNH/ C3, C5 CyNH), 0.87 (s, CH_3 HexNH).

2.1.5.3.12 *HexCyPN-PW*

Pale green viscous liquid; 0.52 g, 89.66%; elemental analysis calcd (%): C 25.59, H 4.71, N 7.46; found: C 26.23, H 5.13, N 7.71; FTIR (cm^{-1}): 3356 (N-H broad), 2926, 2854 (C-H_{alkyl}), 1451, 1407 (C-C_{alkyl}), 1252, 1077 (P-N), 973 (P-O), 892 (W=O), 799 (W-O-W); δ ^{31}P NMR (162 MHz, CDCl_3): 13.25 (m, RPN), 11.06 (m, RPN), 8.98 (m, RPN), -15.22 (s, PW); δ ^1H NMR (400 MHz, CDCl_3): 3.31 (s, NH HexNH/CyNH), 2.99 (s, CH CyNH/ CH_2 ; C1 HexNH), 1.96/1.73/1.56 (m, CH_2 ; C2 HexNH/ CH_2 ; C2, C4, C6 CyNH), 1.29 (s, CH_2 ; C3, C4, C5 HexNH/ C3, C5 CyNH), 0.89 (t, CH_3 HexNH).

2.2 Catalyst Characterization Techniques

2.2.1 Elemental Analysis

Elemental analysis is the measurement of the elemental composition of a material. These techniques can be used to detect the presence of specific elements within a material qualitatively and/or quantitatively. The main application of elemental analysis is to determine the purity of a sample.

2.2.1.1 *Inductively Coupled Plasma Optical Emission Spectroscopy (ICP-OES)*

Inductively coupled plasma optical emission spectroscopy (ICP-OES) is an analytical technique that is used to detect trace amounts of elements in a solution and is sensitive to traces down to parts per billion.

The ICP-OES spectrometer is composed of two parts: the inductively coupled plasma and the optical spectrometer. The plasma is created by igniting argon gas in a radio frequency (RF) coil which has a stable temperature of about 7000 K. The sample solution is introduced directly

inside the plasma flame as a mist using an analytical nebulizer. The elements within the sample collide with the electrons and ions of the plasma which excites electrons within the elements to higher states. As the electrons relax, they emit photons of energy which are quantized and characteristic of the element involved. The wavelengths of the energies produced are recorded by the spectrometer as emission lines and the intensities (measured in counts per second) of these lines are directly proportional to the concentration of the element in the sample solution. The concentration of an element can then be determined by comparison of the emission line intensities with standard calibrated solutions of the corresponding element.²

ICP-OES was used to determine the concentration of phosphorous in our catalyst samples.

Samples for ICP-OES analysis were prepared by digesting 20 mg of catalyst in 4 mL of boiling aqua regia (1 mL conc. HNO₃ and 3 mL conc. HCl). The solution was then diluted to 25 mL with H₂O₂ and submitted for analysis.

For the POM/RPN-SiO₂ catalysts the POM could be digested off the surface using 10 % w/v KOH_{aq}. The concentration of POM on the surface of the sample could be determined from the phosphorus or metal content of the solution. Samples were prepared by boiling 20 mg POM/SiO₂ samples in 25 mL 10 % w/v KOH_{aq}. Once the solution had cooled down to room temperature, it was topped back up to 25 mL with fresh 10 % w/v KOH_{aq} and submitted for analysis.

Samples were submitted to the Microanalysis Service in the University of Liverpool Chemistry Department and analysed on an Agilent 5110 ICP-OES spectrometer with SVDV detection equipped with the sample changer by George Miller.

2.2.1.2 CHN Analysis

CHN analysis was used in this work to elucidate the elemental composition of the RPNs and the catalysts. Analyses of samples were obtained by submission to the Microanalysis Service in the University of Liverpool Chemistry Department.

2.2.2 Microscopy

Microscopy is the use of a microscope to view an object at a higher resolution than can be seen with the human eye. Optical and electron microscopy measure the reflection, diffraction, or refraction of electromagnetic radiation or electron beams that interact with the sample in order to create an image. These images can provide information on the topography and morphology of the samples surface.

2.2.2.1 Scanning Electron Microscopy (SEM)

Scanning electron microscopy (SEM) is a spectroscopic technique used for probing solid surfaces. A focussed beam of high-energy electrons is passed over the surface of the sample and the resulting electron-surface interactions can reveal information about the surface morphology, topography and chemical composition. The electron-surface interactions produce various signals which include secondary electrons, back-scattered electrons and X-rays to list a few. Secondary electrons are most commonly used for imaging samples as their detection is sensitive to the topography and morphology of the sample. Scanning of the surface using secondary electron imaging detects the electrons emitted from very close to the surface and can, consequently, provide image resolution up to about 10 nm.

For typical imaging in the SEM, samples must be electrically conductive at the surface and electrically grounded to avoid accumulation of electrostatic charge. Non-conducting samples

collect charge when scanned by the electron beam and, especially in secondary electron imaging mode, this causes scanning faults and other image artifacts. These materials are usually coated with an ultrathin layer of electrically conducting material, such as metal or water, which is deposited onto the sample either by low-vacuum sputter coating or by high-vacuum evaporation.³

Scanning Electron Microscopy (SEM) of POM/RPN-SiO₂ and RPN-SiO₂ samples was performed by Casper Kunstmann on a FEI Quanta 250 FEG Environmental SEM, operating in “Low Vacuum” mode. This allows for imaging of non-conductive samples by filling the sample chamber with a small amount of pure water vapour (at 100 Pa), which helps dissipate beam induced charge from the sample surface. To image the samples, the dry powder silica particles were deposited directly on double-sided carbon adhesive discs (*Agar Scientific*). All images are obtained at low beam energy (5 kV) to avoid sample damage and again, charging effects.

2.2.3 Thermal Analysis

Thermal analysis techniques are experimental methods for characterising a sample by measuring changes in physio-chemical properties as a function of temperature. Phase changes and decomposition are the properties that are most commonly measured by these techniques.

2.2.3.1 Thermogravimetric Analysis (TGA)

Thermogravimetric Analysis (TGA) is a technique in which the mass of a substance is monitored as a function of temperature whilst the sample is gradually heated in a controlled atmosphere. Decomposition as the result of heating is an inherent property of most chemical compounds. The mass lost by decomposition can be used to determine the thermal stability of

a compound and can also provide information on its structural composition. It can also be used to quantify loss of water, loss of solvent, decarboxylation, pyrolysis, and oxidation to list a few examples.⁴

TGA instrumentation consists of a sample pan that resides in a furnace and is attached to a precision balance. As the sample is heated, the balance measures the change in weight of the sample. The environment inside the furnace can be controlled through a gas inlet, which enables controlled flow of reactive or inert purge gas over the sample, which then exits through an exhaust.

TGA was used in this work to measure the thermal stability of RPN-POM catalyst aggregates and to measure the amount of physisorbed water in the commercially sourced heteropoly acids (supplied as hydrates from Sigma-Aldrich) used in these studies. Samples were analysed using a Perkin Elmer TGA 7. Experiments were conducted under N₂ flow using a heating rate of 20 °C per minute to raise the temperature from room temperature up to 700 °C.

2.2.3.2 Differential Scanning Calorimetry (DSC)

Differential scanning calorimetry provides information about the thermal changes a sample undergoes that do not involve a change in mass, such as phase transitions. The technique measures the difference in the amount of heat that is required to increase the temperature of a sample and a reference as a function of temperature. As the sample undergoes a phase transition, more or less heat flow will be needed to maintain a constant temperature with the reference. The heat required will depend on whether the phase change is exothermic or endothermic. For example, as a solid sample melts to a liquid, heat will be absorbed by the sample as it undergoes the endothermic phase transition from solid to liquid and so it will require more heat flow to increase its temperature at the same rate as the reference. The

converse is true for crystallization of a liquid sample, which is an exothermic process. By monitoring the difference in heat flow between the sample and reference, DSC can measure the amount of heat absorbed or released during such transitions. Subtler physical changes can also be detected, such as glass transitions.⁵

DSC was used in our studies to monitor the phase transitions undergone by our eutectic RPNs. Sample measurements were run by Jessica Smith on a TA Instruments DSC Q2000. Measurements were conducted under a nitrogen atmosphere. Per run, samples were heated to 150 °C at 5 °C/min, cooled to -80 °C at 5 °C/min, and heated to 150 °C at 5 °C/min. Sunflower oil and linseed oil were used as reference samples.

2.2.4 Spectroscopy

Spectroscopy is the study of the interaction between radiation and matter. Electromagnetic radiation in the form of photons – packets of energy – is absorbed by subatomic particles (e.g. protons and electrons) which results in excitations in their energy levels. The energies required for these excitations are quantized and only discrete energies will result in transfer of a particle between energy levels.

Excitations or emissions can translate into changes in the vibrational, rotational or translational levels within a molecule depending on the amount of energy that is absorbed or emitted by photons. The frequency of the photons corresponding to these transitions occur in well-defined regions of the electromagnetic spectrum which is shown in Fig. 2.1. It is through the measurement of photons with well-defined energies and their interactions with matter which gives rise to each spectroscopic technique.⁶

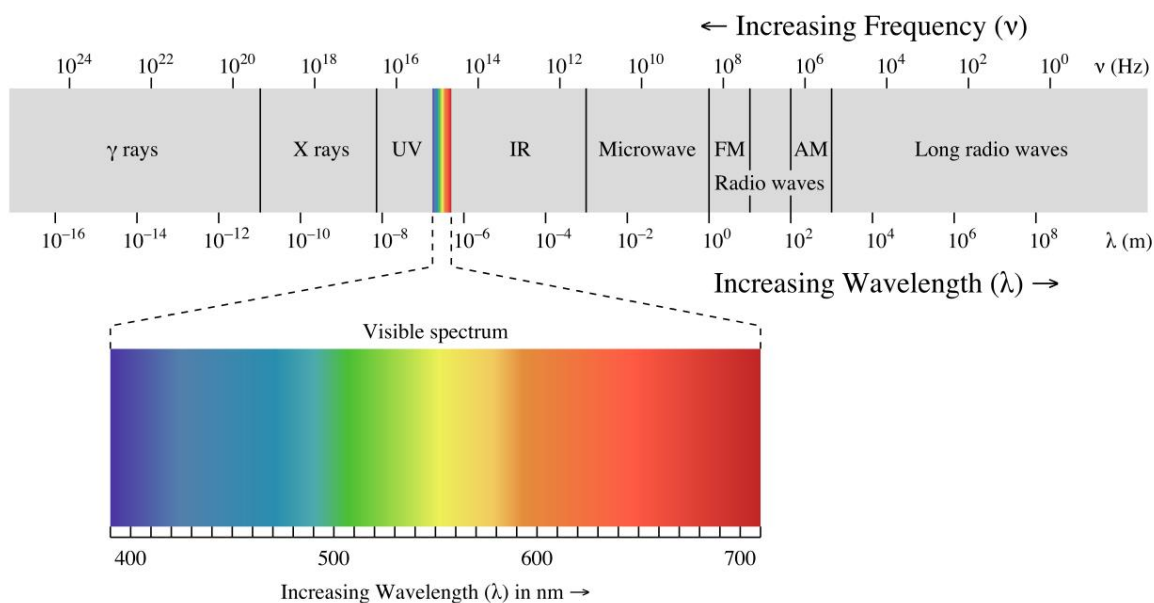


Fig. 2.1. The electromagnetic spectrum (source: Wikipedia article on the electromagnetic spectrum).

2.2.4.1 UV-Visible Spectroscopy

UV-Visible (UV-Vis) spectroscopy is an analytical technique employed to measure the absorbance spectrum of a compound within the ultraviolet and visible regions of the electromagnetic spectrum. The peaks in the spectrum correspond to electronic transitions between the ground state and excited state energy levels of molecules containing π or non-bonding (n) electrons. Ultraviolet (UV) or visible light energy is used to excite these electrons into unoccupied, high-energy anti-bonding orbitals. The exact energy absorbed corresponds to the HOMO-LUMO gap (Highest Occupied Molecular Orbital and Lowest Unoccupied Molecular Orbital, respectively), with a smaller gap requiring low energy, long wavelength light to excite the electron.

Measurements are often conducted using solutions containing a known concentration of a sample complex or compound. A suitable solvent must be selected that will not alter the

electronic transitions within the sample (e.g. the solvent will not substitute ligands on a complex) nor will it have an absorbance in the UV-Vis region that will mask the spectrum of the sample. An aliquot of the solution is transferred to a suitable cuvette cell with a known path length (often 1 cm), with clean solvent in a duplicate cell for use as a reference. This ensures the measured spectrum is made up of peaks due to absorptions by the sample rather than the solvent. Analysis of the resulting spectrum provides information on two important parameters: the position of the absorbance peaks in relation to their wavelength and the intensity of the band. The intensity and the concentration can be used to calculate the extinction coefficient (ϵ) for each peak using the Beer-Lambert law:

$$A = \log_{10}(I_0/I) = \epsilon cl \quad \mathbf{2.1}$$

where A is absorbance, c is the molar concentration and l is the path length in centimetres. The extinction coefficient measures how strongly a substance absorbs light at a given wavelength per molar concentration. An electronic band in the spectrum may have several clear peaks resulting from different vibration states in the molecules (Frank-Condon principle). If the peak is well resolved, an estimate of the vibrational frequency of the excited state responsible for the fine structure can be obtained by measuring the individual peak positions.⁷

In this work, UV spectroscopy was used to measure the phase-transfer ability of different RPNs (iPrPN, iBuPN and BzPN) at different [RPN]/[PW] ratios in a DCE/H₂O system. Measurements were used to detect a change in concentration of PW or its derivative peroxy POM species in the DCE layer resulting from the different ratios of RPN PTCs. Measurements were recorded on a CARY 50 Probe UV/Vis spectrometer in 1 cm quartz cuvettes.

To measure the phase-transfer of PW, a biphasic system was established by combining a 0.5 mL aqueous phase containing PW (6.478×10^{-6} mol) and organic DCE phase containing RPN ($n \times [\text{POM}]$, where $n = 1, 2, 3, 4, 5, 6, \text{ or } 10$) in a 15 mL glass vial. The system was shaken

vigorously at room temperature (~20 °C) to emulsify the two layers and left to settle for two hours. A 1 mL aliquot was taken from the organic layer and diluted to a tenth of its concentration with fresh DCE to ensure absorption was below the saturation limit of the spectrophotometer. Scans were taken in the range of 200 – 800 nm and the maximum PW peak absorbance was measured at ~268 nm. To measure the phase-transfer of peroxo PW, the exact same procedure was followed using H₂O₂ (0.1 mL, 1.01 mmol) instead of H₂O. Max absorbance for peroxo PW was measured at ~292 nm.

2.2.4.2 Fourier Transform Infra-Red Spectroscopy (FTIR)

FTIR spectroscopy is an analytical technique employed to measure the absorbance spectrum of a compound within the infrared region of the electromagnetic spectrum. The frequency of the energy absorbed is discrete and corresponds to the transition energy between the ground state and excited state energy levels which is required for a bond to vibrate, bend or rotate. The absorption peaks in the recorded spectrum of a compound, therefore, indicate the presence of characteristic bonds with vibrations and rotations that occur at these discrete energies.⁷

For this work, solid samples were analysed by FTIR using the diffuse reflectance technique (DRIFTS). This technique measures the diffusely scattered light which is reflected from the surface of the sample. As diffusely reflected light passes through the powder, groups on the surface or in the bulk of the powder can absorb the light, producing a diffuse reflected spectrum. If the powder is strongly absorbing it can be mixed with a diffusely scattering matrix, such as KBr, which lowers absorption and improves throughput of the signal.⁸ A diagram of the set-up of the spectrometer is shown in Fig. 2.2. There are four flat mirrors (M1, M2, M5 and M6) and two ellipsoid mirrors. Mirrors M1, M2 and M3 direct the light from the source to the sample.

2.2.4.3 Nuclear Magnetic Resonance Spectroscopy (NMR)

Nuclear magnetic resonance spectroscopy (NMR) measures the electromagnetic radiation absorbed by a nucleus with a magnetic moment, μ , inside an applied magnetic field (B_o).^{6,7,9}

For a nucleus to have a magnetic moment, it must possess either an odd number of protons or an odd number of neutrons, or both i.e. its spin quantum number, I , must be non-zero. In the absence of a magnetic field, the magnetic states of the nucleus will be in their degenerate state. However, when placed in an external magnetic field the spins can adopt a discrete number of possible orientations which total $2I+1$. The individual spin orientations are given by:

$$m = I, I-1, I-2, \dots, 0, \dots, -I+1, -I \quad 2.2$$

Allowed transitions between spin orientations obey the rule $\Delta m = \pm 1$. It is this splitting of the otherwise degenerate energy levels in a magnetic field that makes NMR spectroscopy possible.

The spin of a nucleus is directly proportional to its magnetic moment, as given by:

$$\mu = \frac{\gamma I h}{2\pi} \quad 2.3$$

where γ is the gyromagnetic ratio of the type of nucleus and h is planks constant.

Some of the most widely investigated nuclei, ^1H , ^{13}C and ^{31}P - all of which have been studied in this work - are $I = \frac{1}{2}$ and so when these nuclei are placed in an external field there are two spin states that arise, $m = +\frac{1}{2}$ and $-\frac{1}{2}$. A single transition is possible between these two states.

The energy difference corresponding to this transition is illustrated in Fig. 2.3.

The frequency of the radiation required for this transition, the resonance frequency, is given by:

$$\nu = \frac{\gamma B_o}{2\pi} \quad 2.4$$

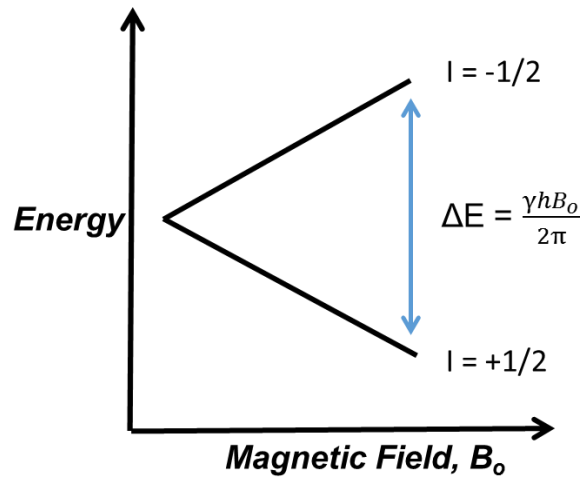


Fig. 2.3. Energy levels for a spin $I = \frac{1}{2}$ nucleus in an externally applied field. Difference in energy between levels corresponds to the single possible transition between the states where B_0 is the strength of the applied field, γ is the gyromagnetic ratio of the nucleus and h is Plank's constant.

The energy of the external field is at a specific resonance frequency that lies within the radio-frequency area of the electromagnetic spectrum. When introduced to this field, the nuclear spins absorb energy that corresponds to the resonance frequency and begin to precess around the direction of the applied field (Fig. 2.4). The rate at which an individual spin precesses around the applied field is called the Larmor frequency.

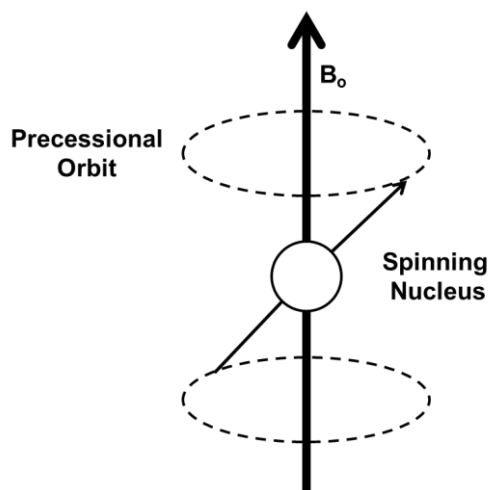


Fig. 2.4. Precession of a nucleus around an applied external field, B_0 .

The effective magnetic field that is experienced by the nucleus, however, is not necessarily the same as the applied field; the motion of the electrons that surround the nucleus can create a field that opposes the applied field which effectively shields the nucleus:

$$B_{eff} = B_0(1 - \sigma) \quad 2.5$$

where σ is the shielding constant. As the local environment around a nucleus varies, so too will the value of σ . This alters the energy and therefore the frequency required to cause a transition, meaning the resonance frequency is characteristic of the localised environment of the nucleus. As contributions provided by σ are usually small, the observed frequency of each resonance (ν_{obs}) is measured relative to a reference frequency (ν_{ref}) produced by a nucleus of the same type in a magnetic environment (e.g. phosphate in phosphoric acid is commonly used for ^{31}P NMR as a reference). The distance a nucleus is “shifted” from this reference frequency is proportional to effect of the environment on the magnetic moment of the nucleus, and is called a *chemical shift*, δ . As these effects are small, the difference is multiplied by a million and so shifts are quoted from the reference peak in terms of ‘ppm’ or ‘parts per million’:

$$\delta = 10^6 \times \frac{\nu_{obs} - \nu_{ref}}{\nu_{ref}} \quad 2.6$$

The reference shift is always stated as 0 ppm, so the chemical shift (ppm) and frequency (Hz) scales are interconvertible using equation

$$\delta = 10^6 \times \frac{\Delta\nu}{\text{spectrometer frequency}} \quad 2.7$$

As different nuclei have different gyromagnetic ratios, the frequencies required for the nuclei to resonate will be different, i.e. the resonance frequencies for different nuclei are often separated by many MHz. As such, as chemical shifts are only measured in Hz it is very unlikely that there will be any overlapping chemical shifts sourced from different nuclei.

2.2.4.3.1 Solution-State Nuclear Magnetic Resonance Spectroscopy

In a sample solution, in the absence of a magnetic field the nuclear spins are orientated in random directions which means that the small magnetic fields that they generate are cancelled out and there is no net magnetic effect. Once an external field is applied and the spins equilibrate, they align in such a way that they create a bulk magnetization along the direction of the applied magnetic field to polarize the sample. The direction of the bulk magnetisation is called the net magnetization vector (M) (Fig. 2.5).

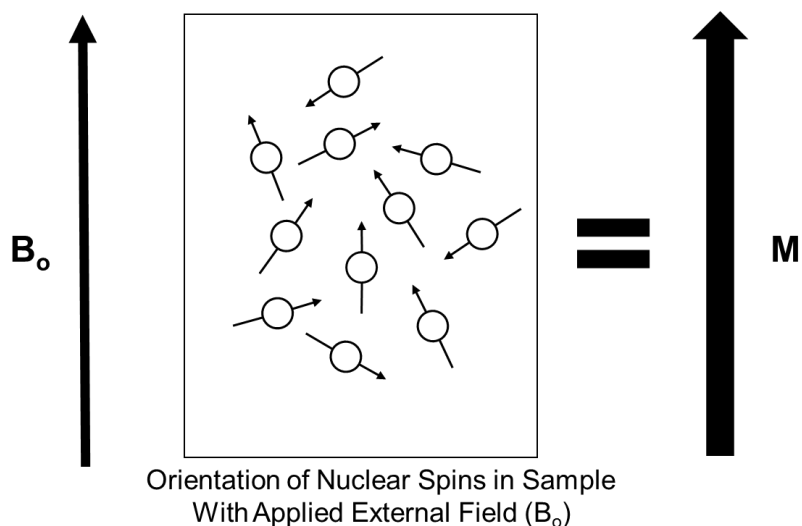


Fig. 2.5. Generation of net magnetization vector of nuclear spins in a sample (M) with application of an external magnetic field (B_0).

This vector is typically visualized along the z axis of a Cartesian plot as shown in Fig. 2.6. (1).

In a typical experiment, outlined in Fig. 2.6, the external field, B_0 , is applied continuously along the z axis to maintain M (1). A second radio frequency (RF) pulse is then applied perpendicular to the applied magnetic field to perturb the net magnetization vector produced by polarization of the sample (2); maximum signal is obtained with a 90° pulse. Precession of M around B_0 occurs as M “relaxes” and realigns itself with the external field (3). This precession is also known as Larmor precession as it is with the individual spins. The oscillating magnetism cuts through a pickup coil producing an electrical signal (a free induction signal). This produces a free induction decay signal (FID) as M realigns with B_0 which is Fourier transformed (FT) to give a plot of absorption vs. frequency. The individual spins give peaks at their corresponding Larmor frequencies which are directly proportional to the energy of their magnetic moment.

The final NMR spectrum is usually displayed in a plot of absorbance vs. ppm. The chemical shifts of the nuclei are determined by their local environments within the molecule i.e. shielding as mentioned above; if two nuclei of the same type are in two inequivalent environments they will spin at different frequencies and, hence, will produce two peaks at separate δ in the spectrum. Integration of the peaks in the spectra of certain nuclei such as ^1H and ^{31}P can be used to calculate the ratio of nuclei in each environment as the absorbance is directly proportional to the moles of the corresponding nuclei. Therefore, these characteristic shifts provide information on the localised environments that are present within the molecule, such as functional groups, which is why NMR is such a powerful tool for the structural elucidation of molecules.

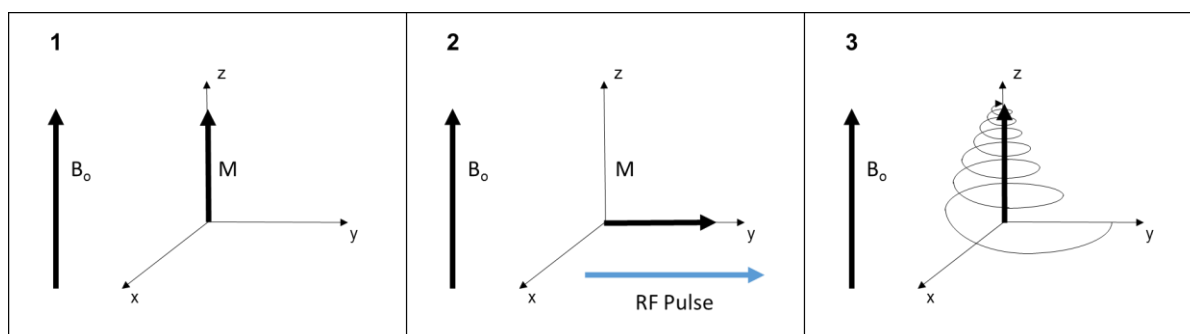


Fig. 2.6. Stages of a typical NMR experiment. **1)** Bulk magnetization of spins in a sample align in the direction of B_0 to give net magnetisation vector, M , at equilibrium. **2)** RF pulse offsets M from equilibrium position. **3)** M precesses at Larmor frequency as it relaxes back to equilibrium position.

^{31}P NMR was used in this work to identify the presence of PMo and PW in organic solutions facilitated by RPN PTC; their shifts are found at -3 ppm and -14 ppm, respectively.¹⁰⁻¹² Their lacunary and peroxy derivatives can also be identified in characteristic peak ranges and so the technique can also be used as an identifier of successful phase-transfer of these species.¹³⁻¹⁵ In

addition, ^{31}P NMR can also be used to identify the successful substitution of all six chloro substituents in the synthesis of organoaminocyclotriphosphazenes from $\text{P}_3\text{N}_3\text{Cl}_6$ and a primary amine.¹ *Hexa*-substituted organoaminocyclotriphosphazenes give singlet peaks with characteristic chemical shifts at ~ 19 ppm.

^1H and ^{13}C NMR were used to identify the alkyl groups of the organoamine substituents.

Solution-state NMR analysis in this work was conducted on a Bruker 400 MHz NMR spectrometer fitted with an auto-sampler. Samples were prepared in organic solutions using a CDCl_3 lock or in aqueous solutions using a D_2O lock. Analysis was run at 25°C .

2.2.4.3.2 Solid State Magic Angle Spinning Nuclear Magnetic Resonance Spectroscopy (MAS NMR)

Solid-state NMR is used to determine the magnetic environments of nuclei in solid state compounds.

Anisotropic nuclear interactions, such as dipolar coupling, quadrupolar coupling and chemical shift anisotropy, modify nuclear spin energy levels which often produce line broadening in NMR spectra. As these interactions are orientation-dependent, the Brownian motion of molecules in solution-state NMR leads to an averaging of anisotropic interactions which means they can be neglected on the time scale of the NMR experiments. In solid samples, molecules are in fixed positions and so anisotropic interactions have a strong effect on the nuclear spins. The spectra of solid samples usually have broad, poorly defined signals that are difficult to analyse. However, by spinning the sample at a frequency of 1 to 130 kHz at the magic angle, θ_m , (ca. 54.74° with respect to the direction of the magnetic field) the broad lines become narrower, increasing the resolution for analysis of the spectrum. This results from the effects of dipolar coupling averaging to zero and nuclear-electron interactions (chemical shift

anisotropy) averaging to a non-zero value. Quadrupolar interactions are partially averaged by MAS which leaves residual secondary quadrupolar interactions which can be seen in the spectra (spinning side bands).

Solid-state NMR experiments were used in this work to characterise solid RPN-SiO₂ and POM/RPN-SiO₂ catalysts. Solid-state NMR experiments were performed by Dong Xiao on a 400 DSX NMR spectrometer, using a 4 mm HXY probe in triple resonance mode with the X channel tuned to ³¹P at 161.9 MHz, and Y channel tuned to ¹³C at 100.5 MHz in ¹³C CP experiments and to ²⁹Si at 79.4 MHz in ²⁹Si CP experiments, respectively.

³¹P DE NMR. Experiments were performed at a MAS rate of 12 kHz using ³¹P rf (radio-frequency) field amplitude pulses and ¹H cw (continuous-wave) decoupling at 83 kHz. 128 to 2048 transients were accumulated with a quantitative recovery delay longer than 5 x T₁. The chemical shifts were referenced to aqueous 85% H₃PO₄ at 0 ppm.

¹³C CP NMR. Experiments were performed at MAS rates of 10 and 14 kHz. The rf field amplitude of ¹H 90° pulses and SPINAL64 decoupling were 83 kHz.¹⁶ For ¹H to ¹³C CP transfer, the amplitude-ramped rf field for ¹H was 60 kHz, while Hartmann-Hahn matched ¹³C rf field was 25-33 kHz at MAS rate of 10 kHz and 30 to 53 kHz at MAS rate of 14 kHz, and the contact time was optimized to be 1-2 ms. 5120 to 47104 transients were accumulated with a recovery delay of 3 s per transient. The chemical shifts were referenced to CH of adamantane at 29.45 ppm.¹⁷

²⁹Si CP NMR. Experiments were performed at a MAS rate of 10 kHz. The rf field amplitude of ¹H 90° pulse and SPINAL64 decoupling was 83 kHz.¹⁶ For ¹H to ²⁹Si CP transfer, the amplitude-ramped rf field for ¹H was 60 kHz, while Hartmann-Hahn matched ²⁹Si rf field was 28-57 kHz, and the contact time was optimized to be 9 ms. 20480 to 51200 transients were

accumulated with a recovery delay of 3 s per transient. The chemical shifts were referenced to the most upfield signal of Q_8M_8 at -109 ppm (corresponding to $SiMe_4$ at 0 ppm).¹⁸

2.2.5 X-ray Diffractometry

X-ray diffraction is used to identify the spacing between atoms or ions that comprise a molecule. The X-rays have the same wavelength as the spacing between the atoms or ions in the planes of a crystalline lattice which causes X-rays that penetrate the crystal to be diffracted. In an experiment, a monochromatic beam of X-ray radiation - created by bombarding a metal with high energy electrons and collimating the beam into one wavelength – is fired at the sample. If the crystal planes are orientated at the correct angle, the diffracted X-rays will constructively interfere in accordance with Bragg's Law, $n\lambda = 2d\sin\theta$ (where n is the order of reflection which has an integer value, λ is the incident X-ray wavelength, d is the planar spacing between atoms in the lattice layers, and θ is the angle of incidence), as illustrated in Fig. 2.7, and produce a diffraction pattern, or diffractogram. From the diffractogram, the symmetries and dimensions of the unit cell, and thus the structure of the sample also, can be solved.¹⁹

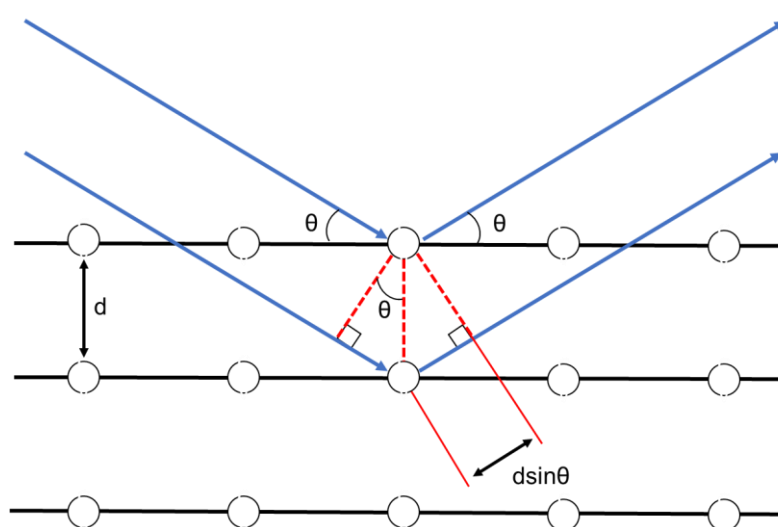


Fig. 2.7. Bragg diffraction by a set of parallel lattice planes.

2.2.5.1 Single Crystal X-ray Diffractometry

Single crystal X-ray diffractometry is used to measure the packing and orientation of molecules in the lattice of a single crystal in three dimensions. A monochromatic beam of X-ray radiation is fired at the surface of a crystal. The sample crystal is mounted on a Mylar tip attached to a goniometer. As the crystal is rotated, the spacing of the atoms in the crystal act as a diffraction grating and diffract the X-rays in 3 dimensions. The detector, which is mounted on a rotating arm, is repositioned around the crystal at different values of 2θ to detect X-rays that are diffracted at different angles. Only reflections that satisfy the Bragg equation produce spots on the diffractogram. The variance in intensity of the spots and the angle of detection relative to the beam source provide information on the geometry of the structure in 3 dimensions.¹⁹

Single crystal X-ray studies were used to determine the packing of the POM and RPN constituents in RPN-POM aggregate catalysts in the solid state, and to help identify the structure of isolated intermediates from oxidation reactions in which they were used as catalysts with H_2O_2 . RPN-POM crystals were grown by dissolving both components separately in methanol and then combining the two solutions in the appropriate [RPN]/[POM] ratios in a vial and allowing the methanol to slowly evaporate off at room temperature and pressure. Crystals of intermediates were isolated by separating off the organic layer from RPN-POM in the presence of H_2O_2 in two-phase systems and allowing the solvent to evaporate off slowly at room temperature and pressure.

Samples were analysed by Dr. Alexander Steiner and Dr. Craig Robertson. Reflections were collected on a Bruker Smart Apex diffractometer using $\text{MoK}\alpha$ radiation ($\lambda = 0.71073 \text{ \AA}$). Structures were refined by full-matrix least-squares against F^2 using all data.²⁰

2.2.5.2 X-ray Powder Diffractometry (XRD)

Powdered crystalline samples can diffract X-rays as the particulate crystals contain ordered lattice planes. The technique is used for the phase identification of crystalline material and can provide information on unit cell dimensions.

Collection of the diffraction patterns of powdered samples is identical to that of single crystal samples, with the exception that the powders are dispersed as a thin film on tape or glass slides which are then attached to the goniometer.

XRD was used in this study for structural determination of powdered catalyst samples and to determine if waxy eutectic RPN-POM catalysts were microcrystalline. Analysis of samples was carried out on a D 5005 Siemens diffractometer using CuK α radiation (1.5418 Å) by the XRD Analytical Services in the University of Liverpool Chemistry Department.

2.2.6 Surface Area and Porosimetry Studies

Heterogeneous catalysts are typically porous solids. Their catalytic activities, selectivities and stabilities are heavily influenced by their morphologies, which are dictated by properties such as total surface area, pore volumes and the distribution of their pore sizes. Pore sizes fall into three different classes:

1. Micropores and ultramicropores - size below 2 nm and below 0.7 nm, respectively,
2. Mesopores – size between 2 nm and 50 nm,
3. Macropores – size above 50 nm.

The type of pore (Fig. 2.8) determines the shape and availability of the pore walls to total surface contributions. Individual catalyst particles generally contain many pores of different shapes, sizes and volumes (pore size distribution). The total surface area of porous solids is much higher than the external area as it includes surface contributions from the pore walls.

Common porous catalysts typically have a total surface area of between 1-1000 m²g⁻¹, whereas their external areas are in the range of 0.01-10 m²g⁻¹.

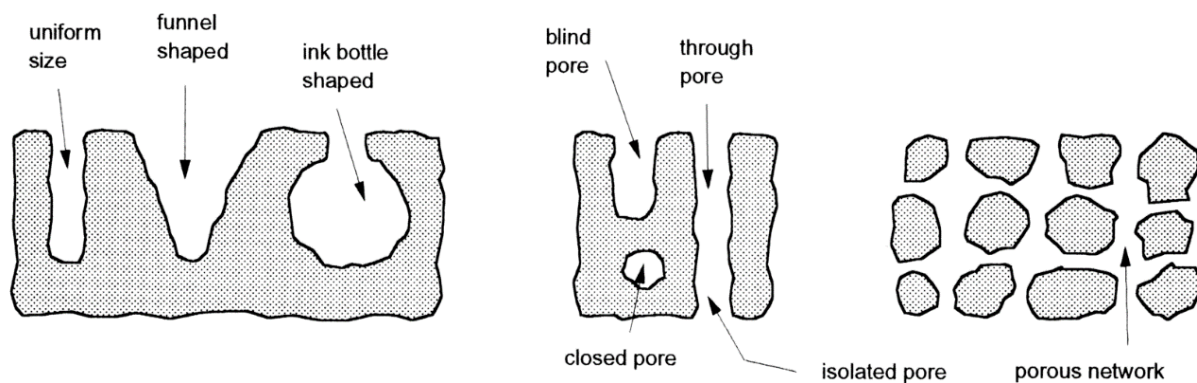


Fig. 2.8. Types of pores.²¹

Nitrogen adsorption at 77K is the most commonly used technique to discern the surface area and porosimetry of solid catalysts. In these studies, the N₂ molecules adsorb to the surface of the sample to form a tightly packed monolayer which is independent of the atoms in the structure of the analyte. An experiment measures the amount of N₂ adsorbed onto the surface of the sample at 77 K as a function of N₂ pressure. A plot of the volume of adsorbed N₂, V , against its relative partial pressure, P/P_o , produces an adsorption isotherm. The shape of the isotherm depends on the porous texture of the sample, or adsorbate, and the four types of adsorption isotherms commonly observed with N₂ adsorption on catalysts are shown in Fig. 2.9.

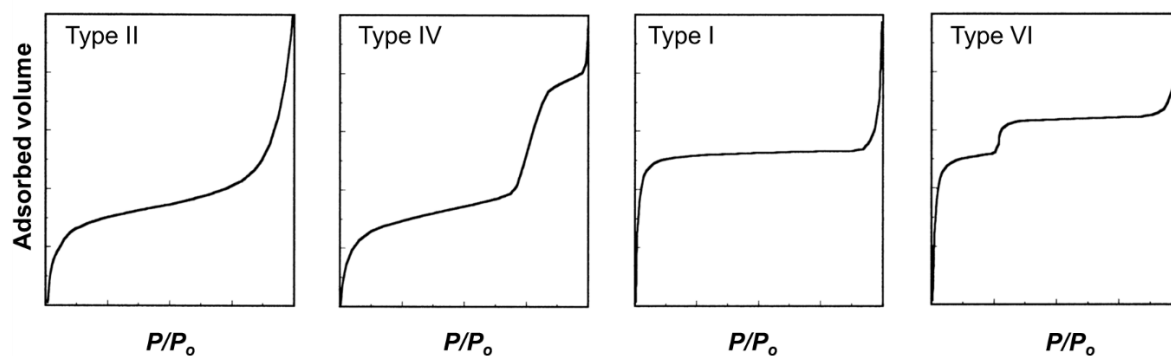


Fig. 2.9. The four types of adsorption isotherms usually observed by nitrogen adsorption on solid catalysts.²¹

Type I describes adsorption by microporous solids, type II describes adsorption by macroporous solids, type IV describes adsorption by mesoporous solids, and type VI describes adsorption by uniform ultramicroporous solids. Details on these isotherms have been described many times in the literature^{21–24} and, as such, only the mesoporous type IV isotherm will be discussed here as this is relevant to the heterogeneous solid catalysts and supports analysed in this work.

At low relative pressures, adsorption of N₂ onto mesoporous solids forms a monolayer. At high relative pressures, adsorption in the mesopores leads to multilayer formation until capillary condensation occurs, which provides a sharp increase in the volume of gas adsorbed (Fig. 2.9, type IV). The larger the mesopores, the higher the relative pressure required for this process to occur.^{21,25}

After saturation of the adsorbate has been reached, the process of N₂ desorption begins. Desorption for microporous and macroporous materials is the opposite process of adsorption. This is also partially true for mesoporous materials, though, evaporation from the mesopores occurs at lower temperatures than capillary condensation which produces a hysteresis in the

isotherm. This is due to the shape of the pores and may also be the result of pore connectivity effects (Fig. 2.8). The four types of hysteresis that can be produced are illustrated in Fig. 2.10.

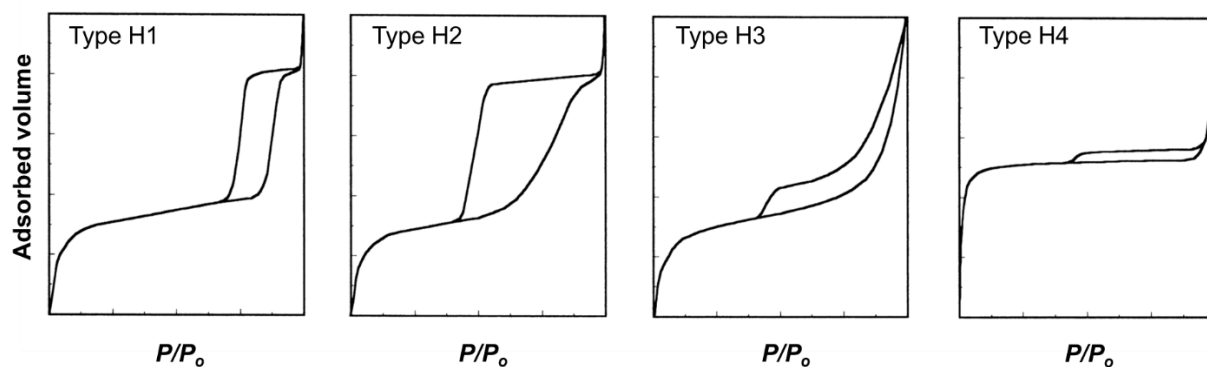


Fig. 2.10. The four hysteresis types of adsorption isotherm usually found by N₂ adsorption.²¹

Types H1 and H2 are attributed to solids composed of particles with cylindrical pore channels, or spheroidal aggregates or agglomerates. The parallel, almost vertical branches of the H1 loop indicates a high degree of pore size uniformity and facile pore connectivity, whereas H2 loops have a steep desorption branch that is typically ascribed to pores that are less uniform in size and shape. The hysteresis loop shapes are also characteristic of pores with narrow openings with larger sized bodies often called “ink-bottle pores.” Condensation in these pores obeys the Kelvin law – the liquid formed at low pressure in the mouth of the pore provides vapour for condensation in the larger pore body – but evaporation of the pore body cannot occur until the pore mouth is empty. Most catalysts with mesopores display H1 or H2 hysteresis.^{21,24}

Types H3 and H4 are characteristic of solids comprised of aggregates or agglomerates of particles which form slit like pores. For type H4 these pores are uniform and for type H3 they are non-uniform in size and/or shape. Hysteresis is usually due to different behaviour exhibited by the pores during desorption compared to during adsorption. For instance, in pores formed by parallel plates the meniscus is flat during adsorption (radius = ∞), but is cylindrical during

desorption (radius = half distance between plates). H3 and H4 hysteresis is often seen in active carbons and zeolites.^{21,24}

Samples that exhibit no hysteresis usually have blind cylindrical, cone-shaped and wedge-shaped pores (Fig. 2.8).

The surface area of a sample is measured by the volume of N₂ required to form a complete monolayer on the samples surface. However, the N₂ molecules can also form multilayers as the monolayer is filled. The BET method compensates for the formation of multilayers and allows measurement of the monolayer by using the BET equation:

$$\frac{1}{V(P_o - P)} = \frac{1}{V_m C} + \frac{(C - 1)}{V_m C} \times \frac{P}{P_o} \quad \mathbf{2.8}$$

where P is the equilibrium pressure, V is the volume of gas absorbed at P , P_o is the saturation pressure, V_m is the volume of gas required to cover the surface in one monolayer, and C is a constant related to the heat of condensation.

A plot of $1/V(P_o - P)$ against P/P_o in the range of $0.05 < P/P_o < 0.35$ produces a linear relationship, the gradient of which provides the value of V_m . Values of P/P_o below 0.05 underestimate adsorption and values above 0.35 overestimate adsorption. The total surface area (S_{total}) and specific surface area (S_{BET}) are calculated by:

$$S_{Total} = \frac{V_m N_a A}{V} \quad \mathbf{2.9}$$

$$S_{BET} = \frac{S_{Total}}{a} \quad \mathbf{2.10}$$

where N_a is the Avogadro's constant, A is the area of one nitrogen molecule (0.162 nm²) and a is the mass of the absorbent sample.

The Barrer, Joiyner and Hallenda (BHJ) method is commonly used to measure the mesopore volume and mesopore size distribution of solid samples. This method describes the adsorption-capillary pore condensation process that occurs in mesopores: in the capillary condensation region ($P/P_o > 0.4$), increase in pressure causes an increase in the thickness of the layer adsorbed on the walls of the pore and capillary condensation in empty pores with a radius of r_c . This effect is described by the Kelvin equation:

$$\ln\left(\frac{P}{P_o}\right) = -\frac{2\gamma w_m \cos\theta}{RT r_c} \quad 2.11$$

where r_c is the radius for the cylindrical pores or the distance between the walls of slit-shaped pores, γ is the surface tension, w_m is the molar volume, and θ is the contact angle.

The model assumes that the pores are either cylindrical or slit shaped and provides a method to calculate the contributions of the thickness of the adsorbed film to the total adsorption, and then the core volume. This, in conjunction with the assumed pore geometry, enables the core volume to be translated into the pore volume, and the core size into the pore size. By examining the isotherm step-by-step in the range $0.42 < P/P_o < 0.98$ in this way, the mesopore volume and mesopore size distribution can be calculated.²¹

The BET method was used to measure S_{BET} and the BHJ method was used to calculate the pore volume and average pore size distribution of the solid samples in this work. A Micrometrics ASAP 2010 instrument was used to conduct N₂ adsorption porosimetry studies of RPN-SiO₂ and PMo/RPN-SiO₂ solid catalyst samples. Samples were pre-treated at 140 °C under vacuum in a tube furnace for 2.5 h and then for a further 2 h at 140 °C on ASAP 2010 to a pressure below 8 μmHg to remove all gasses from the pores.

2.3 Catalyst Reaction Studies

2.3.1 Product Analysis

Gas-liquid chromatography was used for the quantitative analysis of products from the RPN-POM catalysed oxidation reactions with H₂O₂ in this study.

2.3.1.1 Gas-Liquid Chromatography

Gas chromatography is used for the separation and quantitative analysis of compounds in a sample that can be volatilized without decomposition. Separation of the components of the volatilities operates on the principle of phase partition; that is, the different affinities that the components have for two phases –a mobile gas phase and a stationary solid or immobilised liquid phase - and the equilibria they establish as they diffuse between these phases.²⁶

The sample is injected into an injection port where it is volatilised. The gaseous sample is then mobilised through a heated column by an inert or unreactive carrier gas such as nitrogen, helium, hydrogen or argon. A liquid layer on an inert support lining the inside of the column acts as a stationary phase. As the sample passes through the column its constituent molecules interact with the surface groups of the stationary phase which slows the rate at which the components travel through the column; the more strongly a compound interacts with the surface, the more slowly it will pass through the column. The time that it takes a component to pass through the column is called the *retention time*. A constituent's functional groups influence how strongly or weakly they interact with the stationary phase and/or the gas phase. The number, size and type of functional groups will, thus, influence the retention time. The overall size of a constituent will also affect retention time. Different constituents of different sizes and with different functional groups will, therefore, have different retention times.

Once components have passed through the column they then enter a detector where they are analysed using spectroscopic or thermal/electrical conductance techniques. The results are then plotted as a function against time to give the final chromatogram of the sample.

A diagram showing the typical set-up of gas chromatographic instrumentation is shown in Fig. 2.11.

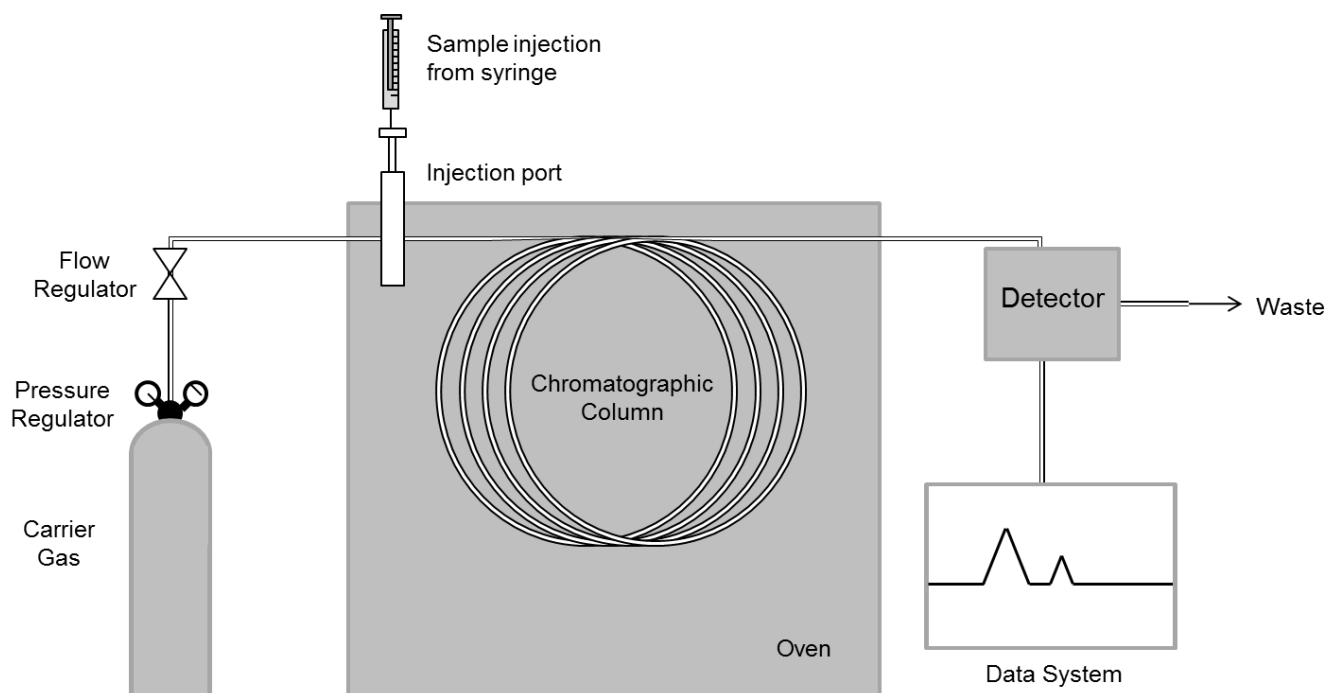


Fig. 2.11. General set-up of gas chromatographic instrumentation.

2.3.1.1.1 Injection Port – Split/Splitless Inlet

Injection ports (or column inlets) provide a method for delivery of the sample onto the GC column. Many GC systems use a split/splitless inlet (Fig. 2.12). This was the type of delivery system used to introduce sample in our work. The sample is injected through a rubber septum using a microliter syringe into the heated inlet where it is volatilised and mixes with the carrier gas. The resulting sample gas is contained inside a quartz glass liner and continued flow of carrier gas forces the sample gas either onto the column or in between the inlet liner and the

injector body and into the split line. If the split valve is open, then the sample gas traveling *via* the latter route is purged out from the system.

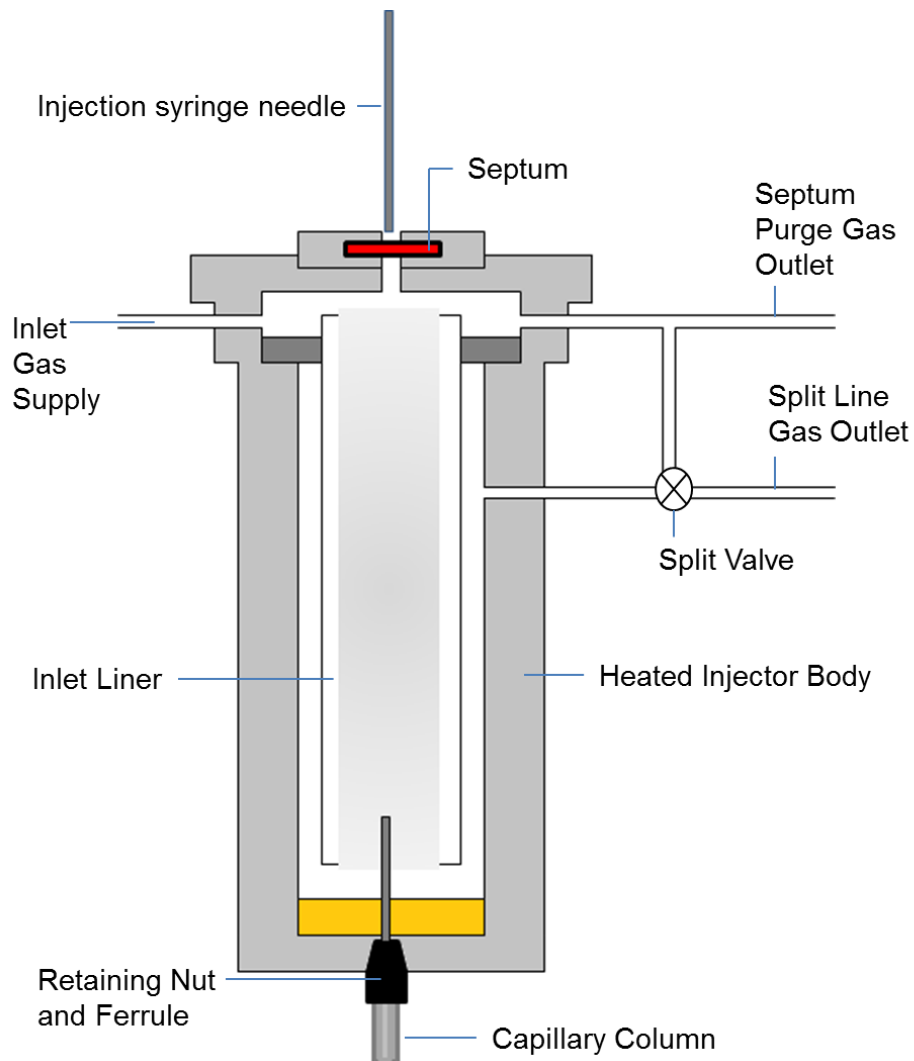


Fig. 2.12. Split/splitless injection port.

The amount of sample entering the column is dependent on the relative flow rates through the column and through the split line. This is called the split ratio. The higher the split ratio the smaller the amount of sample passing through the column. The flow of sample gas through the liner (liner flow) is dependent on both the flow through the split line (split flow) and the flow through the column (column flow)

2.3.1.1.2 Column

In gas chromatography, the column is responsible for the separation of components in a sample mixture. It is the column that contains the stationary phase for the separation process. The most commonly used columns have a thin liquid film (0.1-0.5 μm) constituting the stationary phase which coats the inner wall of the capillary (Fig. 2.13). These columns are termed “capillaries” due to their small inner diameters (0.1-0.5 mm) and typically have lengths of 10-100 m. Although “partition” describes the distribution of a molecule between two immiscible solution phases, the term is still commonly used in gas-liquid chromatography (GLC) to describe the distribution of a given solute/analyte between the gas phase and the stationary liquid phase on the surface of the column. In this case, it is helpful to view the gas phase as a *pseudo*-solvent or gaseous eluent for the volatilised analytes.

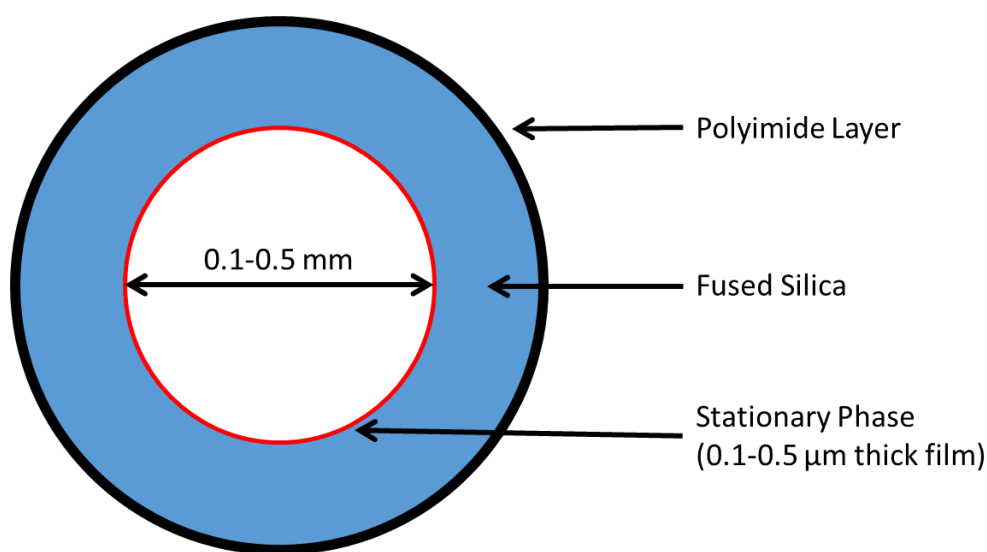


Fig. 2.13. Organisation of layers in an open tubular capillary column.²⁶

The retention of analytes on the column depends on the column's efficiency. This is described in terms of “the height of a theoretical plate” A plate refers to the length of column in which

the analyte equilibrates between the mobile phase and the stationary phase. The more efficient the column is, the smaller plate the height will be, the more equilibrations will occur in the length of the column and the more time the analyte will spend on the column which will result in a longer analyte retention time. A highly efficient GC column is one which is long in length with a narrow internal diameter and thin film stationary phase. Efficient columns provide the best separation of analytes as each analyte will have a different affinity for the stationary phase.

2.3.1.1.3 Stationary Phase

The stationary phase inside the capillary column of a gas chromatogram plays a vital part in the separation of the analytes in a sample. An ideal stationary phase is one that is selective and has a different adsorptivity for each component to ensure separation, and can also operate over a wide temperature range. It also must be chemically and thermally stable, with a low vapour pressure at high operating temperatures.

There are two main types of stationary phase, nonpolar and polar. When a nonpolar stationary phase is used, there will be very little interaction between the sample compounds and the stationary phase, and separation will occur because of the different boiling points of the compounds. When a more polar stationary phase is used, the compounds will be separated due to their different polar interactions with the stationary phase and their different boiling points.

2.3.1.1.4 Column Oven and Temperature Control

The column oven controls the column temperature in the chromatogram. Heating is uniform along the length of the column to ensure thermodynamic equilibrium is maintained throughout the column, which also guarantees that measurements/separations are not effected by

atmospheric temperature. Retention of compounds on a column is temperature dependent. Increasing the temperature typically reduces the retention for most compounds.

2.3.1.1.5 Detector

Once a sample has passed through the column, its presence and/or relative concentration can be measured by a detector. The outlet of the column is directly attached to the detector in the chromatograph for this purpose. One type of detector most commonly used in tandem with gas chromatography is a flame ionisation detector (FID). This detector was used for the analysis of our samples. The analyte is ionised in a flame composed of hydrogen and air. These ions are then impelled by an electrical potential towards an electrode which produces a small current measured in picoamps. This current is then converted to a voltage, amplified, and displayed as a point in a chromatogram of electron volts (eV) vs. time (often min).

The larger the concentration of the analyte that passes through, the more ions will be formed which will induce a stronger current and give a larger reading. If a high concentration of analyte passes into the detector over a very short time interval then a very intense, sharp peak will be produced in the chromatogram. A diagram of an FID is shown in Fig. 2.14.

At the entrance of the detector is a heated zone (300-350 °C) where the carrier gas exits the column and is combined with hydrogen gas before entering the flame chamber. Air enters the chamber through a separate channel. The flow rate of carrier gas, hydrogen and air is usually set to a 1:1:10 ratio. The gas exiting through the jet tip is ignited by the flame ignition coil. The flame is sustained by a continuous flow of hydrogen and carrier gas through the jet tip and the excess of air in the chamber. The reducing zone of the flame is at the centre close to the jet tip. As the analyte passes through the reducing zone of the flame it reacts to form ions. The reaction for hydrocarbons occurs through the steps outlined in equations 2.12 and 2.13.²⁶

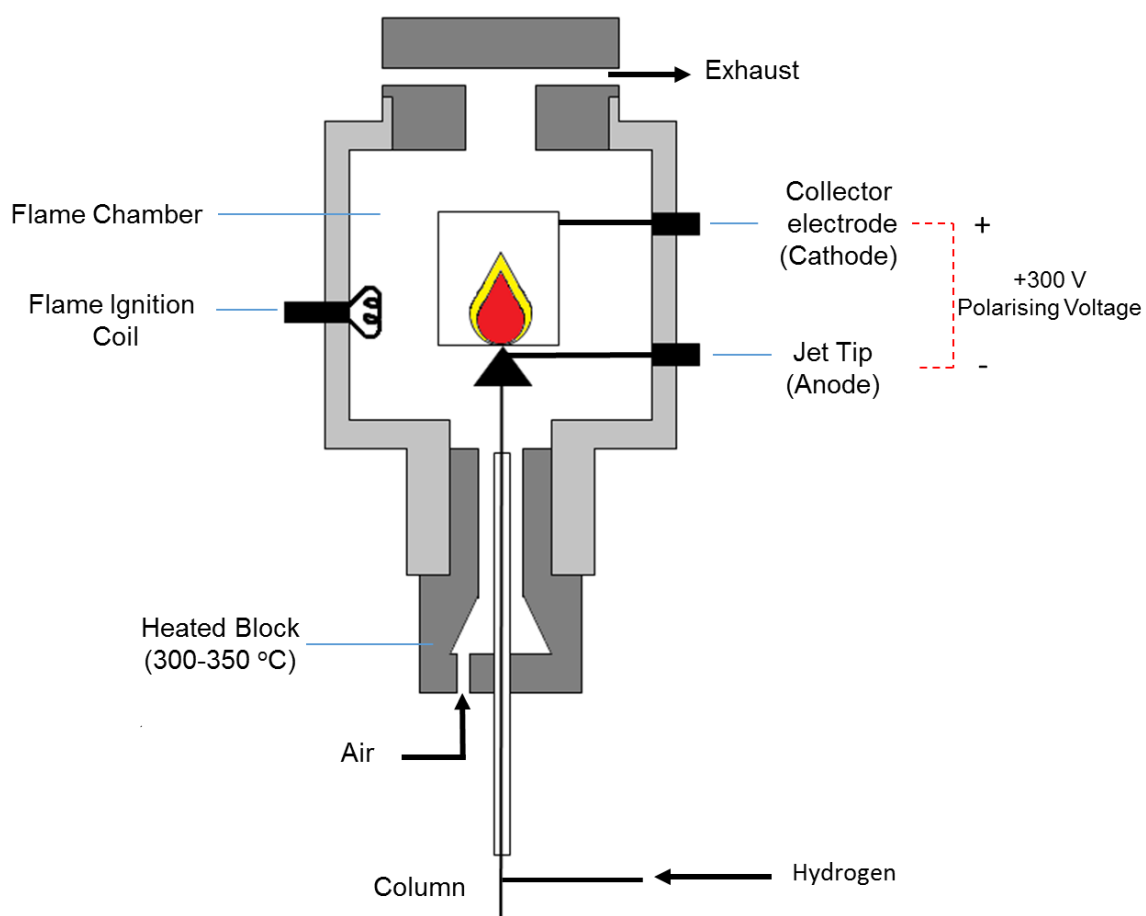
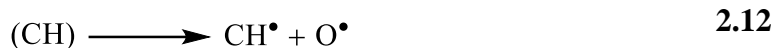


Fig. 2.14. Diagram of a flame ionisation detector (FID).



A potential is applied across the collector electrode and the jet tip to measure the change in current produced from the ions.

FID can detect all organic compounds apart from formic acid. The minimum detectable mass of analyte is about 0.01-0.1 ng.

2.3.1.1.6 Chromatogram

Once a mixture of compounds has been separated through the column and detected by the detector the results are displayed in a chromatogram as a function of retention time versus the output signal of the detector measured in appropriate units (e.g. mV for FID).

2.3.1.2 Calibration of Compounds

It is very difficult to inject the exact same volume of sample onto the GC column each time as each injection uses only microliters of sample. Injecting different volumes of sample into the chromatogram will introduce different amounts of analyte onto the column which will produce signals with different peak areas, i.e. it is impossible to know the exact concentration of a compound that has produced a signal peak in the chromatogram due to the large error associated with the sample injection volume *via* this method. To compensate for this, the *internal standard method* can be used.

When attempting to measure the concentration of an analyte, an internal standard of known concentration is added to the sample, and the relative response factor, R_f , of the analyte must be calculated. This is the ratio between a signal produced by an analyte and the quantity of analyte which produced the signal, using the internal standard as a reference. In mathematical terms, it is the inverse of ratio of the proportionality constants, k , for the relationship between the signal peak areas and concentrations for the analyte and the internal standard (equations 2.14-2.17).

$$S = k \times M \times V \quad \mathbf{2.14}$$

$$S_o = k_o \times M_o \times V_o \quad \mathbf{2.15}$$

$$\frac{S}{S_o} = \frac{k}{k_o} \times \frac{M}{M_o} \times \frac{V}{V_o} \quad \mathbf{2.16}$$

$$\frac{S}{S_o} = \frac{k}{k_o} \times \frac{M}{M_o} \quad 2.17$$

where S is the analyte signal peak area, S_o is the internal standard signal peak area, k is the analyte proportionality constant, k_o is the internal standard proportionality constant, M is the number of moles of analyte, M_o is the number of moles of internal standard, V is the analyte sample volume, and V_o is the internal standard sample volume.

R_f is important as it is used to compensate for the irreproducibility of manual injections. The internal standard must be a spectator in the sample mixture and must not interfere with the signal of the analyte. In this way, if the injection volumes vary slightly between injections, the ratio of peak areas of the analyte and the internal standard will remain constant. Thus, in (eq. 2.16) $V/V_o = 1$ and this term becomes negligible, hence, the peak area of the internal standard can be used as a reference for the value of the peak area for the analyte (eq. 2.17). Even if the concentration of analyte varies between samples, so long as the concentration of the internal standard is known then the concentration of the analyte can be calculated from the ratio of the peak areas and R_f .

R_f can be calculated, or *calibrated*, by injecting solutions (standards) into the GC and recording the peak area counts of the corresponding signals for the internal standard (S_o) and the analyte (S). Each standard has a known concentration of the internal standard (M_o), and a known concentration of analyte (M) which is different for each standard. Rearrangement of eq. 2.17 gives eq. 2.18. A plot of the ratio of signal peak area counts (S/S_o) against the corresponding ratio of the concentrations (M/M_o) for each standard produces a graph which obeys eq. 2.18, the gradient of which is R_f of the analyte to the GC referenced to the internal standard.

$$\frac{M}{M_o} = R_f \times \frac{S}{S_o} \quad 2.18$$

Figs. 2.15 through 2.24 show the calibration plots used to calculate the R_f values for each compound. Table 2.1 summarises the R_f values, retention times and boiling points of reactants and products tested for the epoxidation of olefins and oxidation of benzothiophenes by H_2O_2 . The R_f values were measured using the GC-FID set-up and temperature programmes outlined in Chromatograph Specifications (Section 2.3.1.3 below).

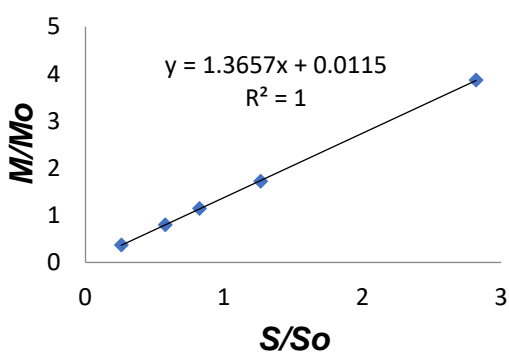


Fig. 2.15. Cyclooctene calibration.

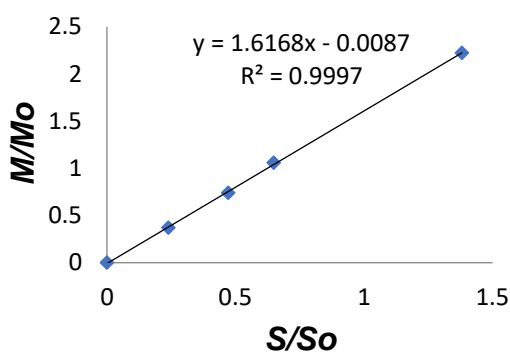


Fig. 2.16. Epoxycyclooctane calibration.

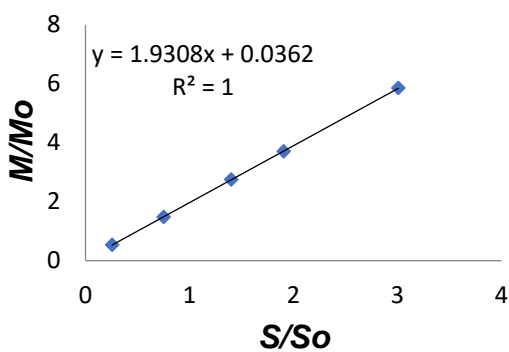


Fig. 2.17. 1-Hexene calibration.

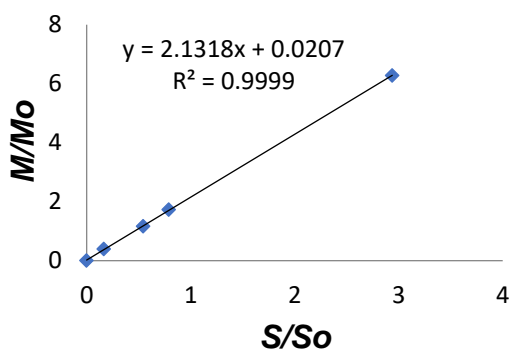


Fig. 2.18. 1,2-Epoxyhexane calibration.

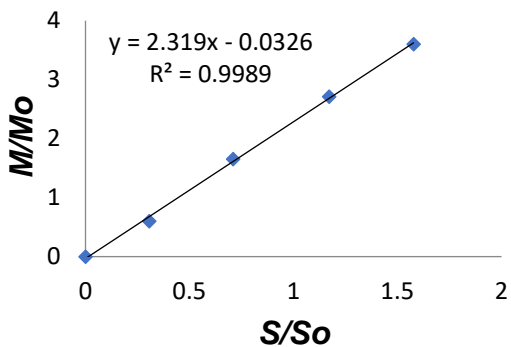


Fig. 2.19. Cyclohexene calibration.

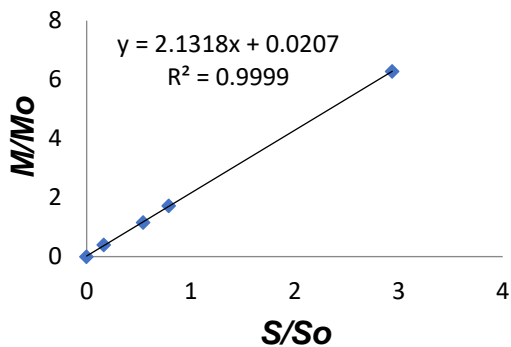


Fig. 2.20. Epoxycyclohexane calibration.

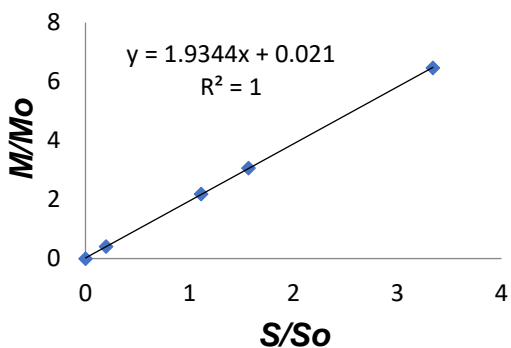


Fig. 2.21. Epoxyoctane calibration.

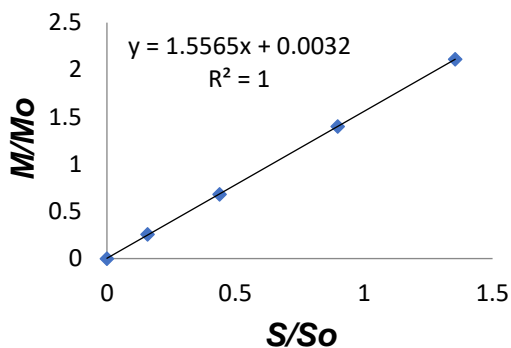


Fig. 2.22. Benzothiophene calibration.

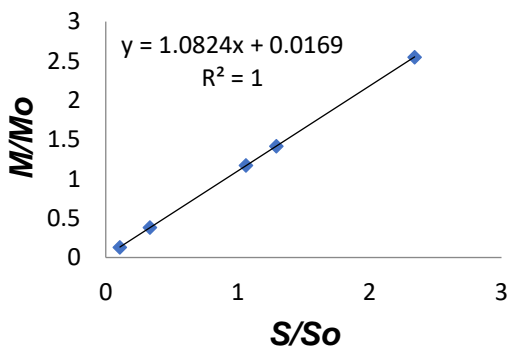


Fig. 2.23. Dibenzothiophene calibration.

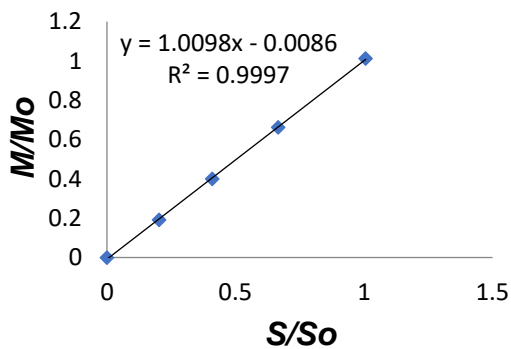


Fig. 2.24. 4,6-Dimethyldibenzothiophene calibration.

Table 2.1. Boiling points, retention times and relative response factors (R_f) of compounds in olefin epoxidation and dibenzothiophene oxidation. *

Compound	Boiling Point (°C)	Retention Time (min)	R_f (rel. to decane)	R_f (rel. to dodecane)
Decane	174	6.9 – 7.0	1.0	-
Dodecane	216	8.4 - 8.5	-	1.0
Cyclooctene	146	5.7 - 5.8	1.37	-
Epoxycyclooctene	189.3	7.9 - 8.0	1.61	-
1-Hexene	63	2.2 - 2.3	1.93	-
1,2-Epoxyhexane	118	4.3 - 4.4	2.14	-
Cyclohexene	83	2.9 - 3.0	-	-
Epoxycyclohexane	130	5.0 - 5.1	2.29	-
1,2-Octene	121	4.1 - 4.2	-	-
1,2-Epoxyoctane	170	6.4 - 6.5	-	1.94
Benzothiophene	221	8.7 - 8.8	-	1.56
Dibenzothiophene	333	13.8 - 13.9	-	1.08
4,6-Dimethyldibenzothiophene	365	15.5 - 15.7	-	1.01

2.3.1.3 Chromatograph Specifications

In this work, samples were run on a Varian Chrompack CP-3380 Gas chromatograph equipped with FID and a 25 m × 0.32 mm × 0.5 μm BP1 (100% dimethyl polysiloxane) capillary column. Nitrogen was employed as a carrier gas at a flow rate of 2 mL/min. Nitrogen was also used as FID make-up gas at a flow rate of 30 mL/min. The split ratio was 1:20. The injector and detector temperatures were set at 250 °C and 300 °C, respectively.

The column oven was set using the following temperature programmes for analysis of reactants and products of olefin epoxidation (Fig.16) and benzothiophene oxidation (Fig. 17) reactions, respectively:

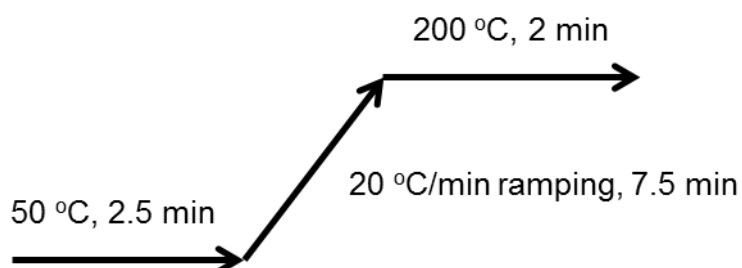


Fig. 2.25. Temperature programme for the GC column for analysis of olefin epoxidation reaction samples.

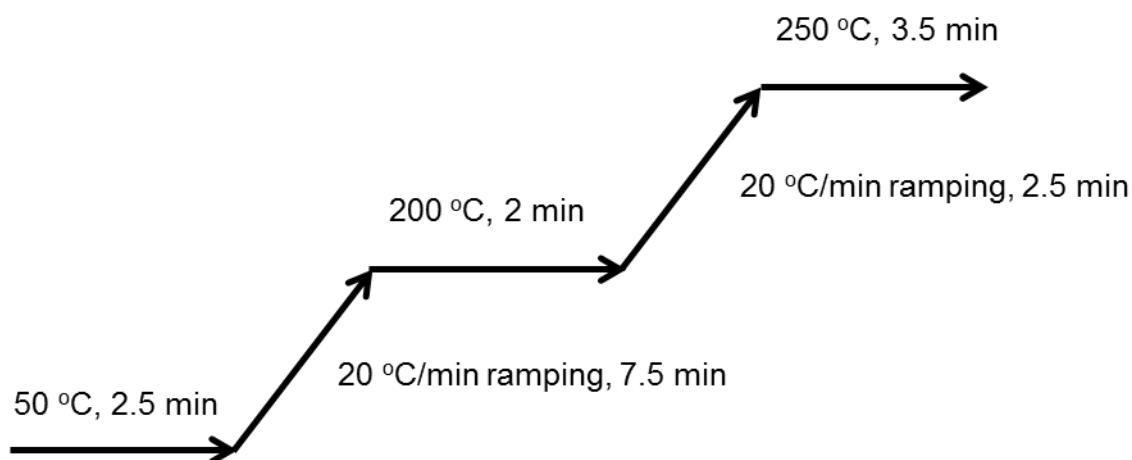
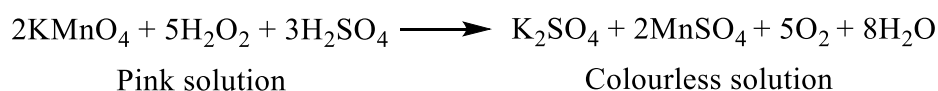


Fig. 2.26. Temperature programme for the GC column for analysis of benzothiophene oxidation reaction samples.

2.3.2 Titrations

Titration is a quantitative analytical technique which is used to determine the unknown concentration of an identified solution. Typically, a solution of known concentration (titrant) is slowly added to a known volume of sample solution with an unknown concentration (titrand) until a notable “end-point” is observed. The end-point can correspond to a colour change, a product precipitating or, in the case of a potentiometric titration, the formation of a peak in the analysed data.

The following reaction occurs when aqueous potassium permanganate solution is added to hydrogen peroxide solution acidified with dilute sulfuric acid:



This reaction is used to determine the concentration of H_2O_2 in a solution. Titration with KMnO_4 gives a colourless solution when H_2O_2 is present and turns the solution pink when all the H_2O_2 has reacted, signifying the end-point.

The remaining H_2O_2 at the end of our biphasic oxidation reactions was determined by titration of the remaining aqueous phase with KMnO_4 (0.005 M) to calculate the H_2O_2 selectivity of the reaction. H_2O_2 selectivity was given by:

$$\text{Epoxidation } \text{H}_2\text{O}_2 \text{ selectivity} = \frac{\text{Product (mol)}}{(\text{Initial } \text{H}_2\text{O}_2 - \text{Final } \text{H}_2\text{O}_2) \text{ (mol)}} \times 100 \quad \mathbf{2.19}$$

Desulfurization H_2O_2 selectivity

$$= \frac{2 \times \text{Conversion of substrate (mol)}}{(\text{Initial } \text{H}_2\text{O}_2 - \text{Final } \text{H}_2\text{O}_2) \text{ (mol)}} \times 100 \quad \mathbf{2.20}$$

2.3.3 Reaction Studies

Unless specified otherwise, all reactions in this study were conducted in a 50 mL jacketed glass reactor equipped with a magnetic stirrer, a reflux condenser and a Jencons Julabo heat circulator. The equipment set-up is shown in Fig. 2.27.

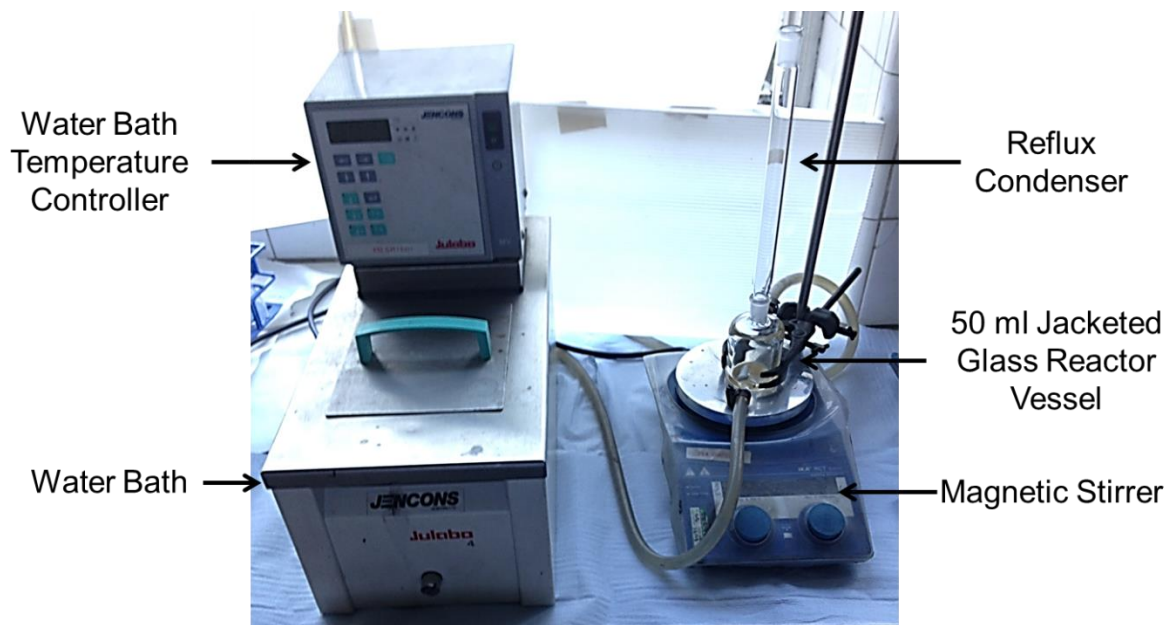


Fig. 2.27. Set-up of equipment for reactions.

In this work, decane or dodecane was used as an internal standard for biphasic oxidation with H_2O_2 . Samples of the organic layer were collected after set time intervals during the reaction and injected into a GC-FID for analysis (for GC specifications, see above). The moles of reactant or product were calculated from the area counts of the corresponding peaks and internal standard peak in accordance with equation 2.21.

$$M = R_f \times \frac{S}{S_o} \times M_o \quad 2.21$$

where R_f is the relative response factor of the reactant or product, S/S_o is the ratio of the signal peak area counts recorded for the analyte and internal standard, and M_o is the known

concentration of internal standard. The yield of product (%) and conversion of reactant (%) were then calculated using equations 2.20 and 2.21, respectively.

$$\text{Epoxide yield} = \frac{\text{Product (mol)}}{\text{Initial H}_2\text{O}_2 \text{ (mol)}} \times 100 \quad 2.22$$

$$\text{Sulfone yield} = \frac{2 \times \text{Product (mol)}}{\frac{2}{3} \text{Initial H}_2\text{O}_2 \text{ (mol)}} \times 100 \quad 2.23$$

$$\text{Conversion} = \frac{(\text{Initial reactant} - \text{Final reactant}) \text{ (mol)}}{\text{Initial reactant (mol)}} \times 100 \quad 2.24$$

The product yield (%) or the conversion of substrate (%) was then plotted against the corresponding reaction time in a scatter plot to trace the progress of the reaction (see example in Fig. 2.28).

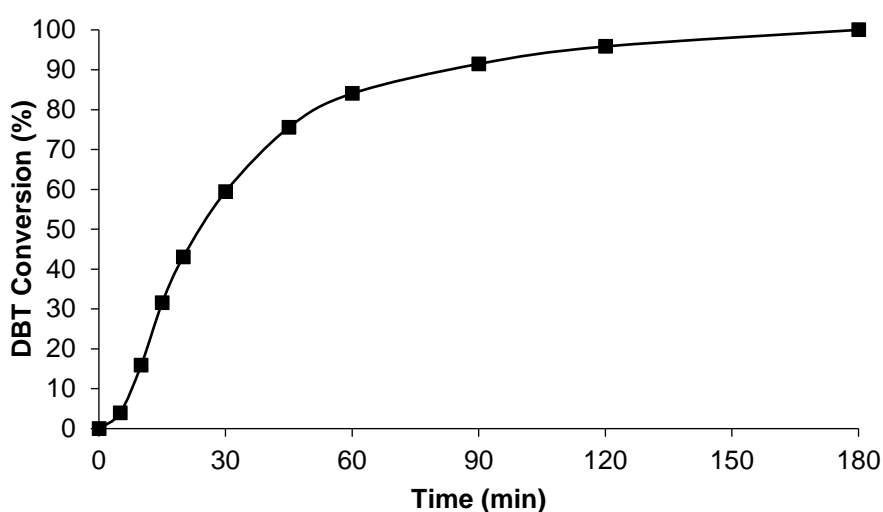


Fig. 2.28. Plot of conversion of DBT versus time for desulfurization of heptane model diesel fuel with H₂O₂ and PMo/BzPN-SiO₂ catalyst.

2.3.3.1 RPN-POM Catalysed Biphasic Oxidation Reactions with H₂O₂

The oxidation of benzothiophenes and epoxidation of alkenes were carried out in an aqueous biphasic system containing toluene, n-heptane or 1,2-dichloroethane as an organic solvent and aqueous H₂O₂ at 25-60 °C in a 50 mL glass reactor equipped with a magnetic stirrer, a reflux condenser and a heat circulator. The methodologies for the reactions are outlined below. The reactions were carried out at a stirring speed of 1000 rpm; at stirring speeds above 500 rpm, the reaction rate did not depend on the stirring speed. Blank experiments showed that no reaction occurred in the absence of POM, and practically no reaction was observed for olefin epoxidation or oxidative desulfurization in the presence of POM without RPN. The reactions were monitored by taking aliquots from the organic phase and submitting them to GC analysis. After reaction, the amount of remaining H₂O₂ was determined by titration with KMnO₄ for the efficiency of hydrogen peroxide use to be estimated. The mean absolute percentage error in conversion and product yield was $\leq 5\%$.

For catalyst reuse, the catalyst was separated after reaction by complete evaporation of the reaction mixture under vacuum, washed with hexane and reused. In the case of DBT oxidation, this procedure led to accumulation of the product sulfone which did not affect catalyst performance in consecutive runs. Excess sulfone could be removed by precipitation from toluene.

2.3.3.1.1 Epoxidation of Olefins

The epoxidation of olefins was carried out using one of two methods:

Method 1: POM (0.0065 mmol), RPN (0.0395 mmol), organic solvent (5 ml), H₂O (0.2 ml) and H₂O₂ (30% w/v, 0.1 ml, 1.014 mmol) were added to the reactor vessel. The resulting

mixture was stirred initially at room temperature whilst the heat circulator was switched on. Once the desired reaction temperature had been established, the reaction mixture was stirred for a further 5 minutes. 5 ml of a solution composed of cyclooctene (6.78 mmol), decane as internal standard (2.13 mmol) and organic solvent was added to start the reaction. Aliquots were taken from the organic layer after 0, 5, 10, 15, 20, 30, 45, 60, 90 and 120 minutes, centrifuged and analysed using GC to track the progress of the reaction.

Method 2: POM (0.0086 mmol), H₂O (0.2 ml), H₂O₂ (30% w/v, 0.1 ml, 1.01 mmol), organic solvent (5 ml) and 5 ml of a solution composed of cyclooctene (9.71 mmol), decane as internal standard (2.13 mmol) and organic solvent were added to the reactor vessel. The resulting mixture was stirred initially at room temperature for 2 minutes to activate the catalyst. The mixture was then heated to reaction temperature and RPN (0.0515 mmol) was added to start the reaction. Aliquots were taken from the organic layer after 0, 5, 10, 15, 20, 30, 45, 60, 90 and 120 minutes, centrifuged and analysed using GC to track the progress of the reaction.

2.3.3.1.2 Oxidative Desulfurization

The heat circulator was first heated up and stabilized at the desired reaction temperature (25-60 °C). Then, organic solvent (5 ml), RPN (0.0023 mmol), hydrogen peroxide (30% w/v, 0.15 ml, 1.5 mmol) and POM (0.0056 mmol) were added to the reactor vessel and stirred for 5 min. Finally, the sulfur compound (0.5 mmol) and standard (0.4 mmol) were dissolved in solvent (5 ml) and added to reaction mixture. Aliquots were taken from the organic layer after 2, 5, 10, 20, 30, 60, 90 and 120 minutes, centrifuged and analysed using GC to track the progress of the reaction.²⁷

2.3.3.2 POM/RPN-SiO₂ Catalysed Biphasic Oxidation Reactions with H₂O₂

The oxidation of benzothiophenes and epoxidation of alkenes were carried out in an aqueous biphasic system containing toluene, n-heptane or 1,2-dichloroethane as an organic solvent and aqueous H₂O₂ at 25-60 °C in a 50-mL glass reactor equipped with a magnetic stirrer, a reflux condenser and a heat circulator. The reactions were conducted using the methodologies outlined below. All reactions were stirred at a rate of 1500 rpm unless specified otherwise. The reaction rate did not depend on the stirring speed in the range of 1000-1500 rpm, which indicates no limitation by external diffusion. The reactions were monitored by taking aliquots from the organic phase and submitting them to GC analysis.

After reaction, the amount of remaining H₂O₂ was determined by titration with KMnO₄ for the efficiency of hydrogen peroxide use to be estimated. The mean absolute percentage error in conversion and product yield was $\leq 10\%$.

2.3.3.2.1 Oxidative Desulfurization

POM (0.0056 mmol), H₂O₂ (30% w/v, 0.15 ml, 1.51 mmol), dodecane as internal standard (0.4 mmol), DBT (0.5 mmol) and heptane (10 ml) were combined in the reactor vessel. The mixture was then stirred for 2 minutes at room temperature to allow the catalyst to activate. The vessel was then heated to reaction temperature and RPN-SiO₂ (0.0056 mmol surface RPN) was added to start the reaction. Aliquots were taken from the organic layer after 0, 5, 10, 15, 20, 30, 45, 60, 90, 120 and 180 minutes, centrifuged and analysed using GC to track the progress of the reaction.

For catalyst reuse, the initial reaction was run using the above procedure. After reaction, the mixture was left to settle and the organic and aqueous layers were carefully decanted off. The

catalyst powder in the reactor vessel was washed with 2 x 5 mL of acetonitrile to remove the sulfone product then washed with heptane (5 mL) using a centrifuge. The catalyst was dried at ambient temperature overnight. The dried catalyst was added back to the reactor along with specified amounts of H₂O₂, dodecane, benzothiophene, and heptane (10 mL) for the next run.

2.3.3.2.2 *Epoxidation of Olefins*

POM (0.0062 mmol), H₂O₂ (10% w/v, 0.3ml, 1.01 mmol), decane (2.13 mmol), cyclooctene (9.71 mmol) and organic solvent (10 ml) were combined in the reactor vessel. The reaction mixture was then stirred for 2 minutes at room temperature to allow the catalyst to activate. The vessel was then heated to reaction temperature and RPN-SiO₂ (0.0062 mmol surface RPN) was added to begin the reaction. Aliquots were taken from the organic layer after 0, 5, 10, 15, 20, 30, 45, 60, 90, 120, 180, 240 and 300 minutes, centrifuged and analysed using GC to track the progress of the reaction.

For catalyst reuse, the initial run used PMo (0.0062 mmol), BzPN-SiO₂ (0.0062 mmol surface BzPN), H₂O₂ (10% w/v, 0.3 mL, 1.01 mmol), decane (2.13 mmol), cyclooctene (0.971 mmol) and DCE (10 mL). The reaction was carried out at 60°C and 1500 rpm stirring speed. After reaction, the catalyst powder was isolated by decanting off the reaction mixture and washed with 2 × DCE washings (5 mL) and dried at room temperature and pressure overnight. Subsequent runs reused catalyst powder with fresh H₂O₂ (0.3 mL, 1.01 mmol, 10% w/w), decane (2.13 mmol), cyclooctene (9.71 mmol) and DCE (10 mL).

2.3.3.3 Epoxidation of Olefins Catalysed by Eutectic RPN-POMs

Eutectic RPN-POM (0.0125 mmol) was added to a vial equipped with a magnetic stirring bar. To this, olefin (3.4 mmol unless otherwise specified) and aqueous H₂O₂ (3 mmol, 30 % w/v) was added which was then stirred in an oil bath at 60°C for 4 hours. After reaction was stopped, toluene (5 mL) containing decane (2.14 mmol) was added to the mixture which was then stirred for an additional 30 seconds. The mixture was then left standing to allow layers to separate before the organic layer was isolated for analysis.

For catalyst reuse, heptane was used in place of toluene as this solubilised the reactants and products but did not appear to solubilize the catalyst. Once products/reactants were removed, catalyst was washed with heptane and dried in an oven at 100 °C for 30 min before re-use.

For kinetic testing at different stirring speeds, HexCyPN-PMo (0.0125 mmol), cyclooctene (30 mmol), decane (2.14 mmol) and aqueous H₂O₂ (3 mmol, 30 % w/w) was added to a 50 mL jacketed glass reactor vessel equipped with a magnetic stirrer, heat circulator and reflux condenser. Reaction was conducted at 60 °C and stirred at the required speed.

The reactions were monitored by taking aliquots from the organic phase and submitting them to GC analysis. Epoxide yield (%) was calculated using eq. 2.20, substrate conversion (%) was calculated using eq. 2.21, H₂O₂ selectivity (%) was calculated using eq. 2.22, and mass balance (%) was calculated using eq. 2.23. The mean absolute percentage error for product yield, conversion, selectivity and mass balance were ≤ 4%.

$$H_2O_2 \text{ selectivity} = \frac{\text{Epoxide product (mol)}}{(\text{Initial substrate} - \text{Final substrate}) \text{ (mol)}} \times 100 \quad \mathbf{2.25}$$

$$\text{Mass balance} = \frac{(\text{Epoxide product} + \text{Final substrate}) \text{ (mol)}}{\text{Initial substrate (mol)}} \times 100 \quad \mathbf{2.26}$$

References

- 1 J. F. Bickley, R. Bonar-Law, G. T. Lawson, P. I. Richards, F. Rivals, A. Steiner and S. Zacchini, *Dalt. Trans.*, 2003, 1235–1244.
- 2 X. Hou and B. T. Jones, in *Encyclopedia of Analytical Chemistry*, ed. R. A. Meyers, Wiley, Chichester, 2000, pp. 9468–9485.
- 3 W. Zhou, R. P. Apkarian and Z. L. Wang, in *Scanning Microscopy for Nanotechnology*, 2007, pp. 1–40.
- 4 A. W. Coats and J. P. Redfern, *Analyst*, 1963, **88**, 906–924.
- 5 G. W. H. Höhne, W. Hemminger and H.-J. Flammersheim, *Differential Scanning Calorimetry An: Introduction for Practitioners*, Springer Berlin Heidelberg, 1996.
- 6 S. Duckett and B. Gilbert, *Foundations of Spectroscopy*, Oxford University Press, New York, 2000.
- 7 A. K. Brisdon, *Inorganic Spectroscopic Methods*, Oxford University Press, New York, 1998.
- 8 J. Mendham, R. C. Denney, J. D. Barnes and M. J. K. Thomas, *Vogel's Textbook of Quantitative Chemical Analysis*, Pearson Education Ltd., 2000.
- 9 J. A. Iggo, *NMR Spectroscopy in Inorganic Chemistry*, Oxford University Press, New York, 1999.
- 10 Z. Zhu, R. Tain and C. Rhodes, *Can. J. Chem.*, 2003, **81**, 1044–1050.
- 11 S. S. Lim, G. I. Park, I. K. Song and W. Y. Lee, *J. Mol. Catal. A Chem.*, 2002, **182**, 175–183.

- 12 Y. Kim and W. Lee, *J. Korean Magn. Reson. Soc.*, 1997, **1**, 45–58.
- 13 J.-M. Brégeault, M. Vennat, J.-Y. Piquemal, Y. Mahha, E. Briot, P. C. Bakala, A. Atlamsani and R. Thouvenot, *J. Mol. Catal. A Chem.*, 2006, **250**, 177–189.
- 14 V. Nardello, J. Marko, G. Vermeersch and J. M. Aubry, *Inorg. Chem.*, 1995, **34**, 4950–4957.
- 15 D. C. Duncan, R. C. Chambers, E. Hecht and C. L. Hill, *J. Am. Chem. Soc.*, 1995, **117**, 681–691.
- 16 B. M. Fung, A. K. Khitrin and K. Ermolaev, *J. Magn. Reson.*, 2000, **142**, 97–101.
- 17 C. R. Morcombe and K. W. Zilm, *J. Magn. Reson.*, 2003, **162**, 479–486.
- 18 E. Brendler, T. Heine, A. F. Hill and J. Wagler, *Z. Anorg. Allg. Chem.*, 2009, **635**, 1300–1305.
- 19 W. Clegg, *X-Ray Crystallography*, Oxford University Press, Oxford, 2015.
- 20 G. M. Sheldrick, *Acta Crystallogr. Sect. A Found. Crystallogr.*, 2007, **64**, 112–122.
- 21 G. Leofanti, M. Padovan, G. Tozzola and B. Venturelli, *Catal. Today*, 1998, **41**, 207–219.
- 22 Malvern Instruments Ltd, *A basic guide to particle characterization*, 2012.
- 23 K. S. W. Sing, D. H. Everett, R. a. W. Haul, L. Moscou, R. a. Pierotti, J. Rouquérol and T. Siemieniewska, *Pure Appl. Chem.*, 1985, **57**, 603–619.
- 24 M. Kruk and M. Jaroniec, *Chem. Mater.*, 2001, **13**, 3169–3183.
- 25 R. Hetterley, PhD Thesis: *Multifunctional Catalysts for the One-Step Conversion of Acetone to Methyl Isobutyl Ketone*, University of Liverpool, 2008.

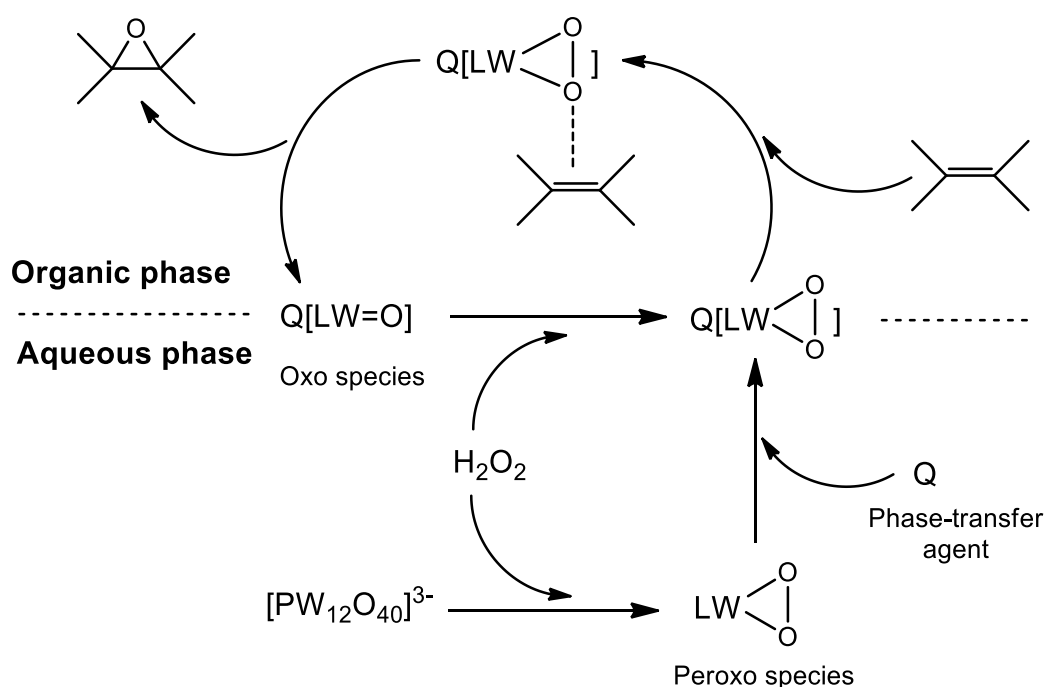
- 26 E. Ludanes, L. Reubsaet and T. Greibrokk, *Chromatography*, Wiley VCH, Weinheim, 2014.
- 27 R. Yahya, PhD thesis: *Polyoxometalate Catalysis for Oxidative Desulfurization*, University of Liverpool, 2015.

3. System One: Homogeneous Catalysis – Biphasic Oxidation Reactions with Hydrogen Peroxide Catalysed by RPN-POM Salt Aggregates

3.1 Introduction

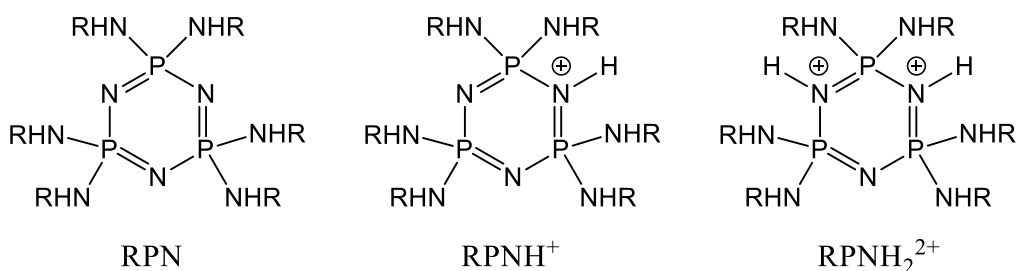
The biphasic oxidation of olefins and desulfurization of fuels are reactions of interest in both industry and academia.¹⁻⁹ Oxidation of olefins is used to produce epoxides which are important precursors for epoxy resins, surfactants and paints, and are key intermediates in organic syntheses.¹⁰⁻¹⁶ Oxidative desulfurization is an emerging technology for the removal of heavy aromatic organosulfur compounds from vehicular diesel fuels, which cannot be easily removed by commercialized processes (e.g. hydrodesulfurization, HDS) without increasing the cost of processing and compromising fuel quality.¹⁷⁻¹⁹ It is important that sulfur-containing compounds are removed from fuels as their combustion produces SO_x species which are harmful to health and the environment. Many of the biphasic systems used for these processes employ polyoxometalates (POMs) - nano-sized metal-oxygen cluster anions - as catalysts because of the rich variety of structures they can possess, their diverse range of mechanical and electronic properties, and the functional versatility that these attributes provide.²⁰ Keggin-type POMs are the most heavily investigated and widely used. These compounds, comprised of twelve oxygen-sharing MO_x polyhedra (most typically M = Mo^{VI}, W^{VI} and V^V) which encapsulate a central tetrahedron ([XO₄]ⁿ⁻, typically X = P^V, Si^{IV} etc.), have found applications in various chemical disciplines,²¹⁻²⁵ of which catalysis has found the most success. There is compelling evidence to suggest that Keggin polyanions are degraded by excess H₂O₂ in

solution to form peroxy POM species, e.g., the Venturello complex $\{\text{PO}_4[\text{WO}(\text{O}_2)_2]_4\}^{3-}$,⁴ which are suggested to be the active intermediates in POM-catalysed oxidations with H_2O_2 .⁴⁻⁹ Oxidation in biphasic systems, which are composed of an organic layer and an aqueous layer (Scheme 3.1), is attractive in catalysis as it can enable product separation through the relative solubilities of the catalyst and product in the two phases. These systems require the use of an efficient phase-transfer catalyst (PTC) that functions as a ligand to transfer the active peroxy species across the solvent interface;⁴⁻⁹ a process which has been extensively researched, both in terms of phase-transfer catalysis in general²⁶ and, specifically, PTC mediated phase-transfer of peroxy POMs.²⁷⁻³⁰ Often quaternary ammonium cations with C_8 - C_{18} alkyl groups are used as phase-transfer agents in these systems; examples include salts of $\pi\text{-C}_5\text{H}_5\text{N}^+(\text{C}_{16}\text{H}_{33})_3$, $(\text{C}_{18}\text{H}_{37})_2(\text{CH}_3)_2\text{N}^+$, $n\text{-C}_{16}\text{H}_{33}(\text{CH}_3)_3\text{N}^+$ and $p\text{-C}_5\text{H}_5\text{N}^+\text{C}_{16}\text{H}_{33}$.³¹⁻³⁸ However, these catalysts can be cumbersome to prepare, and the systems in which they are used can suffer from catalyst deactivation and difficult separation of the catalyst and product once the reaction is completed.⁵



Scheme 3.1. Mechanism of alkene epoxidation with H_2O_2 catalysed by POM in a two-phase system.⁵

In this work, alkylaminocyclotriphosphazenes, $(\text{RNH})_6\text{P}_3\text{N}_3$, labelled hereafter as RPN, have been identified as alternative PTCs to quaternary ammonium cations for POM-catalysed biphasic oxidations with H_2O_2 , due to the remarkable properties that cyclophosphazenes generally possess. Indeed, cyclic and polymeric phosphazenes are renowned for their chemical and thermal robustness which has seen them used as high performance elastomers, fire retardants, electrolytes and biomedical applications.³⁹⁻⁴¹ Alkylaminocyclotriphosphazenes are easy to prepare in one-step reactions from commercially available hexachlorocyclotriphosphazene and a wide range of primary amines.⁴² The phosphazene ring is extremely inert towards concentrated acids and bases, even at elevated temperatures.^{43,44} One or two of the ring nitrogen sites can be protonated to yield mono- or dicationic species, RPNH^+ and RPNH_2^{2+} , respectively (Scheme 3.2),^{45,46} which can be used to form salt complexes with suitable anions.⁴⁷⁻⁵¹ The lipophilic alkylamino substituent groups attached to exocyclic positions at the phosphorus sites of the ring render these compounds soluble in non-polar solvents and also provide numerous hydrogen bonding sites. This provides them with unique surfactant qualities and makes them versatile building blocks for supramolecular assemblies.⁵²



Scheme 3.2. Structures of neutral (RPN), monoprotonated (RPNH^+) and diprotonated (RPNH_2^{2+}) alkylaminocyclotriphosphazenes.

In this work, we have investigated RPN-POM composites as catalysts for biphasic oxidations with H_2O_2 and probed the versatility of RPN as phase-transfer catalysts in these reactions.

3.1.1 RPN-POM Aggregate Salts

In this study, RPN-POM salt aggregate catalysts were typically formed *in situ* in the preparation of the reaction mixtures for biphasic oxidation reactions with H₂O₂. Though the salt aggregates discussed in this section did show catalytic activity when added to these systems pre-formed, they were mostly isolated to examine the intermolecular interactions between the RPNs and POMs in the solid-state and to try to better understand the interactions that may occur in solution.

Characterisation of the RPN-POM aggregate salts was mostly carried out during my undergraduate project and some of the findings have already been published.⁵³ A discussion of their characterisation has been included here to provide a more complete picture of the work that has been undertaken in this study.

RPN-POM aggregate salts were formed through simple self-assembly processes by combining stoichiometric ratios of RPN and heteropoly acid hydrates in methanol. The salt products were isolated by evaporation of the solvent. To produce crystals for single crystal X-ray analysis, components were combined in RPN:POM molar ratios of 4:1 for H₄SiW₁₂O₄₀ and both 3:1 and 6:1 for H₃PMo₁₂O₄₀ and H₃PW₁₂O₄₀, using BzPN, iBuPN and iPrPN. Crystals suitable for X-ray structure determination were obtained from batches [iBuPN:H₄SiW₁₂O₄₀ (4:1)], [iPrPN:H₃PW₁₂O₄₀ (3:1)], [iBuPN:H₃PW₁₂O₄₀ (3:1)] and [iPrPN:H₃PW₁₂O₄₀ (6:1)].

Analysis of [iBuPN:H₄SiW₁₂O₄₀ (4:1)] yielded a [iBuPNH]₄[SiW]·2CH₃OH structure. Evidence of P₃N₃ ring protonation was provided by lengthening of the P-N bonds neighbouring the protonated N sites to 1.66 Å,⁵⁴ compared to ~1.60 Å typically seen in the ring bonds of neutral RPNs.⁵³⁻⁵⁵ The protonated ring atoms were orientated towards the [SiW]⁴⁻ ion within hydrogen-bonding distance, with four [iBuPNH]⁺ ions surrounding one polyanion with a total of twenty NH...O interactions in a single unit; each [iBuPNH]⁺ contributes one ring NH and

four exocyclic NH sites as shown in Fig. 3.1 A. The extended structure in Fig. 3.1 B shows the crystal packing.

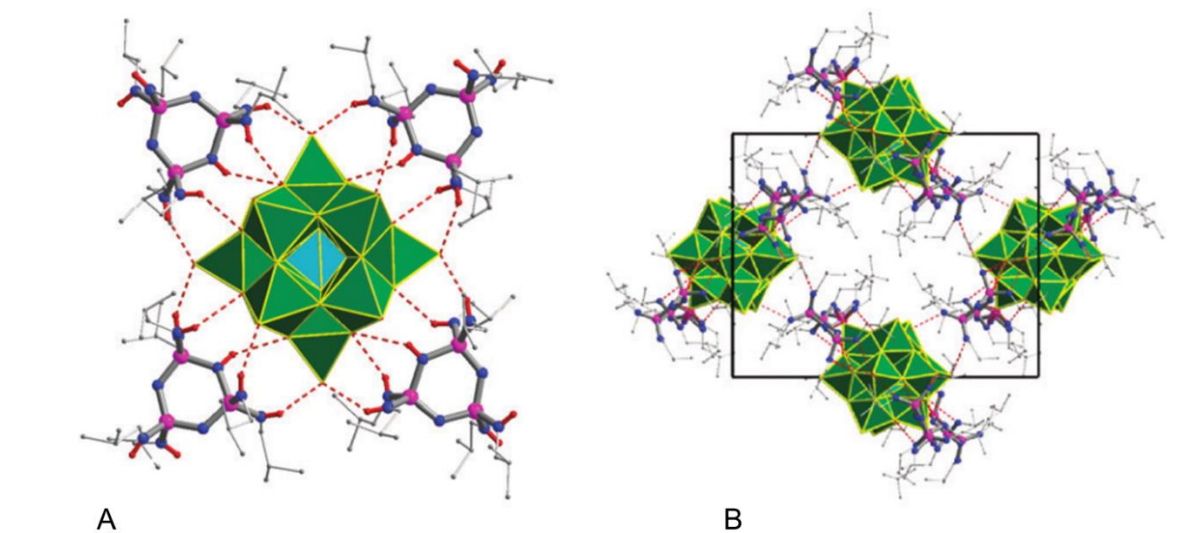


Fig. 3.1 Crystal structure of $[iBuPNH]_4[SiW] \cdot 2CH_3OH$: (a) $[iBuPNH]_4[SiW]$ unit, (b) crystal packing structure. WO_x polyhedra, green; SiO_4 , turquoise; P, purple; N, blue; H, red; alkyl groups, grey; hydrogen bonds, red dotted lines.⁵³

Crystals of 3:1 $[RPN]:[PW]$ yielded $[iPrPNH][iPrPNH_2][PW] \cdot 6CH_3OH$ and $[iBuPNH][iBuPNH_2][PW] \cdot 3H_2O \cdot CH_3OH$ structures, in which RPN is present as mono- and dication, $[RPNH]^+$ and $[RPNH_2]^{2+}$, respectively. The additional proton is disordered between two symmetrically equivalent RPNs through hydrogen-bonding with two MeOH molecules (Fig. 3.2).

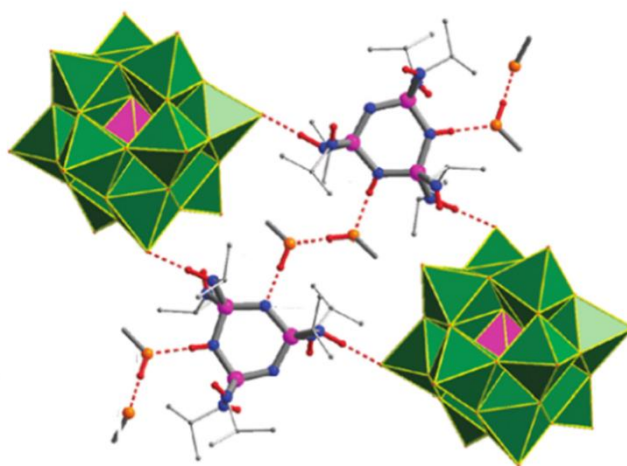


Fig. 3.2. Crystal structure of $[\text{iPrPNH}][\text{iPrPNH}_2][\text{PW}] \cdot 6\text{CH}_3\text{OH}$ highlighting the disorder of the extra RPN cation proton between the two rings through a chain of hydrogen-bonded MeOH molecules.⁵³

Crystals of 6:1 iBuPN and $\text{H}_3\text{PW}_{12}\text{O}_{40}$ were relatively poor and only P and W atoms were distinguishable. Nevertheless, a structure was determined which showed an octahedral arrangement of the phosphazene ligands around a central $[\text{PW}]^{3-}$ ion, with a likely composition of $[\text{iBuPNH}]_3[\text{PW}] \cdot 3\text{iBuPN} \cdot x\text{solvent}$ (Fig. 3.3). It was believed there were only three $[\text{iBuPNH}]^+$ cations due to the total number of protons provided by the parent $\text{H}_3\text{PW}_{12}\text{O}_{40}$ and the charge on the $[\text{PW}]^{3-}$ ion.

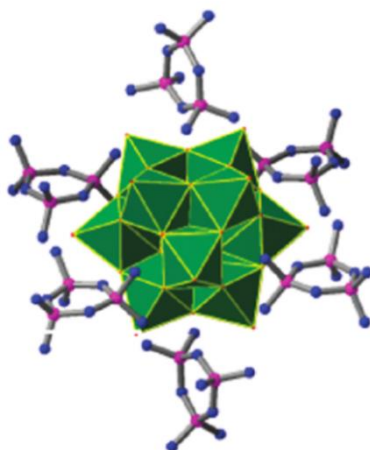


Fig. 3.3. Octahedral assembly of $[\text{iBuPN}]_3[\text{iBuPNH}]_3[\text{PW}]$ modelled from the positions of W and P atoms.⁵³

Preliminary oxidative desulfurization and epoxidation results found RPN-PW catalysts to be most efficient in 6:1 [RPN]:[POM] molar ratio, giving 100% and >99% conversion of DBT to sulfone and conversion of H_2O_2 to epoxide, respectively, in toluene/ H_2O systems using BzPN-PW catalyst. Reactions in this study were also most effective using 6:1 ratio, thus, characterisation of 6:1 RPN-POMs from this work will be discussed here for context.

Elemental analyses of RPN-PWs (see Section 2.1.2) show that the isolated species weren't the pure $(\text{RPN})_6\text{PW}$ as expected. It is likely that there were distributions of the number of RPN coordinating around each PW in a sample, with some uncoordinated RPN washed away during product isolation. Some PW may have also partially degraded to form lacunary PW species which the RPNs can coordinate to and could, therefore, also be present in the samples. Some of the products of PW degradation that weren't coordinated to RPN (e.g. W mono-oxo species) could have remained soluble in the reaction solvent and/or been washed away during filtration, resulting in low W % in the isolated compounds. Another possibility could be that some solvent

molecules may have also been incorporated into the crystal structures of the isolated compounds.

UV-vis spectra of all RPN-PW in MeOH each had a single, broad peak with λ_{max} in the range of 263-268 nm, which correspond with the single, broad peak at 268 nm recorded for PW in MeOH. These broad peaks result from oxygen to W(VI) charge-transfer of the terminal, edge and corner-sharing oxygens in PW W-O bonds. The literature shows that degradation of PW causes λ_{max} of this peak to shift by > 10 nm from 268 nm.⁵⁶ As there was little change in the position of λ_{max} in the salts compared with λ_{max} of PW, this indicated that the PW structure remained intact within the different RPN-PW salts. Peaks in the range of 190-210 nm were typically assigned to RPNs.⁵⁷

FTIR spectra of all RPN-PW compounds showed characteristic peaks for RPN and PW. Fig. 3.4 compares PW and BzPN-PW spectra; characteristic PW peaks can be seen in the BzPN-PW spectrum at 944 cm^{-1} (W=O), 863 cm^{-1} (W-O-W corner-sharing) and 791 cm^{-1} (W-O-W edge-sharing), which confirms that PW or its lacunary derivatives were present in the sample. The peak at 1076 cm^{-1} (P-O) overlaps with the peak at 1091 cm^{-1} (P-N) from the BzPN ring.

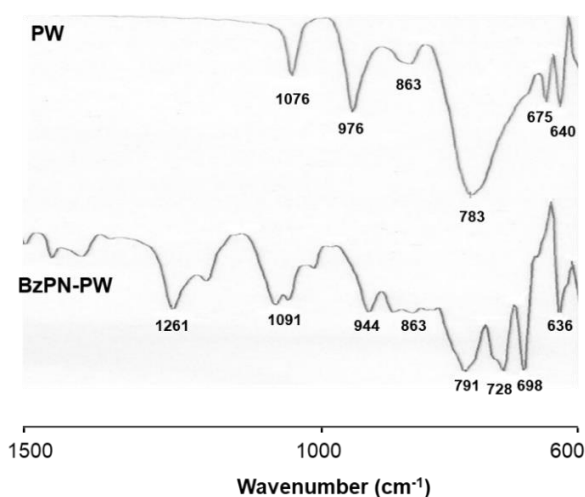


Fig. 3.4. FTIR spectra of PW and BzPN-PW.

TGA for iPrPN, iBuPN and BzPN, as well as for the corresponding PW aggregates, are shown in Fig. 3.5-3.7. These phosphazenes decompose at ~300 °C, with a decomposition onset at 150 °C for iPrPN, 180 °C for iBuPN, and 170 °C for BzPN. The corresponding RPN-PW composites exhibited higher thermal stability, showing decomposition onsets at 260 °C for iPrPN-PW, 280 °C for iBuPN-PW and 195 °C for BzPN-PW.⁵³

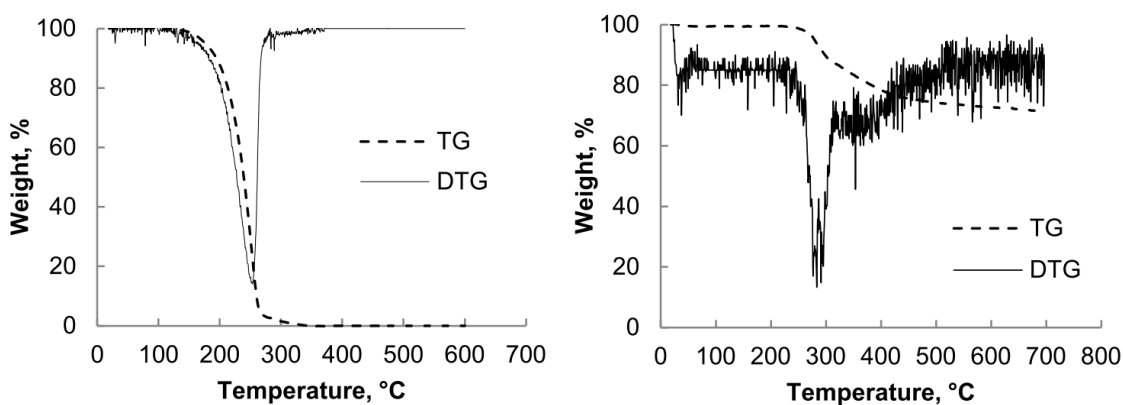


Fig. 3.5. TGA for iBuPN (left) and iBuPN-PW (right) under N₂.

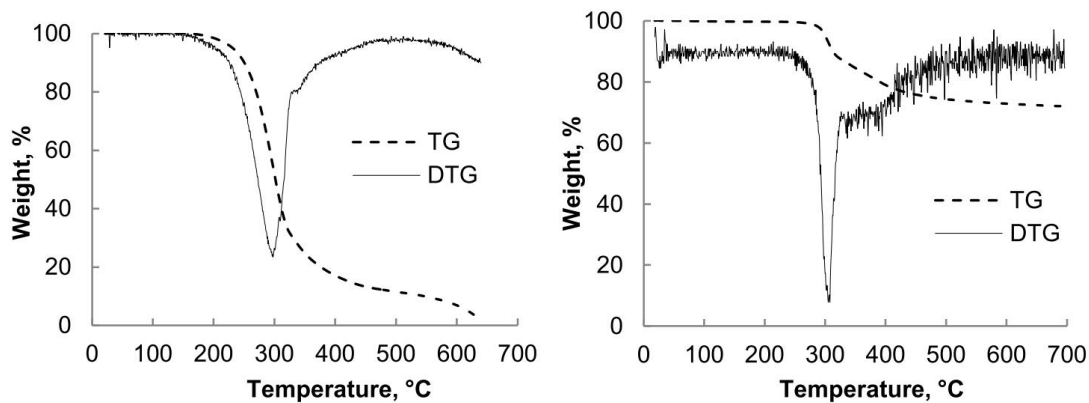


Fig. 3.6. TGA for iPrPN (left) and iPrPN-PW (right) under N₂.

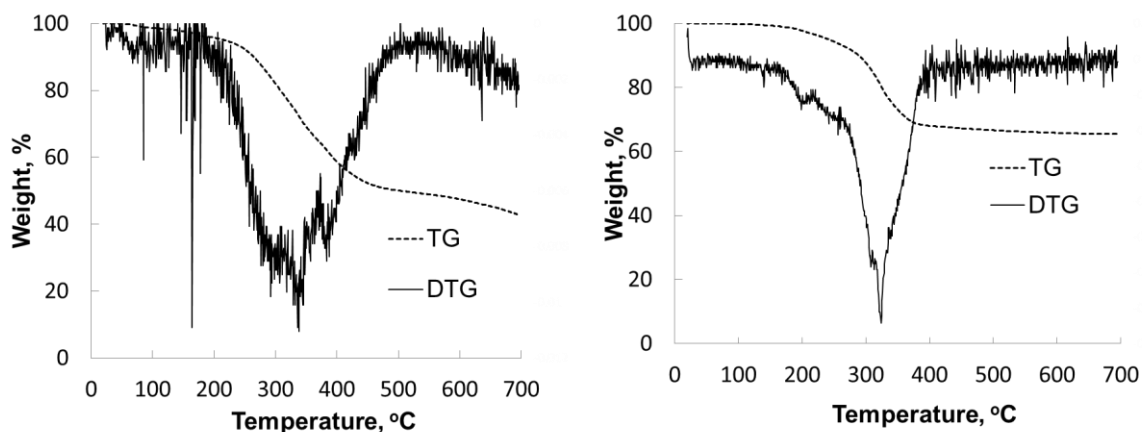


Fig. 3.7. TGA for BzPN (left) and BzPN-PW (right) under N₂.

3.2 Phase-Transfer of POM Facilitated by RPN

Alkylaminocyclophosphazenes, RPN, solubilize Keggin POMs and their peroxy derivatives in non-polar solvents, such as toluene, n-heptane or 1,2-dichloroethane (DCE), making them efficient and recyclable catalysts for biphasic oxidations with hydrogen peroxide through facile phase-transfer of POM facilitated by RPN.

In the absence of RPN, the POMs were insoluble in these organic solvents. After shaking an aqueous solution of H₃PW₁₂O₄₀ with toluene or DCE in the absence of RPN no PW was present in the organic phase. However, in presence of RPN, PW transfer from aqueous to organic phase was clearly observed by ³¹P NMR (Fig 3.8) and UV-Vis spectroscopy (Figure 3.9). The ³¹P NMR of the toluene phase after shaking the iBuPN-PW (2:1)/toluene-H₂O system shows the presence of PW₁₂O₄₀³⁻ anion (peak at ca. -14 ppm) together with a small amount of another anion (ca. -11 ppm), which can be attributed to the PW₁₁O₃₉⁷⁻ lacunary anion as it is known that PW₁₂ undergoes degradation to PW₁₁ at pH > 2.²⁴ The doublet at 13 ppm and triplet at 15 ppm can be attributed to the monoprotonated phosphazene iBuPNH⁺ (Figure 3.8) bound to the PW₁₂ anion. These signals are shifted upfield from the singlet peak of the nonprotonated iBuPN

at 19.6 ppm. After shaking BzPN and PW in a (6:1)/DCE-H₂O system, UV-Vis analysis of the DCE phase shows a broad charge transfer band from PW peaked at 268 nm (Figure 3.9), which confirms the presence of PW in the DCE phase.

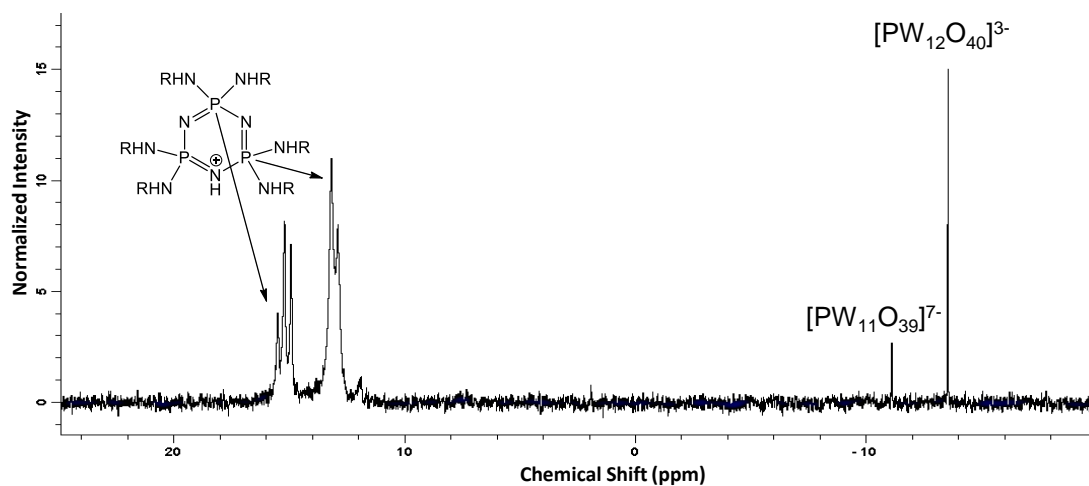


Fig 3.8. ³¹P NMR of organic phase separated from toluene (5 mL) – water (1 mL) biphasic system containing PW (0.15 mmol) and iBuPN (0.31 mmol) after stirring for 20 min at room temperature.

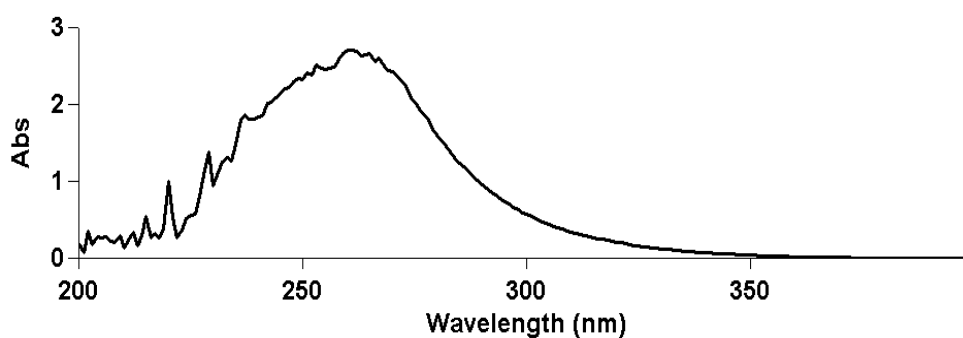


Fig. 3.9. UV-Vis spectrum of DCE phase after shaking the BzPN-PW (6:1)/DCE-H₂O system {PW (6.48 10⁻³ mmol), BzPN (38.9 10⁻³ mmol), DCE (10 mL), H₂O (0.5 mL)}. DCE phase was diluted 1:10 with fresh DCE. λ_{max} at 268 nm.

Fig 3.10 shows the effect of the ratio of [RPN]/[PW] on PW phase-transfer by RPN as a function of absorbance by PW (at ca. 268 nm) for different RPNs. Assuming more absorbance equals a greater amount of PW transferred into the organic layer, BzPN appears to be the most effective PTC, followed by iBuPN and, finally, iPrPN. There appears to be a maximum transfer for iBuPN and iPrPN at a 3:1 ratio, after which, transfer appears to dip and plateau, whereas phase-transfer with BzPN continues to increase beyond a 3:1 ratio, albeit by smaller increments between ratios than was seen before 3:1. It is suggested that these observations are due to the way in which the RPNs can encapsulate the PW with respect to their size. At a stoichiometric ratio of 3:1, three [RPNH]⁺ ions can encapsulate one PW³⁻ ion to give a neutral complex [RPNH]₃PW. Beyond a 3:1 ratio, the smaller iBuPN and iPrPN could increase in coordination number around each PW that has been transferred into the organic layer, meaning that beyond 3:1 ratio the excess RPNs are not transferring any more PW into the organic layer. BzPN, on the other hand, is much bulkier due to the large Bz groups meaning coordination numbers around PW will be smaller than the other RPNs and so increasing [BzPN] continues to increase PW transfer, but at a slower rate above 3:1 [BzPN]/[PW].

Phase-transfer of peroxy PW species was observed after stirring iBuPN-PW (6:1)/toluene-H₂O₂-H₂O and BzPN-PW (6:1)/DCE-H₂O₂-H₂O systems, where H₂O₂ was added in a 150-fold excess to PW. Fig. 3.11 shows the ³¹P NMR spectrum of iBuPN-PW (6:1) in toluene, where the peaks in the range of -5 to +9 ppm can be attributed to several peroxy PW species, including {PO₄[WO(O₂)₂]₄}³⁻.^{7,8} The UV-Vis spectrum of the DCE phase (Fig. 3.12) shows two broad absorption bands at 250 and 292 nm, which can also be assigned to peroxy PW species.

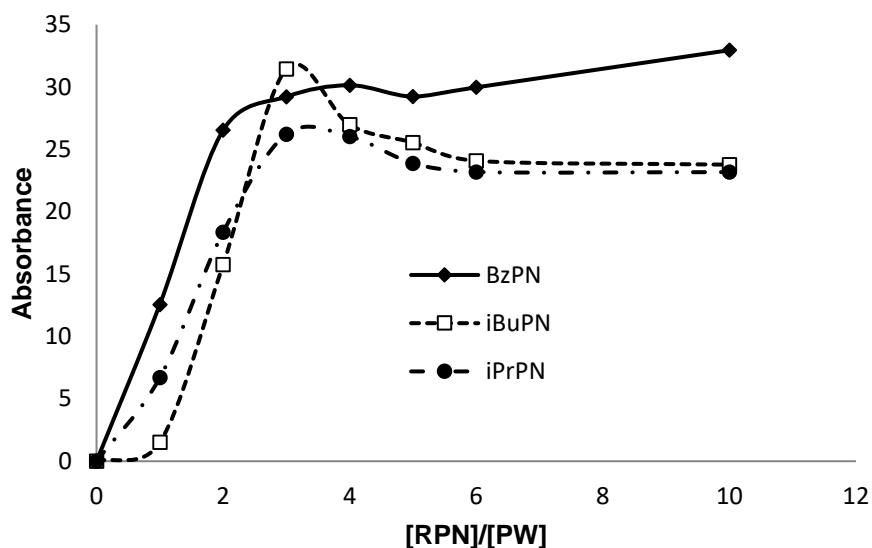


Fig. 3.10. UV-Vis absorbance of PW in the DCE phase in DCE/H₂O system at different RPN/PW molar ratios. PW (6.478×10^{-6} mol), (0.5 mL) H₂O (10 mL) DCE in initial systems with required [RPN] (mol) at RT. Maximum absorbance for the PW peak measured at ~268 nm.

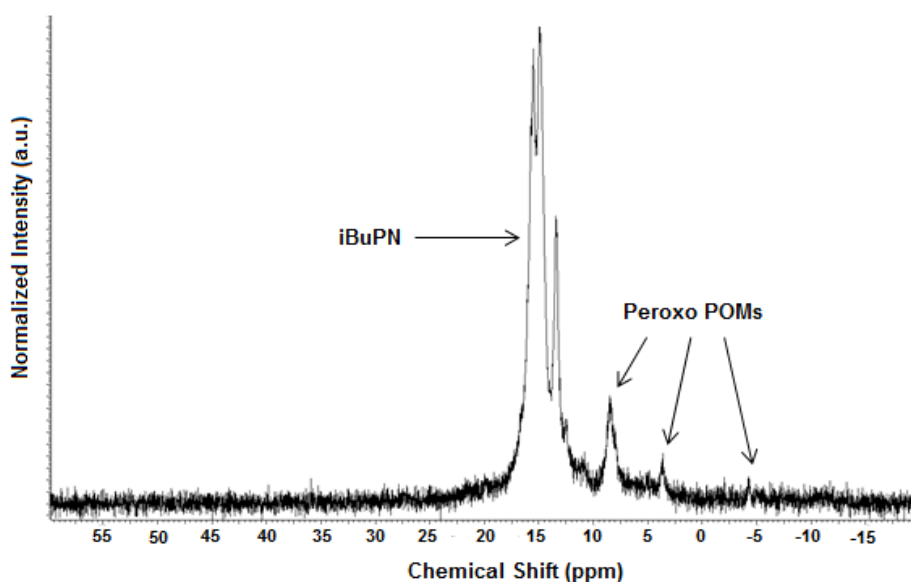


Fig. 3.11. ³¹P NMR of organic phase separated from toluene (3 mL) – water (1 mL) biphasic system containing PW (6.48×10^{-2} mmol), H₂O₂ (10 mmol) and iBuPN (0.39 mmol) after stirring for 20 minutes at room temperature.

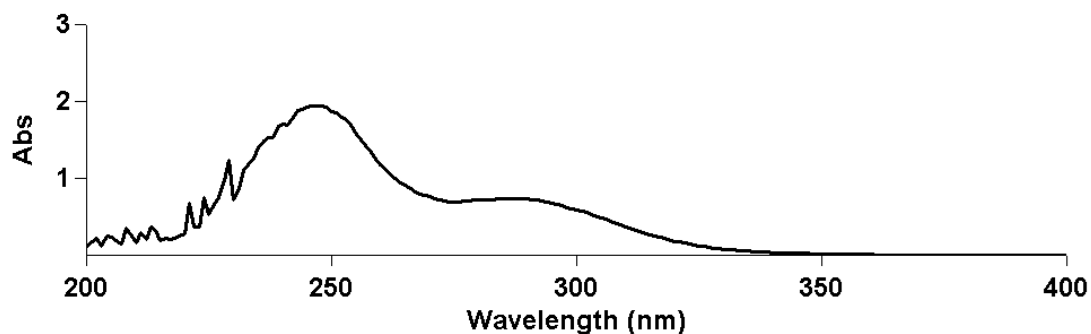


Figure 3.12. UV-Vis spectrum of DCE phase after shaking the PW-BzPN (1:6)/DCE-H₂O₂-H₂O system {PW (6.48 10⁻³ mmol), BzPN (38.9 10⁻³ mmol), H₂O₂ (1.01 mmol), DCE (10 mL), H₂O (0.3 mL)}. DCE phase was diluted 1:10 with fresh DCE. The two bands are peaked at 250 and 292 nm.

3.3 Epoxidation of Alkenes

To test the catalytic ability of the RPN-POM aggregates, the epoxidation of cyclooctene (eq. 3.1) was first examined, which is typically used as the standard screening test for epoxidation catalysts. The reaction was carried out in a biphasic toluene-water system at temperatures ranging from 30-60 °C using 10% H₂O₂ as the oxidant and a 1:6 mixture of PW and BzPN as the catalyst. This catalyst was observed to be very efficient even at 30 °C, yielding >99% epoxycyclooctane with >99% efficiency of H₂O₂ utilization in 3 h reaction time (Table 3.1).

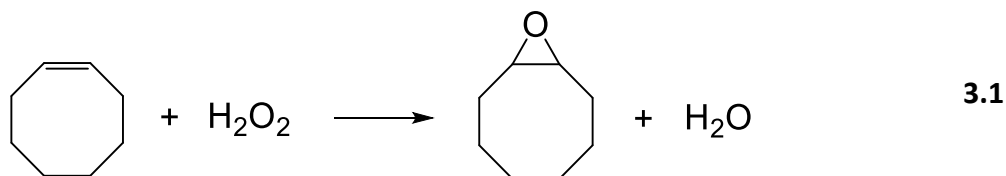


Table 3.1. Epoxidation of olefins catalysed by BzPN-POM in toluene-H₂O biphasic system.^a

Olefin	POM	Time (h)	Yield (%)	H ₂ O ₂ efficiency ^b (%)
Cyclooctene	PW	3.0	99	>99
Cyclooctene	PMo	2.0	99	>99
Cyclohexene	PMo	3.5	69	73
1-Octene	PMo	24	27	27
1-Hexene	PMo	24	25	26

^a At 30 °C, POM (8.59 10⁻³ mmol), [POM]/[BzPN] = 1:6, H₂O₂ (1.01 mmol), olefin (9.71 mmol), toluene (10.0 mL), H₂O (0.3 mL). ^b Epoxide selectivity based on initial [H₂O₂].

Reactions were run using method 2.

Fig. 3.13 demonstrates the relative catalytic activity of different Keggin POMs (PMo, PW and SiW) at 50 °C and pseudo-first order conditions, i.e., [H₂O₂]/[alkene] = 1:10. The relative activity decreases in the series: PMo > PW >> SiW which is in line with the stability of these POMs to hydrolysis.²⁴ SiW shows the lowest activity, with an induction period of ca. 60 min. This is probably due to the high stability of SiW to degradation in aqueous solution,²⁴ which makes it difficult to form the active peroxy species required for catalysis. Cyclooctene epoxidation with PMo at [H₂O₂] << [alkene] occurs as almost a zero-order reaction to give 99% epoxide yield in 0.5 h with >99% H₂O₂ efficiency (Fig. 3.13). It obeys the Arrhenius equation with apparent activation energy of 27.1±2.2 kJ mol⁻¹ (Fig. 3.14). In contrast,

epoxidation with PW obeys a first-order rate law up to 80% conversion (Fig. 3.15) giving 84% epoxide yield (84% H₂O₂ efficiency) (Fig. 3.13).

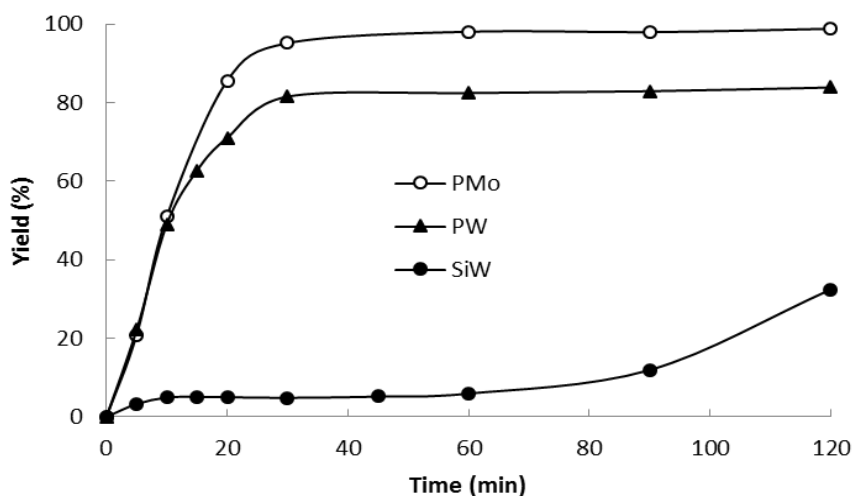


Fig. 3.13. Effect of POM for cyclooctene epoxidation catalysed by POM-BzPN in toluene-H₂O system (50 °C, RPN ($5.15 \cdot 10^{-2}$ mmol), [POM]/[BzPN] = 1:6, H₂O₂ (1.01 mmol), cyclooctene (9.71 mmol), toluene (10.0 mL), H₂O (0.3 mL)). Reactions were run using method 2.

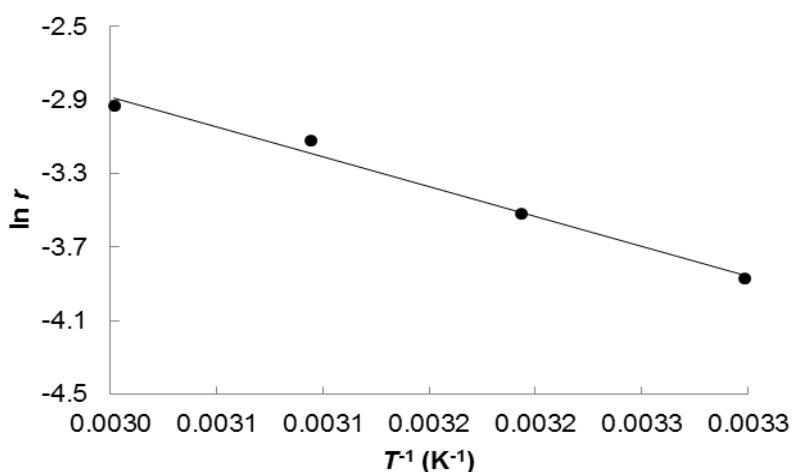


Fig. 3.14. Arrhenius plot for epoxidation of cyclooctene catalysed by BzPN-PMo in toluene-H₂O system (30-60 °C, PMo ($8.59 \cdot 10^{-3}$ mmol), [PMo]/[BzPN] = 1:6, H₂O₂ (1.01 mmol), cyclooctene (9.71 mmol), toluene (10.0 mL), H₂O (0.3 mL); r in mmol min⁻¹; $E_a = 27.1 \pm 2.2$ kJ mol⁻¹). Reactions were run using method 2.

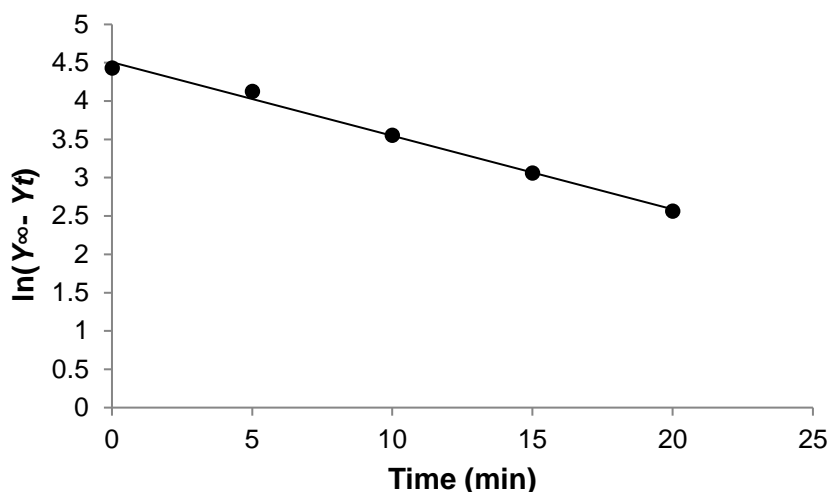
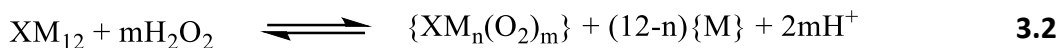


Fig. 3.15. First-order plot for cyclooctene epoxidation catalysed by BzPN-PW in PhMe-H₂O system (50 °C, BzPN (5.15 10⁻² mmol), [PW]/[BzPN] = 1:6, H₂O₂ (1.01 mmol), cyclooctene (9.71 mmol), toluene (10.0 mL), H₂O (0.3 mL); Y_t and Y_∞ are the yields of epoxide at time t and $t = \infty$). Reactions were run using method 2.

These results can be explained assuming a reaction mechanism through equations (3.2) – (3.4), which include degradation of the Keggin POM by hydrogen peroxide to form active peroxy species (3.2), alkene epoxidation (3.3) and regeneration of the active peroxy species (3.4).⁴⁻⁸ Steps (3.2) and (3.4) occur in the aqueous phase or at the interface and step (3.3) in the organic phase. With the least stable POM, PMo, the reaction is probably limited by step (3.3), with steps (3.2) and (3.4) fast and complete. At $[H_2O_2] \ll [alkene]$, this will lead to a zero-order reaction. With more stable PW, the reaction is probably limited by regeneration of peroxy species (3.4), resulting in a first-order reaction. With the most stable SiW, the degradation step (3.2) is likely to be the rate-limiting step.



This mechanism is also supported by the observation of a short induction period in cyclooctene epoxidation with PW when the PW was added last to the reaction mixture to start the reaction (instead of adding the alkene or RPN last using methods 1 and 2, respectively – see section 2.3.3.1.1). This induction period appears to be caused by the relatively slow PW degradation in step (3.2). Similar behavior was also observed in DBT oxidation (see below). In contrast, neither alkene epoxidation nor DBT oxidation showed such behavior with PMo.

In the epoxidation of cyclooctene, the catalytic activity was found to increase with the size of R group in RPN: $i\text{Pr} < i\text{Bu} < \text{Bz}$ (Table 3.2) in a PhMe/H₂O system. This can be explained by increasing phase-transfer efficiency of RPN in this series due to the relative solubility of the substituent R-groups in the organic phase.

Table 3.2. Effect of RPN on cyclooctene epoxidation catalysed by PW in toluene-H₂O two-phase system.^a

RPN	iPrPN	iBuPN	BzPN
Initial rate (mmol min ⁻¹)	0.0090	0.014	0.022

^a At 60 °C, PW (0.020 g, 6.48 10⁻³ mmol), RPN (3.95 10⁻² mmol) RPN, [PW]/[RPN] = 1:6, H₂O₂ (1.01 mmol), cyclooctene (6.78 mmol), toluene (10.0 mL), H₂O (0.3 mL). Reactions were run using method 1.

The catalytic activity also increased with the RPN/POM molar ratio, reaching a plateau at a ratio of 6:1 (Fig. 3.16), which corresponds to complete transfer of catalytically active peroxy-POM from the aqueous to organic phase. This is confirmed by the very close correlation between the initial rate of epoxidation catalysed by BzPN-PW and the intensity of UV-Vis absorption band of peroxy PW species at 292 nm (Fig. 3.16 and Fig 3.17, also discussed earlier, see Fig 3.10). The relationship between iBuPN-PW and the initial rates (Fig. 3.18 and Fig 3.19), however, does not match as closely. This can be explained using the interpretation of the results from the measurements of absorbance vs. [RPN]/[PW] (Fig 3.10 *vide supra*), but with a slight modification; the size of the peroxy PW species that are formed in the presence of H₂O₂ is smaller than the parent PW,³⁴ so iBuPN coordination numbers are smaller, therefore, more iBuPN will be available for phase-transfer, thus increasing the rate.

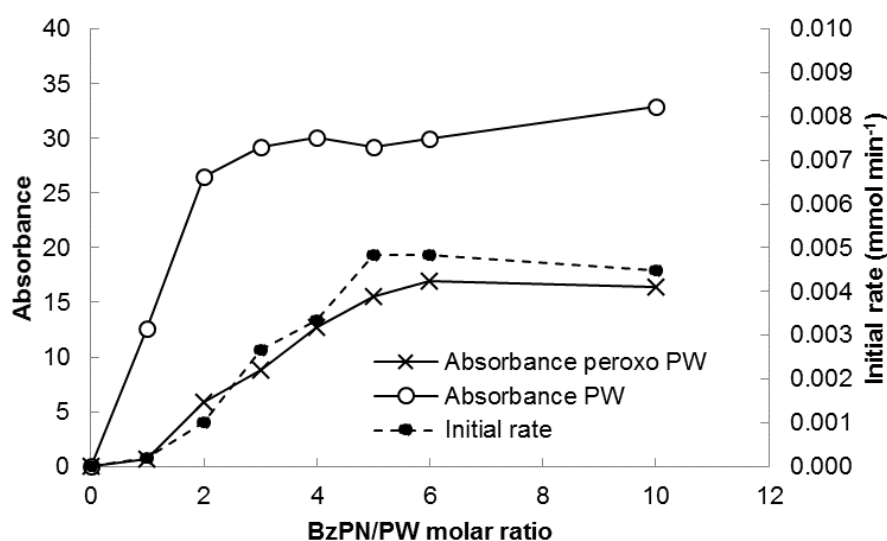


Fig. 3.16. Initial rate of cyclooctene epoxidation catalysed by BzPN-PW in DCE-H₂O two-phase system versus UV-Vis absorbance of PW in the DCE phase at different BzPN/PW molar ratios in the presence and absence of hydrogen peroxide. (Initial rates at 30 °C, DCE (10.0 mL), H₂O (0.3 mL), H₂O₂ (1.01 mmol), cyclooctene (2.71 mmol), PW (6.48 10⁻³ mmol); UV-Vis absorbance of PW and peroxy PW in the DCE phase at 268 and 292 nm, respectively). Reactions were run using method 1.

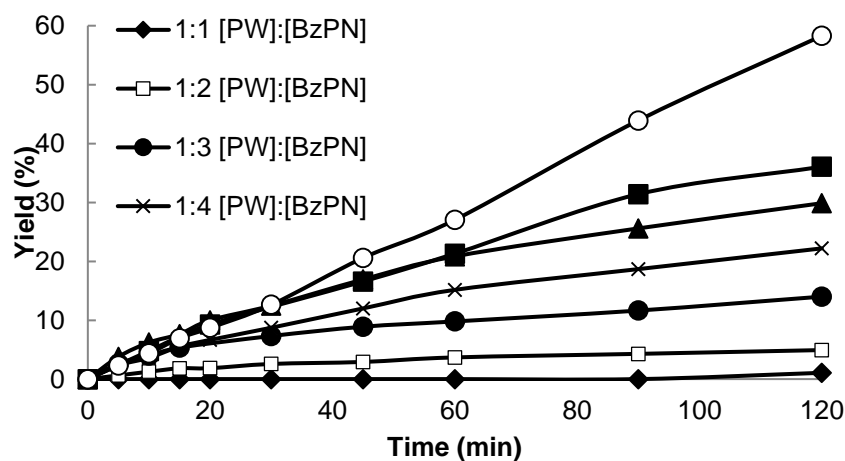


Fig. 3.17. Epoxide yield versus reaction time for cyclooctene epoxidation catalysed by BzPN-PW in DCE-H₂O system at various PW/BzPN molar ratios (30 °C, PW ($6.48 \cdot 10^{-3}$ mmol), H₂O₂ (1.01 mmol), cyclooctene (2.71 mmol), DCE (10.0 mL), H₂O (0.3 mL)). Reactions were run using method 1.

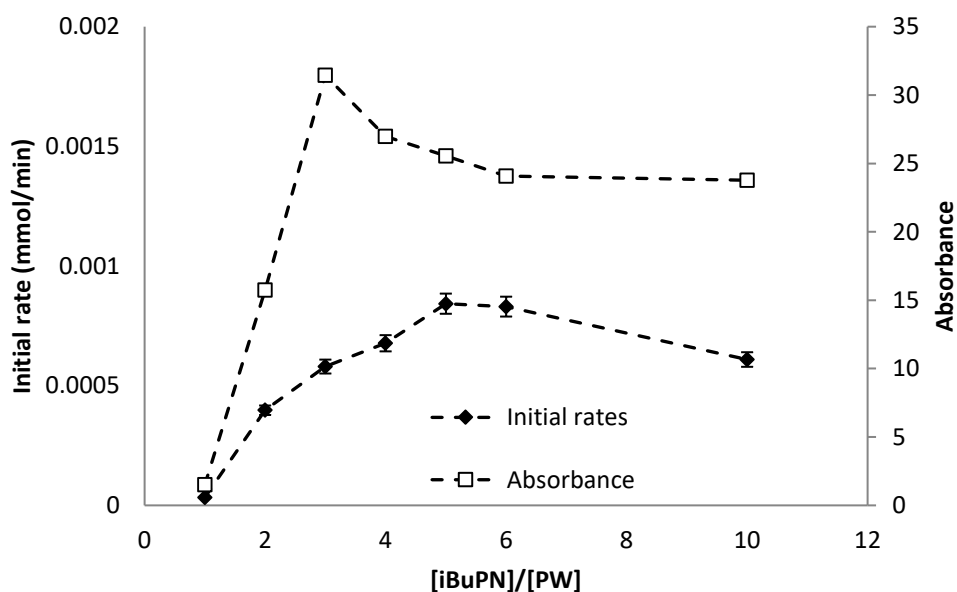


Fig. 3.18. Initial rate of cyclooctene epoxidation catalysed by iBuPN-PW in DCE-H₂O two-phase system versus UV-Vis absorbance of PW in the DCE phase at different iBuPN/PW molar ratios in the presence and absence of hydrogen peroxide. (Initial rates at 30 °C, DCE (10.0 mL), H₂O (0.3 mL), H₂O₂ (1.01 mmol), cyclooctene (2.71 mmol), PW ($6.48 \cdot 10^{-3}$ mmol); UV-Vis absorbance of PW in the DCE phase at 268 nm respectively). Reactions were run using method 1.

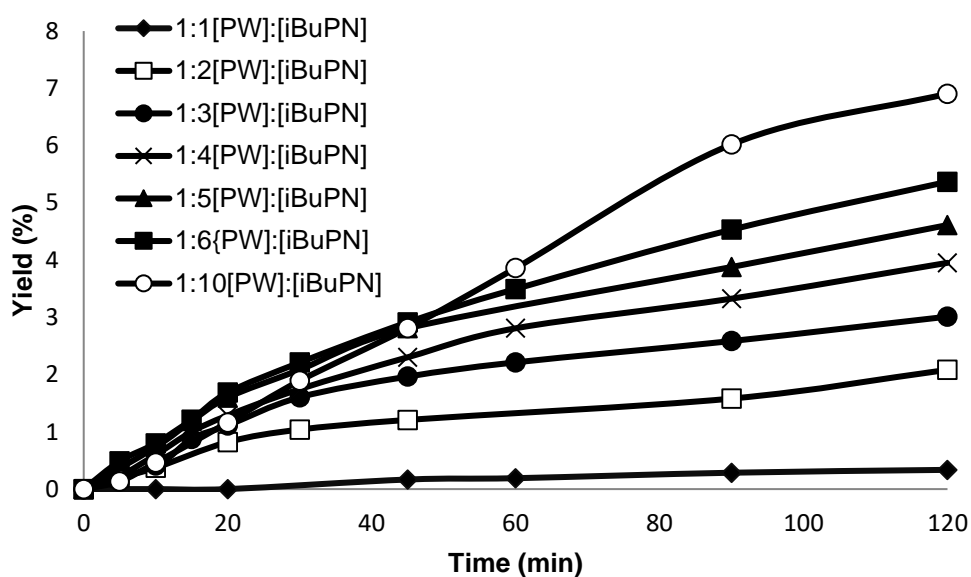


Fig. 3.19. Epoxide yield versus reaction time for cyclooctene epoxidation catalysed by iBuPN-PW in DCE-H₂O system at various PW/iBuPN molar ratios (30 °C, PW (6.48 10⁻³ mmol), H₂O₂ (1.01 mmol), cyclooctene (2.71 mmol), DCE (10.0 mL), H₂O (0.3 mL)). Reactions were run using method 1.

In addition to cyclooctene, the BzPN-PMo catalyst was also active for epoxidation of other alkenes including cyclohexene and terminal linear alkenes such as 1-hexene and 1-octene (Table 3.1). However, the reaction rate and H₂O₂ efficiency decreased significantly in this series in agreement with previous reports.⁴⁻⁸

The BzPN-PMo catalyst can be recovered by vacuum distillation and reused without loss of its activity as demonstrated in Fig. 3.20, which shows five successive runs for the epoxidation of cyclooctene at 60 °C.

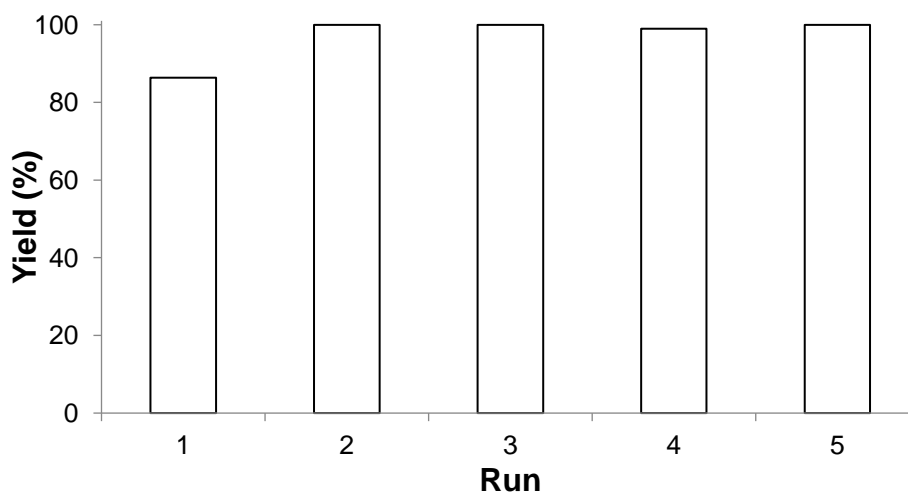


Fig. 3.20. Catalyst reuse for cyclooctene epoxidation catalysed by BzPN-PMo in toluene-H₂O system (60 °C, PMo (8.59×10^{-3} mmol), [PMo]/[BzPN] = 1:6, H₂O₂ (1.01 mmol), cyclooctene (19 mmol), toluene (10.0 mL), H₂O (0.3 mL); (1.01 mmol) H₂O₂ was added at the start of every repeat run). Reactions were run using method 2.

The effect of stirring speed was found to have little effect on the rate of the reaction when increased above 800 rpm using the best reaction conditions (Fig 3.21). This indicates that mass transfer of the peroxy species by BzPN is influenced by the speed of stirring at rates of up to 800 rpm under typical reaction conditions. Therefore, at the 1000 rpm stirring rate used in our reactions mass transfer limitation should be a non-issue.

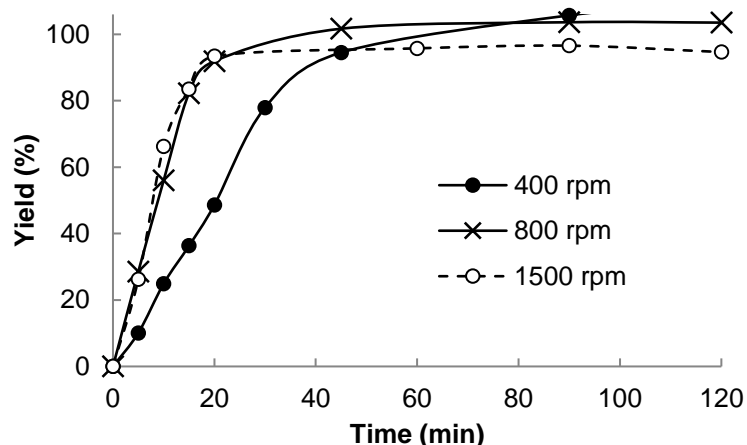


Fig. 3.21. Effect of stirring speed for cyclooctene epoxidation catalysed by BzPN-PMo in PhMe-H₂O system (60 °C, PMo ($8.59 \cdot 10^{-3}$ mmol), [PMo]/[BzPN] = 1:6, H₂O₂ (1.01 mmol), cyclooctene (9.71 mmol), toluene (10.0 mL), H₂O (0.3 mL)). Reactions were run using method 2.

Our catalyst can be compared favorably with one of the best POM epoxidation catalysts – the lacunary silicotungstate $(n\text{Bu}_4\text{N})_4[\gamma\text{-SiW}_{10}\text{O}_{34}(\text{H}_2\text{O})_2]$.⁶ This catalyst epoxidizes cyclooctene with 30% H₂O₂ in homogeneous MeCN solution at 32 °C and otherwise similar conditions, giving also 99% epoxide yield with >99% H₂O₂ efficiency. But in contrast to the straightforward preparation of BzPN-PMo, which can also be prepared *in situ*, the synthesis of lacunary silicotungstate is a more elaborate procedure. Another advantage of the BzPN-PMo system is that molybdenum-based systems are used instead of tungsten, which reduces the catalyst weight by 25-30%.

3.4 Search for Intermediates

In the search for reaction intermediates, we attempted to isolate the Venturello complex $\{\text{PO}_4[\text{WO}(\text{O}_2)_2]_4\}^{3-}$ as a salt aggregate with RPNH^+ counter cations from a PhMe/H₂O₂ system

in the absence of olefin and standard with 1:6 [PW]:[iBuPN] at 60 °C for 30 min. A sample of the organic layer was analysed by ^{31}P NMR. When left to cool down to room temperature, a yellow powder precipitated from the mixture which was isolated by filtration and recrystallized from methanol for single crystal X-ray analysis. A ^{31}P NMR was also recorded for the isolated powder in methanol. The spectrum of the organic layer gave a broad, noisy peak at $\sim \delta 14$ ppm that was ascribed to a mixture of mono- and diprotonated phosphazene species. The broadness of the peak is believed to be due to fast proton exchange at the ring N sites in solution. The ^{31}P NMR spectrum of the yellow powder (Fig. 3.22) showed that PW had degraded in H_2O_2 during the reaction which was evident from the large number of potential phosphate, peroxy and lacunary peaks ranging between $-\delta 5.78$ ppm and $\sim \delta 6.5$ ppm, and the lack of a characteristic PW peak at $-\delta 13$ ppm.³⁴ Accurate assignment of these peaks is difficult, however, it is suggested that the peaks at $-\delta 3.9$, 0.39, 2.96 and 4.72 ppm are ascribed to PW_4O_m , PWO_q , $[\text{HPWO}_4\{\text{WO}(\mu\text{-O}_2)(\text{O}_2)\}_2]^{2-}$, and $\{\text{PO}_4[\text{WO}(\text{O}_2)_2]_4\}^{3-}$ species, respectively, in accordance with the literature.^{7,8} Shifts in the spectrum between $\delta 10.42$ ppm and $\delta 19.28$ ppm may indicate the presence of iBuPN cations or species created by partial degradation of iBuPN.

Attempts to synthesise and isolate a Venturello-type complex with iBuPNH^+ cations for comparison, using a procedure derived from the literature, was unsuccessful.^{24,58}

A tetra(peroxy)tungstate $(\text{iBuPNH})_2[\text{W}(\text{O}_2)_4]$ was isolated from the organic layer of PhMe/ H_2O biphasic system containing H_2O_2 and iBuPN-PW (6:1) after stirring at 50 °C, with the iBuPNH^+ cations solubilizing the tetra(peroxy)tungstate species in the organic solvent. This compound was also synthesized from H_2WO_4 , H_2O_2 and iBuPN in a toluene/ H_2O system and recrystallized from methanol yielding pale yellow crystals. The single crystal X-ray structure consists of the methanol solvate $(\text{iBuPNH})_2[\text{W}(\text{O}_2)_4]\cdot 2\text{MeOH}$. The $\text{W}(\text{O}_2)_4^{2-}$ ion shows the familiar dodecahedral arrangement, which has been observed in crystal structures of other

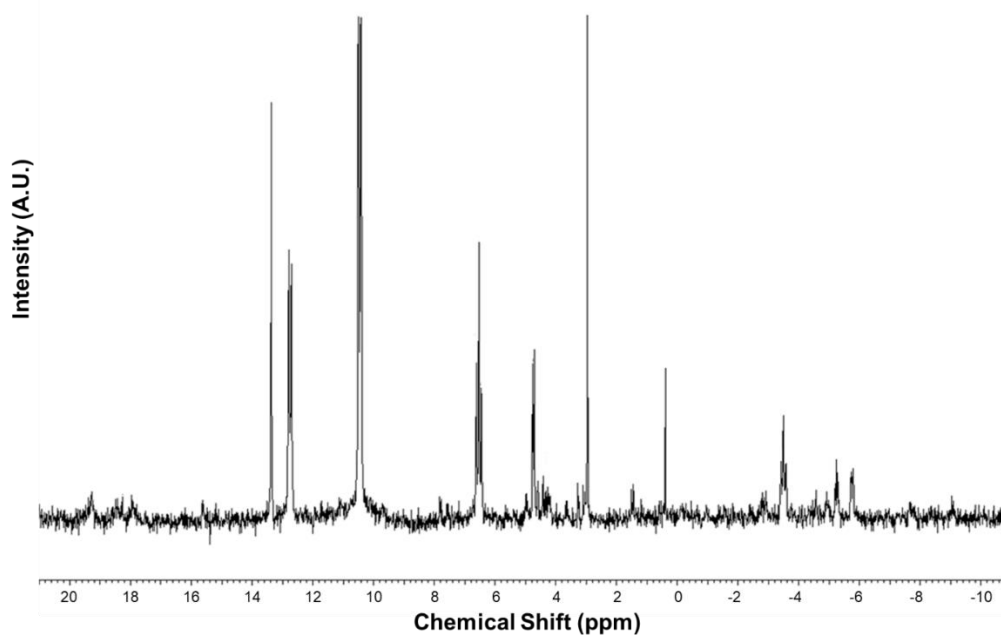


Fig. 3.22. ^{31}P NMR of yellow powder in MeOH (CDCl_3 lock) isolated from a PhMe/ H_2O_2 system in the absence of olefin and standard with 1:6 [PW]:[iBuPN] at 60°C for 30 minutes.

tetra(peroxo)tungstates.^{59–62} Protonation of one ring nitrogen site of the phosphazene is facilitated by the elongation of the associated P-N(ring) bonds (Fig. 3.23).^{63,64} The cationic and anionic components are connected *via* hydrogen bonds between NH functions of the phosphazanium ions and peroxo groups of the addendum complex anions. Every tetra(peroxo)tungstate ion is linked to four phosphazene cations and, in turn, every cation to two anions resulting in a ribbon-like arrangement (Fig. 3.24). Methanol molecules, also incorporated into the crystal structure, connect phosphazene cations via NH...O and OH...N(ring) interactions resulting in a 3D-network (Fig. 3.25). In contrast to alkali metal tetra(peroxo)tungstates, which decompose rapidly at room temperature and can explode on impact,⁶⁵ crystals of $(\text{iBuPNH})_2[\text{W}(\text{O}_2)_4]$ appear to be much more stable under ambient conditions and can be stored for several weeks at room temperature, or for several months when refrigerated, without undergoing noticeable degradation. The enhanced stability may be due to more effective separation of $\text{W}(\text{O}_2)_4^{2-}$ ions by the larger cations.

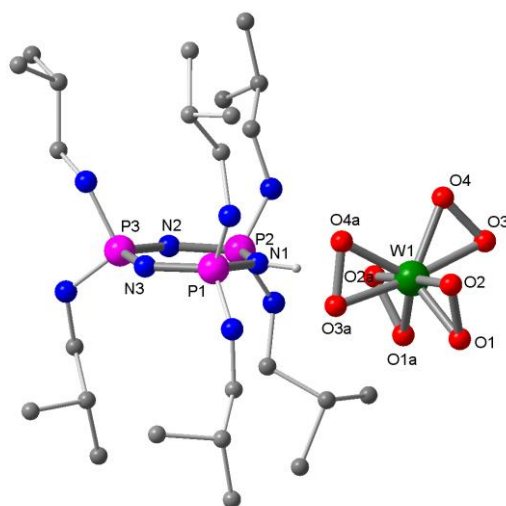


Fig. 3.23. Selected bond lengths (Å) and angles (°) of the crystal structure of (iBuPNH)₂[W(O₂)₄]·2CH₃OH: W1 O1 1.929(5), W1 O2 1.963(5), W1 O3 1.954(6), W1 O4 1.924(6), O1 O2 1.476(8), O3 O4 1.420(10), P1 N1 1.648(6), P2 N1 1.666(6), P2 N2 1.570(6), P3 N2 1.561(6), P3 N3 1.596(6), P1 N3 1.574(5), N3 P1 N1 109.6(3), N2 P2 N1 107.4(3), N2 P3 N3 115.4(3), P1 N1 P2 130.4(3), P3 N2 P2 130.0(4), P1 N3 P3 126.6(4).

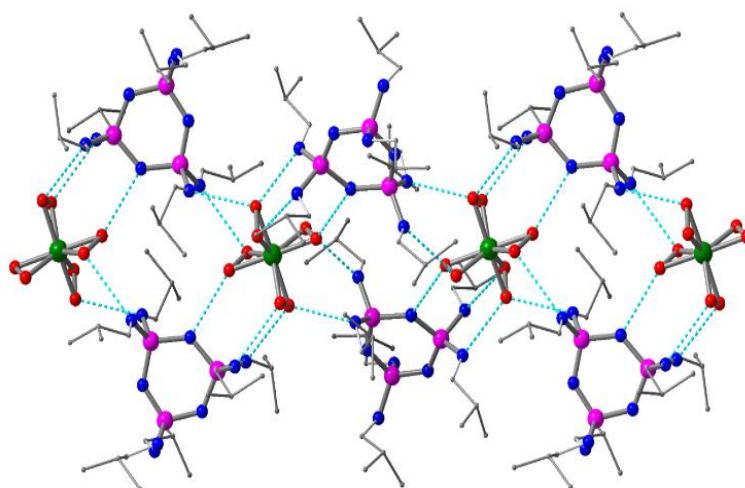


Fig. 3.24. Crystal structure of (iBuPNH)₂[W(O₂)₄]·2CH₃OH highlighting the ribbon-like assembly of anions and cations. W, green; O, red; P, purple; N, blue; C, grey. Hydrogen bonds are illustrated as dashed lines. Hydrogen atoms and the methanol molecules have been omitted for clarity.

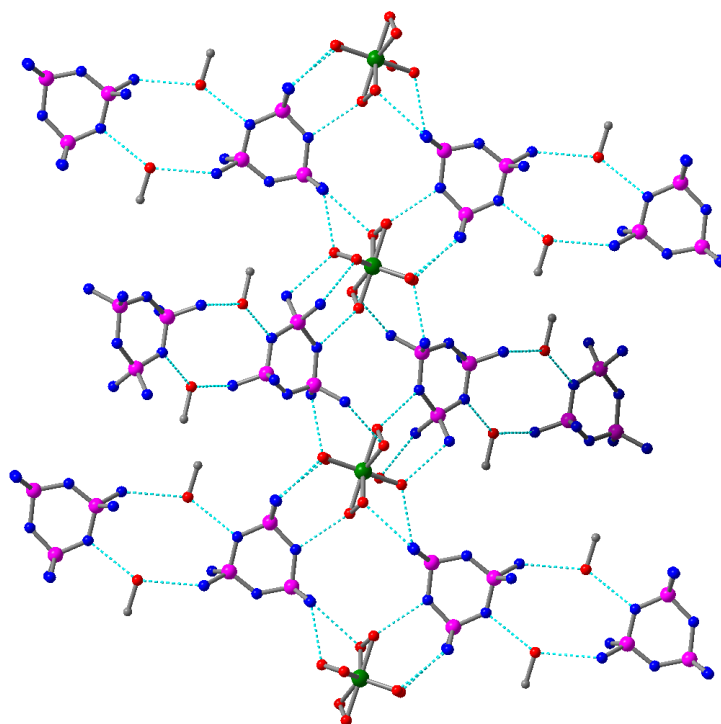


Fig. 3.25. Supramolecular structure of $(i\text{BuPNH})_2[\text{W}(\text{O}_2)_4] \cdot 2\text{CH}_3\text{OH}$ including methanol molecules. Hydrogen bonds are shown as dashed lines; *iso*-butyl groups and H atoms are omitted for clarity.

$(i\text{BuPNH})_2[\text{W}(\text{O}_2)_4]$ was tested as a stoichiometric reagent (in the absence of H_2O_2) in the epoxidation of cyclooctene in toluene as a solvent at 60°C to give 18% epoxide yield based on the peroxo groups present in 2 h reaction time. Further testing under catalytic conditions $\{60^\circ\text{C}$, 1 h reaction time, $(i\text{BuPNH})_2[\text{W}(\text{O}_2)_4]$ ($7.80 \cdot 10^{-2}$ mmol), H_2O_2 (1.01 mmol), cyclooctene (6.78 mmol), toluene (10.0 mL), H_2O (0.3 mL) $\}$ gave an improved 44% epoxide yield (Fig. 3.26), which was comparable to the yield obtained with *i*BuPN-PW (6:1) under similar conditions and the same amount of W(VI) used. It should be noted, however, that the reaction with $(i\text{BuPNH})_2[\text{W}(\text{O}_2)_4]$ had a 20 min induction period, the cause of which is uncertain. Nevertheless, these results show that $(i\text{BuPNH})_2[\text{W}(\text{O}_2)_4]$ is active in alkene epoxidation and

could be an intermediate or, more likely, one of the active intermediates in the reaction in question.

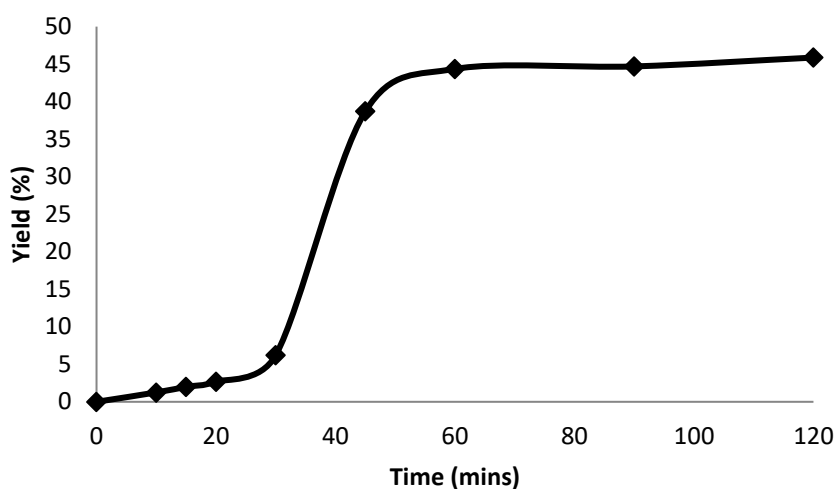
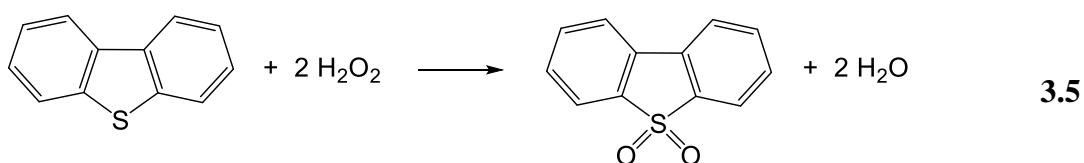


Fig. 3.26. Yield of cyclooctene oxide produced over a 2 h period in the presence of H_2O_2 using pre-formed $(\text{iBuPNH})_2[\text{W}(\text{O}_2)_4]$ as a catalyst.

3.5 Oxidation of Benzothiophenes

It has been reported in the literature that tungsten-based POMs have been used as catalysts for oxidative desulfurization using hydrogen peroxide as a “green” oxidant, providing a promising new method for the removal of heavy organosulfur compounds from transportation fuel.¹⁻³ In these systems, oxidation of dibenzothiophene (DBT) (eq. 3.5) is typically employed as a model reaction for catalyst testing.



Through work mostly conducted by Rana Yahya,⁶⁶ and with contributions from myself, it was found that RPN-POM aggregates are highly active catalysts for DBT oxidation with H_2O_2 in

biphasic systems comprised of PhMe, DCE or n-heptane as an organic solvent and H₂O, yielding DBT sulfone as the only product (Table 3.3). Other benzothiophenes such as benzothiophene (BT) and 4,6-dimethyldibenzothiophene (DMDBT) were also readily oxidized to their corresponding sulfones in this system. As in olefin epoxidation reactions, the POM and RPN components were simply added to form the active RPN-POM catalyst *in situ*.

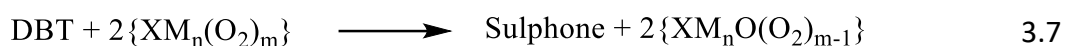
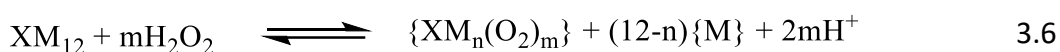
Table 3.3. Oxidation of benzothiophenes by H₂O₂ in toluene-H₂O two-phase system in the presence of BzPN-POM catalyst at 60 °C.^a

Entry	Substrate	POM	Time (h)	Conversion (%)	H ₂ O ₂ efficiency ^b (%)
1	DBT	PMo	0.5	100	99
2	DBT	PW	0.5	100	99
3	DBT	SiW	1.0	0	-
4	BT	PMo	1.5	71	99
5	DMDBT	PMo	1.0	100	99

^a Toluene (10 mL), substrate (0.50 mmol, 1 wt.%), aqueous 30% H₂O₂; molar ratios: [Substrate]/[POM] = 90:1, [Substrate]/[H₂O₂] = 1:3, [BzPN]/[POM] = 6:1. Sulfones were the only reaction products. ^b Reaction selectivity based on H₂O₂.

In DBT oxidation, like cyclooctene epoxidation, PMo exhibited a higher activity than PW, whereas SiW showed no activity at all in agreement with the relative stability of these POMs to degradation in aqueous solution (Table 3.3, entries 1, 2 and 3, respectively).²⁴ In the presence of BzPN-PW (1:6) and BzPN-PMo (1:4) oxidation of DBT proceeded with 100% conversion at 60 °C (Table 3.4, entries 7 and 8, respectively). The mechanism for the reaction can be

summarized using schemes (3.6) – (3.8). As with olefin epoxidation, the Keggin POM precursor initially degrades in the presence H₂O₂ to form active peroxy species (3.6), before oxidizing DBT (3.7) and forming an oxo species, which then reacts with more H₂O₂ to regenerate the active peroxy species (3.8).⁴⁻⁸ Steps (3.6) and (3.8) occur in the aqueous phase or at the interface and step (3.7) in the organic phase. With the least stable POM, P_MO, the reaction is probably limited by step (3.7), with steps (3.6) and (3.8) fast and complete. It should also be noted that step (3.7) requires reaction with two peroxy groups for DBT to undergo full oxidation to the sulfone product.



The reactivity of benzothiophenes decreased in the order: DBT > DMDBT > BT, which is in agreement with previous reports¹⁻³ and can be attributed to the electron donating and steric effects of aromatic and methyl groups in the benzothiophenes. Very little to no decomposition of H₂O₂ to molecular oxygen took place in this system, giving >99% efficiency of H₂O₂ utilization.

The catalytic activity with respect to RPN was found to increase in the order: iPr < iBu < Bz (Table 3.4, entries 1-3) in toluene and DCE, which is line with increasing size of R group phase-transfer efficiency of RPN in this series. The activity also increased with increasing [BzPN]/[POM] molar ratio, levelling off at a ratio of 6:1 (entries 4-9), which agrees with the UV-Vis results regarding the effect of [BzPN]/[POM] ratio on the POM phase-transfer (Fig. 3.16).

Table 3.4. Effect of RPN and [RPN]/[POM] ratio on oxidation of DBT by H₂O₂ in toluene-H₂O two-phase system.^a

Entry	POM	BzPN/POM (mol/mol)	Temperature (°C)	Conversion (%)	H ₂ O ₂ efficiency (%)
1	PW	1:4 ^{c,d}	40	38	>99
2	PW	1:4 ^{c,e}	40	89	>99
3	PW	1:4 ^c	40	94	>99
4	PW	1:1	60	56	>99
5	PW	2:1	60	81	>99
6	PW	4:1	60	97	>99
7	PMo	4:1	60	100	>99
8	PW	6:1	60	100	>99
9	PW	10:1	60	100	>99
10	PMo	1:6	60	100	>99
11 ^f	PMo	1:6	60	33	>99
12 ^f	PMo	1:6 ^g	60	79	>99
13	PMo	1:6 ^g	60	87	>99
14 ^f	PMo	1:6 ^e	60	66	>99

^a Toluene (10 mL), DBT (0.50 mmol, 1 wt.%), aqueous 30% H₂O₂ (0.15 mL); molar ratios: [DBT]/[POM] = 90:1, [DBT]/[H₂O₂] = 1:3, 0.5 h reaction time. DBT sulfone was the only reaction product observed. ^b Reaction selectivity based on H₂O₂. ^c [DBT]/[H₂O₂] = 1:20. ^d iPrPN. ^e iBuPN. ^f Heptane used in place of toluene. ^g HexPN.

Through further investigation into this work, conducted by myself, the catalyst efficiency was found to vary in different solvents with respect to the alkylamino substituents on the phosphazene. Entries 10-14 in Table 3.4 compare DBT oxidation in toluene and heptane using either HexPN, iBuPN or BzPN as a phase-transfer agent. In heptane, DBT conversion with HexPN was greater than with BzPN (79 and 33% respectively), whereas in toluene the conversion with BzPN was greater than with HexPN (100 and 87%) respectively. This observation can be rationalized by the solubility of the phosphazene substituent R groups in each organic solvent; the aliphatic hexyl groups on the RPN render the active POM species more soluble than the aromatic Bz groups in aliphatic hydrocarbon solvents, whereas in aromatic solvents such as toluene this observation is reversed. HexPN also gives a higher conversion in heptane than iBuPN (entries 12 and 14, respectively), probably due to improved solubility of HexPN through larger lipophilic R groups. By changing the alkylamino substituents on the phosphazene ring the solubility of the phase-transfer agent could be tuned to improve catalyst performance in each solvent system. This is important as the oxidation of DBT in aliphatic hydrocarbon solvents such as heptane demonstrates effective desulfurization of a model diesel fuel under biphasic conditions, which is highly desirable in the petrochemical industry.¹⁻³ The sulfone product is insoluble in aliphatic hydrocarbons such as heptane, crashing out as a white powder which enables easy extraction and separation with a suitable, immiscible solvent such as acetonitrile.

100% DBT conversion at 99% H₂O₂ efficiency was observed for both the BzPN-PMo and BzPN-PW catalysts within 30 minutes at 60 °C with a 1:3 [DBT]/[H₂O₂] molar ratio in a PhMe/H₂O system (Table 3.3, entries 1 and 2). The catalysts could also be recovered by vacuum distillation and reused without exhibiting a loss in activity. These results compare well with those obtained using [(CH₃)₃NC₁₆H₃₃]₄W₁₀O₃₂ catalyst under similar conditions, which gave 99.6% DBT conversion and are considered the best reported so far, though H₂O₂

efficiency was not reported.² $[(C_{18}H_{37})_2N(CH_3)_2]_3[PW_{12}O_{40}]$ catalyst also gave 100 % conversion of DBT under similar conditions, and operated through the formation of an emulsion in the system which enabled catalyst separation by centrifugation once the reaction was complete.^{3,67} These catalysts, however, require pre-synthesizing *via* cumbersome procedures,² whereas POM–RPN can be synthesized *in situ* in our system. Another advantage of our system is that molybdenum-based systems can be used instead of tungsten, which reduces the catalyst weight by 25-30%.

3.6 Conclusions

Alkylaminocyclotriphosphazenes are efficient and tuneable phase-transfer agents for POM catalysed biphasic oxidations with hydrogen peroxide. Aliphatic (iBu, iPr and hexyl) and aromatic (BzPN) alkylaminocyclotriphosphazenes have been tested in biphasic systems with organic phases of various polarities to demonstrate that the organoamino substituent groups on the phosphazene ring can be tuned to modify the solubility of the RPN–POM aggregates in different solvents. Reactivity with respect to POMs was found to increase with decreasing aqueous stability in the order $PMo > PW > SiW$. A relatively stable tetraperoxo $(iBuPNH)_2[W(O_2)_4]$ species has been isolated from a biphasic system containing RPN, POM and H_2O_2 . This species was tested in the biphasic epoxidation of cyclooctene with H_2O_2 and was found to be catalytically active.

The catalysts compare well to some of the best reported catalysts for biphasic epoxidation and DBT oxidation with H_2O_2 . However, catalyst recovery by vacuum distillation is not an ideal method as it requires further expenditure of energy to isolate the catalyst which reduces the energy efficiency of the system.

References

- 1 F. M. Collins, A. R. Lucy and C. Sharp, *J. Mol. Catal. A Chem.*, 1997, **117**, 397–403.
- 2 X. Jiang, H. Li, W. Zhu, L. He, H. Shu and J. Lu, *Fuel*, 2009, **88**, 431–436.
- 3 Z. Jiang, H. Lü, Y. Zhang and C. Li, *Chinese J. Catal.*, 2011, **32**, 707–715.
- 4 C. Venturello, E. Alneri and M. Ricci, *J. Org. Chem.*, 1983, **48**, 3831–3833.
- 5 Y. Ishii, K. Yamawaki, T. Ura, H. Yamada, T. Yoshida and M. Ogawa, *J. Org. Chem.*, 1988, **53**, 3587–3593.
- 6 K. Kamata, K. Yonehara, Y. Sumida, K. Yamaguchi, S. Hikichi and N. Mizuno, *Science*, 2003, **300**, 964–6.
- 7 L. Salles, C. Aubry, R. Thouvenot, F. Robert, C. Doremieux-Morin, G. Chottard, H. Ledon, Y. Jeannin and J.-M. Brégeault, *Inorg. Chem.*, 1994, **33**, 871–878.
- 8 D. C. Duncan, R. C. Chambers, E. Hecht and C. L. Hill, *J. Am. Chem. Soc.*, 1995, **117**, 681–691.
- 9 R. Yahya, M. Craven, E. F. Kozhevnikova, A. Steiner, P. Samunual, I. V. Kozhevnikov and D. E. Bergbreiter, *Catal. Sci. Technol.*, 2015, **5**, 818–821.
- 10 R. A. Sheldon and J. K. Kochi, *Metal-catalyzed oxidations of organic compounds: mechanistic principles and synthetic methodology including biochemical processes*, Academic Press, Michigan, 1981.
- 11 C. L. Hill, in *Advances in Oxygenated Processes vol. 1*, ed. A. L. Baumstark, Jai Press Inc., London, 1988, p. 210.
- 12 M. Hudlicky, *Oxidations in Organic Chemistry*, Wiley VCH, 1990.

- 13 A. H. Tullo, *Chem. Eng. News Arch.*, 2004, **82**, 25–31.
- 14 N. Mizuno, K. Yamaguchi and K. Kamata, *Coord. Chem. Rev.*, 2005, **249**, 1944–1956.
- 15 I. Skeist and G. R. Somerville, *Epoxy resins.*, New York: Reinhold Publishing Corporation, 1958., 1958.
- 16 H. Q. Pham and M. J. Marks, in *Ullmann's Encyclopedia of Industrial Chemistry*, Wiley-VCH Verlag GmbH & Co. KGaA, 2000.
- 17 J. Gary, G. Handwerk and M. J. Kaiser, *Petroleum Refining.*, CRC Press, London, 5th edn., 2007.
- 18 C. Song, *Catal. Today*, 2003, **86**, 211–263.
- 19 H. Y. Zhang, G. B. Shan, H. Z. Liu and J. M. Xing, *Chem. Eng. Commun.*, 2007, **194**, 938–945.
- 20 M. T. Pope, *Heteropoly and Isopoly Oxometalates*, 1983.
- 21 C. L. Hill and C. M. Prosser-McCartha, *Coord. Chem. Rev.*, 1995, **143**, 407–455.
- 22 T. Okuhara, N. Mizuno and M. Misono, *Adv. Catal.*, 1996, **41**, 113–252.
- 23 J. T. Rhule, C. L. Hill, D. a. Judd and R. F. Schinazi, *Chem. Rev.*, 1998, **98**, 327–358.
- 24 I. V. Kozhevnikov, *Catalysts for Fine Chemical Synthesis: Catalysis by Polyoxometalates*, Wiley, West Sussex, 2002.
- 25 I. V. Kozhevnikov, *J. Mol. Catal. A Chem.*, 2009, **305**, 104–111.
- 26 C. M. Starks and M. Halper, *Phase-Transfer Catalysis: Fundamentals, Applications, and Industrial Perspectives*, Springer Netherlands, 1994.

- 27 L. J. Csányi and K. Jáky, *J. Mol. Catal.*, 1990, **61**, 75–84.
- 28 L. J. Csányi and K. Jáky, *Phys. Chem. Chem. Phys.*, 2001, **3**, 2018–2024.
- 29 L. J. Csányi, *Transit. Met. Chem.*, 1990, **15**, 371–373.
- 30 L. J. Csányi and K. Jáky, *J. Mol. Catal. A Chem.*, 1997, **1169**, 125–138.
- 31 Y. Matoba, H. Inoue, J.-I. Akagi, T. Okabayashi, Y. Ishii and M. Ogawa, *Synth. Commun.*, 1984, **14**, 865–873.
- 32 X. Zuwei, Z. Ning, S. Yu and L. Kunlan, *Science*, 2001, **292**, 1139–1141.
- 33 Y. Ding, W. Zhao, H. Hua and B. Ma, *Green Chem.*, 2008, **10**, 910–913.
- 34 J.-M. Brégeault, M. Vennat, J.-Y. Piquemal, Y. Mahha, E. Briot, P. C. Bakala, A. Atlamsani and R. Thouvenot, *J. Mol. Catal. A Chem.*, 2006, **250**, 177–189.
- 35 M. Guo, *Green Chem.*, 2004, **6**, 271–273.
- 36 J. Gao, Y. Chen, B. Han, Z. Feng, C. Li, N. Zhou, S. Gao and Z. Xi, *J. Mol. Catal. A Chem.*, 2004, **210**, 197–204.
- 37 N. Zhou, Z. Xi, G. Cao and S. Gao, *Appl. Catal. A Gen.*, 2003, **250**, 239–245.
- 38 Y. Ding and W. Zhao, *J. Mol. Catal. A Chem.*, 2011, **337**, 45–51.
- 39 M. Gleria and R. De Jaeger, *Top. Curr. Chem.*, 2005, **250**, 165–251.
- 40 M. Gleria and R. De Jaeger, *Phosphazenes: A Worldwide Insight*, Nova Science Publishers, New York, 2004.
- 41 A. K. Andrianov, *Polyphosphazenes for Biomedical Applications*, Wiley, 2009.

- 42 J. F. Bickley, R. Bonar-Law, G. T. Lawson, P. I. Richards, F. Rivals, A. Steiner and S. Zacchini, *Dalt. Trans.*, 2003, 1235–1244.
- 43 H. R. Allcock, T. J. Fuller and K. Matsumura, *Inorg. Chem.*, 1982, **21**, 515–521.
- 44 J. Ledger, R. Boomishankar and A. Steiner, *Inorg. Chem.*, 2010, **49**, 3896–904.
- 45 H. R. Allcock, *Chem. Rev.*, 1972, **72**, 315–356.
- 46 D. Feakins, *J. Chem. Soc.*, 1964, 4464–4471.
- 47 T. Moeller and S. G. Kokalis, *J. Inorg. Nucl. Chem.*, 1963, **25**, 875–881.
- 48 O. Schmitz-Dumont and H. Kùlkens, *Z. Anorg. Allg. Chem.*, 1938, **238**, 189–200.
- 49 H. Bode, K. Bùtow and G. Lienau, *Chem. Ber.*, 1948, **81**, 547–552.
- 50 D. B. Sowerby and L. F. Audrieth, *Chem. Ber.*, 1961, **94**, 2670–2675.
- 51 Z. Tun, A. J. Heston, M. J. Panzner, V. Scionti, D. A. Medvetz, B. D. Wright, N. A. Johnson, L. Li, C. Wesdemiotis, P. L. Rinaldi, W. J. Youngs and C. A. Tessier, *Inorg. Chem.*, 2016, **55**, 3283–3293.
- 52 A. Steiner, in *Polyphosphazenes for Biomedical Applications*, John Wiley & Sons, Inc., 2009, pp. 411–453.
- 53 M. Craven, R. Yahya, E. F. Kozhevnikova, R. Boomishankar, C. M. Robertson, A. Steiner and I. V. Kozhevnikov, *Chem. Commun.*, 2013, **49**, 349–351.
- 54 H. R. Allcock, E. C. Bissell and E. T. Shawl, *J. Am. Chem. Soc.*, 1972, **94**, 8603–8604.
- 55 H. R. Allcock, E. C. Bissell and E. T. Shawl, *Inorg. Chem.*, 1973, **12**, 2963–2968.
- 56 Z. Zhu, R. Tain and C. Rhodes, *Can. J. Chem.*, 2003, **81**, 1044–1050.

- 57 H. R. Allcock, in *Phosphorus-Nitrogen Compounds*, Academic Press, Inc., London, 1972, p. 498.
- 58 C. Venturello, J. C. J. Bart and M. Ricci, *J. Mol. Catal.*, 1985, **32**, 107–110.
- 59 M. H. Dickman and M. T. Pope, *Chem. Rev.*, 1994, **94**, 569–584.
- 60 M. Grzywa, W. Nitek and W. Łasocha, *J. Mol. Struct.*, 2007, **828**, 111–115.
- 61 X.-Y. Shi and J.-F. Wei, *Zeitschrift für Krist. - New Cryst. Struct.*, 2006, **221**, 148–150.
- 62 R. Stomberg, *J. Less-Common Met.*, 1988, **143**, 363–371.
- 63 M. A. Benson, S. Zacchini, R. Boomishankar, Y. Chan and A. Steiner, *Inorg. Chem.*, 2007, **46**, 7097–7108.
- 64 P. I. Richards, M. A. Benson and A. Steiner, *Chem. Commun.*, 2003, **9**, 1392–1393.
- 65 M. Grzywa, W. Łasocha and D. Rutkowska-Żbik, *J. Solid State Chem.*, 2009, **182**, 973–982.
- 66 R. Yahya, PhD thesis: *Polyoxometalate Catalysis for Oxidative Desulfurization*, University of Liverpool, 2015.
- 67 H. Lü, J. Gao, Z. Jiang, F. Jing, Y. Yang, G. Wang and C. Li, *J. Catal.*, 2006, **239**, 369–375.

4. System Two: Heterogeneous Catalysis – Oxidation Reactions with H₂O₂ in Multiphase Systems Catalysed by POM Immobilised on RPN-Functionalized Silica Support

4.1 Introduction

In the previous chapter, alkylaminocyclotriphosphazenes, (RPN, R= benzyl, *iso*-butyl or *iso*-propyl) were used as PTC moieties for POM-catalysed oxidative desulfurization and olefin epoxidation with H₂O₂ in two-phase systems comprised of organic solvent and water (System One). The basic N-sites of the phosphazene ring are protonated by heteropoly acids, H_nPOM, forming ion pairs (RPN-POM aggregates) - in which the POM ions are effectively encapsulated by extensive hydrogen bonding with alkylamino (RNH) substituents. The lipophilicity of the alkylamino groups rendered the resulting POM-RPN aggregates soluble in the organic/fuel phase. The solubility of the aggregates could be tuned by varying the alkyl group, R. Thus, high conversion of benzothiophene or yield of epoxide was achieved in solvents such as toluene and heptane using aromatic (benzyl) and aliphatic (*iso*-butyl) RNH groups, respectively. The main issue with these systems, however, was that the catalyst remained soluble in the organic layer once the reaction was complete which made product separation difficult; separation required vacuum distillation to isolate the catalyst which increases system costs and can compromise product yield and purity.

One method to improve catalyst/product separation in liquid systems is to use a solid catalyst. The catalyst is insoluble in the reaction solvent and reactions occur at the liquid/solid interface between the active sites on the catalyst surface and the reactants in the solvent. Examples are shown in Fig. 4.1, which outlines the possible reaction processes for an organic molecule at the surface of a supported metal catalyst in a liquid-solid system, where the metal functions as the active site.^{1,2}

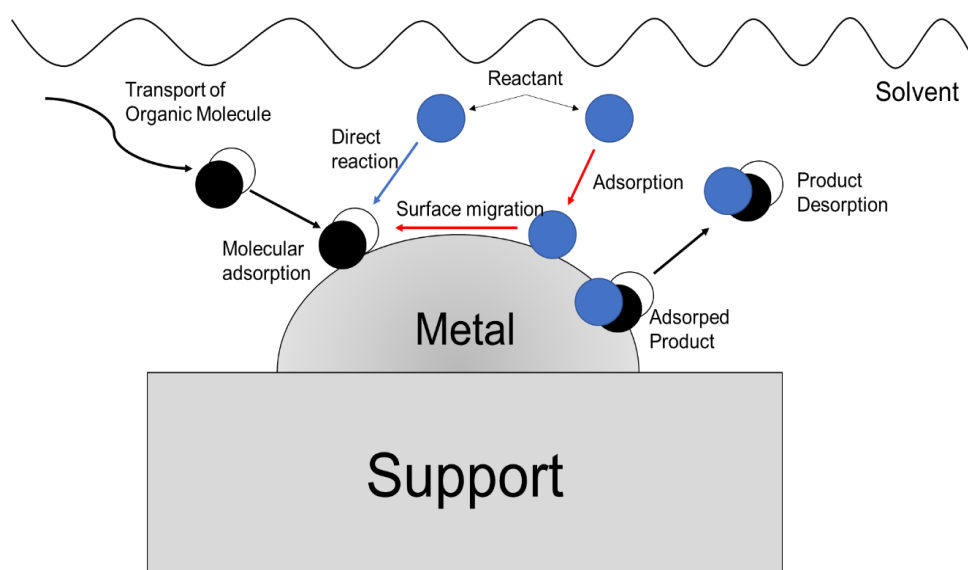


Fig. 4.1. Reaction processes for an organic molecule at the surface of a supported metal catalyst in a liquid-solid system.

Once the molecule has adsorbed onto the catalyst surface, a second reactant can either interact directly from solution, or by adsorbing onto the catalyst surface first and then migrating across the surface before reacting with the adsorbed molecule. The mechanism of the reaction depends on the respective orientations required for the molecule and reactant to react, and whether the reactant needs to be activated on the catalyst surface before it can react with the target molecule. The adsorbed product then desorbs from the catalyst and is transported away from the surface

which then provides space for other reactant molecules to interact with the surface to complete the cycle.

The use of powdered, porous catalysts often increases the reaction rates by improving the available surface area of the catalysts and hence increasing the number of available active sites to the reactants for reaction.^{3,4} An active site can also be a catalyst species that has been immobilised on the surface of a solid support to heterogenize the catalyst in the system. In this way, a catalyst that successfully catalyses a reaction homogeneously but is difficult to separate from the products can still be used to catalyse the same reaction but is now instantly separated from the product once the reaction is complete. Additional advantages of this approach also include enhanced catalytic activity of the active sites through interactions between the support and the catalyst, minimization of metal traces from metal-based catalysts in the product, improved handling, and improved control over the reaction process.³

Many heterogeneous catalysts have been used for the oxidative desulfurization of diesel fuels.^{5–}

¹¹ Systems which use H_2O_2 as an oxidant are attractive as H_2O_2 is cheap, has a high active oxygen atom efficiency, and its only by-product is water.^{12,13} Examples of catalysts that have been used in such systems include $\text{Mo}/\gamma\text{-Al}_2\text{O}_3$,¹⁴ Ti-containing zeolites,¹⁵ Ti^{iv} grafted onto silica,¹⁶ Zr and Hf oxoclusters in a poly(methylmethacrylate) matrix,¹⁷ and a POM-MOF composite to name just a few.¹⁸

Transition metal derivatives are commonly used as catalysts for the oxidation of alkenes with H_2O_2 .¹⁹ However, in homogeneous systems, these compounds can be difficult to separate from the product and can leave traces of toxic heavy-metals in the products. Many of these catalysts can be immobilised on solid supports which can help to resolve these issues. Examples of solid-supported transition metal catalysts for epoxidation with H_2O_2 include: titanium silicate zeolite (TS-1);²⁰ metallocene compounds on mesoporous silica (e.g. Ti-MCM-41);²¹ solid polymer-

supported Mn-Salen complexes;²² methyltrioxorhenium (MTO) supported on poly(4-vinylpyridine) derived polymers,²³ and MTO supported on niobia.²⁴

POMs are particularly effective catalysts in oxidations with H₂O₂, transforming into catalytically active peroxy POM species.²⁵⁻²⁷ Methods for their heterogenization for use as catalysts in liquid-phase organic transformations have been reviewed,²⁸ and the major strategies include: immobilization on solid supports (e.g. mesoporous silicas, MOFs, polymers, metal oxides, and magnetic particles); solidification through the use of inorganic cations such as alkali metals, organic compounds such as organic amine surfactants, or the formation of ionic liquids (particularly those with high melting points); and the formation of POM-based porous frameworks.

Immobilization of POMs onto solid supports is one of the most simple and efficient methods for synthesizing POM-based heterogeneous catalysts. Table 4.1 highlights some of the methods used to immobilize POMs onto various supports and their use as heterogeneous catalysts in either oxidative desulfurization or alkene oxidation with H₂O₂.

Table 4.1. Immobilized POM catalysts and their corresponding reaction studies.²

Support	POM	Immobilization Method	Reaction	Ref
Mesoporous silicas				
IL-modified SiO ₂	[{W(=O)(O ₂) ₂ (H ₂ O)} ₂ (μ-O)] ²⁻	Ion-exchange	Alkene oxidation	29

IL-modified SiO ₂	Na ₇ H ₂ LaW ₁₀ O ₃₆ ·32H ₂ O	Ion-exchange	Oxidative desulfurization	30
MOFs				
MIL-101(Cr)	[PW ₁₁ CoO ₃₉] ⁵⁻ and [PW ₁₁ TiO ₄₀] ⁵⁻	Impregnation	Alkene oxidation	31
MIL-101(Cr)	[PW ₁₁ O ₃₉] ⁷⁻	Impregnation	Alkene oxidation and oxidative desulfurization	32-34
HKUST-1	H ₅ PV ₂ Mo ₁₀ O ₄₀	One-pot synthesis	Oxidative desulfurization	35
Polymers				
Ionic copolymers AM-BM, DIM-CIM Ordered mesoporous polymeric materials Polymer- immobilized ionic liquid phase	PW ₁₂ O ₄₀ ³⁻ and PW ₄ O ₁₆ ³⁻ [PO ₄ {WO(O ₂) ₂ } ₄] ³⁻ [PO ₄ {WO(O ₂) ₂ } ₄] ³⁻	Ion-exchange Ion-exchange Ion-exchange	Alkene oxidation Alkene oxidation Alkene oxidation	36,37 38 39

Cross-linked POM polymers	$[\{CH_2=CH-(CH_2)_6Si\}_xO_ySiW_wO_z]^{4-}$	Copolymerization	Oxidative desulfurization	40
Mesoporous metal oxides				
Ordered mesoporous ZrO ₂	H ₃ PMO ₁₂ O ₄₀ and H ₃ PW ₁₂ O ₄₀	Surfactant- assisted sol-gel copolymerization	Alkene oxidation	41,42
Magnetic nanoparticles				
Fe ₃ O ₄ ferromagnetic NCs PIL-coated magnetic Fe ₃ O ₄	(DODA) ₃ PW ₁₂ O ₄₀ H ₃ PW ₁₂ O ₄₀	Incorporation Ion-exchange	Oxidative desulfurization Alkene oxidation	43 44

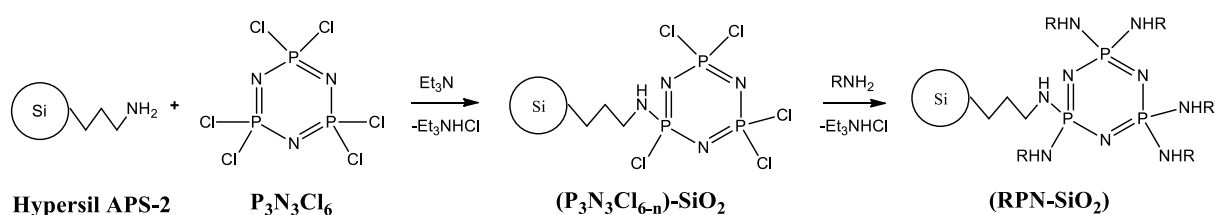
The preparation of many immobilised POM catalysts use an ion-exchange method to graft POM to the surface of the support. In these procedures, the POMs are ionically bonded to cationic functional groups at the surface of the support.

In this chapter, the problem of catalyst separation in RPN-POM catalysed biphasic oxidations with H₂O₂ has been addressed by grafting RPN-POMs to an aminopropyl-functionalized silica support (Hypersil APS-2). The resulting materials, POM/RPN-SiO₂, comprising POMs immobilized onto the silica surface using RPNs as tethers, are reported as heterogeneous catalysts for biphasic oxidative desulfurization and olefin epoxidation with H₂O₂. Discussion

of solid-state NMR data was written in conjunction with Dong Xiao. Figs 4.2-4.5 and 4.9 were created by Dong Xiao and have been used in this work with the consent of the creator.

4.2 Phosphazene-Modified Silica Support

The route for grafting alkylaminocyclotriphosphazenes onto silica is shown in Scheme 4.1. First, the reaction of Hypersil APS-2 surface aminopropyl groups with hexachlorocyclotriphosphazene ($P_3N_3Cl_6$) in the presence of triethylamine produces the chlorocyclotriphosphazene grafted silica ($(P_3N_3Cl_{6-n})-SiO_2$ (where n = grafted aminopropyl linkers). Subsequent reaction with an 8-fold molar excess of RNH_2 yields the final RPN functionalized silica, RPN- SiO_2 .



Scheme 4.1. Grafting RPN onto aminopropyl-modified silica Hypersil APS-2.

Solid-state MAS NMR was used to determine the structure of the RPN- SiO_2 products formed and monitor the step-wise synthesis of BzPN- SiO_2 by recording ^{13}C CP, ^{31}P DE NMR spectra (Fig. 4.2) and ^{29}Si CP NMR spectra (Fig 4.3) of the expected compounds, $(P_3N_3Cl_{6-n})-SiO_2$ and BzPN- SiO_2 , that were isolated after each reaction step.

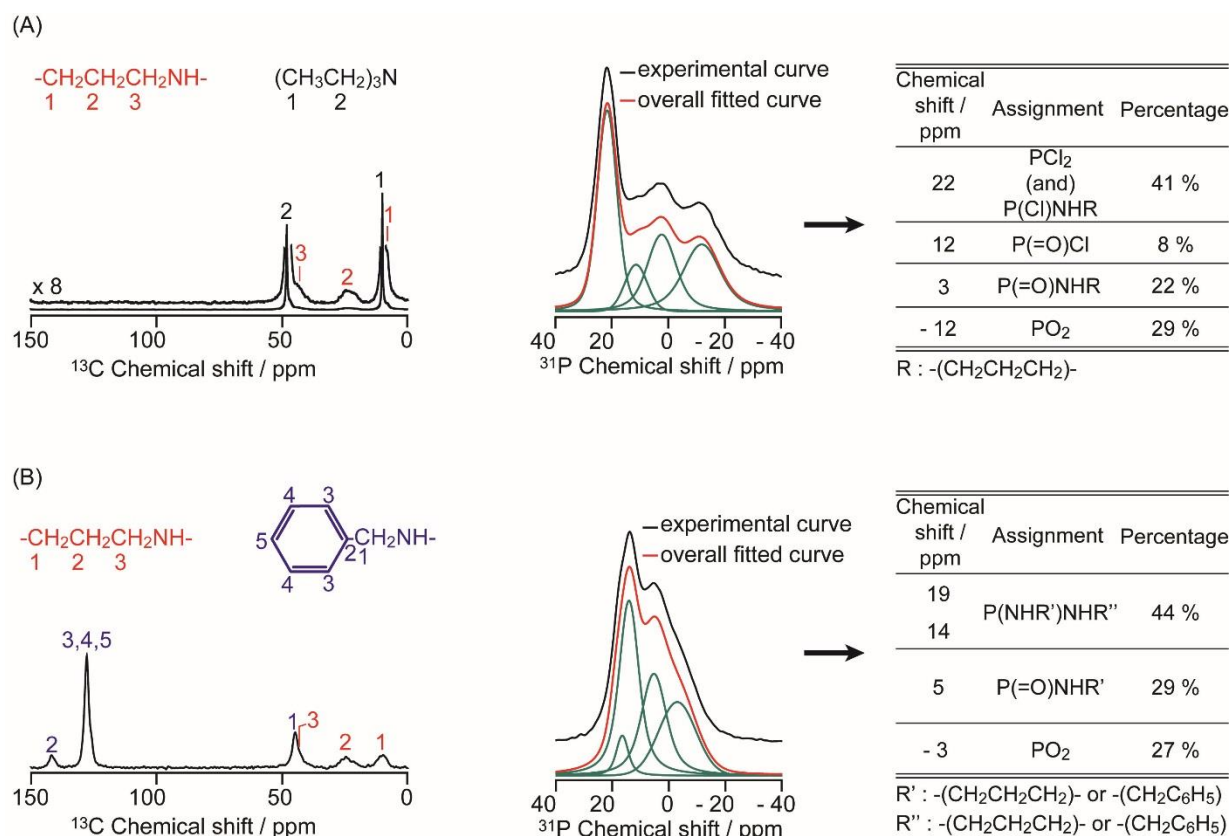


Fig. 4.2. ^{13}C CP MAS (14 kHz) NMR and ^{31}P DE MAS (12 kHz) NMR spectra and quantification of different phosphorus sites of (A) $(\text{P}_3\text{N}_3\text{Cl}_{6-n})\text{-SiO}_2$ and (B) BzPN-SiO_2 . The ^{13}C spectral assignments are given in the corresponding ^{13}C NMR spectra. The deconvolution and quantification of the different phosphorus sites are given with the experimental ^{31}P MAS NMR spectra. Error of integrations was $<10\%$.

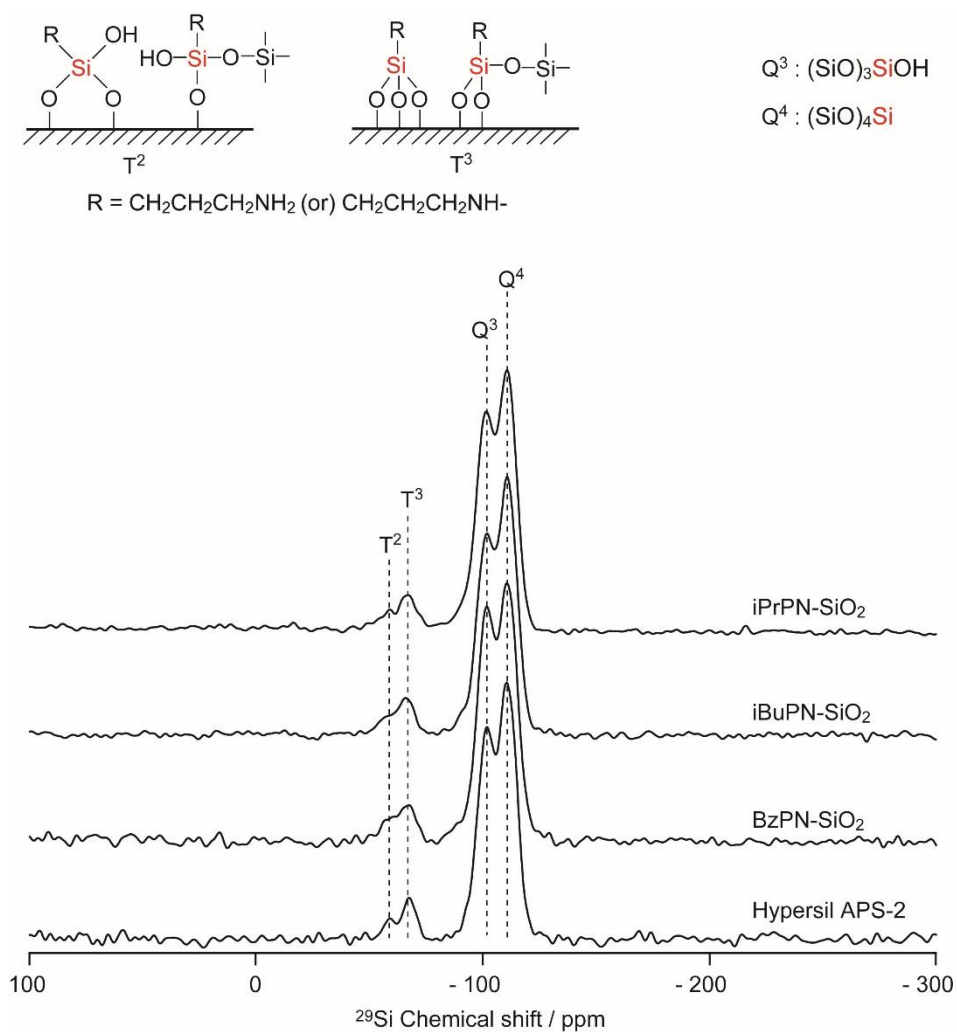


Fig. 4.3. ²⁹Si CP MAS NMR spectra of Hypersil APS-2, BzPN-SiO₂, iBuPN-SiO₂, iPrPN-SiO₂. Spectra were recorded at 9.4 T, MAS rate of 10 kHz. Signals are assigned according to the reference.⁴⁵

The ¹³C spectrum of Hypersil APS-2 shows three distinct peaks in the range of 0 – 50 ppm which can be assigned to the three carbon environments that are present in the aminopropyl surface groups (Fig. 4.4).

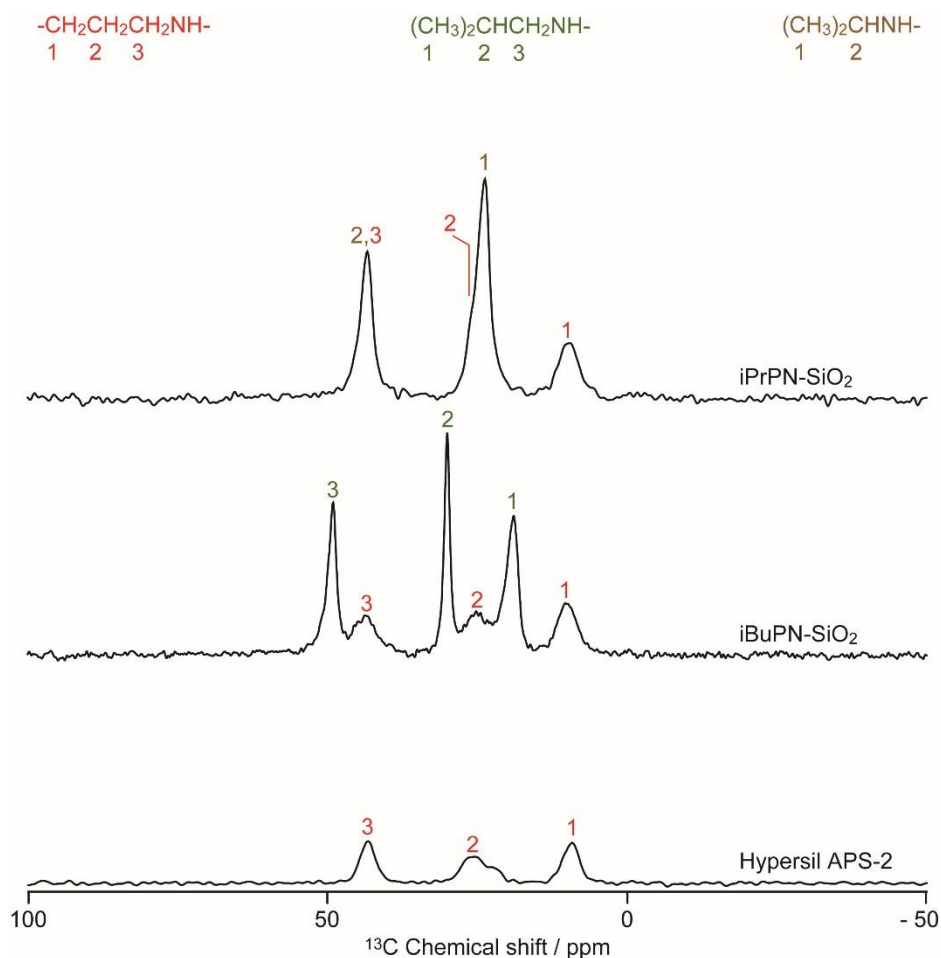


Fig. 4.4. ¹³C CP MAS NMR spectra of Hypersil APS-2, iBuPN-SiO₂, iPrPN-SiO₂. Spectra were recorded at 9.4 T and MAS rate of 10 kHz for iBuPN-SiO₂, iPrPN-SiO₂ and of 14 kHz for Hypersil APS-2. The ¹³C spectral assignments are given in the corresponding ¹³C NMR spectra.

The ¹³C signals of the aminopropyl groups remain after reactions with P₃N₃Cl₆ and then RNH₂, and show little change in the chemical shifts in the spectra for (P₃N₃Cl_{6-n})-SiO₂ and the RPN-SiO₂ products (Figs 4.2 and 4.4), indicating that bonding between these groups and silica surfaces are not destroyed during the preparation procedure and are largely unaffected by reaction with the phosphazene rings. Signals in (P₃N₃Cl_{6-n})-SiO₂ spectrum (Fig. 4.2, A) also show corresponding peaks for triethylamine, the auxiliary base used in the preparation

procedure, which was not completely removed when isolating the $(P_3N_3Cl_{6-n})-SiO_2$ intermediate. Typical signals from aromatic groups ($\delta = 128$ and 142 ppm) are observed in BzPN-SiO₂, which clearly indicate successful immobilization of BzPN on the silica. The spectra of iBuPN-SiO₂ and iPrPN-SiO₂ also indicate successful immobilization of iBu and iPr groups, respectively, and their assignments are shown in Fig. 4.4.

³¹P NMR is indicative of the substitution pattern of cyclophosphazenes. Each P₃N₃ ring has six exocyclic substituent sites that are available for functionalisation with a variety of substituent groups (see P₃N₃Cl₆ structure in Scheme 4.1, the three P atoms each have two exocyclic Cl substituents), and the ³¹P chemical shifts of the three phosphorous atoms are strongly influenced by the electronegativity of the two substituent groups that each atom is bonded to.⁴⁶ It has been shown previously that P-nuclei of phosphazene rings that carry two RNH groups have chemical shifts at around 20-23 ppm,⁴⁷ thus we should expect a narrow distribution of peaks in the spectra of RPN-SiO₂ compounds. However, ³¹P MAS NMR spectra of RPN-SiO₂ compounds (Fig 4.2 and Fig. 4.5) reveal a wider range of shifts stretching from -19 to -4 ppm. Similar shifts have been observed in cyclophosphazenes that have amino and oxo substituent groups; the oxo groups were introduced *via* partial or complete hydrolysis of the PCl₂ groups.⁴⁸ Three regions of shifts can be identified in the ³¹P MAS NMR spectra of RPN-SO₂ (Fig. 4.2 B and Fig. 4.5); these can be assigned to P(NHR')NHR'' at 19 to 14 ppm (see definitions for R' and R'' in Fig 4.2 and Fig 4.5 tables), P(=O)NHR' at 9 to 4 ppm, and PO₂ groups at -2 to -4 ppm. The relative signal contributions for each of these groups is given as a percentage in the corresponding figures.

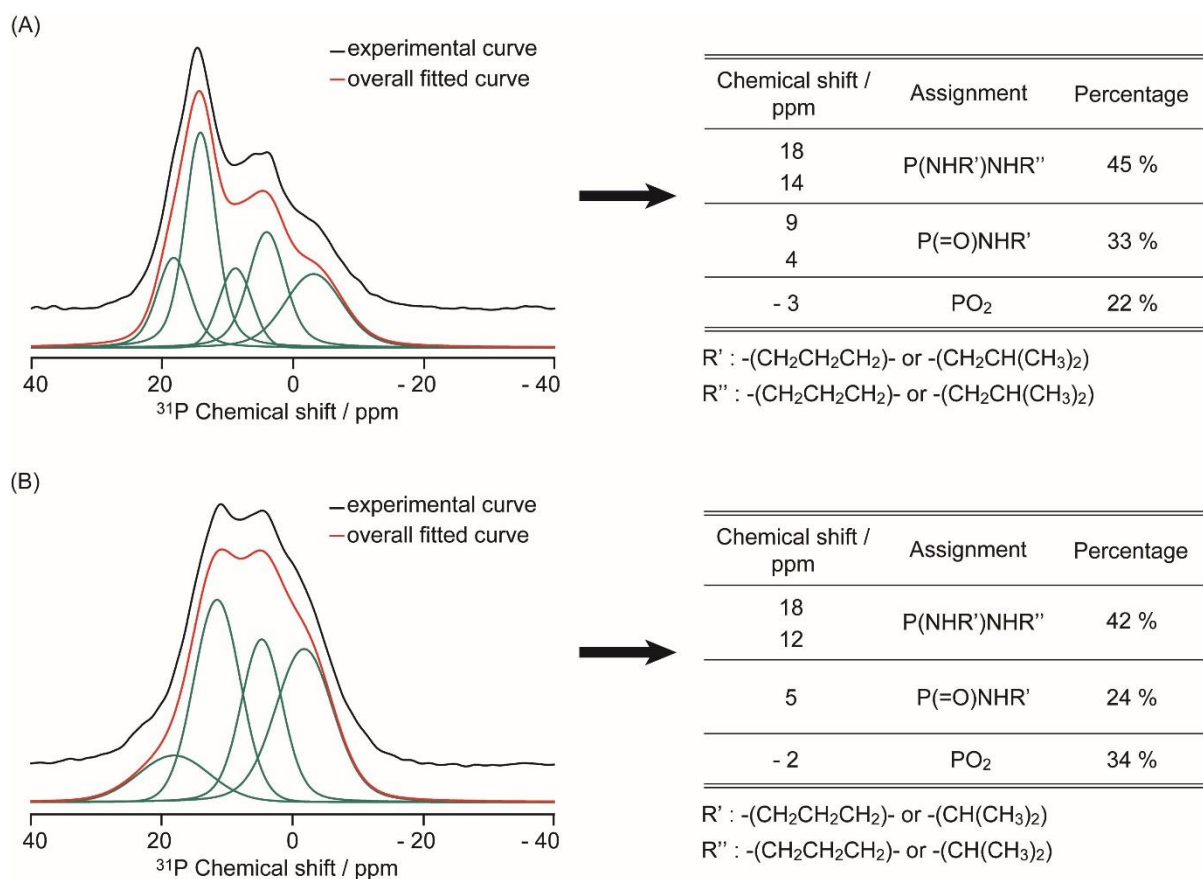


Fig. 4.5. ³¹P DE MAS NMR spectra and the deconvolution and quantification of different phosphorus sites of (A) iBuPN-SiO₂ and (B) iPrPN-SiO₂. Spectra were recorded at 9.4 T, MAS rate of 12 kHz.

It was estimated from the respective contributions in the ³¹P DE MAS NMR spectra using equations (4.1) and (4.2) that the hydrolysis groups occupy up to 40% of the total P exocyclic substituent sites of RPNs in the RPN-SiO₂ samples, with the other 60% of these sites attached to primary amines and/or aminopropyl groups.

$$\text{PO}_2 (\%) + 1/2 (\text{P}(=\text{O}) \text{NHR}') (\%) = \text{Total sites occupied by hydrolysis products} \quad \mathbf{4.1}$$

$$\text{P(NHR')} \text{NHR}'' (\%) + 1/2 (\text{P}(=\text{O}) \text{NHR}') (\%) = \text{Total sites occupied by amine groups} \quad \mathbf{4.2}$$

A range of shifts in the ^{31}P MAS NMR spectrum of $(\text{P}_3\text{N}_3\text{Cl}_{6-n})\text{-SiO}_2$ (Fig. 4.2 A) between 12 and -12 ppm, which have been observed in hydrolysis experiments of $\text{P}_3\text{N}_3\text{Cl}_6$,⁴⁹ strongly suggested that hydrolysis had occurred during the initial grafting of the hexachloro precursor to the silica. It is presumed that residual water bound to silica was responsible for the hydrolysis which was not removed by thermal pre-treatment due to the possibility of destroying surface aminopropyl groups. Indeed, a shoulder at 22 ppm is observed for the C2 resonance (25 ppm) of the aminopropyl groups in the ^{13}C spectrum of Hypersil APS-2 (Fig. 4.4) indicates the presence of ion-pair complexes $\text{Si-O}^-\cdots\text{NH}_3^+\text{-R}$ ($\text{R} = \text{-CH}_2\text{CH}_2\text{CH}_2\text{-}$) which are formed by interactions between the amino groups and silanols in the presence of water.⁴⁵ Hence, this demonstrates the existence of water adsorbed in Hypersil APS-2. It should be noted that similar grafting of cyclophosphazenes onto silica has been reported previously; however, no detailed solid-state MAS NMR work has been undertaken in these cases, which suggests that similar hydrolysis products may have been obtained but not identified.⁵⁰⁻⁵⁴ The spectra in Fig. 4.2 also show that after reaction of $(\text{P}_3\text{N}_3\text{Cl}_{6-n})\text{-SiO}_2$ with benzylamine, the main ^{31}P peak is shifted from 22 ppm in the $(\text{P}_3\text{N}_3\text{Cl}_{6-n})\text{-SiO}_2$ spectrum (A) into the range of 19 to 14 ppm in the BzPN- SiO_2 spectrum (B) which confirms the successful attachment of benzylamino substituent groups.⁴⁷

^{29}Si CP MAS NMR spectra of RPN- SiO_2 are displayed in Fig. 4.3 and show ^{29}Si resonances at -59 ppm, -67 ppm, -102 ppm and -111 ppm which can be assigned to the T^2 , T^3 , Q^3 and Q^4 sites in silica, respectively, of which the T^2 , T^3 sites correspond to the tethering sites of aminopropyl groups to the silica surface.^{45,55}

FTIR analysis of all three RPN- SiO_2 products showed bands in the region of $1300\text{-}1000\text{ cm}^{-1}$ (P-N) and $3400\text{-}3250$ (N-H, amines) which provide further evidence of successful grafting of RPN onto the surface of the silica. An increase in the number and intensity of bands in the $1500\text{ - }1400\text{ cm}^{-1}$ region (C- C_{alkyl}) of RPN- SiO_2 spectra compared with the Hypersil APS-2 spectrum

indicates successful nucleophilic substitution of the phosphazene chloride substituents for the respective primary amines. 1664 cm^{-1} and 1496 cm^{-1} ($\text{C}=\text{C}_{\text{arom}}$), and 878 cm^{-1} , 731 cm^{-1} and 699 cm^{-1} ($\text{C}-\text{H}_{\text{arom}}$) bands in the BzPN-SiO₂ spectrum provide particularly strong evidence of successful substitution with benzylamine groups. Peaks in the range of $2940 - 2970\text{ cm}^{-1}$ in the spectra of RPN-SiO₂ samples before the Hypersil APS-2 background was subtracted could be further evidence of hydrogen-bonding interactions between excess primary amine and the surface silanol groups ($\text{SiOH}\cdots\text{NH}_2$).⁵⁶ P-O stretches from the hydrolysis products in all RPN-SiO₂ spectra appear in the region of $875 - 900\text{ cm}^{-1}$.

Elemental analysis of RPN-SiO₂ provided empirical formulae $\text{C}_{32.4}\text{N}_{9.4}\text{P}_3$, $\text{C}_{24.8}\text{N}_{10.8}\text{P}_3$ and $\text{C}_{18.9}\text{N}_{8.9}\text{P}_3$ for BzPN-SiO₂, iBuPN-SiO₂ and iPrPN-SiO₂, respectively. This provides strong evidence to suggest successful immobilization of the cyclophosphazenes on the silica surface and substitution of the cyclotriphosphazene chlorines with the RNH₂ alkylamines. The loading of the RPN on the surface was found to be 0.12 mmol g^{-1} for iBuPN and 0.14 mmol g^{-1} for iPrPN and BzPN as estimated from the nitrogen and phosphorus content, indicating that phosphazene loading is consistent in the initial steps of the synthesis.

Table 4.2 summarises the elemental analysis of the prepared RPN-SiO₂ samples. The sources of nitrogen atoms in these samples are the N atoms of cyclotriphosphazene rings (three N atoms per ring, N:P = 1:1), as well as the Hypersil APS-2 aminopropyl groups and the RPN substituent amine groups RNH, which each possess a single nitrogen atom. As there are equimolar quantities of P and N present in cyclotriphosphazene rings, the P content was used to determine the quantity of nitrogen provided by the ring nitrogen atoms and the RPN loading for each RPN-SiO₂. The total concentration of aminopropyl linker plus alkylamino substituent (amine N) equals the difference between the total N and the total P content. The ratio of C/Amine N content for each RPN-SiO₂ approximate even distributions of the primary amine and aminopropyl linkers with regards to their concentration on the surface of each sample (e.g.

for BzNH₂ and aminopropyl the C/N ratio are 7 and 3, respectively, and equimolar amounts of both groups on the surface of BzPN-SiO₂ would give a [C]/[Amine N] ratio of 5, such as the value that was calculated using the experimental data).

Table 4.2. Composition of RPN-SiO₂ samples.

RPN-SiO ₂	Total N mmol g ⁻¹	C mmol g ⁻¹	P mmol g ⁻¹	Ring N mmol g ⁻¹	Amine N mmol g ⁻¹	RPN mmol g ⁻¹	C/Amine N	P _{sub} mmol g ⁻¹
Hypersil APS-2	0.40	1.20						
iP-PN-SiO ₂	1.24	2.64	0.42	0.42	0.82	0.14	3.2	0.50
iBuPN-SiO ₂	1.11	2.61	0.37	0.37	0.74	0.12	3.5	0.44
BzPN-SiO ₂	1.34	4.65	0.43	0.43	0.92	0.14	5.0	0.52

The concentration of RNH at the six P exocyclic bonding sites (P_{sub} , Table 4.2) for each RPN can be calculated as $P_{sub} = 2P \times 0.60$, where P is the concentration of phosphazene P given in

Table 4.2 and 0.60 is the 60% PNHR group signal contributions calculated from the ^{31}P DE MAS NMR spectra (Fig 4.2 and Fig. 4.5). Comparison of these values with the corresponding amine N concentration would imply that there is an excess of aminopropyl and primary amine groups present in the RPN-SiO₂ samples that are unreacted with phosphazene. It is suggested that the excess primary amine is hydrogen-bonded to the surface silanol groups which corresponds to peaks at 2940 – 2970 cm⁻¹ in the corresponding FTIR spectra. Such interactions have been reported previously in the literature,⁵⁶ and have demonstrated their stability towards solvent washings under conditions similar to, and harsher than, those used in the preparation of RPN-SiO₂ in this work.^{45,50,56-58}

Fig. 4.6 shows the SEM images of Hypersil APS-2 and BzPN-functionalized Hypersil APS-2 (BzPN-SiO₂). The initial Hypersil APS-2 sample exhibits a uniform array of spherical particles of ~5 μm particle size and it can be seen that this morphology is preserved in the BzPN-functionalized sample, indicating that RPN grafting does not affect the morphology of the initial silica support.

The surface area and porosity of the functionalized supports, RPN-SiO₂, were determined from nitrogen physisorption (BET method). The results are summarised in Table 4.3, together with the loading of surface functional groups. These data show that RPN functionalization had a relatively small effect on the BET surface area due to low RPN loadings, although it slightly reduced the pore volume and pore diameter of the samples, possibly because the RPN groups on the inside of the pore walls of RPN-SiO₂ take up more space than the aminopropyl groups of Hypersil APS-2, resulting in a decrease in the diameter and volume of pores of RPN-SiO₂ compared to Hypersil APS-2. The N₂ adsorption isotherms for Hypersil ASP-2 and BzPN-SiO₂ show a type IV isotherm with a H1 hysteresis loop (Fig. 4.7), indicating a mesoporous structure of uniformly arranged spherical particles,^{59,60} in agreement with the SEM data (Fig. 4.6). The adsorption isotherms for the other RPN-SiO₂ samples (Fig. 4.7) also show type IV isotherms

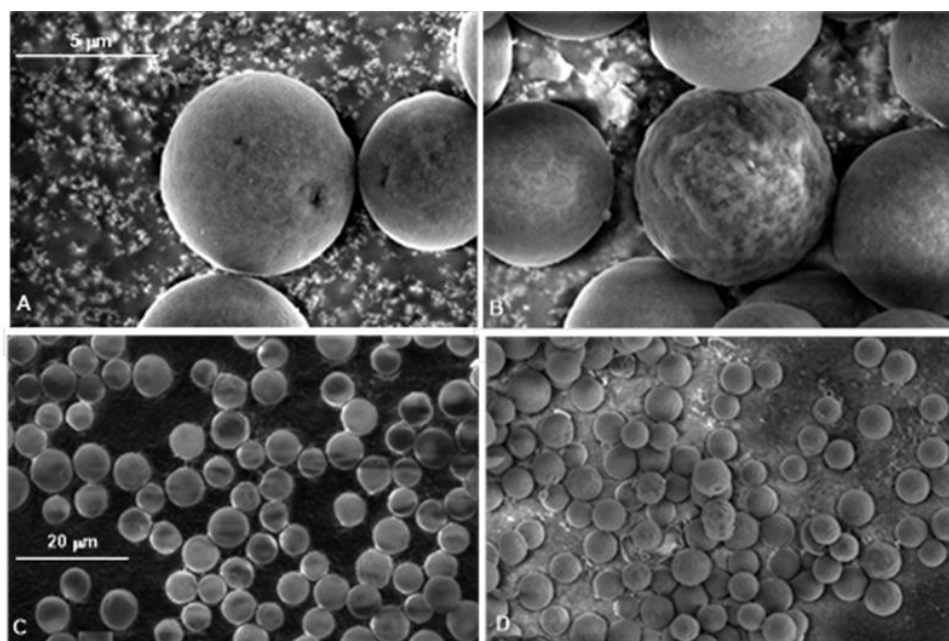


Fig. 4.6. SEM images of Hypersil APS-2 (A, C) and BzPN-SiO₂ (B, D); magnification scale 5 μm for A, B and 20 μm for C, D.

Table 4.3. Surface and porosity data for Hypersil APS-2 and RPN-SiO₂ functionalized supports.^a

Sample	RPN loading mmol g ⁻¹	$S_{\text{BET}}^{\text{b}}$ m ² g ⁻¹	Pore volume ^c cm ³ g ⁻¹	Pore diameter ^d Å
Hypersil APS-2	0.40 ^e	123	0.54	174
iPrPN-SiO ₂	0.14	130	0.49	151
iBuPN-SiO ₂	0.12	109	0.39	144
BzPN-SiO ₂	0.14	116	0.42	143
PMo/BzPN-SiO ₂	0.14	122	0.41	135

^a Samples pre-treated at 140 °C under vacuum. ^b BET surface area. ^c Single point total pore volume. ^d Average pore diameter. ^e aminopropyl group loading.

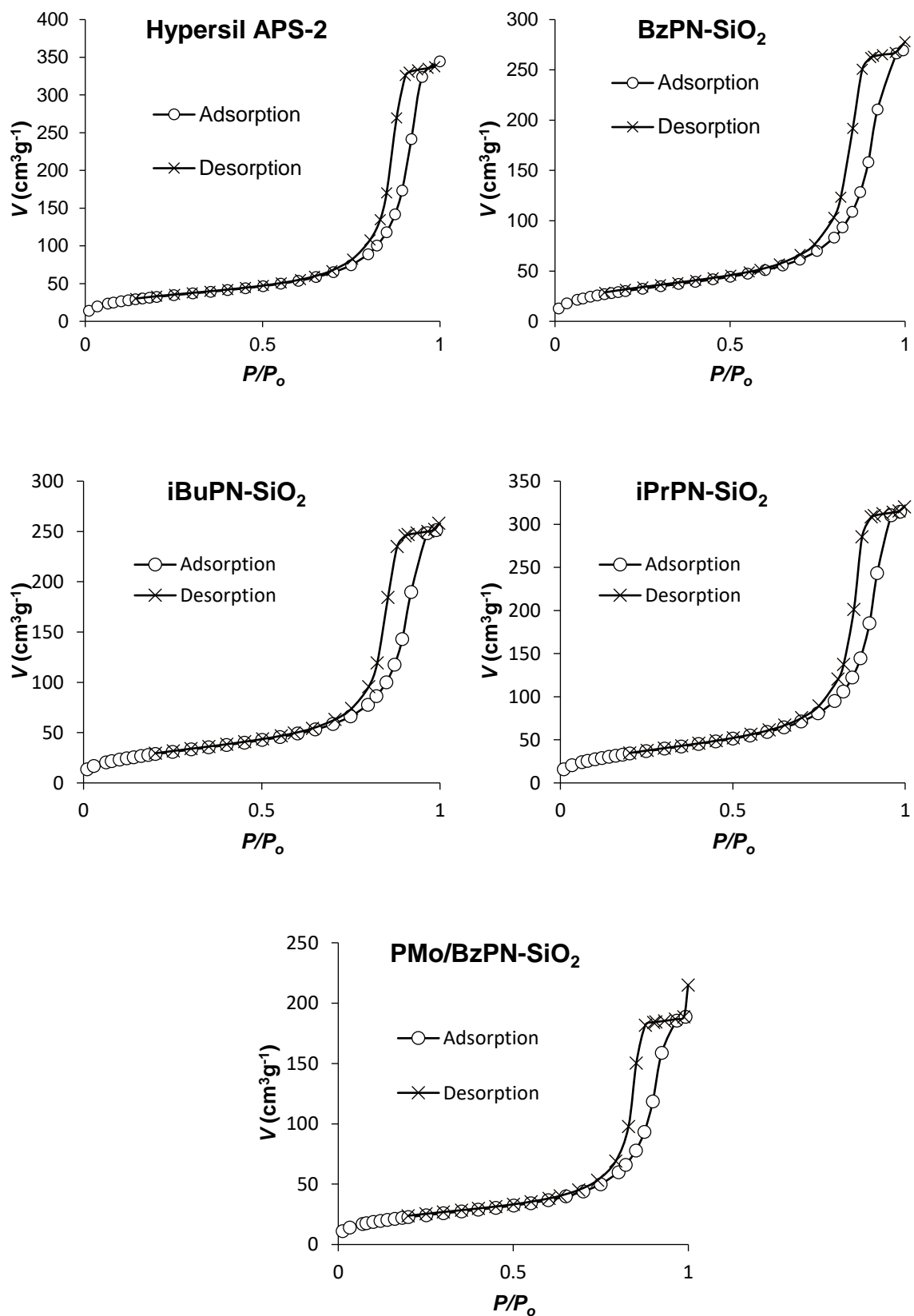
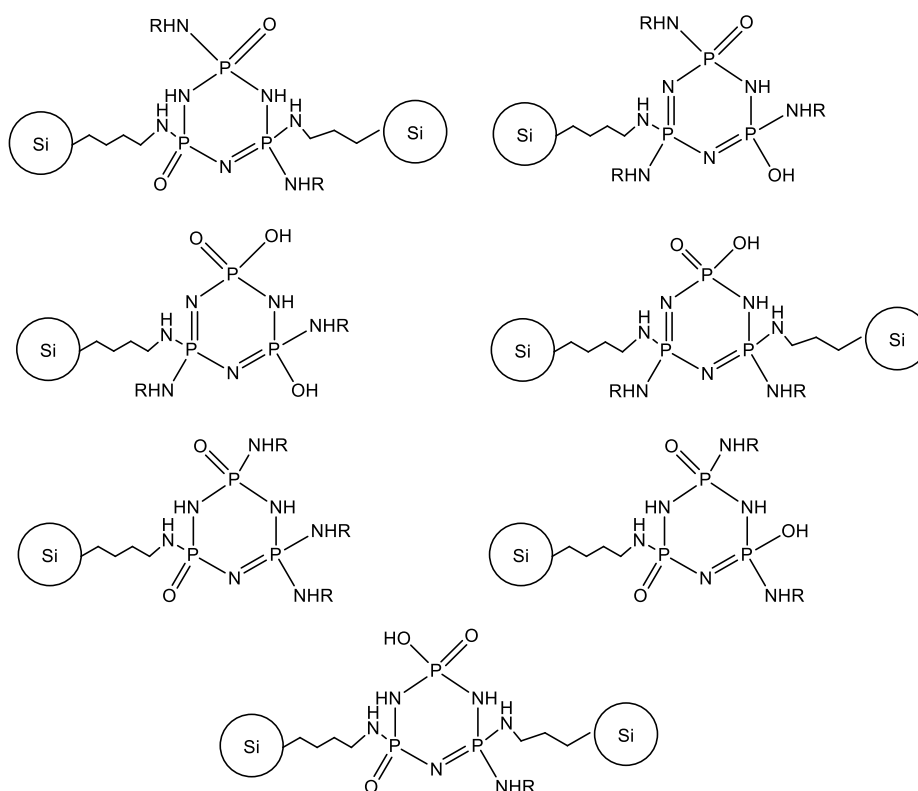


Fig. 4.7. Nitrogen adsorption isotherms for Hypersil APS-2, BzPN-SiO₂, iBuPN-SiO₂, iPrPN-SiO₂ and PMo/BzPN-SiO₂.

with H1 hysteresis loops, which indicates that the mesoporous structure of the silica support has remained intact through the RPN functionalization process.

The RPN-SiO₂ samples retain the 5 μm particle size and mesoporous structure of the parent Hypersil APS-2 support, as shown by BET and SEM analysis (Figs 4.6, 4.7, Table 4.3). Comparison of the elemental analysis with PNHR contributions from ³¹P DE MAS NMR analysis was used to determine the probable structures of RPN grafted on Hypersil APS-2 as shown in Scheme 4.2. Insight into the arrangement of the hydrolysis groups was provided by the literature.^{48,49} However, it should be noted that these structures are derived from the average predicted compositions of the functional groups on the phosphazenes, whereas, there is likely a complex distribution of phosphazene species present on the surface.



Scheme 4.2. Probable structures of RPN-modified Hypersil APS-2.

The phosphazene rings are grafted onto the silica through one or two covalently bonded silica propylamine functional groups with a loading of 0.12 - 0.14 mmol g⁻¹ and appear to be

hydrolysed during the grafting procedure as indicated by ^{31}P DE MAS NMR chemical shifts, most likely by residual water bonded to the silica. ^{31}P DE MAS NMR also shows that, on average, 3.6 (60%) phosphazene exocyclic substituent sites are bonded to either propylamine linkers or have been successfully substituted with the desired primary amine groups, whilst the remaining 2.4 (40%) sites appear to be hydrolysed. Further evidence of functionalisation of the grafted phosphazenes with the desired primary amines is provided by FTIR and ^{13}C CP MAS NMR. Elemental analysis and peaks around 2950 cm^{-1} in the FTIR spectra of RPN-SiO₂ also suggest that there are likely unreacted aminopropyl groups on the surface of the silica, as well as excess primary amine which could be hydrogen-bonded to the surface silanol groups. ^{29}Si CP MAS NMR suggests little change to the silanol (Q³ and Q⁴ sites) or aminopropyl groups (T² and T³ sites) after functionalisation with RPN.

4.3 POM Immobilized on Phosphazene-Functionalized Silica

In this work, Keggin POMs, namely PW₁₂O₄₀³⁻ (PW), PMo₁₂O₄₀³⁻ (PMo) and SiWO₄₀⁴⁻ (SiW), were immobilized onto RPN functionalized silica supports using the corresponding heteropoly acids as the POM precursors (Section 2.1.4.5) and were used as catalysts for deep oxidative desulfurization of model fuel with H₂O₂. Among the POM/RPN-SO₂ catalysts, PMo/BzPN-SiO₂ (PMo/BzPN = 1:1 mol/mol) showed the best desulfurization performance (see below) and was characterised by SEM, BET, solid-state NMR and FTIR.

Fig. 4.8 shows the SEM images of fresh and spent PMo/BzPN-SiO₂ catalysts, the latter was recovered after ODS of DBT (see below). Both catalysts have similar morphology to that of Hypersil APS-2 and BzPN-SiO₂ (Fig. 4.6), which indicates that the loading of PMo and desulfurization reaction has little effect on catalyst morphology as confirmed by the surface and porosity data on freshly prepared PMo/BzPN-SiO₂ catalyst (Table 4.3). It should be noted,

however, that fresh PMo/BzPN-SiO₂ had a higher quantity of smaller particles attached onto the surface as compared to the spent catalyst (Fig. 4.8). Possibly, the smaller particles were washed out during the oxidative desulfurization reaction. PMo/BzPN-SiO₂ also displayed a type IV nitrogen adsorption isotherm with an H1 hysteresis loop (Fig. 4.7), similar to those for Hypersil ASP-2 and BzPN-SiO₂ (Fig. 4.7), which, along with the SEM images, suggests that the catalyst particles remain spherical and fairly uniform in the presence of PMo.

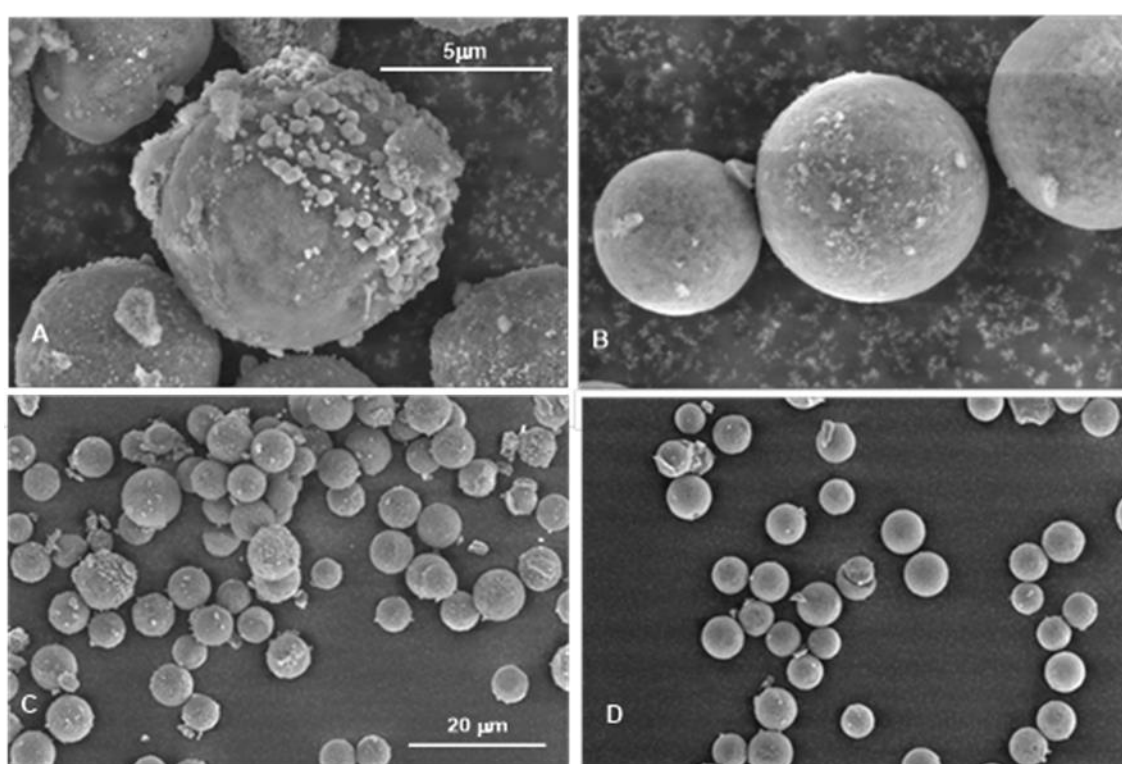


Fig. 4.8. SEM images of fresh PMo/BzPN-SiO₂ catalyst (A, C) and spent catalysts (B, D) recovered after desulfurization reaction; magnification scale 5 μm for A, B and 20 μm for C, D.

The ¹³C CP MAS NMR spectrum of PMo/BzPN-SiO₂ (Fig. 4.9 A) shows the typical signals from the benzylamino groups, while the ²⁹Si CP MAS NMR spectrum confirms the presence

of T² and T³ signals, suggesting that the structure of BzPN-SiO₂ remains intact after loading with PMo. In the ³¹P MAS NMR spectrum (Fig. 4.9 C), two sharp peaks at -3.7 and -4.4 ppm can be assigned to PMo in two different environments- possibly on the surface and in the mesopores-^{61,62} confirming the presence of intact PMo in the catalyst. The broad peaks of BzPN shifted upfield from 14 ppm to 11 ppm suggests protonation of one or two of the phosphazene nitrogens.⁶³

The PMo/BzPN-SiO₂ catalyst also exhibited characteristic peaks of the Keggin anion PMo₁₂O₄₀³⁻ in the FTIR spectrum (Fig. 4.10) at 962 cm⁻¹ (Mo=O), 873 cm⁻¹ (Mo-O-Mo corner-sharing) and 794 cm⁻¹ (Mo-O-Mo edge-sharing), which indicates that PMo remained intact in the catalyst. The intense peak at 1065 cm⁻¹ (P-O) in the FTIR spectrum of PMo/BzPN-SiO₂ is obscured by the broad silica band at 1000-1300 cm⁻¹.

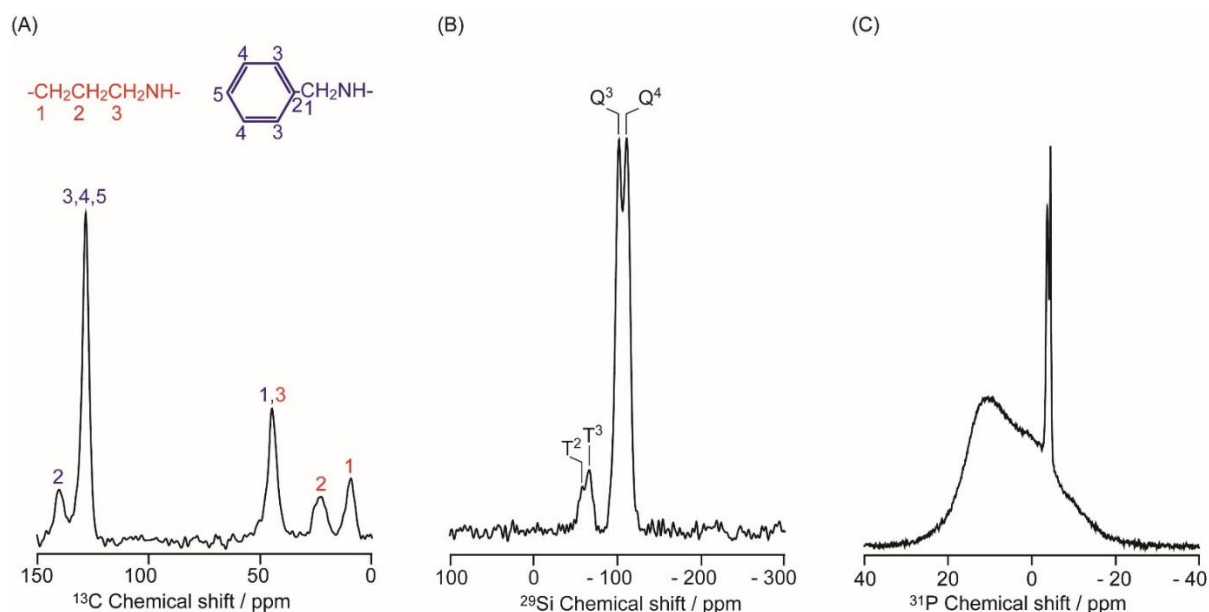


Fig. 4.9. (A) ¹³C CP MAS (14 kHz), (B) ²⁹Si CP MAS (10 kHz) and (C) ³¹P DE MAS (12 kHz) NMR spectra for PMo/BzPN-SiO₂.

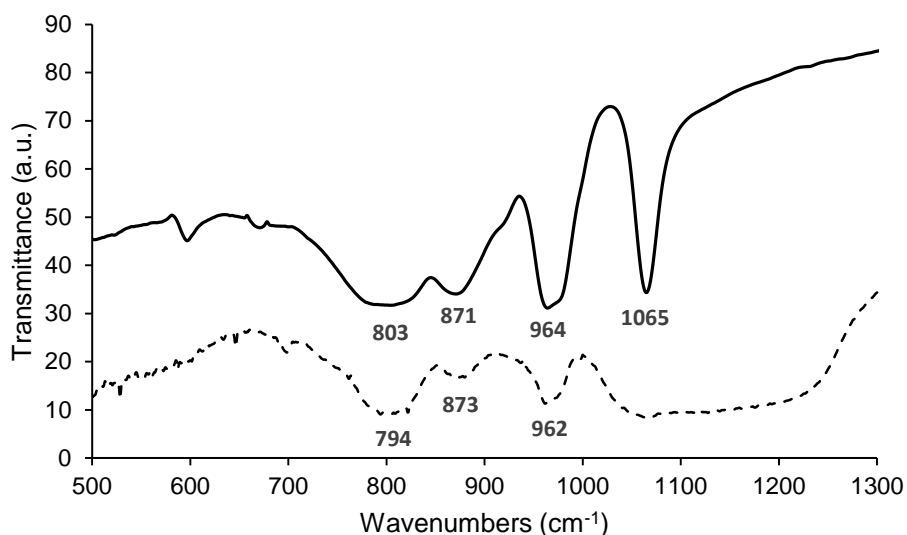
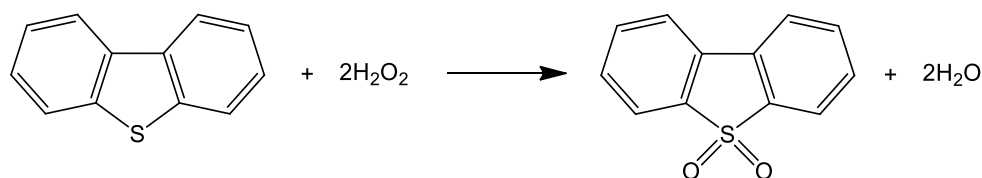


Fig. 4.10. DRIFTS FTIR spectra of PMo/BzPN-SiO₂ (dashed line) and H₃PMo₁₂O₄₀ (solid line) (KBr powder).

In previous work, single-crystal X-ray diffraction was used to characterize the bonding in POM-RPN aggregates (Section 3.1.1.).⁶⁴ It was found that the structures of the POMs remain intact upon aggregation with RPNs and are encapsulated by RPNH⁺ and RPNH₂²⁺ cations through a series of ionic and hydrogen bonding interactions. As characterization of PMo/BzPN-SiO₂ by ³¹P MAS NMR and FTIR suggest that the structure of PMo in the sample remains intact, we would suggest that POM is grafted to the surface of the silica support through ionic and hydrogen bonding interactions with cationic BzPNH_nⁿ⁺ groups. In this case, the cationic BzPN species form as a result of protonation by the H₃PMo₁₂O₄₀ precursor during the preparation procedure.

4.4 Oxidation of Benzothiophenes by H₂O₂ Catalysed by POM/RPN-SiO₂

Keggin-type polyoxometalates (PMo, PW and SiW) immobilized onto the RPN-functionalized silica support, POM/RPN-SiO₂, were used as heterogeneous catalysts for deep oxidative desulfurization of model diesel fuel by H₂O₂. The reactions were tested in a biphasic heptane-H₂O system comprised of n-heptane as a model fuel and benzothiophene (BT, DBT or DMDBT) as an organosulfur compound (Scheme 4.3). In these experiments, the POM/RPN-SiO₂ catalysts were prepared in situ by adding POM (as the corresponding heteropoly acid) and RPN-SiO₂ components separately to the reaction mixture to ensure more efficient pre-activation of the POM by hydrogen peroxide prior to reaction (section 2.3.3.2).



Scheme 4.3. DBT oxidation to sulfone by H₂O₂. Typical reaction conditions are 25 – 70 °C, atmospheric pressure.^{9,18,65-68}

Representative results are given in Table 4.4. The catalytic activity of POMs was found to decrease of the order PMo > PW > SiW (entries 3-5 in Table 4.4, see also Fig. 4.11) in agreement with both the relative stability of these POMs to degradation in aqueous solution and their oxidation potentials. The same activity trend was found previously in biphasic systems with homogeneous POM catalysts (Section 3.5),^{69,70} and can be explained by equations 3.6-3.8 along with their corresponding discussion .

Table 4.4. Oxidation of benzothiophenes by H₂O₂ in heptane-H₂O system using POM/RPN-SiO₂ as catalysts.^a

Entry	POM:RPN	POM	RPN	BT	Temp. °C	Time h	Conv. %	H ₂ O ₂ efficiency ^c %
1	1:4	PMo	- ^b	DBT	60	2	32	22
2	1:1	PMo	BzPN	DBT	60	2	96	68
3	1:1	PMo	BzPN	DBT	60	3	100	68
4	1:1	PW	BzPN	DBT	60	3	70	50
5	1:1	SiW	BzPN	DBT	60	3	55	52
6	1:1	PMo	iBuPN	DBT	60	3	86	61
7	1:1	PMo	iPrPN	DBT	60	3	61	55
8	1:1	PMo	BzPN	DBT	50	3	100	68
9	1:1	PMo	BzPN	DBT	40	3	81	69
10	1:1	PMo	BzPN	BT	60	6	90	80
11	1:1	PMo	BzPN	DMDBT	60	4	100	65

^a POM (0.0056 mmol), 30% H₂O₂ (0.15 mL, 1.51 mmol), dodecane (GC standard, 0.4 mmol), benzothiophene (0.5 mmol) and heptane (10 mL); molar ratio [benzothiophene]/[H₂O₂]=1:3, [POM]/[H₂O₂]=1:270 and [POM]/[benzothiophene]=1:90; stirring speed 1500 rpm. ^b Unmodified Hypersil APS-2. ^c Reaction selectivity with respect to H₂O₂ determined from titration of unconverted H₂O₂ with KMnO₄. H₂O₂ efficiency = 2 × conversion of substrate (mol) ÷ (initial H₂O₂ (mol) – final H₂O₂ (mol)).

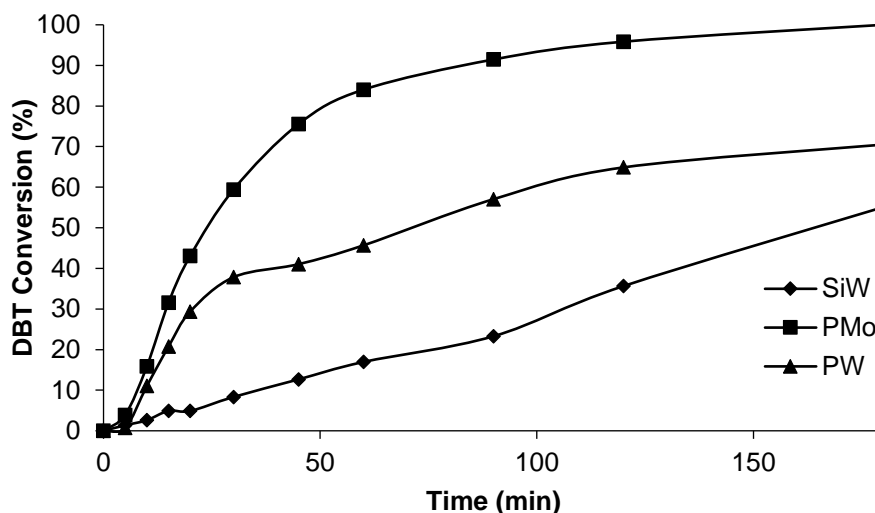


Fig. 4.11. Comparison of activity of POM/BzPN-SiO₂ catalysts (POM/BzPN = 1:1 mol/mol) in DBT oxidation by H₂O₂ in heptane-H₂O system (60 °C, POM (0.0056 mmol), 30% H₂O₂ (0.15 mL, 1.51 mmol), DBT (0.5 mmol), heptane (10 mL)).

Entries 1 and 2 in Table 4.4 compare the catalytic activity of PMo/Hypersil APS-2 and PMo/BzPN-SiO₂ catalyst. The results show that PMo/BzPN-SiO₂ is a more efficient catalyst for the oxidation of DBT than PMo/Hypersil APS-2, giving 95 and 32% DBT conversion at 60 °C in 2h, respectively. The corresponding initial turnover frequencies for these catalysts were calculated to be 1.9 and 0.24 min⁻¹. In terms of turnover rates, PMo/BzPN-SiO₂ is, therefore, 8 times more active than PMo/Hypersil APS-2. This shows that RPN groups in the POM/RPN-SiO₂ catalysts are better tethers for catalytically active POM species on silica than aminopropyl groups of the parent Hypersil APS-2. This can be attributed to the RPN groups that enhance the hydrophobic character of RPN-SiO₂ compared to Hypersil APS-2. With respect to the surface RPN groups, catalytic activity decreases in the order BzPN > iBuPN > iPrPN > PrNH₂ (entries 3, 6, 7 and 1, respectively, Fig. 4.12), in line with decreasing the size of R group. The best catalyst performance with the BzPN group may be attributed to arene-arene π - π interactions between its benzene ring and benzothiophene molecules, which may enhance the

catalytic activity by increasing the local concentration of benzothiophene around the active sites. Another contributing factor may be the basicity of the phosphazene ring, which is affected by the primary amine substituent groups.⁷¹ Increased basicity would strengthen the interaction between the active peroxy-POM species and the RPN surface group to provide more effective immobilisation. This would enable more effective phase transfer of the peroxy-POMs in the reaction mixture as a result.

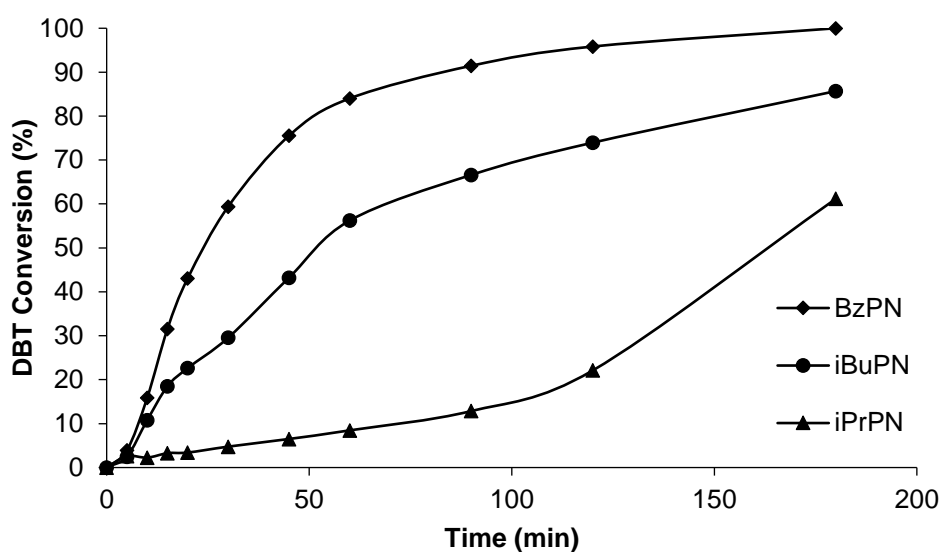


Fig. 4.12. Comparison of activity of PMo catalyst with different RPN-SiO₂ supports for the conversion of DBT to the corresponding sulfone. (PMo/RPN = 1:1 mol/mol) in DBT oxidation by H₂O₂ in heptane-H₂O system (60 °C, PMo (0.0056 mmol), 30% H₂O₂ (0.15 mL, 1.51 mmol), DBT (0.5 mmol), heptane (10 mL)).

The reactivity of benzothiophenes was found to decrease in the order: DBT > DMDBT > BT (Table 4.4, entries 3, 10 and 11). The same trend has been also observed in homogeneous systems (System One, Section 3.5),^{11,63,72-75} and can be attributed to the electron-donating and steric effects of the methyl groups in benzene rings of benzothiophenes.²⁸

As expected, the reaction rate increased with increasing temperature (Fig. 4.13); for the oxidation of DBT with the PMo/BzPN-SiO₂ catalyst, the apparent activation energy was found to be 47 kJ mol⁻¹ in the temperature range 40 – 60 °C (Fig. 4.14).

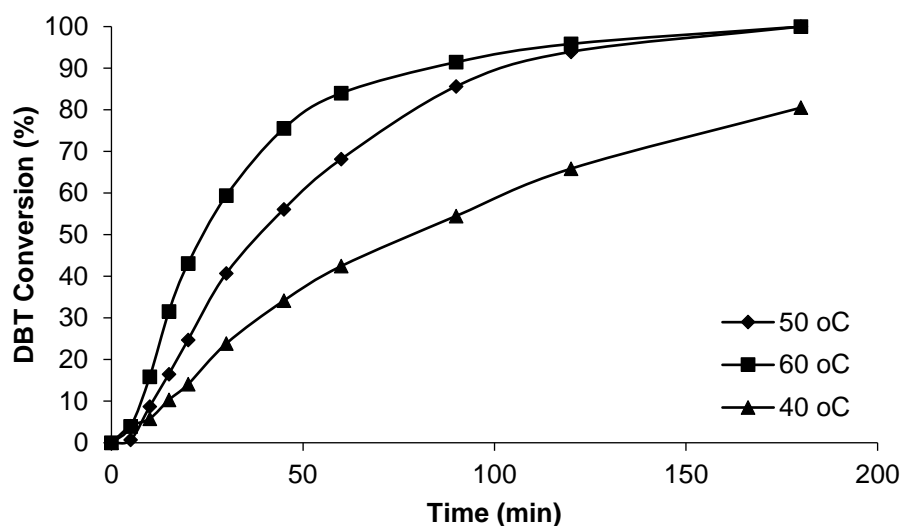


Fig. 4.13. Comparison of activity of PMo/BzPN-SiO₂ at different temperatures (PMo/BzPN = 1:1 mol/mol) in DBT oxidation by H₂O₂ in heptane-H₂O system (PMo (0.0056 mmol), 30% H₂O₂ (0.15 mL, 1.51 mmol), DBT (0.5 mmol), heptane (10 mL)).

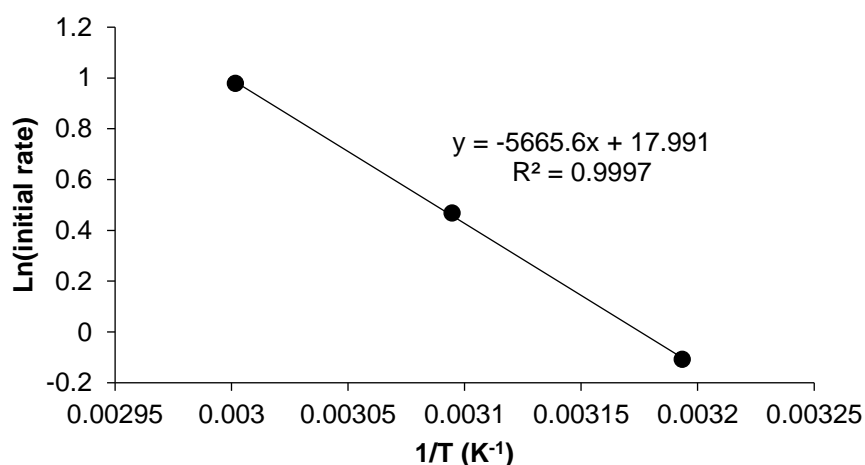


Fig. 4.14. Arrhenius plot of initial rates for DBT oxidation by H₂O₂ catalysed by PMo/BzPN-SiO₂ (PMo/BzPN = 1:1 mol/mol) in heptane-H₂O₂ system (PMo (0.0056 mmol), 30% H₂O₂ (0.15 mL, 1.51 mmol), DBT (0.5 mmol) and heptane (10 mL). $E_a = 47$ kJ mol⁻¹.

Most importantly, the PMo/BzPN-SiO_2 catalyst was found to be more active than its homogeneous analogue, PMo-BzPN (System One). PMo/BzPN-SiO_2 ($\text{PMo/BzPN} = 1:1$) yielded 94% DBT conversion in 2 h at 50 °C, whereas DBT was only converted up to 28 and 49% with PMo/BzPN in a 1:1 ratio and 1:6 ratio, respectively, under the same reaction conditions (Fig. 4.15).⁶³ This may be explained by adsorption of DBT onto the surface of PMo/BzPN-SiO_2 silica support increasing the local concentration of DBT around the active catalyst sites. Interactions between the active surface groups and DBT may be aided by the flexible aminopropyl tethers between silica and BzPN, which increase the mobility of the active peroxy-POM/BzPN units at the silica surface.

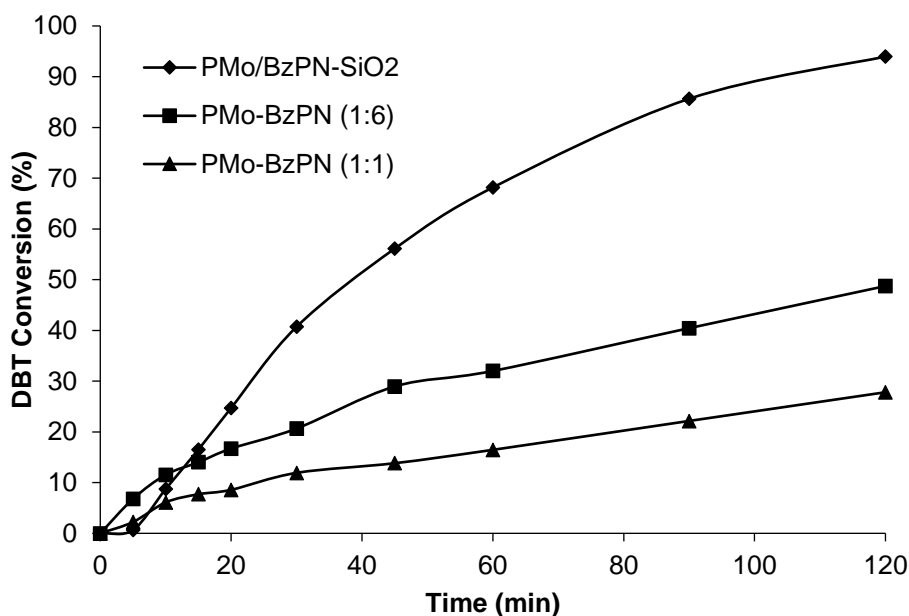


Fig. 4.15. Comparison of heterogeneous PMo/BzPN-SiO_2 ($\text{PMo/BzPN} = 1:1$) and homogeneous PMo-BzPN ($\text{PMo/BzPN} = 1:1$ or $1:6$) catalysts for oxidation of DBT with H_2O_2 (50 °C, PMo (0.0056 mmol), 30% H_2O_2 (0.15 mL, 1.51 mmol), DBT (0.5 mmol) and heptane (10 mL)).

The PMo/BzPN-SiO₂ catalyst is not only more active in the oxidation of benzothiophenes with H₂O₂ than its homogeneous analogue, but it also provides the advantages of heterogeneous catalysts, namely easier and cleaner catalyst separation from fuel by simple filtration. The solid PMo/BzPN-SiO₂ catalyst could be easily recovered and, after washing with acetonitrile to remove the sulfone product, could be reused at least three times in the oxidation of DBT at 60 °C for 6 h per run, giving 100% DBT conversion after each use. These results are shown in Fig. 4.16. It can be seen that the initial rate of DBT conversion has decreased in the first reuse (Run 2), and there was a further decline in the reaction rate in the second reuse (Run 3). This may be due to loss of catalyst by transfer during the catalyst recovery procedure and/or leaching of the active species from the catalyst during the reaction and/or during the recovery procedure. Comparison of the SEMs measured for fresh and spent PMo/BzPN-SiO₂ catalyst (Fig 4.8) shows that fresh PMo/BzPN-SiO₂ had a higher quantity of smaller particles attached onto the surface compared to the spent catalyst. It is possible that the smaller particles were washed out during the oxidative desulfurization reaction, or during the isolation and washing of the catalyst after the reaction. If these particles are immobilised catalytically active species, this could indicate leaching.

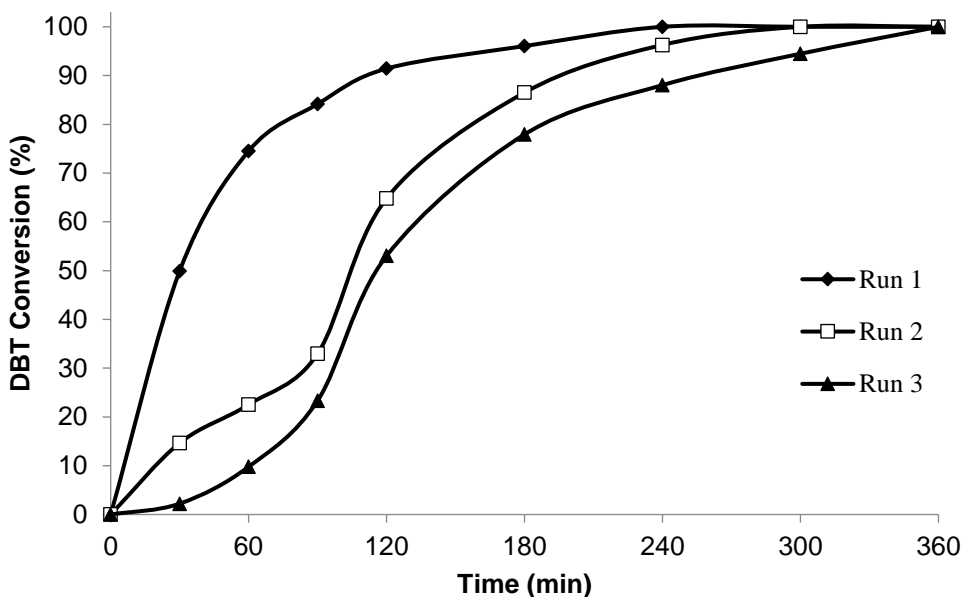
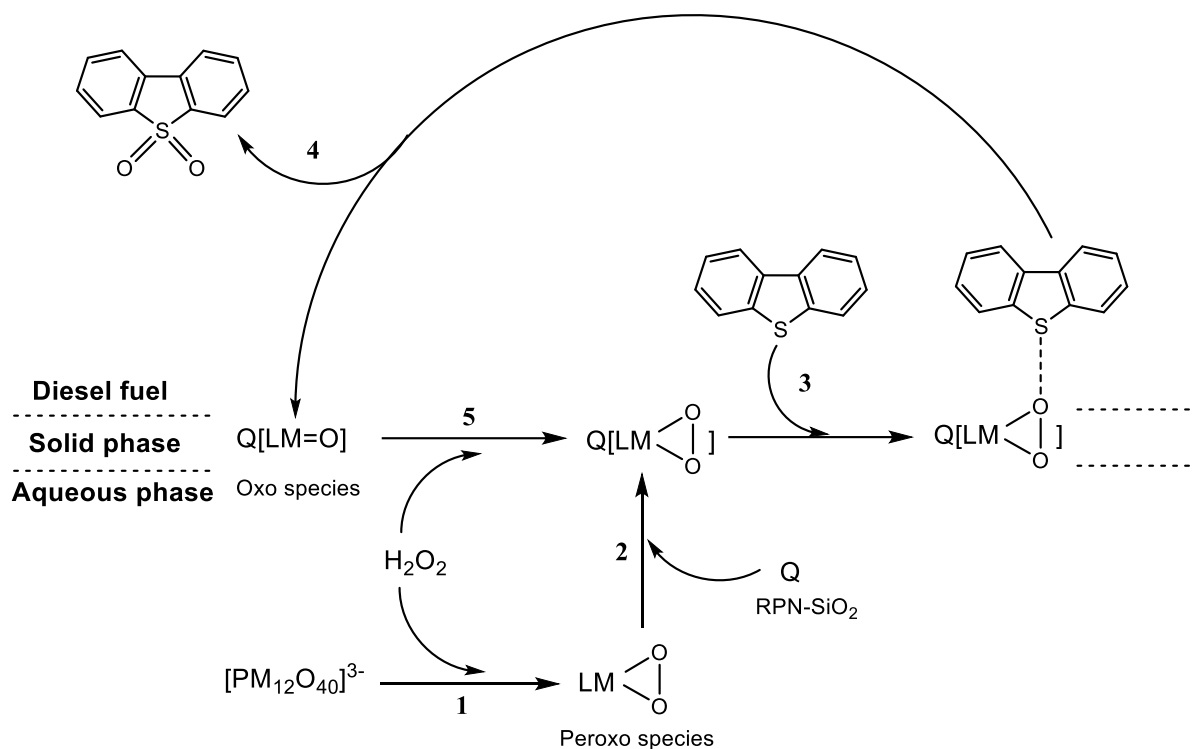


Fig 4.16. Reuse of PMo/BzPN-SiO₂ catalyst for DBT conversion to DBT sulfone by H₂O₂ in heptane/H₂O system. Initial run used (0.0129g, 0.0056 mmol) PMo, (0.0592 g, 0.0056 mmol WRT surface BzPN) Hypersil APS-2 (BzPN), (0.15 ml, 1.51 mmol, 30% w/v) H₂O₂, (0.4 mmol) dodecane, (0.5 mmol) DBT and (10 ml) heptane. Reaction temperature was 60°C and stirring speed was 1500 rpm. Subsequent runs reused catalyst powder produced *in situ* after solvent washings with fresh (0.15 ml, 1.51 mmol, 30% w/v) H₂O₂, (0.4 mmol) dodecane, (0.5 mmol) DBT and (10 ml) heptane.

The PMo/BzPN-SiO₂ catalyst compares well regarding its activity with other heterogeneous catalysts that have been reported recently for the oxidation of DBT with hydrogen peroxide using a 2-5 mol/mol ratio H₂O₂/DBT in model diesel fuel.¹⁶⁻¹⁸ For example, Ti^{iv} grafted onto silica gives 99% DBT conversion to sulfone in isooctane with 10-60% H₂O₂ at 60 °C in 8 h reaction time.¹⁶ With hybrid catalysts comprising Zr and Hf oxoclusters in poly(methylmethacrylate) matrix, 84% DBT conversion to sulfone with 94% selectivity has been obtained in n-octane with 30% H₂O₂ at 65 °C in 24 h.¹⁷ A polyoxometalate-MOF

composite comprising $PW_{11}Zn$ and 2-aminoterephthalic acid in n-octane-[BIMIM]PF₆ biphasic system at 50 °C gives 70% DBT conversion in 4 h and ~100% in 6 h reaction time, though this was obtained using a 50-fold molar excess of 30% H₂O₂ over DBT.¹⁸ In this system, the ionic liquid [BIMIM]PF₆ has been used to extract the product sulfone from the model diesel. In comparison, PMo/BzPN-SiO₂ catalyst gives 100% DBT conversion in heptane with 30% H₂O₂ at 60 °C in 3 h reaction time.

The proposed reaction scheme for oxidation of DBT in model diesel fuel (heptane) by H₂O₂ catalysed by POM/RPN-SiO₂ in this system is shown in Scheme 4.4. In the initial step POM degrades in the presence of H₂O₂ in the aqueous phase to form catalytically active peroxopolyoxometalate species (1).⁶⁹ These species are then heterogenized by interaction with the surface RPN groups of the RPN-SiO₂ support (2) *via* ionic and hydrogen bonding interactions (RPN forms cationic species through protonation of ring nitrogen sites in the presence of strong Brønsted acids).^{63,64,71,76} The active peroxopolyoxometalate species then oxidise DBT in the diesel fuel to DBT sulfone (3). The sulfone, poorly soluble in heptane and insoluble in water, precipitates out (4). The supported POM, now an oxo species, is regenerated by H₂O₂ from the aqueous phase to reform the active peroxo-POM species (5), thus completing the catalytic cycle. In this multiphase system, intense stirring is essential to facilitate the heterogeneously catalysed oxidation process. Sulfur-free diesel fuel could be separated from the catalyst and sulfone product by filtration once the reaction had reached completion. The sulfone can be separated from the catalyst by solvent extraction, and the catalyst can be reused.



Scheme 4.4. Proposed reaction scheme for oxidation of DBT by H_2O_2 catalysed by POM/RPN- SiO_2 in three-phase system.

4.5 Epoxidation of Olefins

As with oxidative desulfurization, Keggin-type polyoxometalates (PMo, PW and SiW) immobilized onto the RPN-functionalized silica support, POM/RPN- SiO_2 , were used as heterogeneous catalysts for epoxidation of cyclooctene by H_2O_2 . The reactions were tested in a biphasic system comprised of n-heptane, toluene or DCE as an organic solvent and aqueous H_2O_2 (10% w/v). In these experiments, the POM/RPN- SiO_2 catalysts were prepared *in situ* by adding POM (as the corresponding heteropoly acid) and RPN- SiO_2 components separately to the reaction mixture to ensure more efficient activation of the POM by hydrogen peroxide prior to reaction (section 2.3.3.2).

The catalytic activity of iBuPN-SiO₂ and PMo was first compared with the activity of unmodified Hypersil APS-2 with PMo to see if functionalisation of the commercially available silica with RPN can enhance catalytic activity in epoxidation of cyclooctene with H₂O₂. The reaction was run in a heptane/H₂O system and the results are illustrated in Fig. 4.17. The reaction with PMo/iBuPN-SiO₂ catalyst shows an improved yield of 24% over 5% given by PMo with unmodified silica with surface aminopropyl groups after 180 min. Functionalisation with RPN improved catalytic activity as was also previously reported for oxidative desulfurization. This is possibly due to more effective intermolecular interactions between the

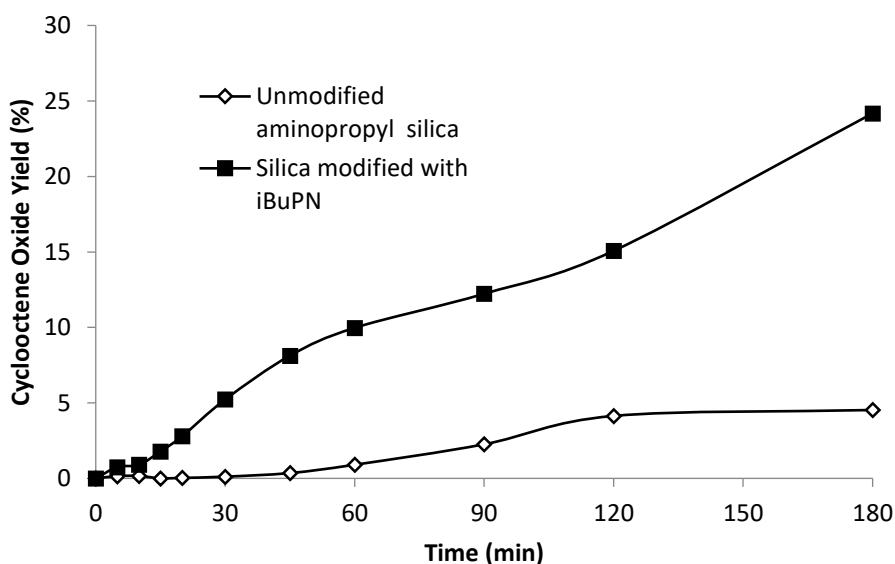


Fig. 4.17. Comparison of catalytic activity of Hypersil APS-2-PMo and PMo/iBuPN-SiO₂ in biphasic epoxidation of cyclooctene by H₂O₂. PMo (0.0062 mmol), unmodified Hypersil APS-2 or iBuPN-SiO₂ (0.0062 mmol with respect to iBuPN), H₂O₂ (1.01 mmol, 10% w/v), decane (2.13 mmol), cyclooctene (9.71 mmol) and heptane (10 mL). Reaction temperature was 60 °C and stirring speed 1500 rpm.

active peroxo POM species and the surface phosphazenes than between peroxo POM and propylamine (i.e. stronger ionic interactions and more available hydrogen bonding groups). More effective interactions would enable more effective immobilisation of the active peroxo species on the catalyst surface which would increase the concentration of active peroxo POM species available to cyclooctene for reaction.

The effect of polyoxometalate on activity was measured using different polyoxometalates and iBuPN-SiO₂ as a support in a heptane/H₂O system (Fig. 4.18.). As previously seen in the desulfurization of dibenzothiophene with POM/RPN-SiO₂ catalysts, and in the epoxidation of olefins using System One (Section 3.3), catalytic activity with respect to the final cyclooctene oxide yield decreases in the order PMo > PW > SiW. However, as shown in Fig. 4.18, the initial rate of reaction increases in the order PW > PMo > SiW which indicates that PW is the most active catalyst in these reactions. After 60 min, the reaction with PW starts to slowly deactivate, whilst the reaction with PMo proceeds at an almost constant rate. Both reactions fully deactivate after 180 minutes. Faster deactivation of the PW catalysed reaction may be due to faster thermal decomposition of H₂O₂ in the presence of PW catalyst species than PMo catalyst species.

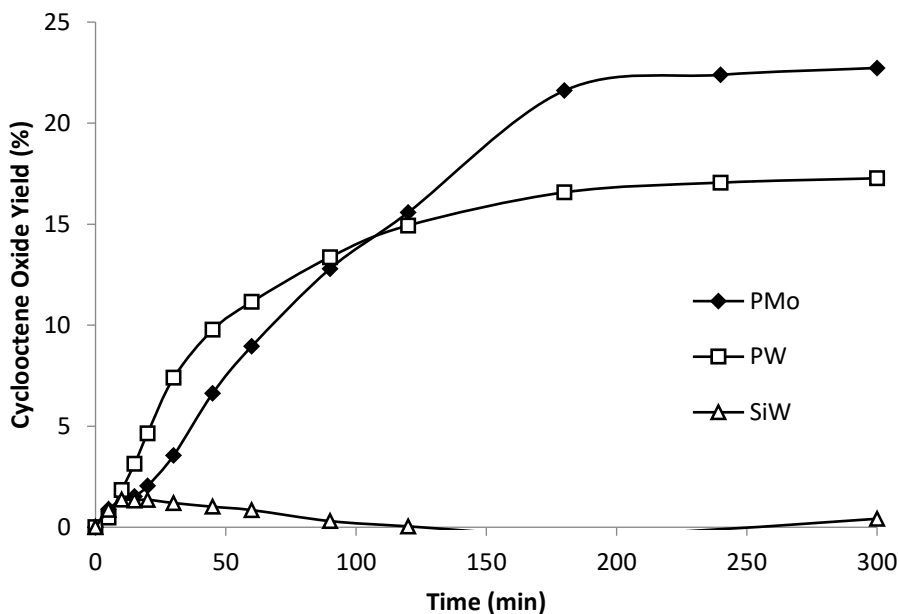


Fig. 4.18. Effect of POM on biphasic epoxidation of cyclooctene with H_2O_2 catalysed by POM/iBuPN-SiO₂. Per run used POM (0.0062 mmol), iBuPN-SiO₂ (0.0062 mmol with respect to iBuPN), H_2O_2 (0.3 mL, 1.01 mmol, 10% w/v), decane (2.13 mmol), cyclooctene (9.71 mmol) and heptane (10 mL). Reaction temperature was 60°C and stirring speed 1500 rpm.

The reaction conditions were further optimised by running the reaction in systems using different solvents and different RPN-SiO₂ supports. These results are summarised in Table 4.5. The activity in different solvents decreases in the order of DCE > toluene > heptane regardless of which RPN-SiO₂ is used. This is likely the result of general solvent effects (e.g. solubility and solvent binding) imposing on interactions between cyclooctene and the active catalyst groups. Any improvements in activity with the change in R group will likely be a reduction of these effects provided by the group. However, evidence of leaching (see below) suggests that the activity in different solvents may result from changes in solubility of the leached active catalyst species provided by the RPN R group. In DCE and in heptane, the activity decreases in the order Bz > iBu > iPr (entries 3, 6 and 9, and entries 1, 4 and 7, respectively) in line with

increasing size of R group. The observed order could be attributed to increasing solubility of the R group.

Table 4.5. Comparison of RPNs and effect of solvent on biphasic epoxidation of cyclooctene by H₂O₂.^a

Entry	RPN-SiO ₂	Solvent	Cyclooctene	H ₂ O ₂
			Oxide Yield (%)	Selectivity (%)
1	iBu	Heptane	23	23
2	iBu	Toluene	67	67
3	iBu	DCE	73	73
4	Bz	Heptane	25	25
5	Bz	Toluene	48	48
6	Bz	DCE	76	76
7	iPr	Heptane	19	19
8	iPr	Toluene	55	55
9	iPr	DCE	70	70

^aPMo (0.0062 mmol), RPN-SiO₂ (0.0062 mmol with respect to surface RPN), H₂O₂ (1.01 mmol, 10% w/v), decane (2.13 mmol), cyclooctene (9.71 mmol) and solvent (10 mL). Reaction time 5 h, temperature 60°C and stirring speed 1500 rpm.

In toluene, activity decreases in the order of iBu > iPr > Bz (entries 2, 5 and 8, respectively) which shows greater activity for the aliphatic R groups over the aromatic R group. None of the reactions gave 100% epoxycyclooctane yield and titrations showed > 97% H₂O₂ had been used up in most reactions (selectivity in line with yield), indicating thermal decomposition of H₂O₂.

Catalyst reuse was tested using the best system, PMo/BzPN-SiO₂ with DCE organic solvent at 60 °C and 1500 rpm stirring speed, and each run was stopped after 5 hours. The results are shown in Fig. 4.19.

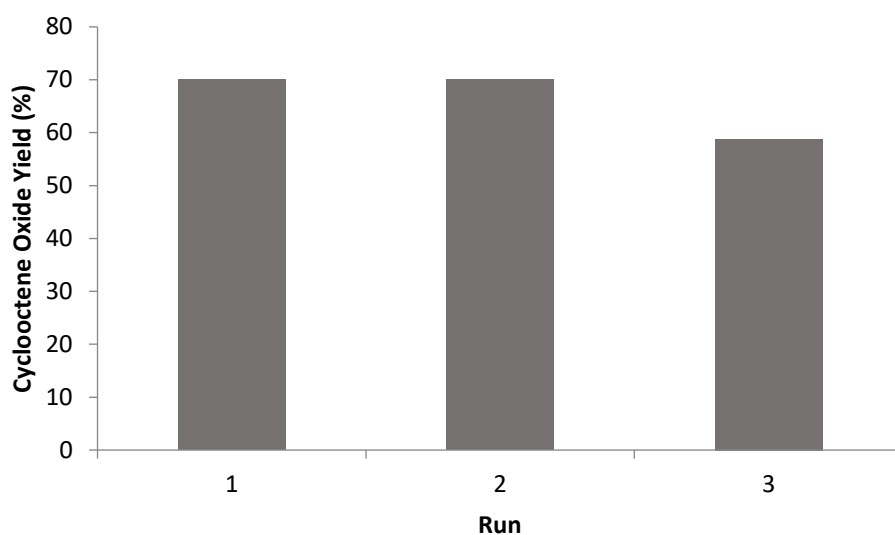


Fig. 4.19. Reuse of PMo/BzPN-SiO₂ catalyst for biphasic epoxidation of cyclooctene by H₂O₂ in DCE/H₂O system. Initial run used PMo (0.0062 mmol), BzPN-SiO₂ (0.0062 mmol with respect to BzPN), H₂O₂ (0.3 mL, 1.01 mmol, 10% w/v), decane (2.13 mmol), cyclooctene (9.71 mmol) and DCE (10 mL). Reaction temperature was 60°C and stirring speed 1500 rpm. Subsequent runs reused catalyst powder produced *in situ* (after solvent washings) with fresh H₂O₂ (0.3 mL, 1.01 mmol, 10% w/v), decane (2.13 mmol), cyclooctene (0.971 mmol) and DCE (10 mL). Reaction time was 300 min per run.

The catalyst could be isolated and reused twice without any notable loss in catalytic activity, giving a 70% yield cyclooctene oxide for the first two runs. After three runs, the yield had dropped to 59%, indicating a loss in catalytic activity. This could be the result of catalyst leaching or loss of catalyst through transfer after each use.

To test if catalyst leaching had occurred, the ^{31}P NMR spectrum of the organic layer was measured after each run. The volume was greatly reduced by evaporation at room temperature to increase the concentration of any leached catalyst. The spectra showed no signals for PMo, peroxy PMo species or BzPN, indicating that leaching may not be the cause of catalyst deactivation.

As a further test to see if leaching in this solvent system was possible, BzPN-SiO₂, PMo and H₂O₂ was stirred under reaction conditions in DCE/H₂O. The DCE layer was isolated and analysed by UV/Vis (Fig. 4.20). A peak at 248 nm is comparable to one that was observed at 247 nm by Rana Yahya in the UV-vis spectrum of a BzPN-PMo (6 :1) DCE/H₂O mixture with H₂O₂ (Fig. 4.21).⁷⁷ This peak was believed to be caused by a PMo species, which indicates that there is a strong possibility of leaching of BzPN-PMo from PMo/BzPN-SiO₂ in a DCE/H₂O solvent system.

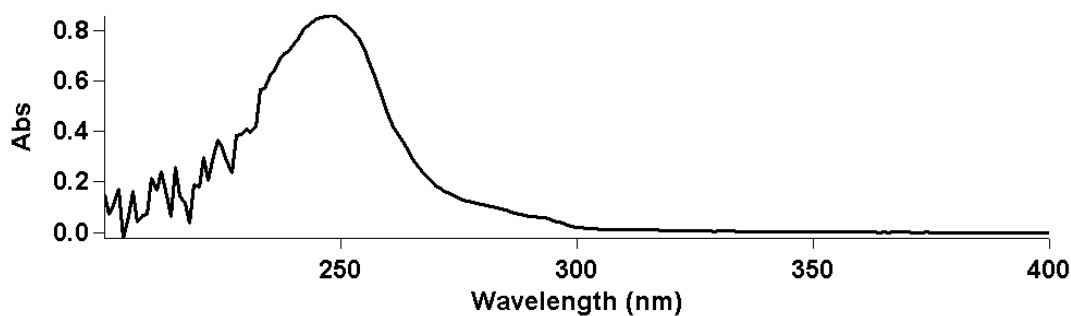


Fig. 4.20. UV-Vis spectrum of DCE layer after stirring BzPN-SiO₂, PMo and H₂O₂ in DCE-H₂O system to check for catalyst leaching. PMo (0.0062 mmol), BzPN-SiO₂ (0.0062 mmol with respect to BzPN), H₂O₂ (1.01 mmol) and DCE (10 mL). Reaction temperature 60°C and stirring speed 1500 rpm. Concentration of DCE sample after reaction diluted to 1/10 for analysis.

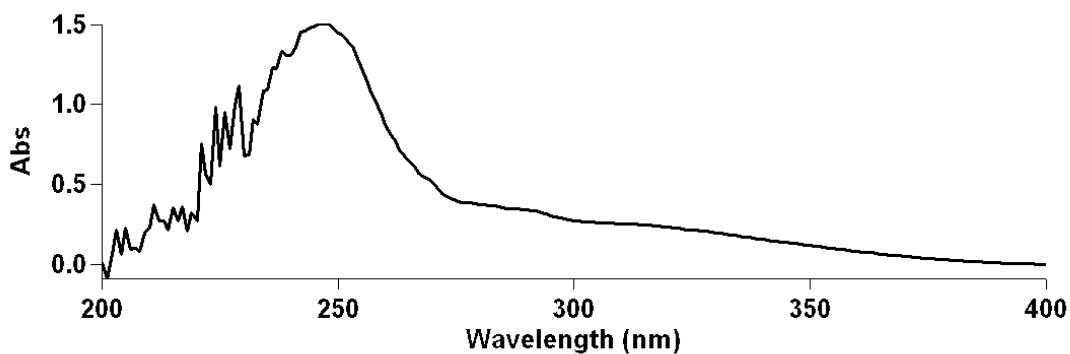


Fig. 4.21. UV-Vis spectrum of DCE layer after shaking PMo-BzPN (1:6)/DCE-H₂O₂-H₂O system {PMo (0.0065 mmol), BzPN (0.0039 mmol), H₂O₂ (1.01 mmol), DCE (10 mL), H₂O (0.3 mL)}. The band is peaked at 247nm.⁷⁷

The catalytic activity of the best POM/RPN-SiO₂, PMo/BzPN-SiO₂, was compared with its homogeneous counterpart, BzPN-PMo, using conditions from System One (Fig. 4.21). Equimolar amounts of PMo were used in reactions with both phase-transfer moieties. BzPN-PMo was much more catalytically active than PMo/BzPN-SiO₂, giving > 99% yield compared to 40 % yield after 120 min, respectively. This could be due to the homogeneity of BzPN-PMo improving the availability of the active peroxy POM species to the target olefin. The reaction with BzPN-PMo appears to occur instantaneously and at a fast rate, whereas there is a clear 30 min induction period with PMo/BzPN-SiO₂. However, it must be noted that a 6-fold excess [BzPN]/[PMo] was used for BzPN-PMo due to BzPNs inability to effectively solubilise active POM species for catalysis at low concentrations as shown in Section 3.3, Figs 3.16 and 3.17.

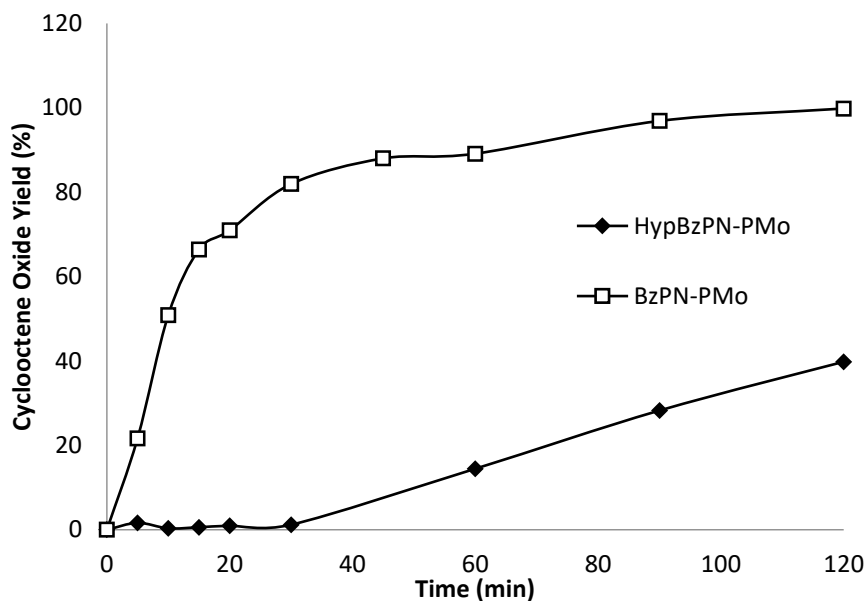


Fig. 4.22. Comparison of biphasic epoxidation of cyclooctene by H_2O_2 using PMo/BzPN-SiO₂ or BzPN-PMo as a catalyst. Per run used PMo (0.0086 mmol), BzPN-SiO₂ (0.0086 mmol with respect to BzPN) or BzPN (0.0515 mmol), H_2O_2 (0.3 mL, 1.01 mmol, 10% w/v), decane (2.13 mmol), cyclooctene (9.71 mmol and toluene (10 mL). Used 1: 1 PMo: BzPN-SiO₂ and 1:6 PMo: BzPN.

The PMo/BzPN-SiO₂ in DCE/H₂O system compares modestly to those reported for other catalysts in the literature which use functionalized silica materials as POM supports. MCM-41 silica supports modified with quaternary ammonium functionalities were used to immobilize PW with electrostatic interactions. This system used 3.15: 3.78 [cyclooctene]/[H₂O₂] mol/mol with 35 % (w/w) H₂O₂ at 50 °C in CH₃CN/H₂O system and gave 20% cyclooctene conversion with 95% epoxide selectivity after 16 h.⁷⁸ PW immobilized on dihydroimidazolium-based ionic liquid-modified SiO₂ was used at 1 mol% with respect to [cyclooctene] in CH₃CN/H₂O system with 30% (w/w) H₂O₂ as oxidant and 5:1 [cyclooctene]/[H₂O₂] mol/mol at 60 °C.⁷⁹ The reaction gave >99% epoxide yield with >95% selectivity after 1 h.

The reaction scheme for the system is likely the same as shown in Scheme 4.4, only steps 3 and 4 - where the active peroxy species on the surface of the catalyst react with the target olefin - are slow, resulting in long reaction times. The mechanism for the leached species is probably similar to the Venturello-Ishii mechanism shown in Scheme 1.7.

4.6 Conclusions

In this study, phosphazene-modified silica supports, RPN-SiO₂ (R= benzyl, *iso*-butyl or *iso*-propyl), were prepared by grafting phosphazenes (RPN) onto the commercial Hypersil APS-2 aminopropyl-modified silica. Keggin-type polyoxometalates (PMo, PW and SiW) have been immobilized on RPN-SiO₂ supports using the corresponding heteropoly acids as precursors to afford the POM/RPN-SiO₂ catalysts. Both the supports and the best catalyst, PMo/RPN-SiO₂, have been characterized by elemental analysis, BET, SEM, multinuclear MAS NMR and FTIR. The heterogenized POM catalysts have been tested for oxidative desulfurization of a model diesel fuel and epoxidation of cyclooctene in biphasic systems with hydrogen peroxide as the oxidant.

Oxidative desulfurization was tested using a benzothiophene in n-heptane as a model fuel. The catalytic activity has been found to decrease with respect to the RPN alkylamino group in the order benzyl > *iso*-butyl > *iso*-propyl and increase with respect to POM in the order PMo > PW > SiW, which is in line with the size of the R group and the stability of the POMs to degradation in aqueous solution, respectively. The most effective catalyst, PMo/BzPN-SiO₂, gave 100% DBT conversion after 3 h at 60 °C with 68% H₂O₂ efficiency and was found to outperform other recently reported heterogeneous catalysts for similar systems. The catalyst could be reused at least three times, giving 100% DBT conversion in 6 h after each use; however, there was a notable loss in the rate of reaction between runs, which may have been caused by leaching

of the catalytically active species and/or loss of catalyst by transfer between vessels, either during the reaction or during the catalyst recovery procedure. Comparison of PMo/BzPN-SiO₂ with its homogenous analogue, BzPN-PMo, found PMo/BzPN-SiO₂ to be more catalytically active; PMo/BzPN-SiO₂ (PMo/BzPN = 1:1) yielded 94% DBT conversion in 2 h at 50 °C, whereas DBT was only converted up to 28 and 49 % with PMo/BzPN in a 1:1 ratio and 1:6 ratio, respectively, under the same reaction conditions. The PMo/BzPN-SiO₂ could be more easily separated from the reaction mixture than BzPN-PMo after the reaction, although, if the active species of PMo/BzPN-SiO₂ had leached during the reaction and remained solubilized in the fuel layer then this would still need to be removed.

Epoxidation of cyclooctene was tested in biphasic systems using n-heptane, toluene or DCE as an organic solvent and aqueous 10% w/v H₂O₂ as an oxidant. Catalytic activity in terms of final epoxide yield increases with respect to POM in the order PMo > PW > SiW in line with the stability of the POMs to degradation in aqueous solution. Reactions with PW appeared to be the most active in terms of initial reaction rates, but deactivated faster than reactions catalysed by PMo, possibly due to faster thermal degradation of H₂O₂ in the presence of catalytically active PW species. With respect to organic solvent, catalytic activity decreases in the order of DCE > toluene > heptane. UV-vis analysis of the organic layer after stirring the catalyst under reaction conditions in DCE/H₂O system gives a strong peak at λ_{max} 248 nm, which can be assigned to PMo species. This, along with the gradual loss of catalytic activity seen in reuse experiments, provides strong evidence of catalyst leeching. Changes in catalytic activity with respect to the organic solvent may result from changes in solubility of the leached active catalyst species provided by the RPN R group. In the best biphasic system, DCE/H₂O, the activity of RPNs is of the order Bz > iBu > iPr in line with increasing size of R group, though the activity of RPN was found to vary in the other solvents. Again, this could result from improved solubility of leached catalyst species in different solvents provided by the R group.

The best catalyst system, PMo/BzPN-SiO₂ in DCE/H₂O, gave 76% yield after 5 h at 60 °C with 76 % H₂O₂ efficiency, meaning the epoxidation reaction was competing with thermal decomposition of H₂O₂. The system shows modest catalytic activity when compared to similar types of catalysts in slightly different systems.

References

- 1 M. Bowker, *The Basis and Applications of Heterogeneous Catalysis*, Oxford University Press, Oxford, 1998.
- 2 Y. Zhou, G. Chen, Z. Long and J. Wang, *RSC Adv.*, 2014, **4**, 42092–42113.
- 3 O. Trapp and J. Troendlin, in *Molecular Catalysts*, Wiley-VCH Verlag GmbH & Co. KGaA, 2014, pp. 393–406.
- 4 X. S. Zhao, X. Y. Bao, W. Guo and F. Y. Lee, *Mater. Today*, 2006, **9**, 32–39.
- 5 S. P. Hernandez, D. Fino and N. Russo, *Chem. Eng. Sci.*, 2010, **65**, 603–609.
- 6 W. Lei, W. Wenya, N. Mominou, L. Liu and S. Li, *Appl. Catal. B Environ.*, 2016, **193**, 180–188.
- 7 D. Wang, N. Liu, J. Zhang, X. Zhao, W. Zhang and M. Zhang, *J. Mol. Catal. A Chem.*, 2014, **393**, 47–55.
- 8 M. Zhang, W. Zhu, H. Li, M. Li, S. Yin, Y. Li, Y. Wei and H. Li, *Colloids Surfaces A Physicochem. Eng. Asp.*, 2016, **504**, 174–181.
- 9 J. Zhang, A. Wang, Y. Wang, H. Wang and J. Gui, *Chem. Eng. J.*, 2014, **245**, 65–70.
- 10 M. Vazylyev, D. Sloboda-Rozner, A. Haimov, G. Maayan and R. Neumann, *Top. Catal.*, 2005, **34**, 93–99.
- 11 Z. Jiang, H. Lü, Y. Zhang and C. Li, *Chinese J. Catal.*, 2011, **32**, 707–715.
- 12 R. Noyori, M. Aoki and K. Sato, *Chem. Commun.*, 2003, 1977–1986.
- 13 W. R. Sanderson, *Pure Appl. Chem.*, 2000, **72**, 1289–1304.
- 14 J. L. Garcia-Gutierrez, G. A. Fuentes, M. E. Hernandez-Teran, P. Garcia, F. Murrieta-

- Guevara and F. Jimenez-Cruz, *Appl. Catal. A Gen.*, 2008, **334**, 366–373.
- 15 D. Zhao, J. Zhang, J. Wang, W. Liang and H. Li, *Pet. Sci. Technol.*, 2009, **27**, 1–11.
- 16 J. M. Fraile, C. Gil, J. A. Mayoral, B. Muel, L. Roldán, E. Vispe, S. Calderón and F. Puente, *Appl. Catal. B Environ.*, 2016, **180**, 680–686.
- 17 M. Vigolo, S. Borsacchi, A. Soraru, M. Geppi, B. M. Smarsly, P. Dolcet, S. Rizzato, M. Carraro and S. Gross, *Appl. Catal. B Environ.*, 2016, **182**, 636–644.
- 18 D. Julião, A. C. Gomes, M. Pillinger, R. Valença, J. C. Ribeiro, B. de Castro, I. S. Gonçalves, L. Cunha Silva and S. S. Balula, *Eur. J. Inorg. Chem.*, 2016, **2016**, 5114–5122.
- 19 A. Goti and F. Cardona, *Hydrogen Peroxide in Green Oxidation Reactions: Recent Catalytic Processes*, 2013, vol. 53.
- 20 M. G. Clerici and P. Ingallina, *J. Catal.*, 1993, **140**, 71–83.
- 21 T. Maschmeyer, F. Rey, G. Sankar and J. M. Thomas, *Nature*, 1995, 378, 159–162.
- 22 T. S. Reger and K. D. Janda, *J. Am. Chem. Soc.*, 2000, **122**, 6929–6934.
- 23 R. Saladino, V. Neri, A. R. Pelliccia, R. Caminiti and C. Sadun, *J. Org. Chem.*, 2002, **67**, 1323–1332.
- 24 A. O. Bouh and J. H. Espenson, *J. Mol. Catal. A Chem.*, 2003, **200**, 43–47.
- 25 C. Venturello, J. C. J. Bart and M. Ricci, *J. Mol. Catal.*, 1985, **32**, 107–110.
- 26 C. Venturello, E. Alneri and M. Ricci, *J. Org. Chem.*, 1983, **48**, 3831–3833.
- 27 J.-M. Brégeault, M. Vennat, J.-Y. Piquemal, Y. Mahha, E. Briot, P. C. Bakala, A. Atlamsani and R. Thouvenot, *J. Mol. Catal. A Chem.*, 2006, **250**, 177–189.

- 28 Y. Zhou, G. Chen, Z. Long and J. Wang, *RSC Adv.*, 2014, **4**, 42092–42113.
- 29 K. Yamaguchi, C. Yoshida, S. Uchida and N. Mizuno, *J. Am. Chem. Soc.*, 2005, **127**, 530–531.
- 30 Y. Chen and Y. Song, *Chempluschem*, 2014, **79**, 304–309.
- 31 N. V. Maksimchuk, M. N. Timofeeva, M. S. Melgunov, A. N. Shmakov, Y. A. Chesalov, D. N. Dybtsev, V. P. Fedin and O. A. Kholdeeva, *J. Catal.*, 2008, **257**, 315–323.
- 32 C. M. Granadeiro, A. D. S. Barbosa, P. Silva, F. A. A. Paz, V. K. Saini, J. Pires, B. De Castro, S. S. Balula and L. Cunha-Silva, *Appl. Catal. A Gen.*, 2013, **453**, 316–326.
- 33 S. S. Balula, C. M. Granadeiro, A. D. S. Barbosa, I. C. M. S. Santos and L. Cunha-Silva, *Catal. Today*, 2013, **210**, 142–148.
- 34 S. Ribeiro, C. M. Granadeiro, P. Silva, F. A. Almeida Paz, F. F. de Biani, L. Cunha-Silva and S. S. Balula, *Catal. Sci. Technol.*, 2013, **3**, 2404–2414.
- 35 Y. Liu, S. Liu, S. Liu, D. Liang, S. Li, Q. Tang, X. Wang, J. Miao, Z. Shi and Z. Zheng, *ChemCatChem*, 2013, **5**, 3086–3091.
- 36 Y. Leng, W. Zhang, J. Wang and P. Jiang, *Appl. Catal. A Gen.*, 2012, **445–446**, 306–311.
- 37 Y. Leng, J. Wu, P. Jiang and J. Wang, *Catal. Sci. Technol.*, 2014, **4**, 1293–1300.
- 38 S. P. Maradur, C. Jo, D. H. Choi, K. Kim and R. Ryoo, *ChemCatChem*, 2011, **3**, 1435–1438.
- 39 S. Doherty, J. G. Knight, J. R. Ellison, D. Weekes, R. W. Harrington, C. Hardacre and H. Manyar, *Green Chem.*, 2012, **14**, 925–929.

- 40 M. Carraro, G. Fiorani, L. Mognon, F. Caneva, M. Gardan, C. MacCato and M. Bonchio, *Chem. - A Eur. J.*, 2012, **18**, 13195–13202.
- 41 G. S. Armatas, G. Bilis and M. Louloudi, *J. Mater. Chem.*, 2011, **21**, 2997–3005.
- 42 E. Skliri, I. N. Lykakis and G. S. Armatas, *RSC Adv.*, 2014, **4**, 8402–8409.
- 43 A. Nisar, Y. Lu, J. Zhuang and X. Wang, *Angew. Chemie - Int. Ed.*, 2011, **50**, 3187–3192.
- 44 Y. Leng, J. Zhao, P. Jiang and J. Wang, *ACS Appl. Mater. Interfaces*, 2014, **6**, 5947–5954.
- 45 G. S. Caravajal, D. E. Leyden, G. R. Quinting and G. E. Maciel, *Anal. Chem.*, 1988, **60**, 1776–1786.
- 46 H. R. Allcock, *Phosphorus-Nitrogen Compounds*, Academic Press, Inc., London, 1972.
- 47 J. F. Bickley, R. Bonar-Law, G. T. Lawson, P. I. Richards, F. Rivals, A. Steiner and S. Zacchini, *Dalt. Trans.*, 2003, 1235–1244.
- 48 J. Ledger, R. Boomishankar and A. Steiner, *Inorg. Chem.*, 2010, **49**, 3896–904.
- 49 D. G. Gabler and J. F. Haw, *Inorg. Chem.*, 1990, **29**, 4018–4021.
- 50 A. Boscolo Boscoletto, M. Gleria, R. Milani, L. Meda and R. Bertani, *Surf. Interface Anal.*, 2009, **41**, 27–33.
- 51 R. Milani, A. Sassi, A. Venzo, R. Bertani, L. Fambri and M. Gleria, *Des. Monomers Polym.*, 2007, **10**, 555–573.
- 52 R. Milani, M. Gleria, A. Sassi, R. De Jaeger, A. Mazzah, L. Gengembre, M. Frere and C. Jama, *Chem. Mater.*, 2007, **19**, 4975–4981.

- 53 P. K. Khatri, B. Singh, S. L. Jain, B. Sain and A. K. Sinha, *Chem. Commun.*, 2011, **47**, 1610–1612.
- 54 A. Sassi, R. Milani, A. Venzo and M. Gleria, *Des. Monomers Polym.*, 2006, **9**, 627–647.
- 55 S. De Monredon-Senani, C. Bonhomme, F. Ribot and F. Babonneau, *J. Sol-Gel Sci. Technol.*, 2009, **50**, 152–157.
- 56 A. Piers and C. H. Rochester, *J. Chem. Soc.*, 1995, **1**, 359–365.
- 57 C. H. Rochester and G. H. Yong, *J. Chem. Soc., Faraday Trans. 1*, 1980, **76**, 1158–1165.
- 58 A. Piers and C. H. Rochester, *J. Colloid Interface Sci.*, 1995, **174**, 97–103.
- 59 M. Kruk and M. Jaroniec, *Chem. Mater.*, 2001, **13**, 3169–3183.
- 60 K. S. W. Sing, D. H. Everett, R. a. W. Haul, L. Moscou, R. a. Pierotti, J. Rouquérol and T. Siemieniewska, *Pure Appl. Chem.*, 1985, **57**, 603–619.
- 61 S. S. Lim, G. I. Park, I. K. Song and W. Y. Lee, *J. Mol. Catal. A Chem.*, 2002, **182**, 175–183.
- 62 Y. Kim and W. Lee, *J. Korean Magn. Reson. Soc.*, 1997, **1**, 45–58.
- 63 M. Craven, R. Yahya, E. F. Kozhevnikova, C. M. Robertson, A. Steiner and I. V. Kozhevnikov, *ChemCatChem*, 2015, **8**, 200–208.
- 64 M. Craven, R. Yahya, E. F. Kozhevnikova, R. Boomishankar, C. M. Robertson, A. Steiner and I. V. Kozhevnikov, *Chem. Commun.*, 2013, **49**, 349–351.
- 65 M. Craven, R. Yahya, E. F. Kozhevnikova, C. M. Robertson, A. Steiner and I. V. Kozhevnikov, *ChemCatChem*, 2016, **8**, 200–208.

- 66 R. Yahya, M. Craven, E. F. Kozhevnikova, A. Steiner, P. Samunual, I. V. Kozhevnikov and D. E. Bergbreiter, *Catal. Sci. Technol.*, 2015, **5**, 818–821.
- 67 J. M. Fraile, C. Gil, J. A. Mayoral, B. Muel, L. Roldán, E. Vispe, S. Calderón and F. Puente, *Appl. Catal. B Environ.*, 2016, **180**, 680–686.
- 68 M. Vigolo, S. Borsacchi, A. Soraru, M. Geppi, B. M. Smarsly, P. Dolcet, S. Rizzato, M. Carraro and S. Gross, *Appl. Catal. B Environ.*, 2016, **182**, 636–644.
- 69 I. V. Kozhevnikov, *Catalysts for Fine Chemical Synthesis: Catalysis by Polyoxometalates*, Wiley, West Sussex, 2002.
- 70 I. V. Kozhevnikov, *Chem. Rev.*, 1998, **98**, 171–198.
- 71 D. Feakins, *J. Chem. Soc.*, 1964, 4464–4471.
- 72 F. M. Collins, A. R. Lucy and C. Sharp, *J. Mol. Catal. A Chem.*, 1997, **117**, 397–403.
- 73 X. Jiang, H. Li, W. Zhu, L. He, H. Shu and J. Lu, *Fuel*, 2009, **88**, 431–436.
- 74 A. W. Bhutto, R. Abro, S. Gao, T. Abbas, X. Chen and G. Yu, *J. Taiwan Inst. Chem. Eng.*, 2016, **62**, 84–97.
- 75 J. Zhang, A. Wang, X. Li and X. Ma, *J. Catal.*, 2011, **279**, 269–275.
- 76 H. R. Allcock, *Chem. Rev.*, 1972, **72**, 315–356.
- 77 R. Yahya, University of Liverpool, 2015.
- 78 D. Hoegaerts, B. F. Sels, D. E. De Vos, F. Verpoort and P. A. Jacobs, *Catal. Today*, 2000, **60**, 209–218.
- 79 K. Yamaguchi, C. Yoshida, S. Uchida and N. Mizuno, *J. Am. Chem. Soc.*, 2005, **127**, 530–531.

5. System Three: Epoxidation of Olefin with H₂O₂ Catalysed by Eutectic RPN-POMs

5.1 Introduction

In Chapter 3, phosphazene-polyoxometalate aggregates (RPN-POMs) comprising Keggin type polyanions (POMs), $[XM_{12}O_{40}]^{m-}$ {X = P^V ($m = 3$) and Si^{IV} ($m = 4$)}, and lipophilic aminocyclotriphosphazene cations $[(RNH)_6P_3N_3H_n]^{n+}$ ($n = 1$ or 2) are shown to be catalysts for biphasic epoxidation of alkenes with H₂O₂ (System One). Although the aggregates provided good yields and selectivities in these reactions, separation of the catalyst from the products once the reaction had reached completion was difficult due to the catalyst remaining solubilised in the organic, product-containing layer. The reaction also required the use of volatile organic solvents such as toluene which are considered harmful and toxic to the environment. In Chapter 4, POM was immobilized onto a solid silica support (Hypersil APS-2) through functionalization of the silica surface with RPN and subsequent interaction between the surface RPN and POM. These catalysts, POM/RPN-SiO₂, successfully catalysed the oxidative desulfurization of a model fuel and the epoxidation of cyclooctene with H₂O₂ (System Two). However, epoxide yields in the latter reaction were much lower with the heterogeneous POM/RPN-SiO₂ catalysts than they were with their homogeneous RPN-POM analogues, and still required the use of volatile organic solvents.

Avoiding the use of volatile organic solvents in a reaction system is important as this drives down costs, reduces the number of toxic and/or hazardous components in a reaction mixture, can simplify product purification as solvent separation is not required post-synthesis, and

reaction rates are often increased due to a higher concentration of the reactants.¹⁻³ In the last 30 years there has been much interest in the use of ionic liquids (ILs) - molten salts that exist in the liquid state at temperatures below 100 °C⁴ - as reaction media in place of volatile organic solvents⁵⁻¹¹ due to their reported non-flammability, recyclability and low toxicology.¹²⁻¹⁵ Their use in catalytic reactions is a topic that has been the subject of many reviews,¹⁶⁻¹⁸ with many ILs also operating as catalysts through appropriation of one of the constituent ions (often organometallic cations).^{4,19-22}

For an ionic liquid to replace a solvent in a reaction system, it must be a liquid at the operational temperature of the reaction that is to be mediated. Many ILs are liquids under ambient conditions (Room Temperature Ionic Liquids- RTILs).²³⁻²⁵ The methods for the suppression of IL melting points have been well researched.²⁶⁻²⁸ One particularly successful approach is to use mixtures of ionic liquids or their constituent ions to influence the melting points, as well as other properties of ionic liquids.^{24,29,30} Hydrogen-bond donor molecules can be added to tailor the properties of ILs also.³¹ The eutectics formed by mixing ILs and also by the addition of hydrogen-bond donors typically have melting points that are lower than either of the individual components and are termed *deep eutectic ionic liquids* or *Deep Eutectic Solvents* (DESs).³¹⁻³³ Like their conventional ionic liquid analogues, DESs have found application as solvents in catalysis³⁴ and synthesis,³⁵ as they often have low-cost components, low volatility, high thermal stability, are bio renewable, biodegradable, non-toxic, and can even be water compatible.^{32,34-36} Their physiochemical properties are also highly tuneable.³²

In recent years, there has been a growing interest in the use of POM-based ILs in oxidation reactions with H₂O₂ to develop reaction-induced phase separation of catalysts for better catalyst-product separation or to forgo the use of volatile organic solvents in the reaction altogether by purposing the POM-ILs as catalysts and a reaction medium. A temperature-responsive poly(N-isopopylacrylamide) functionalised with a Disperse Red moiety, quaternary

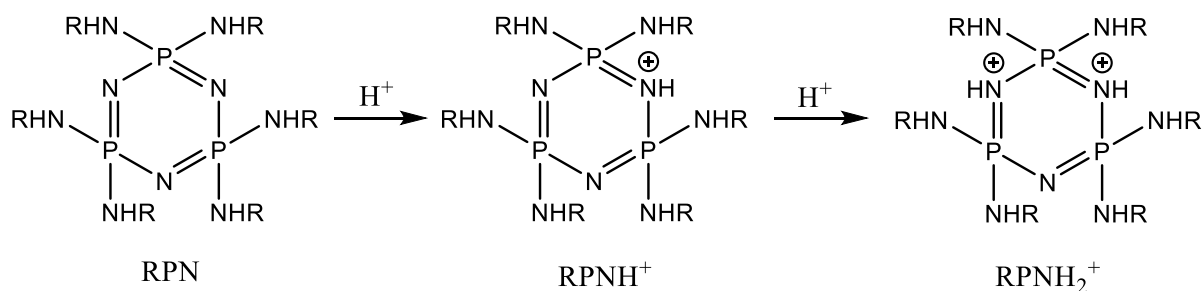
ammonium unit and PW has been reported as a catalyst for the oxidation of alcohols with H₂O₂.³⁷ The catalyst formed a thermo-regulated, stable emulsion species at 90 °C in water which raised the catalytic activity and improved catalyst separation. A series of thermo-regulated self-precipitating POM-based RTILs with PEG chain-functionalized N-dodecylimidazolium cations have been used as catalysts for epoxidation with H₂O₂.^{38,39} The catalyst solubility in each case increased as the temperature was increased during the reaction and could self-separate at room temperature once the reaction had reached completion. N-Methylimidazolium peroxotungstate [HMIm]₂[W₂O₁₁], an RTIL, could act as a reaction-induced phase separation catalyst for the epoxidation of alkenes with H₂O₂.⁴⁰ The reaction system was found to switch from a tri-phase to an emulsion and then to a biphasic during the reaction, and, finally, to complete self-precipitation of the catalyst at the end of the reaction, making catalyst recovery and reuse very convenient. Interestingly, the catalyst could also be used in the absence of an organic solvent, though it was found that the epoxide yield dropped from 100 to 66 % when a suitable organic solvent was not used.

To improve separation and to avoid using volatile organic solvents in the reaction systems used in this study (thus, making the reaction “greener”), it was our aim to suppress the melting points of RPN-POM’s for use as catalytically active DESs. This was done by creating mixed organoamino substituent phosphazenes using a combinatorial approach to introduce disorder into the RPN-POMs and thus suppress the melting point.

5.1.1 Combinatorial Approach to Forming Eutectic RPNs

RPNs have a rigid, cyclic backbone of alternating P-N bonds. The P atoms have two exocyclic bonds each that can coordinate to a variety of different groups such as halides, amines, alcohols and thiols. The ring nitrogens have a basicity which is governed by the substituent groups; with

organoamino substituents (RNH), one or two ring N atoms can be protonated in the presence of a strong Brønsted acid to form mono- and di-cationic species as illustrated in Scheme 5.1.⁴¹



Scheme 5.1. Protonation of organoamino phosphazenes (RPNs) with Brønsted acids.

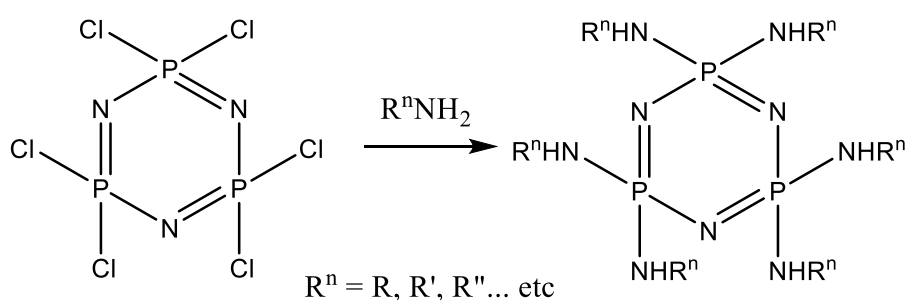
The most common synthetic route to making RPNs involves forming the ring structure with halide substituent groups in the first step. The substituent groups then undergo nucleophilic substitution, providing a route to easy functionalization.^{42–44} Functionalization with organoamines enabled formation of solid RPN-POM aggregates through intramolecular hydrogen-bonding and ionic interactions of the cationic species with POMs *via* the amine groups and ring N sites.

RPNs with single organoamino substituents are crystalline at room temperature due to the formation of well-ordered lattices through a network of intermolecular hydrogen-bonding interactions (see Section 1.4.4.6.2).⁴⁵ The complex aggregates that these compounds form with POMs are also fairly well-ordered, with many examples forming crystal lattice structures which have been characterised by single-crystal X-ray diffraction (see examples in Fig. 3.1 – 3.3).⁴⁶

To depress the melting point of both the RPNs and RPN-POM aggregates to produce room temperature liquids and ionic liquids, respectively, disorder must be introduced into the system to disrupt symmetry. However, for the protonated phosphazene species to operate as a cation constituent in a DES, the method for introducing this disruption: i) must not affect the stability or basicity of the phosphazene ring in a considerable manner; ii) must not inhibit the availability

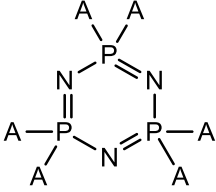
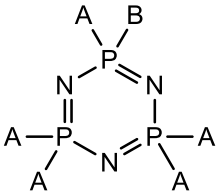
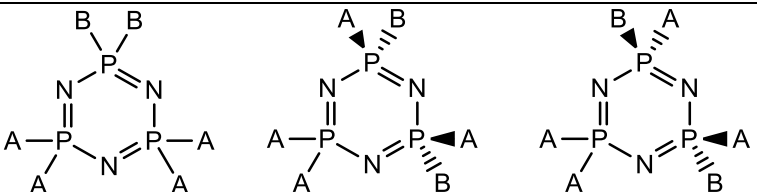
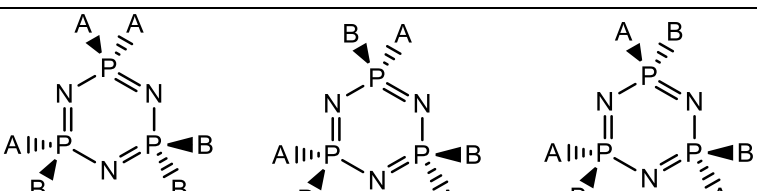
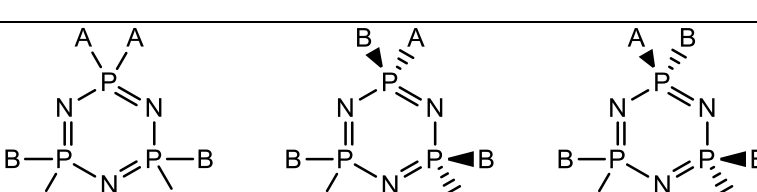
of the ring nitrogen sites for bonding or forming cationic species; iii) must not dramatically reduce the number of bonding sites available for complexation with counter anion species.

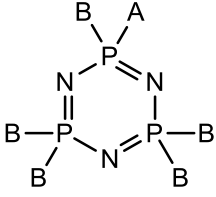
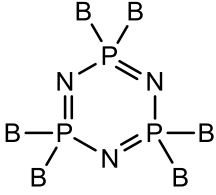
Nucleophilic substitution of the chloride substituent groups of the precursor $P_3N_3Cl_6$ compound with two or more primary amine substituents creates a distribution of unique compounds or a “library” of mixed-substituent phosphazenes in which there are various component phosphazenes with different ratios of each organoamino group (Scheme 5.2). The arrangement of the different organoamines around the ring can alter the symmetry of each phosphazene molecule, which also gives rise to additional isomers and enantiomers. This is illustrated in Table 5.1 for an ideal eutectic RPN mixture synthesized using equal quantities of two primary amines (A and B) and assuming that there is an equal probability of substitution with either amine at any of the six exocyclic P sites. Table 5.2 shows the total number of unique permutations that can be produced when varying the number of primary amines used in the reaction mixture, assuming there is no preference for substitution of one amine over the other(s).



Scheme 5.2. Synthesis of eutectic RPNs.

Table 5.1. Possible permutations for RPN synthesized using binary mixture of amines.

Composition	Stereoisomers	Frequency ^a
A ₆	 D _{3h}	1
A ₅ B	 C _{s(v)}	6
A ₄ B ₂	 C _{2v} C _{s(v)} C ₂	15
A ₃ B ₃	 C ₁ C _{3v} C _{s(v)}	20
A ₂ B ₄	 C _{2v} C _{s(v)} C ₂	15

AB_5	 <p style="text-align: center;">$Cs(v)$</p>	6
B_6	 <p style="text-align: center;">D_{3h}</p>	1

$A = RNH$, $B = R'NH$

^aThis is the relative proportion of a given composition with respect to the distribution of all potential compounds that may form.

Table 5.2. The maximum number of unique compounds that can be achieved from amine mixtures.

No. of primary amines	No. of unique compounds (excluding enantiomers)	No. of unique compounds (including enantiomers)
1	1	1
2	13	16
3	92	138
4	430	720
5	1505	2675
6	4291	7856

There is a clear exponential increase in the total number of unique compounds that can be made by increasing the number of primary amine substituents available for substitution in the reaction mixture; for instance, in a binary mixture of amines there are a total of 16 permutations possible with 13 unique compounds, whereas, by adding another amine to give a ternary amine mixture, the number of possible permutations increases to 138 with a total of 92 unique compounds. Increasing the number of unique and unsymmetrical compounds in a mixture increases the disorder in the mixture, making it more difficult for the components to form ordered lattice structures which, therefore, suppresses the melting point. This can be explained using the equation for the change in Gibbs free energy, ΔG (5.1):²⁶

$$\Delta G = \Delta H - T\Delta S \quad 5.1$$

where ΔH is the change in lattice enthalpy, T is the temperature, and ΔS is the change in entropy. At equilibrium, $\Delta G = 0$, and so the temperature for the melting point is given by:

$$T = \frac{\Delta H}{\Delta S} \quad 5.2$$

Introducing a mixture of components into the system will disrupt intermolecular interactions by disrupting symmetry, which reduces the change in enthalpy whilst simultaneously increasing the change in entropy (disorder). Hence, this leads to a suppression of the melting point. Increasing the number of primary organoamino substituents in the reaction mixture should, therefore, increase disorder and thus further suppress the melting point of the mixture of compounds formed. Equally, with the addition of an appropriate anion to the protonated cationic species in these mixtures, the resulting aggregates should display disorder as the arrangement of the different phosphazene components in the mixture will be random.

5.2 Preparation of Eutectic RPNs

All eutectic RPNs were prepared by Rebekah Upton. Samples were synthesized by refluxing a binary or ternary mixture of primary amines with $P_3N_3Cl_6$ under an inert N_2 atmosphere at 120 °C. All isolated products were liquids at room temperature. The compounds were characterised using FTIR, 1H and ^{31}P NMR, CHN microanalysis, mass spectrometry and differential scanning calorimetry (DSC).

FTIR analysis of all mixed RPNs gave spectra with characteristic peaks in the ranges of 3050-3500 cm^{-1} (broad, N-H), 2800-2950 cm^{-1} (C-H_{alkyl}), and 1300-1500 cm^{-1} (C-C_{alkyl}) which indicate the presence of primary amine groups.⁴⁵ Examples of these peaks can be seen in the spectrum for HexCyPN in Fig. 5.1, in which the spectrum for the parent $P_3N_3Cl_6$ is also shown. Comparison of the P-N peaks in the range of 1050-1300 cm^{-1} for HexCyPN and 700-1250 cm^{-1} for $P_3N_3Cl_6$ shows multiple, sharper peaks for HexCyPN due to the presence of cyclic P-N and exocyclic P-N bonds with the amine substituents, whereas there is only a single, broad peak for $P_3N_3Cl_6$ from the cyclic P-N bonds. Similar peaks in this range are present in the spectra for all of the RPN products and can be used to indicate successful substitution of Cl with primary amines.⁴⁷

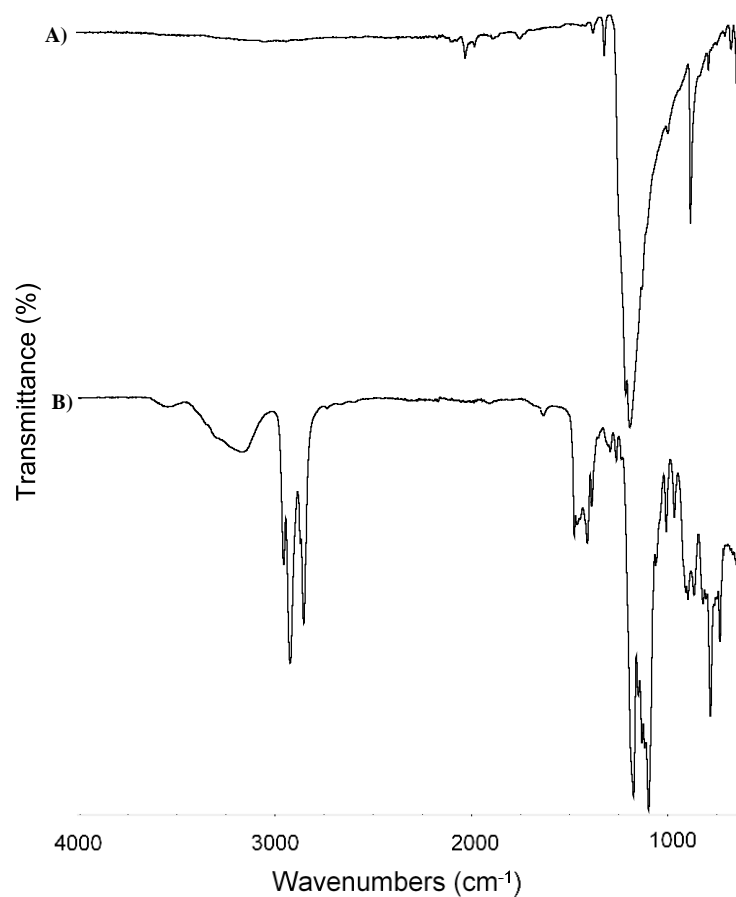


Fig. 5.1. FTIR spectra of (A) P₃N₃Cl₆ and (B) HexCyPN.

³¹P NMR was used to indicate the successful substitution of multiple primary amines on the phosphazene rings in syntheses using binary and ternary amine mixtures. Fig. 5.2 compares the spectra of RPN species synthesized from mono (HexPN) binary (HexiBuPN) and ternary (HexiBuBuPN) mixtures of primary amines.

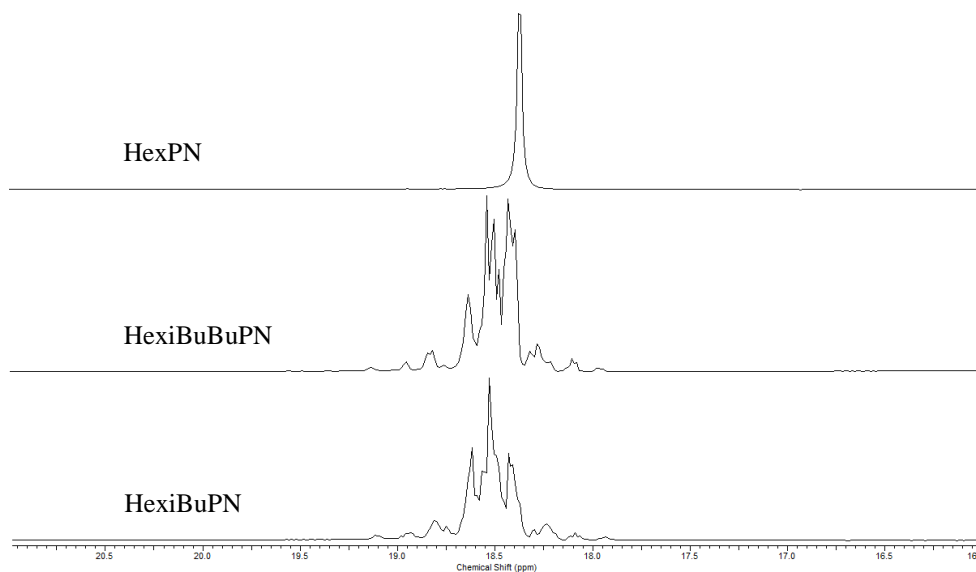


Fig. 5.2. ^{31}P NMR spectra of mixed RPNs synthesized from mono (HexPN), binary (HexiBuPN) and ternary (HexiBuBuPN) mixtures of primary amines.

Substitution with a single amine (here hexylamine, see HexPN spectrum) produces a single peak in ^{31}P NMR spectrum as all phosphorus atoms are in magnetically equivalent environments. Using a mixture of amines (HexiBuPN and HexiBuBuPN) produces multiple overlapping signals. This is because, using a binary mixture of amines as an example, there are up to 13 unique compounds and 3 enantiomers that may form in total (see Table 5.2), and in some of these compounds the phosphorus atoms are in magnetically inequivalent environments which produce peak splitting. All of the peaks have similar chemical shifts; therefore, the peaks overlap in the spectrum. Substitution using a ternary mixture of alkylamino substituent groups, (HexiBuBuPN), increases the number of potential unique compounds to 92 and 46 enantiomers (see Table 5.2), resulting in the production of more unique compounds with different P environments and different chemical shifts. Thus, we see more overlapping peaks in the spectrum.

Another interesting result is that the ^{31}P NMR spectra of compounds with mixed amino substituents can show favoured substitution of one amine compared to the other(s). For example, iBuPN and HexPN have chemical shifts at 19.6 ppm¹ and 18.4 ppm, respectively. It may be expected that phosphazene compounds with an equal substitution of both amines, i.e. $\text{P}_3\text{N}_3(\text{HexNH})_3(\text{iBuNH})_3$, would produce a distribution of peaks which would lie centrally between the shifts of the iBuPN and HexPN as isomers of $\text{P}_3\text{N}_3(\text{HexNH})_3(\text{iBuNH})_3$ would be the main products produced (see Table 5.1 for relative distributions). Therefore, for HexiBuPN, synthesized from a binary mixture of iBuNH₂ and HexNH₂, the average position of the peaks would be expected to lie at 19 ppm. In the measured HexiBuPN spectrum in Fig. 5.2, the average position of the multiple overlapping peaks is shifted upfield from this expected position towards HexPN shift at 18.5 ppm, which could indicate a slight preference for hexylamine substitution over isobutylamine substitution. This phenomenon can be seen more clearly by comparing HexPN, CyPN and HexCyPN shifts in Fig. 5.3.

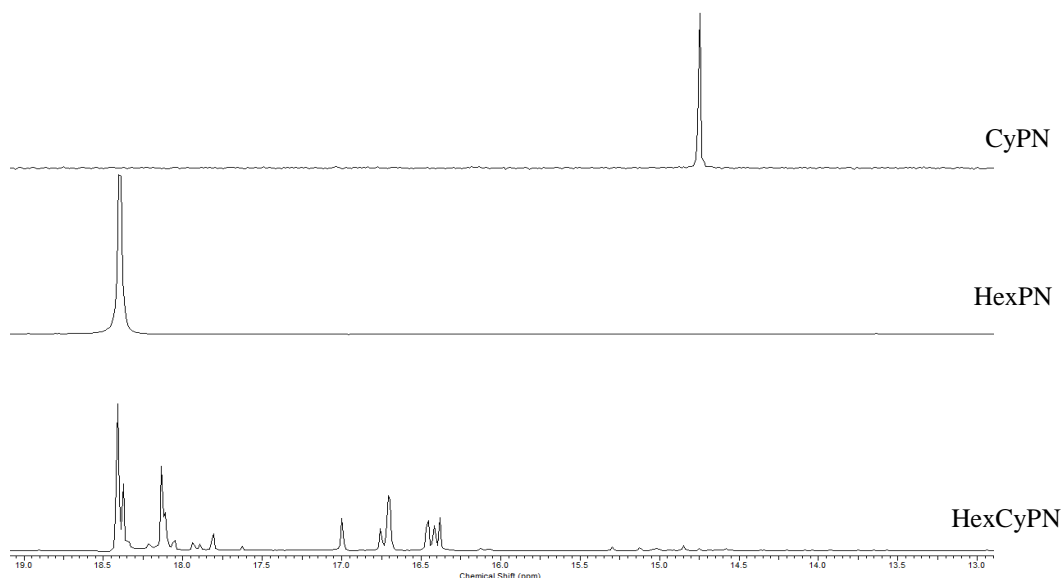


Fig. 5.3. Comparison of the ^{31}P NMR spectra of CyPN, HexPN and HexCyPN showing the preferred substitution of HexNH₂ over CyNH₂ in the synthesis of HexCyPN.

The most intense peaks in HexCyPN spectrum appear around 18.3 ppm which likely indicates that there is a greater hexylamine contribution to the phosphorus signals in the HexCyPN sample than from cyclohexylamine, hence, there is a greater preference for hexylamine substitution over cyclohexylamine substitution.

Elemental analysis of mixed RPNs shows a close correlation with theoretical values, which were calculated based on the mass of compounds which have equal substitution of all amines, as it was predicted by statistical distribution calculations that these would possess the average mass of all the compounds in the mixture. Mixtures with benzylamine substituents - the most carbon-rich amine used for the syntheses of these compounds – have, on average, slightly higher experimentally recorded C content than was predicted by the theoretical calculations, indicating a preference for benzylamine substitution over other amines. This observation is also corroborated with high intensity signals from BzPN contributions in NMR data and mass spectrometry data which show slightly greater proportions of benzylamine-containing compounds in mixtures synthesized using hexylamine and/or cyclohexylamine substituents also. In addition, it should be noted that substitution with cyclohexylamine is also generally less favourable than with other substituents, which is likely due to steric effects resulting from its relatively large, bulky size. As mentioned previously, ^{31}P NMR of cyclohexylamine-containing mixed substituent compounds show peaks with very weak signals at shifts associated with higher degrees of cyclohexylamine substitution. The mass spectra for eutectic RPNs such as HexBzCyPN, HexCyPN and BzCyPN even show low intensities of ions with high degrees of cyclohexylamine substitution, and high intensities of ions with high degrees of substitution of the other substituents. This is illustrated in the mass spectrum of BzCyPN in Fig. 5.4. The molecular weights of $(\text{BzNH})_6\text{P}_3\text{N}_3$ (BzPN) and $(\text{CyNH})_6\text{P}_3\text{N}_3$ (CyPN) are 771 and 724, respectively. With the most intense peak at 764 and the most prominent peaks found in the range of 748-772 m/z, it is clear that substitution with BzNH_2 is preferred over CyNH_2 .

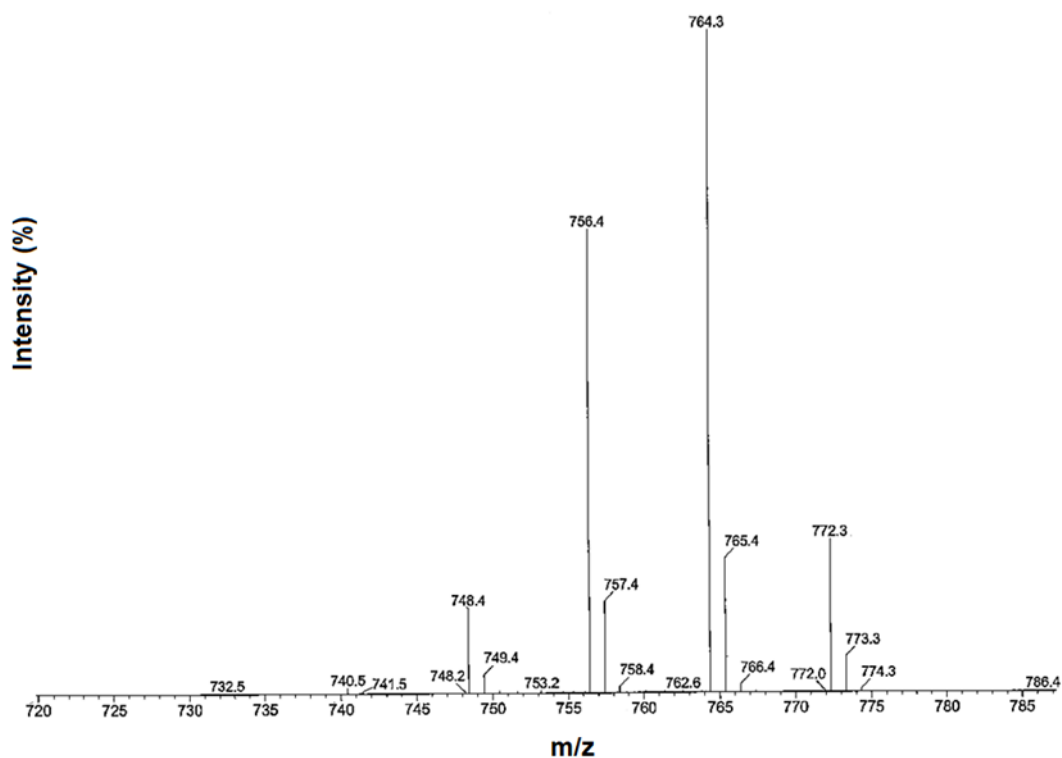


Fig. 5.4. Mass spectrum of BzCyPN.

^1H NMR was used in addition to the other techniques to identify the presence of primary amines in the mixed RPN mixtures.⁴⁷ In some of the spectra the overlap of signals made assignment of some of the proton environments difficult. $^1\text{H}^{13}\text{C}$ HMQC (Fig. 5.5) and ^1H COSY (Fig 5.6) analysis could be used to more clearly assign peaks in ^1H NMR spectra to the correct alkylamino groups. These techniques could prove useful for the synthesis of RPNs using a larger mixture of amines.

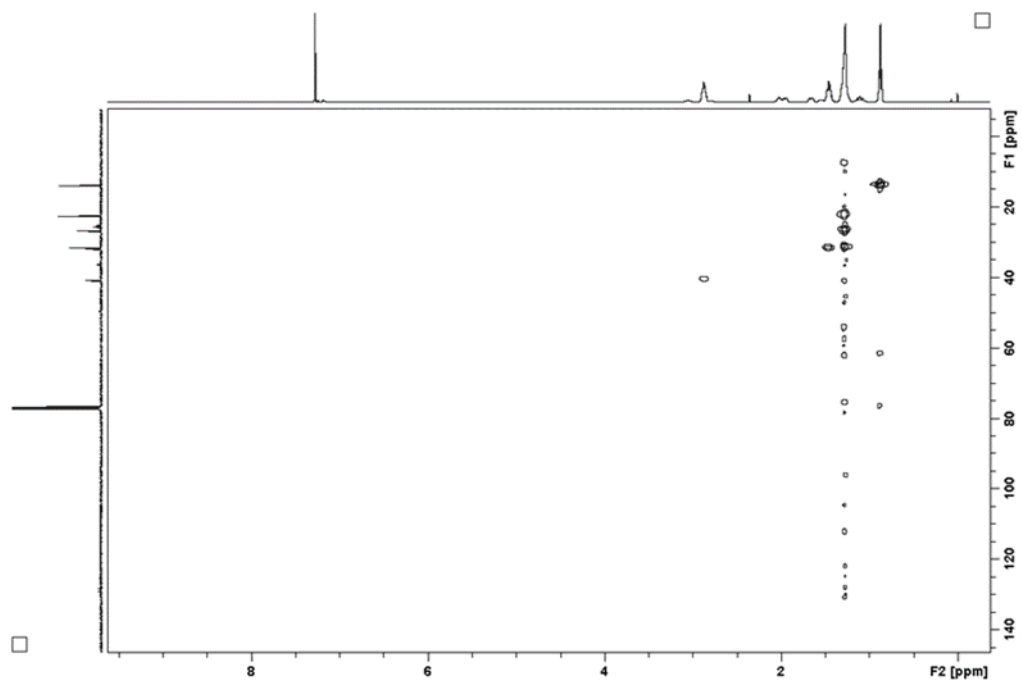


Fig. 5.5. $^1\text{H}^{13}\text{C}$ HMQC for HexCyPN.

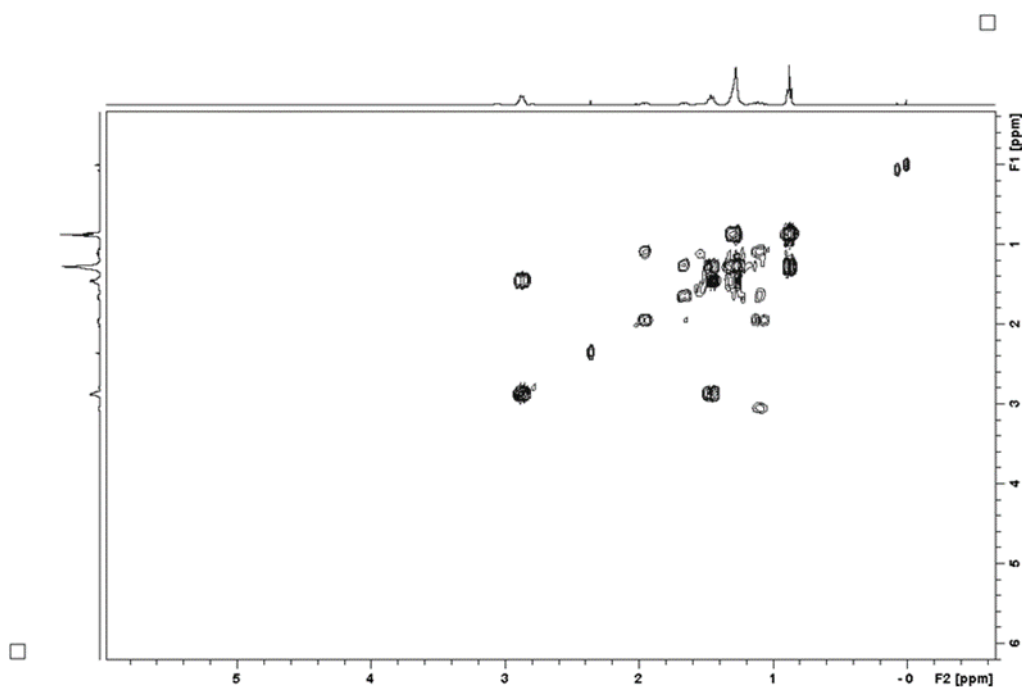


Fig. 5.6. ^1H COSY for HexCyPN.

DSC was used to determine the phase transitions of the eutectic RPNs (Figs 5.7-5.14). The change in heat flow was measured using a temperature cycle program which first heated the

samples from 25 °C up to 150 °C, then cooled the samples down to -80 °C, and finally heated the samples back up to 150 °C. The first stage of heating has been omitted for clarity in Figs 5.7-5.14. With the possible exception of HexBuPN (Fig. 5.9), the samples all appear to have glass transitions (T_g), indicating that they do not form completely ordered lattice structures due to disorder caused by the mixture of substituent groups. This is expected as the samples are all liquids at room temperature.

Samples with Bz substituent groups (Figs, 5.7, 5.11 and 5.12) typically have higher T_g , possibly due to a preference for substitution of BzNH₂ over other substituents (see above) and stronger intermolecular interactions resulting from π -bonding between the large number of Bz groups. Interestingly, HexBzPN (Fig. 5.11) and HexBzCyPN (Fig. 5.12) show broad melting point (T_m) peaks at 37 and 22 °C, respectively, which suggest the presence of microcrystalline species in the samples. These could form due to ordered bonding between component RPNs with high numbers of BzPN substituents facilitated by π -bonding interactions between Bz groups. Hex groups are less bulky than Cy groups, meaning they are less likely to interfere with these bonding interactions through steric hindrance, which is why BzCyPN (Fig. 5.7) only has a T_g and HexBzPN has a T_g and a T_m . The lower T_g and T_m for HexBzCyPN compared to HexBzPN, therefore, result from increased disorder from the extra Cy substituent and the steric hindrance this group provides in intermolecular bonding interactions.

HexBuPN (Fig 5.9) and iBuBuPN (Fig. 5.14) both show eutectic T_m peaks at ca. 3 and 19 °C respectively, indicating microcrystallinity. The peaks are stronger in HexBuPN as both Hex and Bu are linear aliphatics, which enables better ordering within the lattice. The peaks in iBuBuPN are weaker because, although iBu and Bu are similar in size which can provide some order, iBu is branched which provides steric hindrance and, thus, disorder.

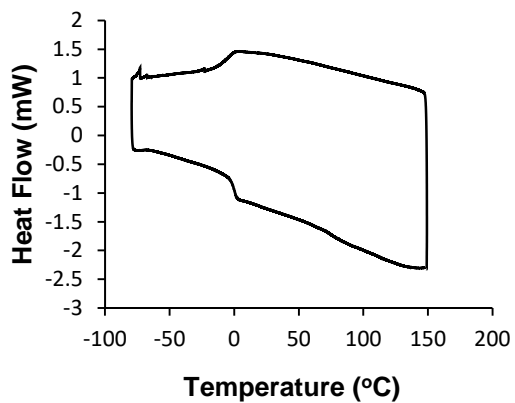


Fig. 5.7. DSC curve for BzCyPN.

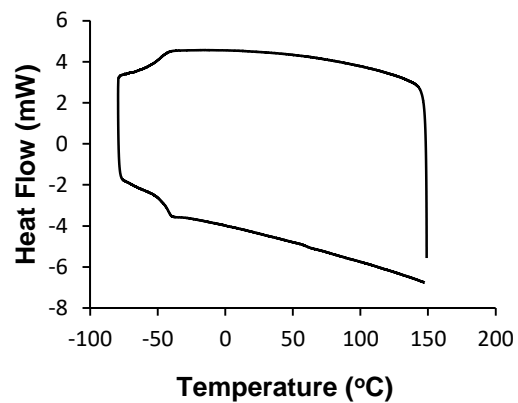


Fig. 5.8. DSC curve for HexiBuPN.

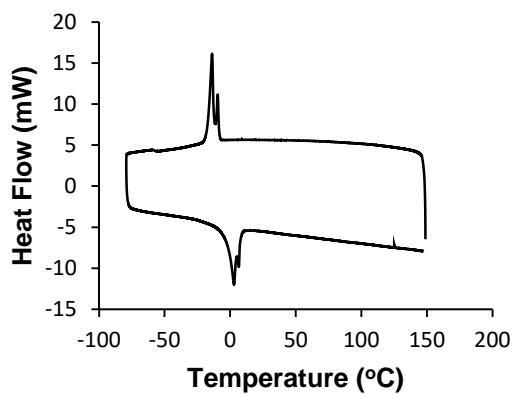


Fig. 5.9. DSC curve for HexBuPN.

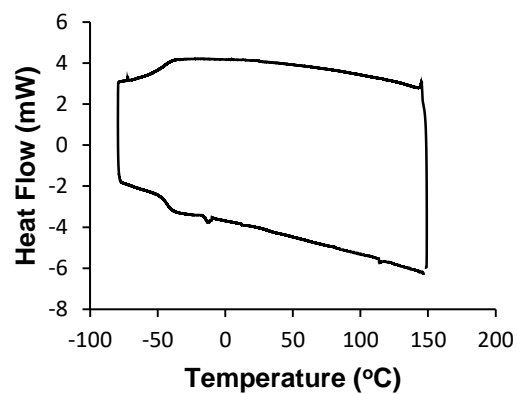


Fig. 5.10. DSC curve for HexiBuBuPN.

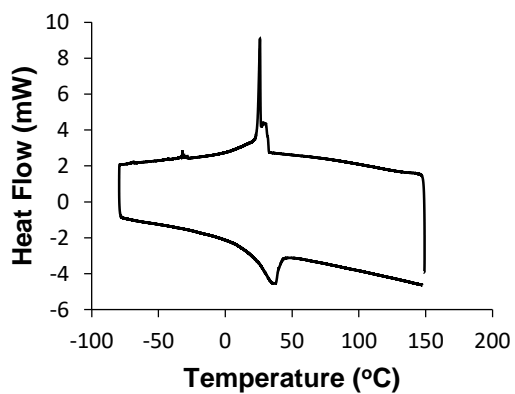


Fig. 5.11. DSC curve for HexBzPN.

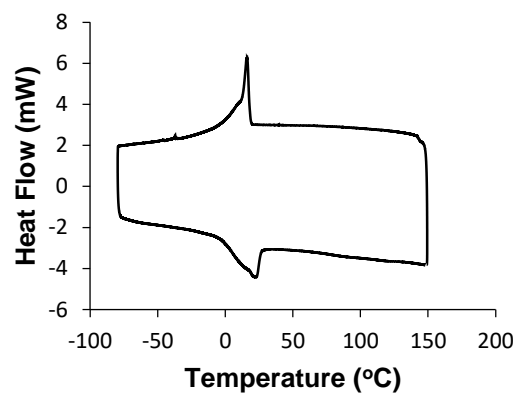


Fig. 5.12. DSC curve for HexBzCyPN.

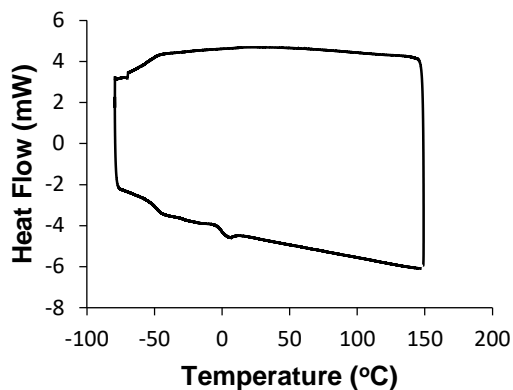


Fig. 5.13. DSC curve for HexCyPN.

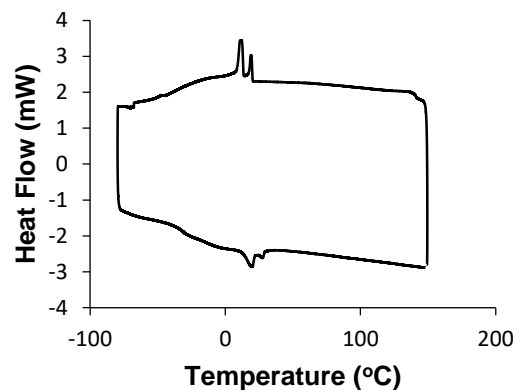


Fig. 5.14. DSC curve for iBuBuPN.

5.3 Preparation of Eutectic RPN Salts

Eutectic RPN salts (henceforth referred to as eutectic RPN-X, where X = Cl⁻, NO₃⁻ or POM) were prepared by stirring solutions of eutectic RPN with aqueous HCl, HNO₃ or HPA at room temperature (samples were synthesized by Rebekah Upton). Eutectic RPN-Cl and RPN-NO₃ samples were prepared in DCM/H₂O biphasic systems, and eutectic RPN-POM samples were prepared in ethanol. Solvents were removed by rotary evaporation. All eutectic RPN-Cl and eutectic RPN-NO₃ samples were waxes at room temperature, whereas eutectic RPN-POMs were generally viscous liquids with a few exceptions.

FTIR of eutectic RPN-NO₃ samples show an NO₃ peak at around 1350 cm⁻¹ in the spectra, and characteristic POM peaks were clearly distinguishable in the fingerprint region of the spectra for eutectic RPN-POMs, as shown in the spectrum of HexBzCyPN-PMo (Fig. 5.15); characteristic peaks of the Keggin anion PMo at 1059 cm⁻¹ (P-O), 949 cm⁻¹ (Mo=O), 874 cm⁻¹ (Mo-O-Mo corner-sharing) and 783 cm⁻¹ (Mo-O-Mo edge-sharing) indicate that PMo remains largely intact in HexBzCyPN-PMo.

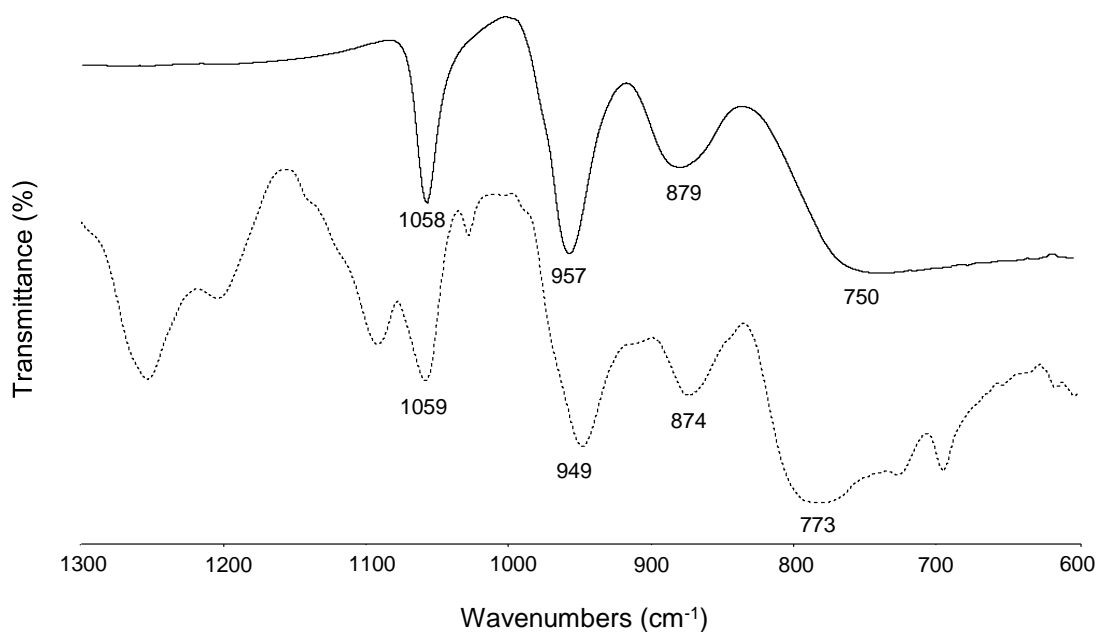


Fig. 5.15. FTIR spectra of HexBzCyPN-PMo (dashed line) and $\text{H}_3\text{PMO}_{12}\text{O}_{40}$ (solid line).

The melting points of all RPN-X DESs are recorded in Table 5.3. With single substituent RPNs, there is a general decrease in melting point in line with increasing size of the counter-anion. Eutectic RPN-X containing RPNs with only aliphatic substituents show a decrease in melting point with increasing size and charge distribution of the counter anion, presumably from greater interionic distances and weaker ionic interactions. RPNs with Bz substituents appear to show unusually high melting points when coordinated to nitrate counter-ions, though, it is currently unknown why this is.

Table 5.3. Melting points of RPN-X DESs.

RPN	Salt Melting point* (°C)					
	Counter-Anion					
	None	Cl ⁻	NO ₃ ⁻	POMs		
PMo				PW	SiW	
HexBzPN	-	60-64	72-78	50-57	52-58	-
HexCyPN	-	64-68	60-63	-	-	-
BzCyPN	-	48-52	96-102	96-104	98-110	108-120
HexCyBzPN	-	55-60	82-85	56-63	-	-
HexiBuPN	-	54-58	52-58	56-62	-	-
HexBuPN	-	73-76	44-51	-	-	-
iBuBuPN	-	142-144	130-132	-	-	-
HexiBuBuPN	-	58-64	34-39	-	-	-
HexPN	40-41	106-109	90-93	-	N/A	N/A
BzPN	82-84	128-130	129-133	74-80	N/A	N/A
iBuPN	60-61	202-204	188-190	N/A	N/A	N/A

* “-“ indicates salt was a liquid at room temperature (20.5 °C)

XRD analysis shows that many eutectic RPN-Cl and RPN-NO₃ are microcrystalline waxes (Figs 5.16 and 5.17, respectively). Peaks with 2θ values between 4-6° give D values in range of 22-12 Å which is indicative of the distance between the two lipophilic R-group layers sandwiching a polar phosphazene ring layer. Peaks with greater values of 2θ indicate short-range order within the layers; as Cl⁻ and NO₃⁻ anions are small, they can sit in-plane between phosphazene rings and interact with the RPN cations through ionic and hydrogen bonding networks which produces this short-range order.

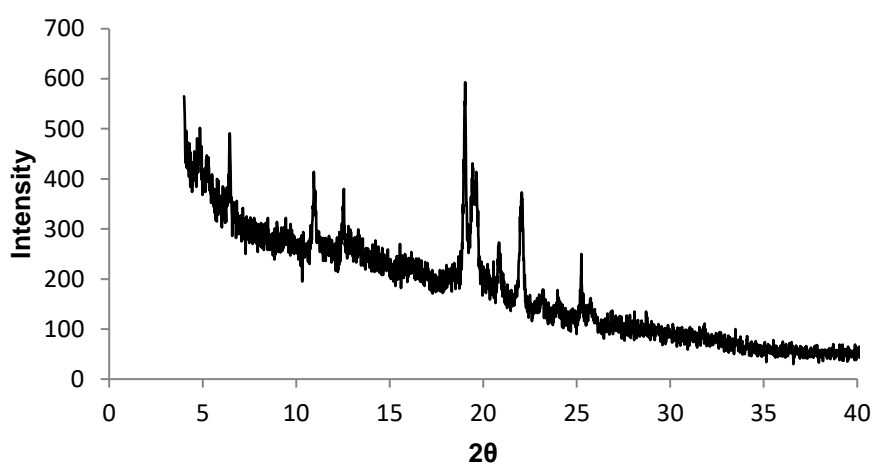


Fig. 5.16. XRD of HexCyPN-Cl.

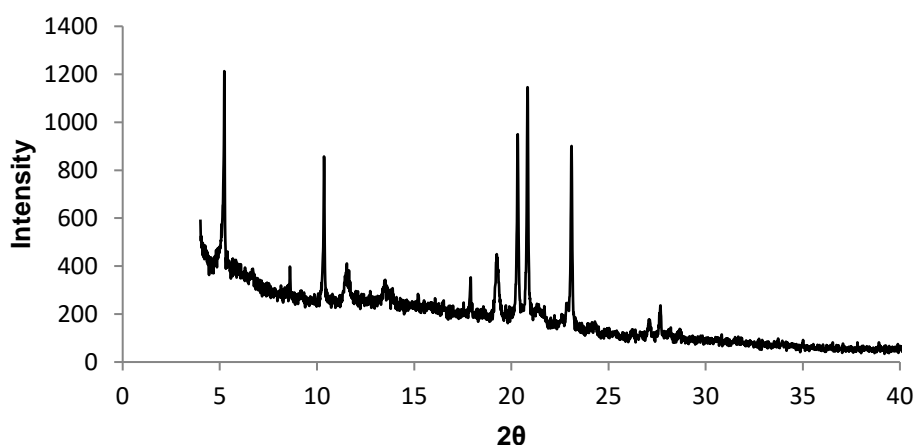


Fig. 5.17. XRD of HexBuPN-NO₃.

Bonding with small anions creates a degree of order within the mixed phosphazenes, which are otherwise disordered liquids, leading to the formation of bilayers composed of lipophilic R group layers sandwiching a polar in-plane network of ring cations and counter-anions as illustrated in Fig. 5.18. The substituent R groups in the lipophilic layers of these bilayers interact with those in lipophilic layers of other bilayers through electrostatic interactions, creating layered sheets which gives rise to the micro-crystallinity in the waxes.

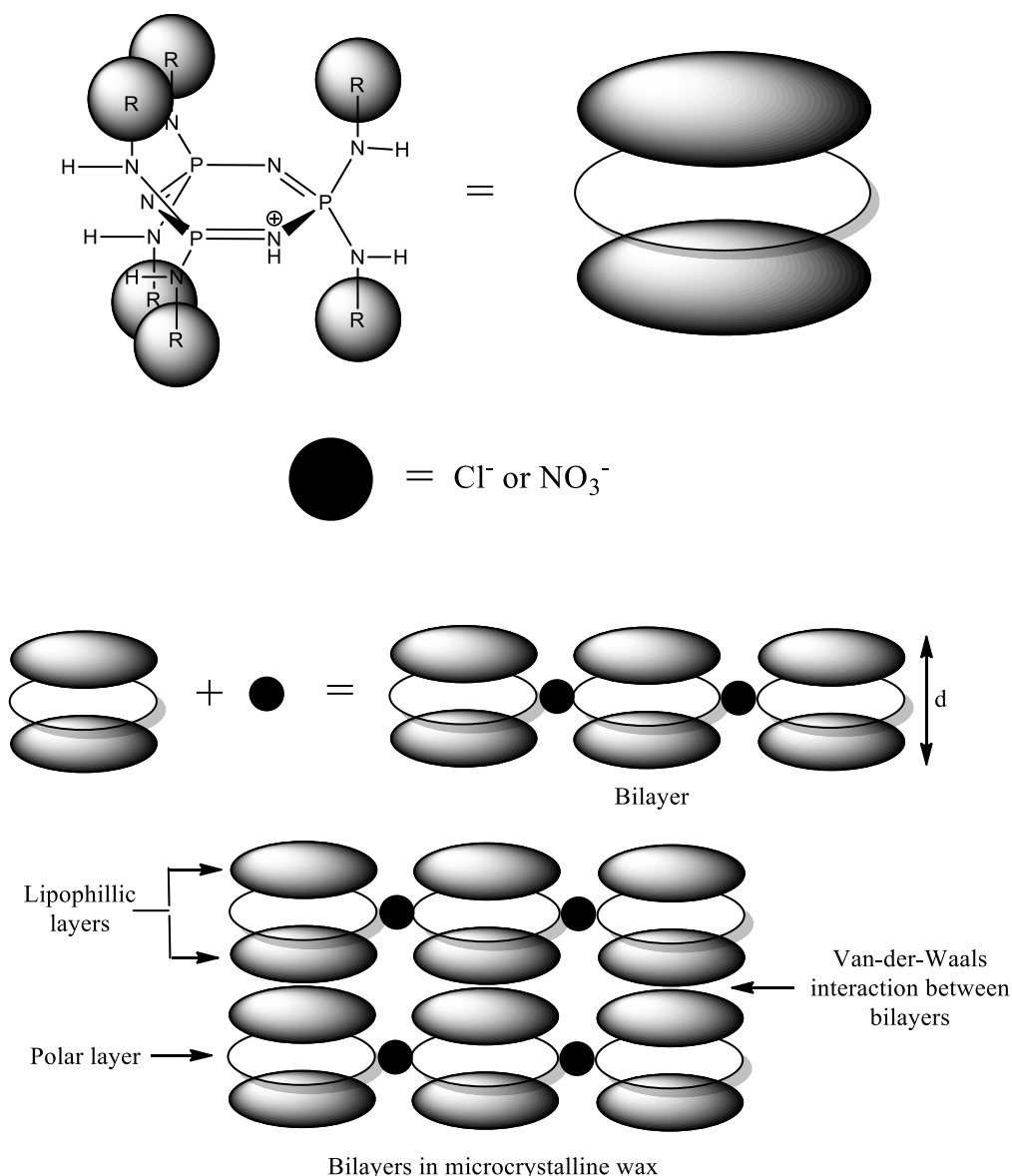


Fig. 5.18. Schematic representation of the proposed ordering of RPNH^+ and Cl^- or NO_3^- in bilayers in microcrystalline RPN-Cl and RPN- NO_3 waxes.

The formation of bilayers in single crystal X-ray structures of singly-substituted RPN-Cl and RPN-NO₃ salts have been observed previously in the group. The structure of BzPN-Cl displayed in Fig. 5.19 (A) clearly shows the arrangement of the [BzPNH]⁺ and Cl⁻ ions in the ionic layer; each Cl⁻ interacts with three neighbouring [BzPNH]⁺ ions through hydrogen bonds with protonated ring N sites and amine groups on the benzylamine substituents. (B) shows the packing of the BzPNs to form the bilayer in which the lipophilic benzyl groups sandwich the ionic layer. (C) shows the stacking of the bilayers. The benzyl groups in the lipophilic layers are well-ordered and so stacking between the bilayers is also ordered, the electrostatic interactions are strong, and so an ordered crystalline lattice can form. In eutectic RPN-Cl, the R groups in the lipophilic layers are randomly arranged and are not well ordered, resulting in poor electrostatic interactions and so only waxes can form.

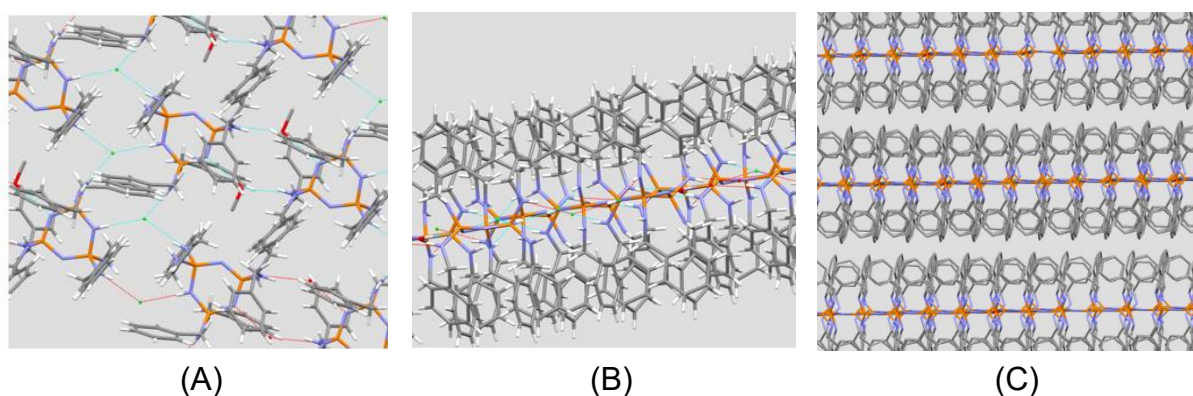


Fig. 5.19. Single-crystal X-ray structure of BzPN-Cl. (A) shows short-range order in ionic layer between [BzPNH]⁺ and Cl⁻ ions. (B) shows the structure of the bilayer, where the lipophilic benzyl groups sandwich the ionic layer. (C) shows the ordered packing of the bilayers (N, purple; P, orange; C, grey; H, white; O, red; Cl⁻, green; H-bonds, blue dotted lines).

The use of POM counter-anions mostly produced viscous liquids. However, some waxy compounds were formed in certain eutectic RPN-POM combinations. XRD patterns indicate

that the structures formed in these waxes are largely amorphous with potential long-range ordering, as shown in Fig. 5.20.

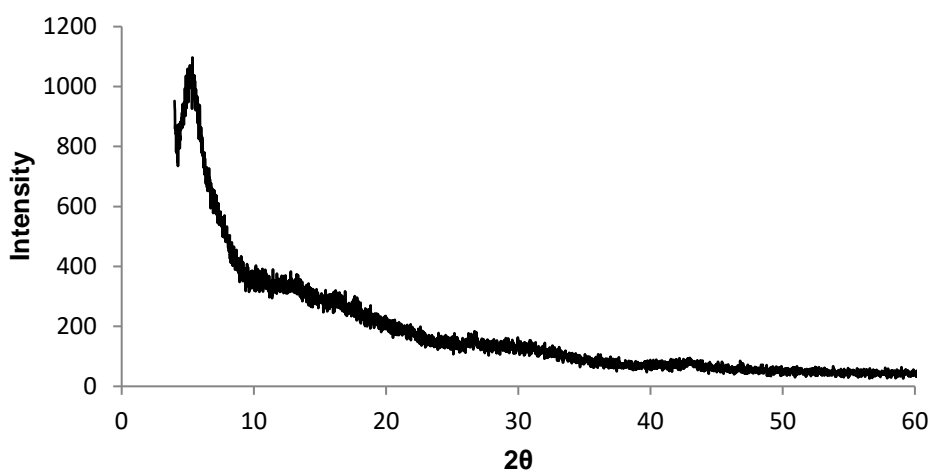


Fig. 5.20. XRD of HexiBuPN-PMo.

The POMs are too big to sit in between phosphazene rings so instead the phosphazenes coordinate around the large spherical POM structures through hydrogen bonding and ionic interactions in a surfactant-like manner, as seen previously in single crystal X-ray structures of RPN-POM aggregates using single substituent RPNs (Section 3.1.1).⁴⁶ Bilayers cannot form between RPNs as the lipophilic R-groups are more disordered in a 3 dimensional orientation (long-range disorder), as shown in Fig. 5.21. There will still be some hydrogen bonding, ionic and van-der-Waals interactions between different RPN-POM aggregates that form either fluxionally (liquids) or non-fluxionally (waxes) *in situ*. The waxes formed are, therefore, not microcrystalline. The only notable exception is with BzCyPN-POM, as substitution of benzylamine is greatly preferred over cyclohexylamine. This leads to generation of more compounds with more benzylamine substituents resulting in slightly more ordered packing in

the RPN-POM complexes that are made (Fig. 5.22). Packing may even be aided by π -interactions between benzyl groups.

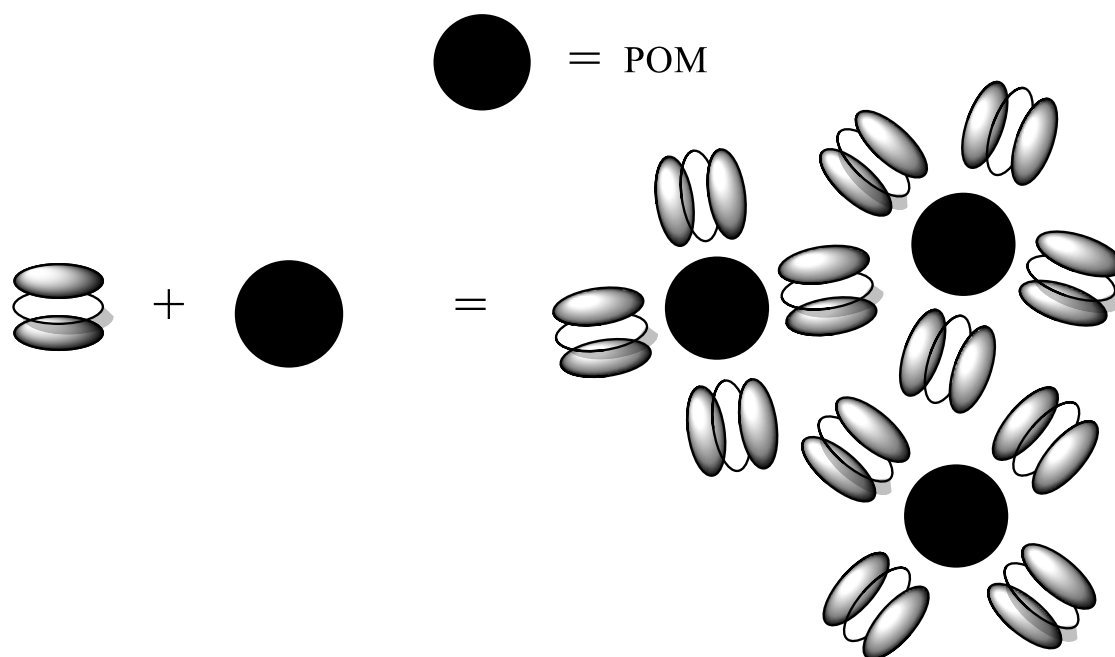


Fig. 5.21. Schematic representation of the proposed packing of RPNH⁺ and POM ions in eutectic RPN-POM composites.

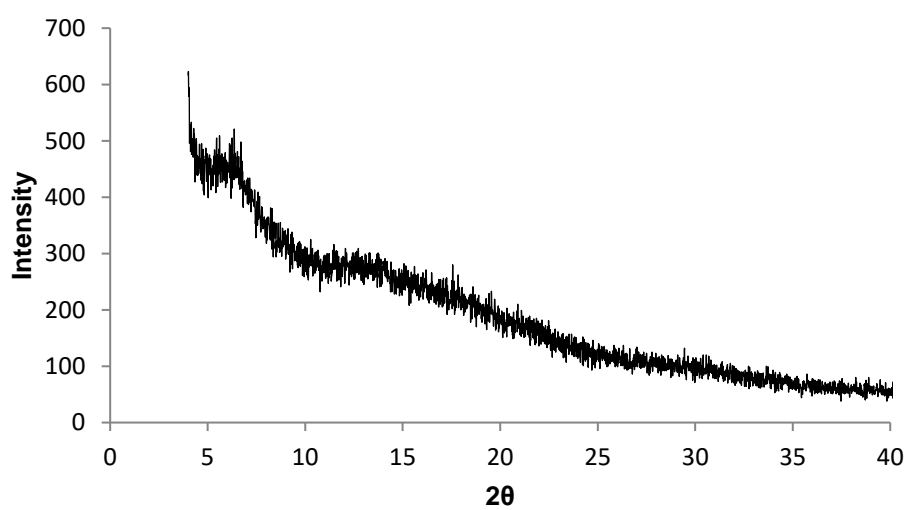


Fig. 5.22. XRD of BzCyPN-PMo.

The ^{31}P NMR spectra of eutectic RPN-POMs show strong singlet peaks at \sim -15 ppm for PW and \sim -4 ppm for PMo with no lacunary POM peaks present, indicating that the POMs have not degraded during preparation. All phosphazene signals are shifted upfield and formed broader, smoother, overlapping peaks compared to those of the starting RPNs. This can be accredited to protonation of the phosphazene ring sites and fast proton exchange between intra- and inter-molecular N ring positions.

5.4 Epoxidation of Olefins Catalysed by Eutectic RPN-POM

Epoxidation of cyclooctene by H_2O_2 was conducted in biphasic RPN-POM/ H_2O system in the absence of solvent using the method outlined in Section 2.3.3.3. Representative results are shown in Table 5.4. HexCyPN-PMo was used as a reaction medium/ catalyst and 1.1:1 molar ratio of [cyclooctene]/[H_2O_2] was used with a slight stoichiometric excess of cyclooctene to improve epoxide selectivity whilst minimising waste. Initial reactions were run for 4 h at 60 $^\circ\text{C}$ and gave 95% epoxide yield with 98 % epoxide selectivity (entry 1). In an attempt to improve the epoxide yield, the reaction time was increased to 6 h which saw a decrease in both epoxide yield and selectivity to 90 % and 92 %, respectively (entry 2). A decrease in mass balance to 93 % indicated the formation of another unidentified product which was represented by a peak in the chromatogram. It was believed to be a hydrolysis product from the epoxide, however further testing showed that this peak was not cyclooctene diol.

Reducing [cyclooctene]/[H_2O_2] reduced the product yield and selectivity (entry 3), possibly favouring hydrolysis or over-oxidation of epoxide products over epoxidation as [cyclooctene] began to drop off towards the end of the reaction.

After 1 hour, the reaction had not reached completion (entry 4), showing that this system conducted cyclooctene epoxidation slower than System One, which used homogeneous BzPN-PMo-based catalyst in the presence of organic solvent and gave 99 % conversion after 30 min.

Table 5.4. Optimization of reaction conditions for HexCyPN-PMo catalysed epoxidation of cyclooctene with H₂O₂.

No.	Reaction time (h)	Reaction temp. (°C)	Substrate (mmol)	Cyclooctene oxide yield (%)	Cyclooctene conversion (%)	Mass balance (%)	Selectivity (%)
1	4	60	3.4	95	85	99	98
2	6	60	3.4	95	90	93	92
3	4	60	3.24	92	92	93	92
4	1	60	3.4	37	31	102	105
5	4	30	3.4	21	28	90	64

HexCyPN-PMo (0.0125 mmol) catalyst, H₂O₂ oxidant (3.0 mmol, 30% w/w). [HexCyPN-PMo]/[H₂O₂] 1: 240 mol/mol, [cyclooctene]/[H₂O₂] = 1.1:1 mol/mol.

Reducing the temperature to 30 °C (entry 5) greatly slowed down the rate of the reaction but illustrated that the catalyst is still active at temperatures close to ambient conditions.

In our search for the best possible RPN-POM IL catalyst, we created a library of different eutectic RPNs with PMo and tested their catalytic activity in epoxidation of cyclooctene with H₂O₂. The results are recorded in Table 5.5. Single-substituent RPN-PMo BzPN-PMo and HexPN-PMo were included for comparison.

Table 5.5. Comparison of RPNs with PMo as catalysts for epoxidation of cyclooctene with H₂O₂.

RPN	Cyclooctene oxide yield (%)	Cyclooctene conversion (%)	Mass Balance (%)	Selectivity (%)
HexCyPN	95	85	99	98
HexBzCyPN	80	73	98	97
HexBzPN	92	86	96	94
HexPN	96	84	100	100
HexiBuBuPN	92	83	98	98
BzPN	94	79	103	104
HexBuPN	96	81	104	105
BzCyPN	66	64	95	92
iBuBuPN	86	81	95	94
HexiBuPN	92	88	94	93

RPN-PMo (0.0125 mmol) catalyst, H₂O₂ oxidant (3.0 mmol, 30% w/w), [RPN-PMo]/[H₂O₂] = 1: 240, [Cyclooctene]/[H₂O₂] = 1.13: 1, 60 °C reaction temperature and 4 h reaction time.

Catalytic activity generally decreases with the increasing number of substituent amines used to functionalize the phosphazene: RPN > RR'PN > RR'R''PN (where R = primary amine), with the most effective catalysts being HexPN-PMo, BzPN-PMo, HexBuPN-PMo and HexCyPN-PMo. Eutectic RPNs including Bz and Cy together generally give lower product yields – probably due to bulky groups providing steric hindrance to catalytically active species *in situ*. Catalytic activity of the single-substituent phosphazenes indicates that use of an organic solvent

(as used in System One, Section 3.3) is not necessary for the reaction to occur. However, HexPN-PMo solubilizes well in heptane, which was used as a solvent for product extraction, which makes separation of catalyst and product difficult when using this catalyst. BzPN-PMo is not a liquid at the 60 °C reaction temperature, therefore, it is more accurate to describe this system as BzPN-PMo aggregates solubilized in cyclooctene than *vice versa*. Cy in HexCyPN-PMo reduces the solubility of RPN-POM species in heptane, which now makes solvent extraction of products more viable through the use of heptane. A comparison of the catalytic activity of HexCyPN-POM with regards to different POMs is summarized in Table 5.6. The catalytic activity increases with respect to POM in the order: PMo > PW > SiW in line with the results obtained in homogeneous and heterogeneous systems (Chapter 3 and 4). The activity with respect to POM can be described using equations 3.2-3.4 and the corresponding explanation in Section 3.3.

Table 5.6. Comparison of POM's as catalysts with HexCyPN for epoxidation of cyclooctene with H₂O₂.

POM	Cyclooctene oxide yield (%)	Cyclooctene conversion (%)	Mass Balance (%)	Selectivity (%)
PMo	95	85	99	98
SiW	29	34	92	75
PW	43	56	81	68

HexCyPN-POM (0.0125 mmol) catalyst, H₂O₂ oxidant (3.0 mmol, 30% w/w), [HexCyPN-POM]/[H₂O₂] = 1: 240, [Cyclooctene]/[H₂O₂] = 1.13: 1, 60 °C reaction temperature and 4 h reaction time.

Catalyst reuse was tested following the procedure outlined in Section 2.3.3.3; the results are shown in Table 5.7. The catalyst could be re-used at least 4 times to give > 91% yield of epoxycyclooctane without any appreciable loss in selectivity or mass balance, indicating very little to no loss in catalytic activity and little to no loss of catalyst in the extraction process. ³¹P NMR analysis on the extraction solvent phases did not show any characteristic peaks for either the phosphazenes, POMs, or degraded POM species, indicating very little to no loss of the catalyst by dissolution during the extraction procedure. The increase in catalyst activity in runs 2 and 3 to 95 and 99%, respectively, are probably due to formation of active peroxo PMo species after the first run which are then readily available in the subsequent runs.⁴⁸⁻⁵⁰ RPN-POM ILs, therefore, show promise as catalytically active media for the development of solvent-less oxidations with H₂O₂.

Table 5.7. Catalyst reuse experiments for epoxidation of cyclooctene with H₂O₂ catalysed by HexCyPN-PMo.

Run	Cyclooctene oxide yield (%)	Cyclooctene conversion (%)	Mass Balance (%)	Selectivity (%)
1	91	85	95	95
2	95	90	94	93
3	99	93	95	94
4	91	84	96	96

HexCyPN-PMo (0.0125 mmol) catalyst, H₂O₂ oxidant (3.0 mmol, 30% w/w), [HexCyPN-PMo]/[H₂O₂] = 1: 240, [Cyclooctene]/[H₂O₂] = 1.13: 1, 60 °C reaction temperature and 4 h reaction time.

Epoxidation of 1-hexene was also tested and the results are shown in Table 5.8. The reactions were run for 4 h and 18 h and show little to no epoxide yields. In both cases, there was a variety of product peaks present in the chromatograms and the intensity of these product peaks were much larger after the reactions were run for 18 h. Hexene conversions of 30 % and 64 % for 4 h and 18 h, respectively, suggest that these peaks are products of other hexene side reactions, which implies that hydrolysis products and/or polymers are likely formed.

Table 5.8. Epoxidation of 1-hexene with H₂O₂ catalysed by HexCyPN-PMo.

Reaction time (h)	Epoxyhexane yield (%)	Hexene conversion (%)	Mass Balance (%)	Selectivity (%)
4	1	30	75	2
18	0	64	N/A	0

HexCyPN-PMo (0.0125 mmol) catalyst, H₂O₂ oxidant (3.0 mmol, 30% w/w), [HexCyPN-PMo]/[H₂O₂] = 1: 240, [Hexene]/[H₂O₂] = 1.17: 1, 60 °C reaction temperature.

The effect of stirring speed on the reaction was measured using an excess of cyclooctene ([cyclooctene]/[H₂O₂] = 10:1) so that the reaction could be monitored by the measurement of aliquots after pre-determined time intervals. The results in Fig. 5.23 show that after a 4 h time period the reaction produced the same product yield (ca. 95 %) regardless of stirring at speeds above 500 RPM. Comparison of yields obtained after 60 min (Fig. 5.24) show that above 1000 RPM stirring speed the reaction is no-longer under the influence of mass transport or diffusion limitations as an effect of mechanical agitation.

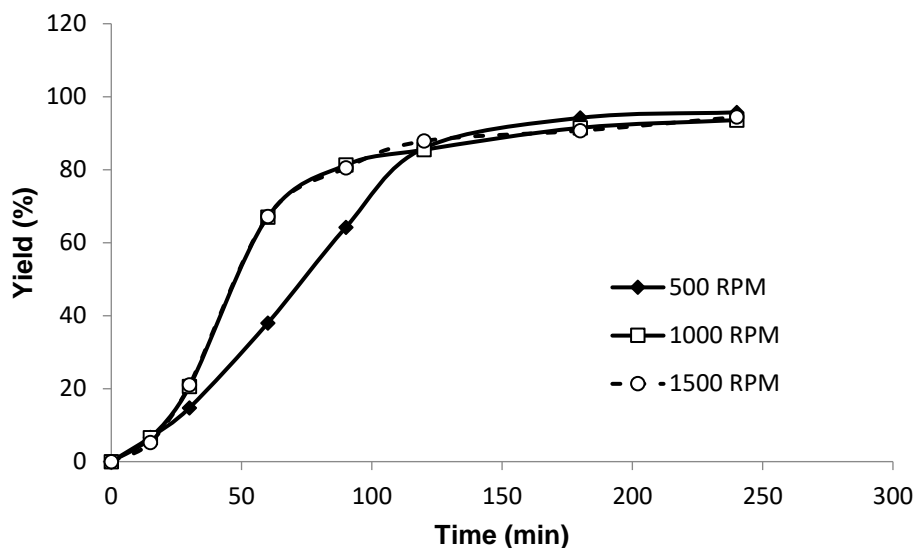


Fig. 5.23. Effect of stirring speed on cyclooctene epoxidation by H_2O_2 with HexCyPN-PMo catalyst at 60 °C. The reaction system included HexCyPN-PMo (0.0125 mmol), cyclooctene (30 mmol), decane (2.14 mmol) and hydrogen peroxide (3.0 mmol, 30 % w/w).

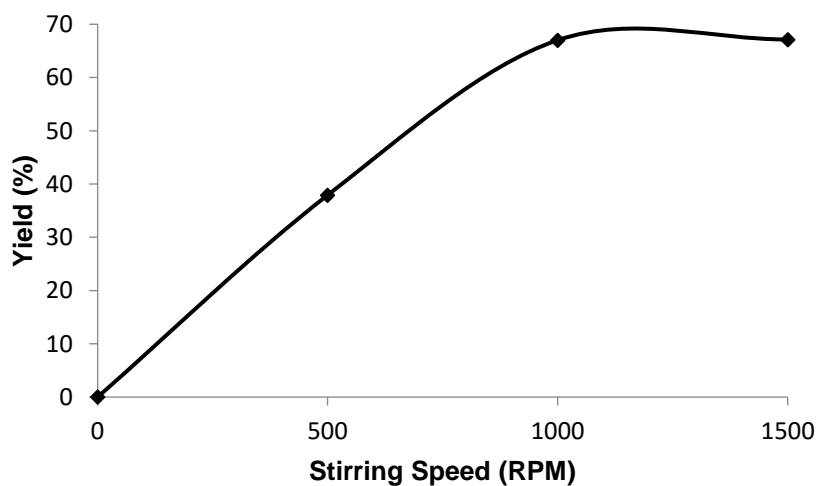


Fig. 5.24. Comparison of epoxide yields achieved after 60 min at 60 °C and different stirring speeds for cyclooctene epoxidation by H_2O_2 with HexCyPN-PMo catalyst. The reaction system included HexCyPN-PMo (0.0125 mmol), cyclooctene (30 mmol), decane (2.14 mmol) and hydrogen peroxide (3.0 mmol, 30 % w/w).

The eutectic RPN-POM catalysts compare very well with IL catalysts used in the solventless epoxidation of olefins with H₂O₂. Two POM-RTILs, prepared by pairing alkylimidazolium cations with Venturello ions (Fig. 5.25), were tested under almost identical conditions to those used in this study (cyclooctene (3.0 mmol), [cyclooctene]/[H₂O₂] = 1:1 (mol/mol), 60 °C reaction temperature, 4 h reaction time).³⁸

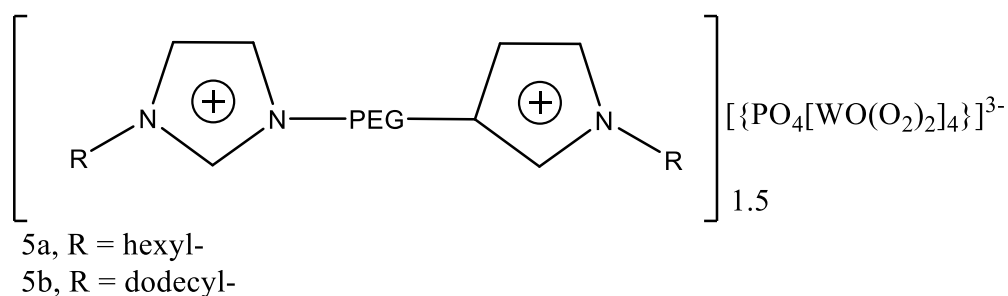


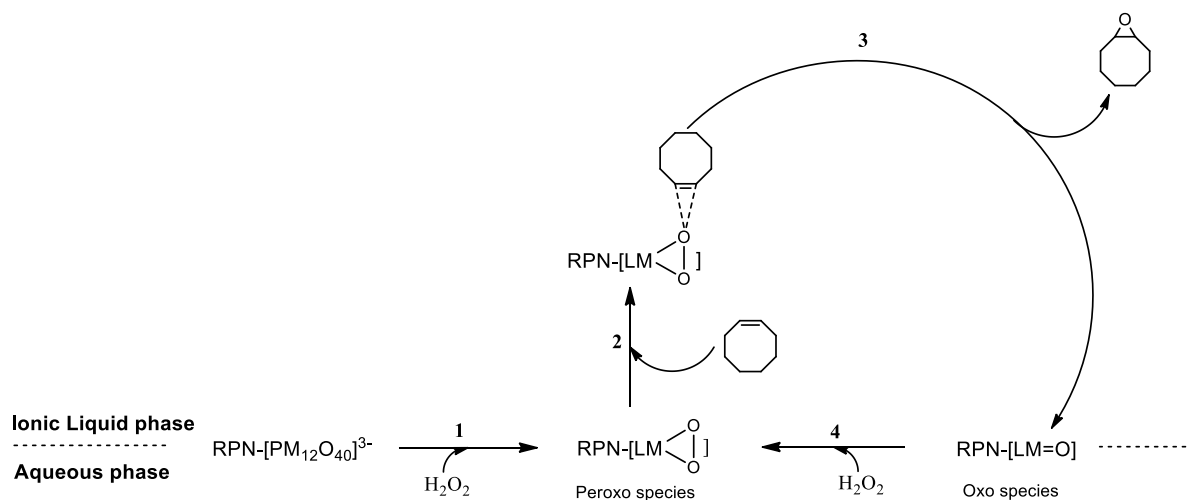
Fig. 5.25. Structure of POM-RTILs, comprised of alkylimidazolium cations and Venturello ions, which were used as catalysts for the epoxidation of olefins with H₂O₂ in the absence of solvent.³⁸

Reactions with 5a and 5b gave 96 and 95 % cyclooctene epoxide yields, respectively, with 99% selectivity. HexCyPN-PMo gave practically identical results, with 95 % yield and 98% selectivity. Catalyst reuse of 5b saw a gradual decline in activity from 95-90 % over the first 4 runs, whereas with HexCyPN-PMo there was no obvious decline in activity, with epoxide yields in the range of 91 - 99% and an average selectivity of ca. 95%. The procedure for making 5a and 5b appears to be much more laborious than that used for the synthesis of HexCyPN-PMo.

Guanidinium-based phosphotungstates with guanidinium ionic liquids have also been used as catalyst/solvent systems for epoxidation of cyclooctene with 1.3 equivalents of 30 % H₂O₂.⁵¹ A 79% epoxide yield with 95% selectivity was obtained in initial runs at 60 °C after 24 h. After pre-activation in previous runs, improved yields of up to 97 % could be obtained. In

comparison, HexCyPN-PMo requires only a 4 h reaction time and gives up to ca. 16% higher epoxide yield from the initial run. In addition, it is also worth noting that HexCyPN-PMo uses Mo instead of W, which can decrease the catalyst weight by up to 25%.

The proposed reaction scheme for epoxidation of cyclooctene with H_2O_2 catalysed by eutectic RPN-POM ionic liquid is shown in Scheme 5.3. In the initial step 1, POM degrades in the presence of H_2O_2 at the interface to form a catalytically active peroxy POM species. The active peroxy POM species interact with cyclooctene in step 2 to form epoxide and an oxo POM species (step 3). The oxo POM interacts with H_2O_2 at the interface to regenerate the active peroxy POM (4), thus completing the catalytic cycle. Once the reaction is complete, the epoxy cyclooctane product can be separated from the catalyst ionic liquid by solvent extraction, and the catalyst can be reused.



Scheme 5.3. Proposed mechanism for epoxidation of cyclooctene by H_2O_2 catalysed by a mixed RPN ionic liquid.

5.5 Conclusions

Eutectic RPN-POMs have been demonstrated to be efficient catalysts for the epoxidation of olefins with H_2O_2 . Reactions do not require the use of volatile organic solvents in these systems, and the catalyst and product can be easily separated once the reaction is complete through solvent extraction of the product, which was much more difficult for single substituent amine RPN-POMs as they were also soluble in these solvents. HexCyPN-PMo could be recycled at least 4 times without any observable loss in catalytic activity. Activity with respect to POM increased with decreasing aqueous stability ($\text{PMo} > \text{PW} > \text{SiW}$) and PMo-based catalysts performed well compared to other previously reported POM-based ILs in similar reaction systems.

Additionally, it was shown that eutectic RPNs, formed by reacting $\text{P}_3\text{N}_3\text{Cl}_6$ with a mixture of primary amines using a combinatorial approach, can be used as a base to produce eutectic ionic liquids by combining these with suitable Brønsted acids (HCl , HNO_3 and HPA).

References

- 1 A. Loupy, in *Modern Solvents in Organic Synthesis. Topics in Current Chemistry*, Springer, Berlin, Heidelberg, 1999, vol. 206.
- 2 R. S. Varma and Y. Ju, in *Green Separation Processes*, Wiley-VCH Verlag GmbH & Co. KGaA, 2006, pp. 53–87.
- 3 K. Tanaka and F. Toda, *Chem. Rev.*, 2000, **100**, 1025–1074.
- 4 P. Wasserscheid and W. Keim, *Angew. Chemie Int. Ed.*, 2000, **39**, 3772–3789.
- 5 M. Lombardo, M. Chiarucci and C. Trombini, *Green Chem.*, 2009, **11**, 574–579.
- 6 P. Mastrorilli, C. F. Nobile, R. Paolillo and G. P. Suranna, *J. Mol. Catal. A Chem.*, 2004, **214**, 103–106.
- 7 S. Anjaiah, S. Chandrasekhar and R. Grée, *J. Mol. Catal. A Chem.*, 2004, **214**, 133–136.
- 8 S. T. Handy, *J. Org. Chem.*, 2006, **71**, 4659–4662.
- 9 E. Janus, I. Goc-Maciejewska, M. Lozynski and J. Pernak, *Tetrahedron Lett.*, 2006, **47**, 4079–4083.
- 10 Y. Xiao and S. V. Malhotra, *Tetrahedron Lett.*, 2004, **45**, 8339–8342.
- 11 C. E. Song, *Chem. Comm.*, 2004, **82**, 1033–1043.
- 12 T. Welton, *Chem. Rev.*, 1999, **99**, 2071–2083.
- 13 J. P. Hallett and T. Welton, *Chem. Rev.*, 2011, **111**, 3508–3576.
- 14 R. D. Rogers and K. R. Seddon, *Science (80-.)*, 2003, **302**, 792–793.
- 15 M. J. Earle and K. R. Seddon, *Pure Appl. Chem.*, 2000, **72**, 1391–1398.

- 16 J. S. Wilkes, *J. Mol. Catal. A Chem.*, 2004, **214**, 11–17.
- 17 H. Olivier-Bourbigou and L. Magna, *J. Mol. Catal. A Chem.*, 2002, **182–183**, 419–437.
- 18 R. A. Sheldon, *Chem. Commun.*, 2001, 2399–2407.
- 19 T. Welton, *Coord. Chem. Rev.*, 2004, **248**, 2459–2477.
- 20 S. V Malhotra, V. Kumar and V. S. Parmar, *Curr. Org. Synth.*, 2007, **4**, 370–380.
- 21 H. Olivier-Bourbigou, L. Magna and D. Morvan, *Appl. Catal. A Gen.*, 2010, **373**, 1–56.
- 22 A. C. Cole, J. L. Jensen, I. Ntai, K. L. T. Tran, K. J. Weaver, D. C. Forbes and J. H. Davis, *J. Am. Chem. Soc.*, 2002, **124**, 5962–5963.
- 23 J. S. Wilkes, J. A. Levisky, R. A. Wilson and C. L. Hussey, *Inorg. Chem.*, 1982, **21**, 1263–1264.
- 24 K. N. Marsh, J. A. Boxall and R. Lichtenthaler, *Fluid Phase Equilib.*, 2004, **219**, 93–98.
- 25 S. K. Poole, P. H. Shetty and C. F. Poole, *Anal. Chim. Acta*, 1989, **218**, 241–264.
- 26 I. Krossing, J. M. Slattery, C. Daguinet, P. J. Dyson, A. Oleinikova and H. Weingärtner, *J. Am. Chem. Soc.*, 2006, **128**, 13427–13434.
- 27 S. Aparicio, M. Atilhan and F. Karadas, *Ind. Eng. Chem. Res.*, 2010, **49**, 9580–9595.
- 28 D. Rooney, J. Jacquemin and R. Gardas, *Top. Curr. Chem.*, 2009, 290, 185–212.
- 29 H. Niedermeyer, J. P. Hallett, I. J. Villar-Garcia, P. A. Hunt and T. Welton, *Chem. Soc. Rev.*, 2012, **41**, 7780–7802.
- 30 G. Chatel, J. F. B. Pereira, V. Debbeti, H. Wang and R. D. Rogers, *Green Chem.*, 2014, **16**, 2051–2083.

- 31 E. L. Smith, A. P. Abbott and K. S. Ryder, *Chem. Rev.*, 2014, **114**, 11060–11082.
- 32 Q. Zhang, K. De Oliveira Vigier, S. Royer and F. Jérôme, *Chem. Soc. Rev.*, 2012, **41**, 7108–7146.
- 33 M. Skopek, M. a Mohamoud, K. S. Ryder and a R. Hillman, *Chem. Commun.*, 2009, **44**, 935–937.
- 34 P. Liu, J.-W. Hao, L.-P. Mo and Z.-H. Zhang, *RSC Adv.*, 2015, **5**, 48675–48704.
- 35 S. Khandelwal, Y. K. Tailor and M. Kumar, *J. Mol. Liq.*, 2016, **215**, 345–386.
- 36 G. Garcia, S. Aparicio, R. Ullah and M. Atilhan, *Energy & Fuels*, 2015, **29**, 2616–2644.
- 37 H. Hamamoto, Y. Suzuki, Y. M. A. Yamada, H. Tabata, H. Takahashi and S. Ikegami, *Angew. Chemie - Int. Ed.*, 2005, **44**, 4536–4538.
- 38 H. Li, Z. Hou, Y. Qiao, B. Feng, Y. Hu, X. Wang and X. Zhao, *Catal. Commun.*, 2010, **11**, 470–475.
- 39 J. Chen, L. Hua, W. Zhu, R. Zhang, L. Guo, C. Chen, H. Gan, B. Song and Z. Hou, *Catal. Commun.*, 2014, **47**, 18–21.
- 40 Y. Qiao, Z. Hou, H. Li, Y. Hu, B. Feng, X. Wang, L. Hua and Q. Huang, *Green Chem.*, 2009, **11**, 1955–1960.
- 41 D. Feakins, *J. Chem. Soc.*, 1964, 4464–4471.
- 42 S. S. Krishnamurthy, A. C. Sau and M. Woods, *Adv. Inorg. Chem. Radiochem.*, 1978, **21**, 41–112.
- 43 C. W. Allen, *Chem. Rev.*, 1991, **91**, 119–135.
- 44 V. Chandrasekhar and S. Nagendran, *Chem. Soc. Rev.*, 2001, **30**, 193–203.

- 45 J. F. Bickley, R. Bonar-Law, G. T. Lawson, P. I. Richards, F. Rivals, A. Steiner and S. Zacchini, *Dalt. Trans.*, 2003, 1235–1244.
- 46 M. Craven, R. Yahya, E. F. Kozhevnikova, R. Boomishankar, C. M. Robertson, A. Steiner and I. V. Kozhevnikov, *Chem. Commun.*, 2013, **49**, 349–351.
- 47 H. R. Allcock, in *Phosphorus-Nitrogen Compounds*, Academic Press, Inc., London, 1972, p. 498.
- 48 C. Venturello, J. C. J. Bart and M. Ricci, *J. Mol. Catal.*, 1985, **32**, 107–110.
- 49 Y. Ishii, K. Yamawaki, T. Ura, H. Yamada, T. Yoshida and M. Ogawa, *J. Org. Chem.*, 1988, **53**, 3587–3593.
- 50 I. V. Kozhevnikov, in *Catalysts for Fine Chemical Synthesis: Catalysis by Polyoxometalates*, eds. S. M. Roberts, I. V. Kozhevnikov and E. Derouane, Wiley, West Sussex, 2002, pp. 117–166.
- 51 L. Gharnati, O. Walter, U. Arnold and M. Döring, *Eur. J. Inorg. Chem.*, 2011, 2756–2762.

6. General Conclusions

Oxidation reactions are used in both industry and academia for a variety of applications such as the manufacture of chemicals, materials, fuels, and the production of key intermediates in the synthesis of drugs. The oxidation reactions used in these processes are selective as they target specific reactant(s) to produce specific product(s),¹⁻³ and are often carried out in liquid phase systems using an oxidizing agent. Hydrogen peroxide is an attractive agent as it is relatively cheap to purchase, it has an atom efficiency of 47% in oxidation reactions, and its only by-product is water.⁴ A catalyst is required to activate H₂O₂ before it can react with the target substrate. Keggin-type polyoxometalates (POMs) – nano-sized metal oxygen cluster anions with the formula [XM₁₂O₄₀]⁸⁻ⁿ comprised of twelve oxygen-sharing MO₆ octahedra (most typically M = Mo^{VI}, W^{VI} and V^V) which encapsulate a central tetrahedron ([XO₄]ⁿ⁻, typically X = P^V, Si^{IV} etc.) – are particularly good catalysts for this purpose, and reactions of this type typically operate using the Venturello-Ishii system.⁵ In this system, the POMs decompose in the presence of excess hydrogen peroxide to form peroxy complexes (e.g. the Venturello complex,⁶ {PO₄[WO(O₂)₂]₄}³⁻) which are the active species in these reactions. These species are hydrophilic and are solubilised in water whereas the target reactants are lipophilic and thus are dissolved in an organic solvent; the two immiscible solutions form a liquid-liquid biphasic system. Phase-transfer catalysts (PTC), typically quaternary ammonium cations, are employed to facilitate the migration of the active peroxy species between the two phases for the oxidation reaction to occur, and enables regeneration of the active species at the interface.⁷

Epoxidation of olefins and oxidative desulfurization of diesel fuels are both important reactions that can operate *via* the Venturello-Ishii system. Oxidation of olefins is used to produce epoxides which are important precursors for epoxy resins, surfactants and paints, and are key

intermediates in organic syntheses.⁸⁻¹² Oxidative desulfurization is an emerging technology for the removal of heavy aromatic organosulfur compounds from vehicular diesel fuels, which cannot be easily removed by commercialized processes, such as hydrodesulfurization, HDS, without increasing the cost of processing and compromising fuel quality.¹³⁻¹⁵ The removal of these compounds is important as their combustion produces SO_x gasses which are harmful to health and the environment. As such, there have been increasingly strict environmental regulations imposed on the sulfur content of diesel fuels used in transportation vehicles which has decreased from 2000 to 10 ppm over the last 20 years.¹⁶⁻¹⁸

In this study, it has been demonstrated that phosphazene-polyoxometalate (RPN-POM) aggregate salts – comprised of alkylaminocyclotriphosphazenes, (RNH)₆(P₃N₃) (henceforth, RPN, where R = *iso*-butyl, *i*Bu; *iso*-propyl, *i*Pr; hexyl, Hex; benzyl, Bz; Cy, cyclohexyl; Bu, butyl) and Keggin-type polyanions – are effective catalysts for olefin epoxidation and desulfurization of diesel fuel using H₂O₂. Three different RPN-POM catalyst systems have been developed in this study. System One used RPN-POM aggregates as catalysts for the oxidation of a target substrate (an olefin or benzothiophene) with H₂O₂ in an aqueous biphasic system in a continuation of our previous work.¹⁹ The study of this system mainly focussed on the effect of the RPN phase-transfer catalyst moiety on the catalytic activity with respect to the organic solvent used. System Two employed a heterogeneous RPN-POM catalyst, POM immobilised on RPN-functionalised silica (POM/RPN-SiO₂), for oxidation reactions with H₂O₂ in a triphasic system, with the aim of improving the ease of catalyst-product separation, compared to System One, whilst maintaining good conversions or yields of benzothiophenes or epoxides, respectively. In System Three, eutectic ionic liquids, comprised of RPNs with mixed organoamino substituent groups (eutectic RPNs) and POMs, were presented as multifunctional solvent-catalysts for epoxidation of olefins with H₂O₂. This system was

developed to be a green reaction system by avoiding the use of volatile organic solvents in the reaction mixture.

In System One, catalytic activity with respect to POM in both olefin epoxidation and oxidative desulfurization typically increased in line with decreasing aqueous stability and in the order: PMo > PW > SiW. With respect to RPN, activity decreased with decreasing the size of R group in the order: Bz > iBu > iPr, which can be explained by increasing phase-transfer efficiency of RPN due to the relative solubility of the substituent R groups in the organic phase. The best catalyst, BzPN-PMo ([BzPN]/[PMo] = 6:1), gave >99 % cyclooctene oxide yield with >99% H₂O₂ efficiency after 30 min in PhMe/H₂O system with 10:1 ratio [cyclooctene]/[H₂O₂] and 1:118 ratio [PMo]/[H₂O₂]. The system could be reused at least 5 times without observing any loss in catalyst activity. For oxidative desulfurization, 100% DBT conversion at 99% H₂O₂ efficiency was observed for both the BzPN-PMo and BzPN-PW catalysts within 30 minutes at 60 °C with a 1:3 [DBT]/[H₂O₂] molar ratio in a PhMe/H₂O system. Moreover, in heptane/H₂O systems, in which heptane was used as a diesel fuel analogue, the sulfone product precipitated from the system due to immiscibility. Activity in this system was found to increase with the use of aliphatic substituent groups on RPN, with the most efficient catalyst, HexPN-PMo, converting 79% DBT to sulfone with >99% H₂O₂ efficiency.

The main issue with this system, however, was that the catalyst remained soluble in the organic layer once the reaction was complete which made product separation difficult (separation required vacuum distillation to isolate the catalyst which increases system costs and can compromise pure product qualities and yields). To improve catalyst separation, System Two was developed. RPN-POM was heterogenized using a mesoporous silica support (Hypersil APS-2), giving POM/RPN-SiO₂ catalyst. The catalysts were synthesized by first functionalizing the silica with P₃N₃Cl₆ using aminopropyl tethers, substituting the chloride groups for primary amine groups to give the desired RPN, and then, finally, immobilizing the

POM onto the surface through ionic and H-bonding interactions with the RPN groups. Analysis of the RPN-SiO₂ support showed that some of the RPNs had been hydrolysed which produced a diverse range of RPN derivatives on the surface. Despite this, POM immobilization was successful and POM/RPN-SiO₂ were found to be effective catalysts for oxidative desulfurization and olefin epoxidation with H₂O₂.

The product yield of olefin epoxidation and conversion of thiophene in oxidative desulfurization reactions was found to increase with respect to POM with decreasing aqueous stability and increasing oxidative potential in the order: PMo > PW > SiW, and increase with increasing the size of R group with respect to RPN in the order: BzPN > iBuPN > iPrPN, independent of the solvent system used. The best catalyst in oxidative desulfurization, PMo/BzPN-SiO₂, gave >99% DBT conversion with 68% H₂O₂ efficiency after 3 h in heptane/H₂O – in which heptane was used as a model fuel - at 60 °C with [DBT]/[H₂O₂]=1:3, [POM]/[H₂O₂]=1:270 and [POM]/[DBT]=1:90. The catalyst could be reused at least three times, giving 100% DBT conversion in 6 h after each use, although, there was a notable loss in the rate of reaction between runs which may have been caused by leaching of catalytically active species and/or loss of catalyst by transfer between vessels either during the reaction or during the catalyst recovery procedure. At 50 °C using PMo/BzPN-SiO₂ (PMo/BzPN = 1:1) as a catalyst a 94% DBT conversion was yielded in 2 h, whereas DBT was only converted up to 28 and 49 % with the homogenous analogue, PMo/BzPN, in a 1:1 ratio and 1:6 ratio, respectively, using System One. The PMo/BzPN-SiO₂ could be more easily separated from the reaction mixture than BzPN-PMo after the reaction, although, if the active species of PMo/BzPN-SiO₂ leached during the reaction and remained solubilized in the fuel layer then this would still need to be removed. For olefin epoxidation, the system was much less active than System One, with the best system, PMo/BzPN-SiO₂ catalyst in 1,2-dichloroethane (DCE), giving 76% yield of cyclooctene oxide and 76% H₂O₂ efficiency after 5 h at 60 °C with

[cyclooctene]/[H₂O₂] ≈ 10:1, [POM]/[H₂O₂] = 1:63 and [POM]/[cyclooctene] = 1:1600. Though catalyst separation was easier in this system than in System One, catalyst activity was much slower and reuse showed gradual loss in activity, giving 59% cyclooctene oxide yield after the 3rd run. UV-vis measurements indicated that catalytically active PMo species appeared to have leached into the DCE layer; as fresh DCE was used for each run in reuse experiments, leached catalytically active species were likely discarded between runs, which probably caused the observed decline in yield and activity.

In System Three, eutectic ionic liquids - comprised of RPNs with mixed organoamino substituent groups (eutectic RPNs) and POMs - were used as multifunctional solvent-catalysts for epoxidation of olefins with H₂O₂. The eutectic RPNs were first synthesized using a combinatorial approach by reacting P₃N₃Cl₆ with two or three primary amines and then the eutectic RPN-POMs were yielded by combining with POM in stoichiometric amounts in ethanol and evaporating off the solvent. The system conducted reactions in the absence of volatile organic solvents, making them greener than those conducted using System One or System Two. One of the best systems, HexCyPN-PMo, was used as solvent-catalyst which gave 95% cyclooctane oxide yield with 98% selectivity with respect to cyclooctene conversion at 60 °C in a 4 h reaction time with [PMo]/[H₂O₂] = 1:240 and [Cyclooctene]/[H₂O₂] = 1.13:1. The epoxide product could be isolated using extraction with heptane and the catalyst could be reused at least 4 times with no loss in activity. In addition, eutectic RPNs were used as a base to produce a range of eutectic ionic liquids by combining these with different Brønsted acids (HCl, HNO₃ and HPA). These were used to observe the effect of anion size on the packing and the melting point of the salts produced with eutectic RPNs. It was found that with smaller ions, such as Cl⁻, many compounds formed microcrystalline waxes composed of ordered bilayers in which the anions sat in plane with the hydrophilic phosphazene ring cations, and this ionic plane was sandwiched between two lipophilic amino-substituent layers. With larger POM

anions, the salts typically formed viscous fluids or low-melting waxes due to RPNH^+ operating as ligands around the POM spheres, creating relatively disordered structures.

In all three systems, activity with respect to POM increased with decreasing aqueous stability and increasing oxidative potential in the order: $\text{PMo} > \text{PW} > \text{SiW}$. This is in line with the ability of POM to form peroxo POMs in the presence of H_2O_2 which are the active intermediate species in epoxidation and oxidative desulfurization reactions with H_2O_2 . The only exception to this was observed for the epoxidation of olefins with POM/RPN- SiO_2 in which PW showed higher initial activity than PMo, though PW was found to deactivate much sooner and give a lower epoxide yield. Fast deactivation with PW may occur due to faster rate of thermal degradation of H_2O_2 in the presence of the PW catalytically active species. Activity with respect to RPN was relative to the catalyst system used. In systems One and Two, activity increased with increasing the size of substituent R group in PhMe/ H_2O and DCE/ H_2O systems for epoxidation in the order: $\text{Bz} > \text{iBu} > \text{iPr}$, which for the homogeneous system, System One, can be explained by increasing phase-transfer efficiency of RPN due to the relative solubility of the substituent R groups in the organic phase. In the heterogeneous system, System Two, this is may be due to a number of factors: i) *pseudo*-liquid behavior of the groups in the organic solvent providing partial solubility of the active surface groups which makes them more available to the target olefin for reaction; ii) increased basicity of RPN which likely binds the active peroxo POMs better to the catalyst surface, making them more available to olefin in the organic phase; iii) increased solubility of any leached catalytically active species in the organic layer provided by the R group, which would make them more available for reaction with the target olefin.

For oxidative desulfurization in System One, the same activity was observed for systems with toluene and DCE, but with heptane/ H_2O it was found that aliphatic R groups, particularly Hex, provided higher catalytic activity than aromatic Bz, which again can be explained by increasing

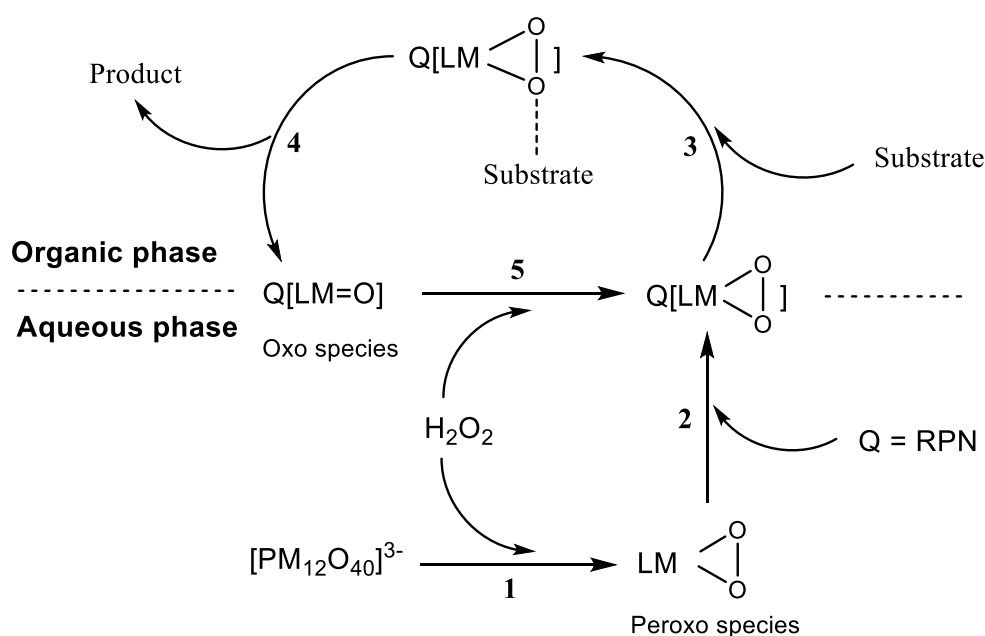
phase-transfer efficiency of RPN due to the relative solubility of the substituent R-groups in the organic phase. For System Two, which used a heptane/H₂O solvent system, activity unexpectedly decreased in the order Bz > iBu > iPr. This is probably due mostly to increased solubility with R group of the leached active species from the surface of the catalyst. With respect to the active species that remain attached to the catalyst surface (either on the surface or in the pores), it is possible that the pseudo-liquid behavior that the groups provide at the surface may make the active peroxy groups more available for reaction. The basicity of the phosphazene rings may also have an effect as the activity increases with increasing basicity of RPN which is likely due to more effective bonding of the peroxy POM to the surface of the support.²⁰ It is also possible that π - π arene-arene interactions between the Bz group and the benzothiophene rings increased the localized concentration of the benzothiophenes around the peroxy groups which made them more available for reaction.

The reactivity of benzothiophenes in oxidative desulfurization in System One and System Two was found to decrease of the order: DBT > DMDBT > BT which can be attributed to the electron-donating and steric effects of the benzene rings and the methyl groups of benzothiophenes.

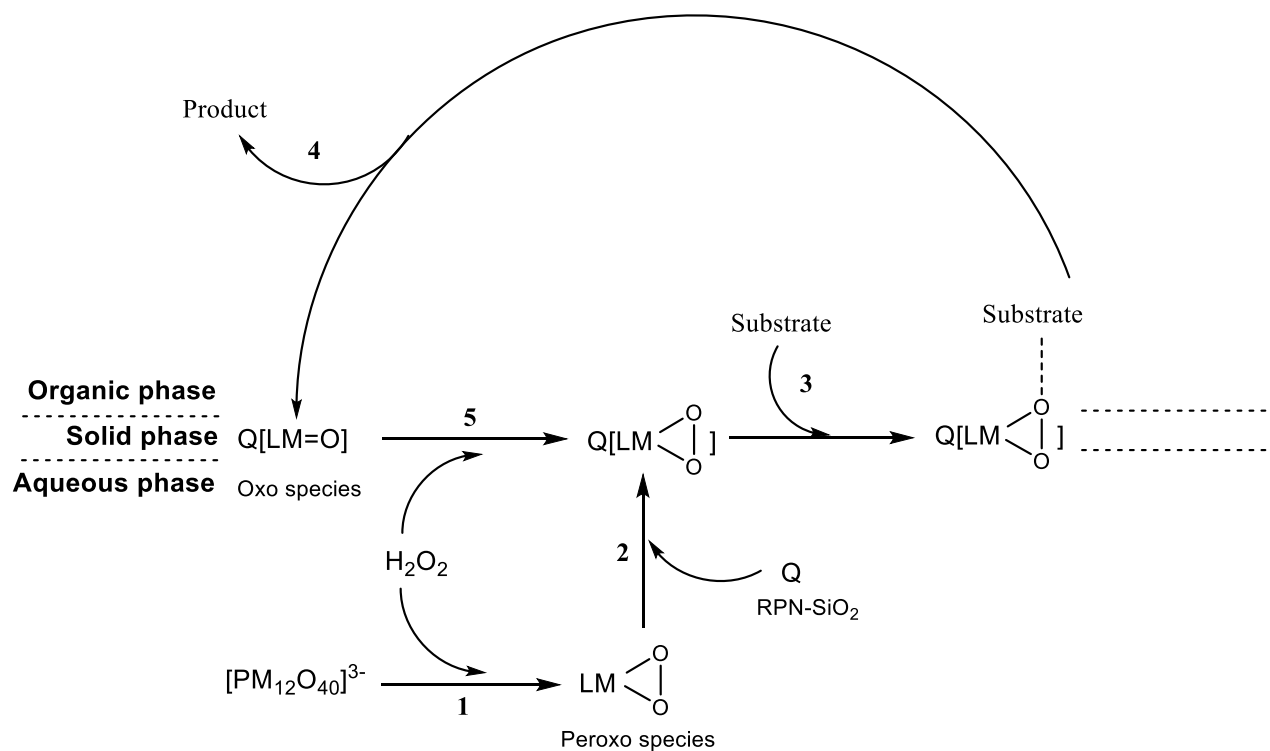
In System Three, the R groups influenced the melting point (T_m) of the eutectic RPNs and the corresponding eutectic RPN-POM catalysts. With the range of different primary amines used in this study, catalytic activity generally decreased in the order: RPN > RR'PN > RR'R''PN, although, differences in conversions and selectivities between some of the best RPNs, R'RPN and RR'R''PNs were not significant, namely HexPN (96% yield, 100% selectivity), HexCyPN (95% yield, 98% selectivity) and HexiBuBuPN (92% yield, 98% selectivity), respectively. It is notable that Hex is a substituent in all three of these compounds which may play some part with steric effects and solubility. It is not entirely certain how the choice and number of amines used to make the eutectic RPNs and, subsequently, eutectic RPN-POMs effects the catalytic

activity; a larger variety of eutectic RPNs using other primary amines would be needed to shed more light on this. Nevertheless, it can be concluded that: i) RPN-POM ILs with low melting points can be synthesized using eutectic RPNs that have been synthesized using a combinatorial approach and ii) the results produced in this study provided preliminary results which proved that these eutectic RPN-POMs can be used as solvent-catalysts. However, more work is required to understand the effect of the RPN substituents on the catalytic activity of these compounds.

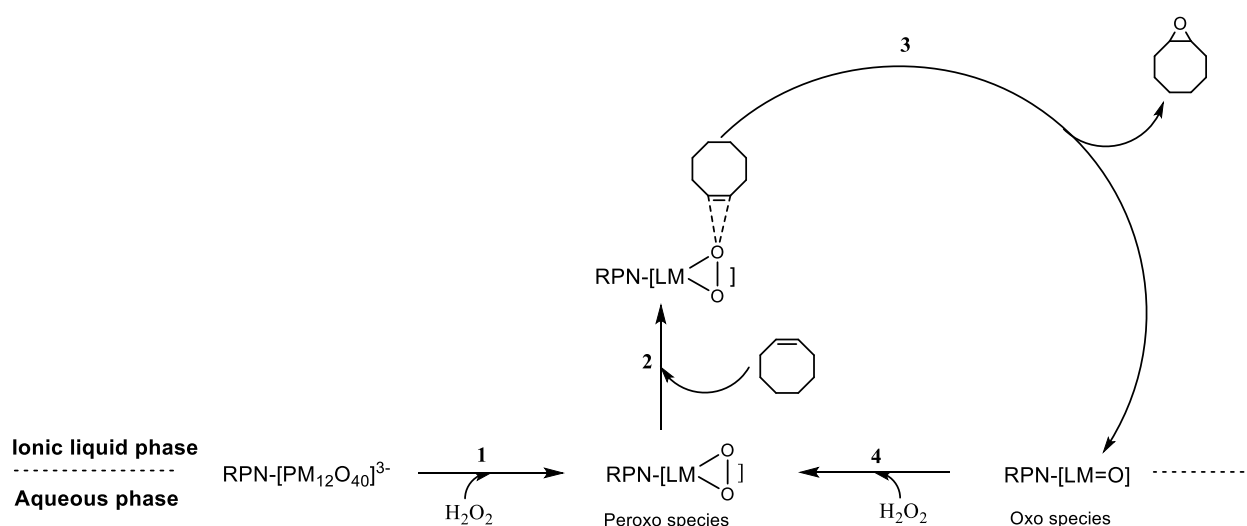
Mechanisms for all three systems have been proposed and are outlined in Schemes 6.1-6.3.



Scheme 6.1. Proposed mechanism for System One - biphasic oxidations with H_2O_2 in organic solvent/ H_2O system with RPN-POM catalysts.



Scheme 6.2. Proposed mechanism for System Two: multiphase oxidations with H₂O₂ catalysed by solid POM/RPN-SiO₂ in organic solvent/H₂O system.



Scheme 6.3. Proposed mechanism for System Three: oxidations with H₂O₂ catalysed by multifunctional eutectic RPN-POM solvent-catalyst IL.

In all three mechanisms, the first step is the degradation POM in the presence of H_2O_2 to a lacunary peroxy POM species, $\text{LM}(\text{O}-\text{O})$, which is the active catalyst species in the oxidation reactions. The mechanism for System One (Scheme 6.1) is identical to that of the Venturello-Ishii system, the only difference is instead of a quaternary ammonium cation this system uses an RPN cation as a phase-transfer catalyst moiety. In this system, the active peroxy catalyst species complexed with RPN (denoted here as $\text{RPN}[\text{LM}(\text{O}-\text{O})]$) operates in the organic layer and is regenerated at the interface in the catalytic cycle. The mechanism for System Two (Scheme 6.2) is very similar to that of scheme one, only the active peroxy catalyst species supported on $\text{RPN}-\text{SiO}_2$, $\text{Q}[\text{LM}(\text{O}-\text{O})]$, are solid and thus heterogenized from both liquid phases and, therefore, operate with reactants in both phases in a third phase through a solid-liquid interface. In the mechanism for the System Three (Scheme 6.3), the eutectic RPN-POM catalyst (an ionic liquid) operates as both a reaction solvent and a catalyst with the active species regenerated at the interface with aqueous H_2O_2 .

Each of these systems has its advantages and disadvantages. System One provides high conversions and yields, and high H_2O_2 efficiency in short reaction times (<0.5 h) for olefin epoxidation and oxidative desulfurization but requires vacuum distillation to separate the product and catalyst at the end of the reaction which increases energy costs. In addition, the fact that the system is effective for both oxidative desulfurization and olefin epoxidation could mean that if the system were used for oxidative desulfurization of diesel fuels then the quality of the fuel could also be compromised by reaction of the alkene components to form epoxides. System Two provides automatic product-catalyst separation in both reactions and completely removes DBT and DMDBT, and 90% BT in the oxidative desulfurization of heptane model fuel in 3 h. With heptane as organic solvent, epoxidation was very poor, providing 25 % epoxide yield after 5 h, indicating that the system showed promise for use in oxidative desulfurization of diesel fuel without greatly compromising fuel quality, though, further testing

with simultaneous desulfurization and epoxidation in heptane/H₂O system would be needed to confirm this. Nevertheless, epoxide yields and H₂O₂ efficiencies were much lower, and reaction times were much longer for System Two compared to System One. The preparation and characterization of the RPN-SiO₂ supports for System Two was also much more difficult than for System One.

System Three was only investigated for epoxidation of olefins due to time constraints on the project. The best catalysts in this system gave average epoxide yields of ca. 95% and $\geq 98\%$ selectivity in 4 h, which is better than the results from using System Two but worse than results from using System One, though, it must be noted that System Three used 1:1.1 molar ratio [H₂O₂]/[olefin] whereas Systems One and System Two required 1:9.7 molar ratio to avoid over-oxidizing the epoxide product. Catalyst-product separation in System Three was easier than System One, which was done using solvent extraction at room temperature, although, catalyst separation was automatic in System Two. The main drawback of the eutectic RPN-POM catalysts used in System Three is that they are viscous fluids and so are much more difficult to handle compared to RPN-POM catalysts used in System One and POM/RPN-SiO₂ used in System Two which are both powders.

Future work could include expanding the range of different RPNs and POMs used in each of the different systems to discover if there are more effective combinations than those used in this study. A range of different supports could be investigated for immobilizing RPN and POMs for use as heterogeneous catalysts such as alumina or activated carbon; indeed, we have ongoing work within the group which is investigating the oxidation of model diesel fuels with H₂O₂ using supported RPN-POMs on activated carbon. Copolymerized phosphazene rings using linkers such as *p*-xylene could also be used as a support to immobilize POMs for use as catalysts.

Catalyst leaching could be tested for in both olefin epoxidation and oxidative desulfurization reactions using System Two by reusing the organic layer with fresh H₂O₂ in the absence of solid catalyst. If the reaction proceeds then this would be evidence that catalytically active species had leached from the POM/RPN-SiO₂ catalyst and operate homogeneously in reactions using System Two. Additionally, ICP could also be used to detect Mo or W from POM species in the organic layer after a reaction, which could also indicate catalyst leaching.

It would also be worth investigating desulfurization of actual diesel fuel with the catalyst systems in this study as a true test of their effectiveness for industrial application. Additionally, a greater range of oxidation reactions with hydrogen peroxide could also be investigated for these systems to improve their range of potential applications.

With many nations recently committing to the banning diesel and petroleum fueled vehicles over the next 30 years, to maintain the relevance of these systems it would also be useful to test their effectiveness in the oxidative desulfurization of biofuels.

As mentioned above, handling of the eutectic RPN-POM catalysts was difficult due to them being viscous fluids at room temperature. Freezing them to form glasses with liquid nitrogen could be one method to improve handling. Another method could be to add a hexa-mono-substituted RPN, such as BzPN, as an additional H-bond donor to the eutectic RPN-POM to provide more order in the structure and possibly create low melting waxes (T_m below the reaction temperature) and improve handling of the solvent-catalyst. It would also be interesting to test the effectiveness of the eutectic RPN-POM system for oxidative desulfurization of diesel fuels with H₂O₂. Ideally, a eutectic RPN-POM could be developed as an emulsion catalyst to provide self-separation of catalysts, reactants and products by the system once the reaction has reached completion.

It would also be useful to simultaneously conduct olefin epoxidation and desulfurization reactions with a wide variety of thiophenes and olefins in a model fuel with each of the systems. If oxidative desulfurization is much more favorable and practically none of the olefins reacted it would then mean that the system could carry out oxidative desulfurization without impacting on the quality of the fuel. For System Two, epoxidation of cyclooctene in heptane/H₂O₂ with PMo/BzPN-SiO₂ was poor, whereas desulfurization with DBT, BT and DMDBT was efficient, meaning that this system already shows early promise for this application.

References

- 1 G. Centi and S. Perathoner, in *Encyclopedia of Catalysis*, John Wiley & Sons, Inc., 2002.
- 2 A. Weiss, in *Modern Biooxidation*, Wiley-VCH Verlag GmbH & Co. KGaA, 2007, pp. 193–209.
- 3 A. Scarso and G. Strukul, in *Stereoselective Synthesis of Drugs and Natural Products*, John Wiley & Sons, Inc., 2013.
- 4 R. Noyori, M. Aoki and K. Sato, *Chem. Commun.*, 2003, 1977–1986.
- 5 Y. Ishii, K. Yamawaki, T. Ura, H. Yamada, T. Yoshida and M. Ogawa, *J. Org. Chem.*, 1988, **53**, 3587–3593.
- 6 C. Venturello, J. C. J. Bart and M. Ricci, *J. Mol. Catal.*, 1985, **32**, 107–110.
- 7 I. V. Kozhevnikov, in *Catalysts for Fine Chemical Synthesis: Catalysis by Polyoxometalates*, eds. S. M. Roberts, I. V. Kozhevnikov and E. Derouane, Wiley, West Sussex, 2002, pp. 117–166.
- 8 R. A. Sheldon and J. K. Kochi, *Metal-catalyzed oxidations of organic compounds: mechanistic principles and synthetic methodology including biochemical processes*, Academic Press, Michigan, 1981.
- 9 C. L. Hill, in *Advances in Oxygenated Processes vol. 1*, ed. A. L. Baumstark, Jai Press Inc., London, 1988, p. 210.
- 10 M. Hudlicky, *Oxidations in Organic Chemistry*, Wiley VCH, 1990.
- 11 A. H. Tullo, *Chem. Eng. News Arch.*, 2004, **82**, 25–31.
- 12 N. Mizuno, K. Yamaguchi and K. Kamata, *Coord. Chem. Rev.*, 2005, **249**, 1944–1956.

- 13 J. Gary, G. Handwerk and M. J. Kaiser, *Petroleum Refining.*, CRC Press, London, 5th edn., 2007.
- 14 C. Song, *Catal. Today*, 2003, **86**, 211–263.
- 15 H. Y. Zhang, G. B. Shan, H. Z. Liu and J. M. Xing, *Chem. Eng. Commun.*, 2007, **194**, 938–945.
- 16 N. Palaić, K. Sertić-Bionda, D. Margeta and Š. Podolski, *Chem. Eng. J. Biochem. Eng. J.*, 2015, **29**, 323–327.
- 17 European Union, *Off. J. Eur. Union*, 2009, L140/88-L140/113.
- 18 *Tier 3 Gasoline Sulfur Standard's Impact on Gasoline Refining*, 2004.
- 19 M. Craven, R. Yahya, E. F. Kozhevnikova, R. Boomishankar, C. M. Robertson, A. Steiner and I. V. Kozhevnikov, *Chem. Commun.*, 2013, **49**, 349–51.
- 20 H. R. Allcock, in *Phosphorus-Nitrogen Compounds*, Academic Press, Inc., London, 1972, pp. 249–266.